Inaugural dissertation

for

obtaining the doctoral degree

of the

Combined Faculty of Mathematics, Engineering and Natural Sciences

of the

Ruprecht – Karls – University

Heidelberg

Presented by

M.Sc. Aurelia Dorothea Saftien

Born in: Filderstadt, Germany 3rd of November 1994

Oral examination: 24th of September 2024

Investigating Fungi – Mammalian Host Interactions in Health and Disease Using Organoids and Mouse Models

Referees: Prof. Dr. Ralf Bartenschlager

Prof. Dr. Eran Elinav

Table of contents

1 Abbreviations

µg	Microgram
µL	Microliter
µM	Micromolar
ABX	Antibiotics
ALF	Acute Liver Failure
ALT	Alanine Aminotransferase
AmpB	Amphotericin B
APAP	Acetaminophen
APC	Adenomatous Polyposis Coli
AST	Aspartate Aminotransferase
ATCC	American Type Culture Collection
ATP	Adenosine Triphosphate
AUC	Area Under The Curve
BILT3	Bilirubin Total Gen. 3
BME	Cultrex Basement Membrane Extract
BMP15	Bone Morphogenetic Protein 15
bp	Base pairs
BSL2	Biosafety Level 2
CDKN2A	Cyclin-dependent Kinase Inhibitor 2A
cDNA	Complementary DNA
CFU	Colony Forming Units
CLEC7A	C-type Lectin Receptor 7A
CRC	Colorectal Cancer
CRISPR	Clustered Regularly Interspaced Short Palindromic Repeats
CT	Cycle Threshold
CYP2E1	Cytochrome P450 2E1
DDW	Deuterium-depleted Water
DEG	Differentially Expressed Genes
DILI	Drug-induced Liver Injury
DKFZ	German Cancer Research Center, Germany
DMEM	Dulbecco’s Modified Eagle Medium
DNA	Deoxyribonucleic Acid
EGF	Epidermal Growth Factor

ELISA	Enzyme-linked Immunosorbent Assay
EMIL	Epithelium-Microenvironment Interaction Laboratory
ERBB2	Epidermal Growth Factor 2
ERα	Estrogen Receptor Alpha
EtOH	Ethanol
FACS	Fluorescence-activated Cell Sorting
FC	Fold Change
FCS	Fetal Calf Serum
FITC	Fluorescein Isothiocyanate
FMT	Fecal Microbiota Transplant
FN 1	Fibronectin 1
fw	Forward
g	Gram
g	Rcf
GAPDH	Glyceraldehyde 3-phophate Dehydrogenase
GF	Germ-free
GFP	Green Fluorescent Protein
GGT2	Gamma-Glutamyl Transferase 2
GSH	Glutathione
h	Hour
H&E	Hematoxylin/eosin
hC	Human Colon Organoid Medium
HEPES	(4-(2-hydroxyethyl)-1-piperazineethanesulfonic acid
HR	Hormone Receptor
IBD	Inflammatory Bowel Disease
ID	Identity
Iglv1	Immunoglobulin Lambda Variable 1
IL	Interleukin
INF	Interferon
Inv	Invitrogen PureLink DNA Extraction Kit
IPA	3-(1H-Indol-3-yl)-propionic acid
ITS	Internal Transcribed Spacer
JP	Dr. Jens Puschhof
kg	Kilogram

L	Liter
MAMPs	Microbe-Associated Molecular Patterns
MAPK	Mitogen-activated Protein Kinase
mDixon	Modified Dixon
MetOH	Methanol
min	Minutes
mL	Milliliter
MLN	Mesenteric Lymph Node
MLNA	Modified Leeming and Notman Agar
MMP	Matrix-Metalloproteinase
MMTV	Mouse Mammary Tumor Virus
n	Number
NAFLD	Nonalcoholic Fatty Liver Disease
NAPQI	N-acetyl-p-benzoquinoneimine
NLR	Nod-like Receptor
Nlrp	Nucleotide-binding Oligomerization Domain, Leucine rich Repeat and Pyrin domain containing
nM	Nanomolar
OD	Optical Density
p.adj	Adjusted p value
PBS	Phosphate Buffered Saline
PCA	Principal Component Analysis
PCR	Polymerase Chain Reaction
PR	Progesterone Receptor
PSC	Primary Sclerosing Cholangitis
PTK2B	Protein Tyrosine Kinase 2 Beta
QF	Qiagen Fast Tissue Kit
QP	Qiagen Power Soil Pro Kit
qPCR	Quantitative Polymerase Chain Reaction
RAG1	Recombination Activating Gene 1
RFP	Red Fluorescent Protein
RNA	Ribonucleic Acid
rpm	Revolutions Per Minute
rv	Reverse

SAGE1	Sarcoma Antigen 1
SCN9A	Sodium Voltage-Gated Channel Alpha Subunit 9
SPF	Specific Pathogen Free
SW	Swiss-Webster
TAA	Thioacetamide
TCA	Tricarboxylic Acid
TEM	Transmission Electron Microscopy
TGF	Transforming Growth Factor
Th	T helper
TP53	Tumor protein P53
WIS	Weizmann Institute of Science, Israel
Wnt	Wingless-related integration site
yH2AX	Phosphorylated H2A Histone Family Member X
YM	Yeast Extract Malt Extract
YPD	Yeast Extract Peptone Dextrose
ZT	Zeitgeber

2 Summary

Emerging from the shadows of the numerically superior bacterial microbiome, fungi - comprising 0.1 – 2 % of the microorganisms inhabiting our body - are rapidly gaining recognition for their significant impacts on their surroundings. These commensal fungi, referred to as the mycobiome, reside mainly in the gut but can also be detected in other niches of the body. They interact with their environment, namely the surrounding bacteria and their host in many ways, by secreting metabolites, cross talking with the immune system, or breaching the intestinal barrier and shifting into an infectious state under specific conditions. Research on commensal fungi has only recently come into focus and suggested important roles for them, with shifts in their community composition associated with many different diseases. As mechanistic studies are still largely lacking, further research is required to understand the complex interactions between fungi and host to untangle causative connections.

To investigate the interplay between commensal fungi and their mammalian host I established and characterized various set-ups with increasing complexity. I focused on five commensal fungi species that are frequently detected in stool sequencing studies: *Candida albicans*, *Candida tropicalis*, *Saccharomyces cerevisiae*, *Malassezia globosa*, and *Malassezia restricta*. By characterizing their growth behavior and metabolite production in vitro, I determined key differences between individual species. Exposure of human intestinal organoids to fungal supernatants did not reveal direct effects on organoid growth or DNA damage. Therefore, I established a fungi-organoid coculture system to model live fungi-host epithelium interaction, which also allows the study of intracellular fungi. While it was possible to detect these, the coculture set-up appeared to be a more accurate representation of an infectious disease setting rather than a commensal one, potentially due to the lack of an immune system. To model a commensal state, I thus turned to mouse colonization models, after adapting different fungi detection methods. Two of the fungi successfully colonized the intestine of mice without causing systemic infection with varying degrees of background microbiomes. I characterized the colonization through transcriptomics of the intestinal mucosa and serum metabolomics, where I could detect species-specific fungal signatures. Additionally, I determined that ex-germ-free mice outside the germ-free facility acquire a natural microbiome that not only caused fungal colonization resistance, but also heavily influenced the transcriptomic and metabolomic output. This was similar in antibiotics-treated mice. Therefore, to characterize the isolated fungi signal while ruling out several confounding factors, I inoculated isolator-housed germ-free mice with a single fungi species. Furthermore, I calibrated an acetaminophen-induced acute liver failure model to show that intestinal *C. albicans* colonization on its own could reduce liver damage, while *C. albicans*-

driven assembly of a bacterial community exacerbated it. In addition to that, *C. albicans* colonization could exert a systemic effect on its host in a breast cancer mouse model by lightening the tumor burden. At the same time, the fungi colonization appeared to increase the metastasis rate, which was potentially mediated via the secretion of serum metabolites. Overall, I could identify several new axis of interaction between commensal fungi and their mammalian host, which influenced progression of two different diseases.

3 Zusammenfassung

Pilze, die aus dem Schatten des ihnen zahlenmäßig überlegenen bakteriellen Mikrobioms auftauchen, machen 0,1 – 2 % der Mikroorganismen aus, die auf unserem Körper leben und gewinnen rasch Anerkennung für ihre bedeutenden Auswirkungen auf ihre Umgebung. Diese kommensalen Pilze, die als Mykobiom bezeichnet werden, leben hauptsächlich im Darm, können aber auch in anderen Nischen des Körpers nachgewiesen werden. Sie interagieren in vielerlei Hinsicht mit dem menschlichen Wirt sowie den Bakterien in ihrer Umgebung, indem sie Metaboliten absondern, mit dem Immunsystem kommunizieren oder unter bestimmten Bedingungen die Darmbarriere durchbrechen und in einen infektiösen Zustand übergehen. Die Forschung über kommensale Pilze ist erst vor kurzem in den Fokus gerückt und hat Veränderungen in ihrer Gemeinschaftszusammensetzung mit vielen verschiedenen Krankheiten in Verbindung gebracht. Da mechanistische Studien weitgehend fehlen, ist weitere Forschung erforderlich, um die komplexen Interaktionen zwischen Pilzen und Wirt zu verstehen und kausale Zusammenhänge zu entwirren.

Um das Zusammenspiel zwischen kommensalen Pilzen und ihrem Säugetierwirt zu untersuchen, habe ich verschiedene Versuchsaufbaue mit zunehmender Komplexität etabliert und charakterisiert. Ich konzentrierte mich auf fünf kommensale Pilzarten, die häufig in Stuhlsequenzierungsstudien nachgewiesen werden: *Candida albicans*, *Candida tropicalis*, *Saccharomyces cerevisiae*, *Malassezia globosa* und *Malassezia restricta*. Durch die Charakterisierung ihres Wachstumsverhaltens und ihrer Metabolitenproduktion in vitro habe ich wesentliche Unterschiede zwischen den einzelnen Arten festgestellt. Die Exposition menschlicher Darmorganoide gegenüber Pilzkulturüberständen zeigte keine direkten Auswirkungen auf das Wachstum der Organoide oder auf DNA-Schäden. Daher habe ich ein Pilz-Organoid-Kokultursystem etabliert, um die Interaktion von lebenden Pilzen mit dem Wirts-Epithel zu modellieren, das auch die Untersuchung intrazellulärer Pilze ermöglicht. Während es möglich war, solche zu detektieren, schien das Kokultur-Setup eher einen infektiöse als einen kommensalen Zustand zu modellieren, möglicherweise aufgrund des Fehlens eines Immunsystems. Um einen kommensalen Zustand experimentell nachzustellen, wandte ich mich daher Mauskolonisationsmodellen zu, nachdem ich verschiedene Methoden zum Nachweisen von Pilzen angepasst hatte. Zwei der Pilze kolonisierten erfolgreich den Darm von Mäusen, ohne eine systemische Infektion zu verursachen, mit unterschiedlichen Mikrobiomen im Hintergrund. Ich charakterisierte die Kolonisation durch Transkriptomik der Darmmukosa und Serum-Metabolomik, wobei ich artspezifische Pilzsignaturen nachweisen konnte. Zusätzlich stellte ich fest, dass

ehemals-keimfreie Mäuse außerhalb der keimfreien Anlage ein natürliches Mikrobiom erwerben, das nicht nur eine Resistenz gegenüber Pilzkolonisation verursachte, sondern auch das transkriptomische und metabolomische Ergebnis stark beeinflusste. Dies war ähnlich bei antibiotisch behandelten Mäusen. Um das isolierte Pilzsignal zu charakterisieren und mehrere Störfaktoren auszuschließen, inokulierte ich daher isolatorgehaltene keimfreie Mäuse mit einer einzigen Pilzart. Darüber hinaus kalibrierte ich ein Paracetamol-induziertes Modell für akutes Leberversagen, um zu zeigen, dass eine intestinale *C. albicans*-Kolonisation allein den Leberschaden verringern konnte, während die durch *C. albicans* getriebene Ansammlung einer Bakteriengemeinschaft diesen verschärfte. Darüber hinaus konnte die *C. albicans*-Kolonisation in einem Brustkrebsmausmodell eine systemische Wirkung auf ihren Wirt ausüben, indem sie die Tumorlast verringerte. Gleichzeitig schien die Pilzkolonisation die Metastasierungsrate zu erhöhen, was möglicherweise durch die Sekretion von Serum-Metaboliten vermittelt wurde. Insgesamt konnte ich mehrere neue Interaktionsachsen zwischen kommensalen Pilzen und ihrem Säugetierwirt identifizieren, die den Verlauf zweier verschiedener Krankheiten beeinflussten.

4 Introduction

4.1 The Microbiome

The human microbiome consists of an estimated three trillion bacteria and is predicted to outnumber the amount of human genes by 100-fold [1-3]. While the vast majority of microbes inhabit the gut, followed by the oral cavity, skin, and vaginal tract, formerly considered sterile tissues such as the lung, liver, and breast tissue have recently been discovered to harbor a low biomass microbiome as well [4-7] (**Figure 1**). This colonization is thought to start during birth and is shaped by diet, host genetics, and environmental factors throughout life [8-10]. Although the microbiota composition in humans is variable, the usual dominant taxa are *Bacteroides* in the gut, *Streptococcus* in the oral cavity, *Propionibacterium* and *Staphylococcus* in the skin, and *Lactobacillus* in the vaginal tract [11]. In mice, the microbiome configuration is similar to humans on a phyla level in the gut, predominantly consisting of *Bacteroidetes* and *Firmicutes*, while on a genera level the types of bacteria are similar but the relative abundance is quite different [12-14]. Even though the genetic similarity between the human and mouse microbiome is very low, with an estimated 4 % shared genes, the functional similarity is considered to be close to 95 % [15].

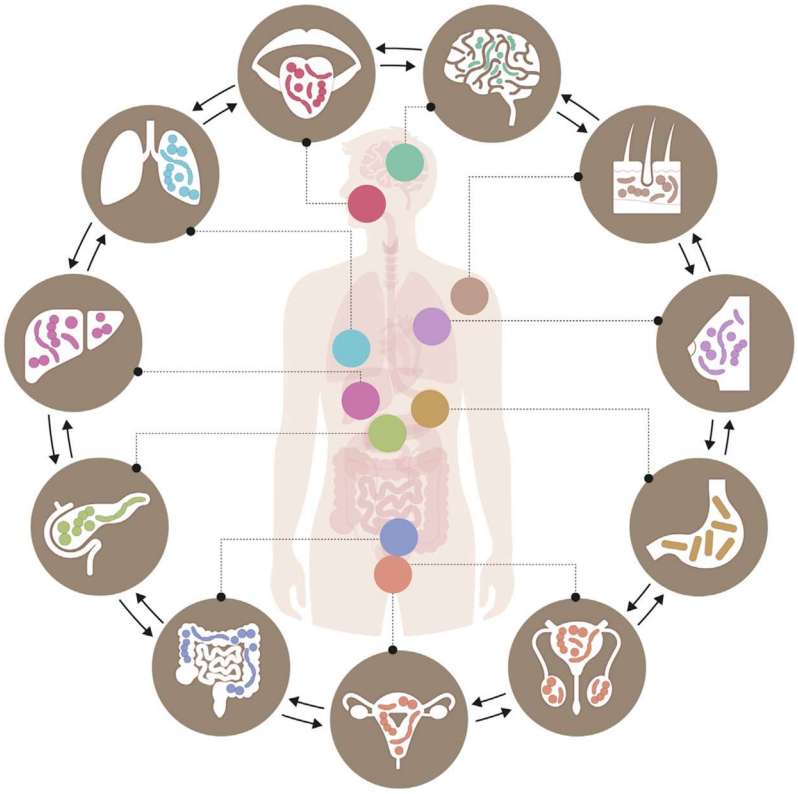

Figure 1: Microbial niches across the human body. Many different body sites have been described to contain a microbiome. From the top clockwise: brain, skin, breast, stomach, male and female genitourinary tract, intestine, pancreas, liver, lung, oral cavity. Adapted from [16].

The gut microbiome interacts with its host in various ways, by supporting digestion, releasing metabolites, and modulating the immune system [17, 18]. Dysbiosis, the state of misbalance of the microbiome, has been associated with different types of cancer [16] as well as gut-associated noncommunicable diseases, such as Inflammatory Bowel Disease (IBD), but also others affecting more distant body sites, like cardiovascular disease [19, 20]. More possible routes are for example, the so-called gut-brain axis that can mediate Amyotrophic Lateral Sclerosis or depression, the gut-liver axis for Nonalcoholic Fatty Liver Disease (NAFLD), or the gut-lung axis for asthma [21-24]. While shifts in the microbiome configuration are often the starting point for microbiome research, providing mechanistic evidence for causal relationships is much more difficult and complicated. These challenges include the existence of several species that are taxonomically distinct but functionally similar, differences between community- and single species-driven effects, under-explored variations between strains within species, or strong environmental influences contributing to issues regarding data reproducibility [25-27].

Additionally, the microbiome has been shown to shape the therapeutic response, for instance in the context of immune therapies, as well as has been used as an actual therapy [16]. The classical approach for this has been via fecal microbiota transplants (FMT), which is used to treat *C. difficile* infections [28]. Alternative ways aiming to modulate the microbiome include the use of prebiotics to selectively feed health-promoting bacteria; probiotics with the purpose of supplementing specific beneficial strains; or postbiotics, which implies to administer microbial-derived compounds, although these methods can also lead to adverse effects [29-31].

Importantly, while the majority of the microbiome consists of bacteria, non-bacterial components like viruses, archaea, as well as eukaryotic protists and fungi, are vastly understudied.

4.2 Fungi

As a kingdom, fungi are distinct from plants, bacteria, and animals. They are eukaryotes and have a cell wall which is composed of glucans, chitin, and glycoproteins [32]. There are two main categories of fungi based on their growth morphology patterns. Fungi that grow in a unicellular form are commonly known as yeasts, while fungi that form multicellular tubular structures called hyphae are classified as molds. However, there are also further morphologies that are somewhere in the middle, such as pseudohyphae, moreover some fungi are able to switch morphology depending on environmental factors such as temperature, pH, or nutrient availability (**Figure 2**) [33].

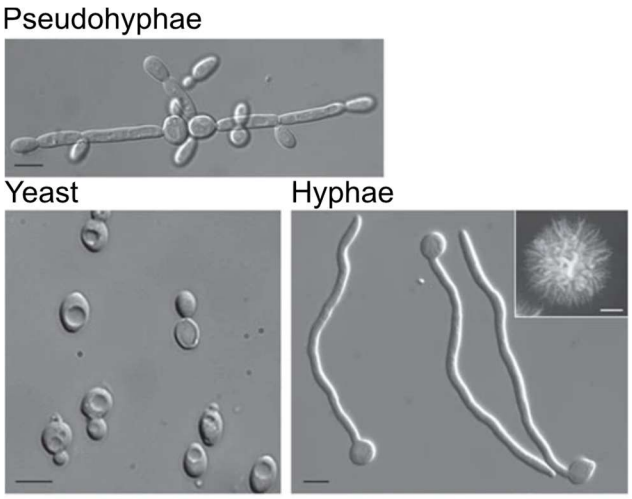

Figure 2: Fungal morphologies. *Candida albicans* growth in different morphologies, inset in hyphae panel shows colony growing on hyphae-inducing Spider medium. Scale bar main panels = 5 µm, hyphae inset = 1 mm. Adapted from [34, 35].

In the past, the focus of the research about the interactions of fungi with their human hosts had been concentrated on infectious diseases, especially due to the emergence of multi drug resistant strains [36]. However, commensal fungi that are part of our natural microbiome and their influence on the host have recently come into focus, even though some of them can become opportunistic under specific circumstances like immune suppression.

4.2.1 The Mycobiome

Fungi represent around 0.01 to 2 % of the total gut microbiome, although due to their cell size that is larger than the average bacteria cell, the actual biomass could be trumping these estimates [37-39]. The fungal microbiome, also termed the mycobiome, is present mainly in the gut, but also in other body sites, like the oral cavity, vaginal tract, skin, or lung, assumedly wherever a bacterial microbiome can be detected (**Figure 1**) [40-43]. Description of a core mycobiome has been a challenging unmet task due to the extensive variability observed across individuals and over time

[44, 45]. This variability is even more pronounced compared to that of bacteria. The intestinal mycobiome has been the best described because of relatively easy access to a proxy of its content via fecal samples. However, it often remains unclear whether the species detected are naturally inhabiting commensals or transient and if they are derived from dietary or other environmental sources [44, 45]. The two main phyla detected are usually Ascomycota and Basidiomycota, with *Candida*, *Saccharomyces*, and *Malassezia* as the main taxa [44, 45]. Similar to the bacterial microbiome, the mycobiome composition is heavily influenced by host diet, environment, lifestyle, urbanity, and host genetics [46-49]. Fungal colonization begins during birth and early life, and changes throughout it [50]. Shifts in the mycobiome configuration have started to be associated with different diseases, from IBD and colorectal cancer (CRC), to airway inflammation, and Alzheimer's disease, but also for example, Graft-versus-host disease [51-55]. Similar trends to the bacterial microbiome are emerging in mycobiome research; however, discoveries and mechanistic studies are lagging behind and only recently started to emerge.

The way in which the gut mycobiome can influence the host can be separated into four different categories: direct cell-cell interactions with the epithelium, secretion of metabolites, communication with the immune system, and interactions with the bacterial community (**Figure 3**).

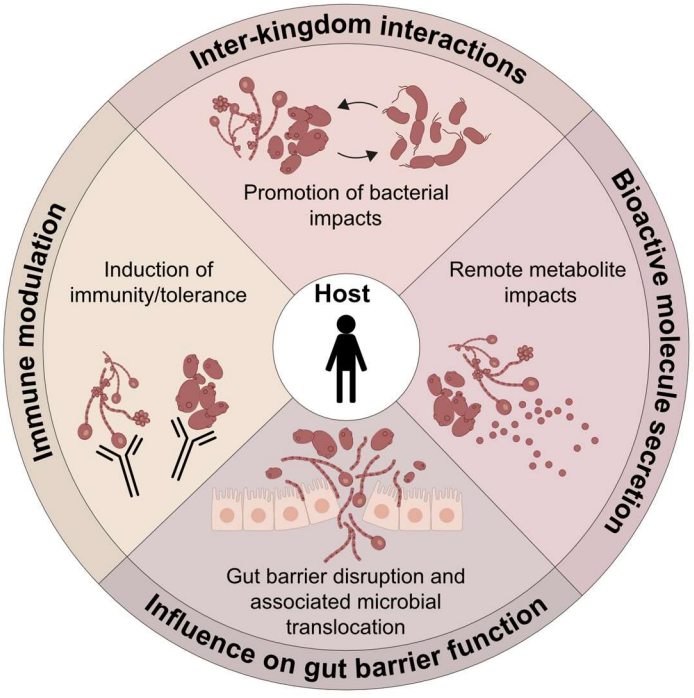

Figure 3: Fungi-host interactions. Fungi can interact with their human host in various ways: through the secretion of metabolites that can reach remote body sites, through disruption of the gut barrier leading to systemic infections, by modulating the immune system, or through the enhancement of bacterial effects. Adapted from [56].

The host intestinal epithelium with its mucus layer serves as a barrier and is the first line of defense also against infections. This has been most well studied for the opportunistic commensal *Candida albicans*, which can disseminate into a systemic infection when the barrier is impaired [57].

While the secretion of bioactive metabolites and their impact on the mammalian host is well studied for bacteria, particularly for short chain fatty acids, this is less clear for commensal fungi species [58, 59]. It has been long known that fungi are capable of producing metabolites that can strongly impact human physiology. *Aspergillus* species like *Aspergillus flavus* produce aflatoxins, which are Group 1 carcinogens well-known to cause liver cancer [60-62]. Fungal metabolites have also been used as biomarkers to detect systemic infections of *Aspergillus* or *Cryptococcus* [63-65]. However, research on fungal metabolites in a commensal setting merits further studies.

Recognition of fungal microbe-associated molecular patterns (MAMPs), typically carbohydrates from their cell wall such as glucans, by the immune system is mediated by pattern recognition receptors (PARPs) on epithelial and myeloid cells. These receptors include C-type lectin receptors (e.g. Dectin, Lectin, or Mincle) as well as Nod-like receptors (NLR) [66]. Signaling via SYK-CARD9, SYK-PLCy2, MYD88, or TRIF leads to interleukin-1β (IL-1β), IL-6, IL-12, IL-23, TGF-β, or interferon γ (INF γ) secretion, and triggers a T helper (Th) 1 and Th17 cell response [66, 67]. The adaptive immune system also responds to fungi colonization, which is evidenced by the presence of cross-reactive anti-*Saccharomyces cerevisiae* antibodies (ASCAs), utilized as a diagnostic tool in IBD [68-70].

Interactions between fungi and bacteria are manifold and not surprising given their proximity in the same niche. From cooperation to competition, different types of co-existence have been reported, including the formation of polymicrobial biofilms [71, 72]. These interactions are most prominently visible when the microbiome is perturbed, such as an overgrowth of fungi after antibiotics treatment [73-75].

In 2022, two studies systematically profiled the presence of intratumoral fungi, introducing a novel niche where a mycobiome can reside [76, 77]. Previously, intracellular fungi had only been considered in an infectious disease context, while these studies detected fungi cells within both, macrophages and epithelial cells in the tumor microenvironment [78, 79]. However, controversy in the analysis methods used for detection of low biomass intratumoral fungi and bacteria have recently been highlighted, contesting many of the claims based on issues with genomic database contaminations [80].

Overall, fungi can interact with their mammalian host in various ways, but research on specific fungi species is limited to date to few candidates, such as *Candida albicans* and *Saccharomyces cerevisiae*, and even for those, studies vary greatly in quality and methods applied, requiring further research.

4.2.2 Fungi of interest

In order to select the fungi of interest to study in this thesis, I applied several criteria when searching in the literature. Fungi should be prevalent in several sequencing studies, in larger quantities, and could potentially be human commensals based on their growth conditions (37 °C and in an anaerobic atmosphere). Based on these inclusion criteria, fungi like *Debaromyces* and *Penicillium*, which are food-born and unable to grow at 37 °C were excluded from this study [44]. *Aspergillus* species were also out of scope, since even though they can survive in the gut, they are more common in the environment, suggesting that they might be transient rather than natural colonizers [44]. Considering the three largest sequencing cohorts of the healthy human mycobiome at the time, including the fungal dataset from the Human Microbiome Project, I selected the following five fungi [44-46] (**Figure 4**).

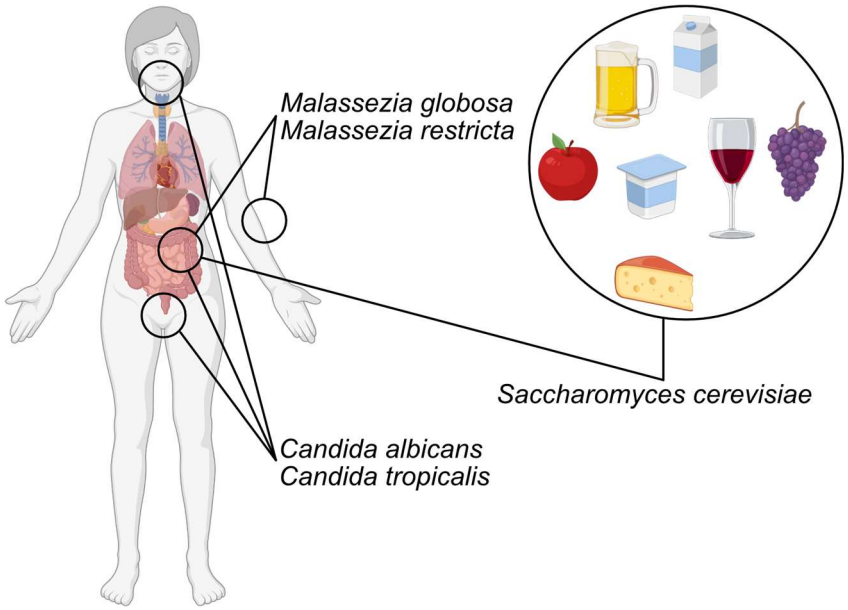

Figure 4 Ecological niches of five selected fungi candidates. *Candida albicans* and *Candida tropicalis* have been detected in samples of the intestine, oral cavity, and vaginal tract. *Malassezia globosa* and *Malassezia restricta* are skin commensals but have additionally been identified in intestinal samples. *Saccharomyces cerevisiae* is present as a live organism or with remaining DNA in many food types and measured in intestinal samples. Created with biorender.

4.2.2.1 *Candida albicans*

Candida albicans, the most well-studied commensal fungi serves as a model organism for mycobiome research [57]. Easy to grow, it has been found to thrive as a commensal of humans in the intestine, oral cavity, and vaginal tract due to its adaptation to these environments (**Figure 4**) [40, 43, 45]. Detected in all human stool sequencing studies, *C. albicans* is often the most common fungi species, normally absent in the mouse intestine. Depending on environmental conditions, this fungi is able to switch across morphologies, its yeast state is more associated with commensalism, while a switch into hyphae structures represents a key virulence factor for infectious disease [57]. This opportunistic behavior can cause local or systemic infections, the latter are oftentimes linked to highly resistant biofilms on catheters in clinics and can be fatal [71, 81]. In a hyphae state, *C. albicans* can produce a cytolytic peptide toxin, called Candidalysin, which has been associated with increased inflammasome activation, and cell proliferation pathway upregulation, and has thus been speculated to be connected to CRC [56, 82-85]. Additionally, clinical strains isolated from patients suffering from oral cancers have been shown to possess increased Acetaldehyde and Nitrosamine production capabilities, which can cause DNA damage [86-88]. Furthermore, *C. albicans* colonization has been also suggested to contribute to metastasis. In experimental models, this was shown to happen via matrix-metalloproteinase (MMP) and oncometabolite production, and through sequencing studies an upregulation of metastasis-associated pathways was detected in tumors containing intratumoral *C. albicans* [76, 89]. Despite being relatively well studied, there are still open questions, particularly in regards to causality.

4.2.2.2 *Candida tropicalis*

Candida tropicalis is the second most common *Candida* species in the human gut and unlike *C. albicans* it can be detected in the mouse intestine (**Figure 4**). It is polymorphic and, as *C. albicans*, can also produce Candidalysin, however, potency and gene expression of the toxin are regulated differently [90]. *C. tropicalis* has been found at increased levels in CRC, contributing to increased tumor burden in a germ-free intestinal cancer model, and in Crohn's disease patients, associated with worsening colitis [91, 92].

4.2.2.3 *Saccharomyces cerevisiae*

The well-known baker's and brewer's yeast *Saccharomyces cerevisiae* is detected in large quantities in several sequencing studies [45, 46]. However, due to its high prevalence in our diet, it is still unclear if it is a "natural" commensal or transient fungi in our intestine, and if it is alive or merely dead cells. The live yeast can be found on many fruits, and its DNA is present in many products after fermentation processes (**Figure 4**). Unlike the *Candida* species it cannot form

hyphae. Contrastingly, while some strains like *S. boulardii* are commercially sold as a probiotic, *S. cerevisiae* has been associated with worsening of colitis in a mouse model [93, 94]. Despite *S. cerevisiae* being a popular model organism particularly for genetics screens, its potential role as a commensal is still unexplored.

4.2.2.4 Malassezia globosa

Malassezia globosa is a well-known skin commensal that grows in the sebaceous glands, leveraging the external sources of lipids to grow, since it lost its fatty acid synthase genes [95]. It is associated with several skin diseases like Pityriasis versicolor and Seborrheic dermatitis. It is frequently detected in stool sequencing studies although it remains unclear if it actually colonizes the intestine or is merely taken up during e.g. food intake (**Figure 4**). *M. globosa* only grows in yeast form, and requires specific growth media with lipids supplementation [96]. Interestingly, it has been associated with pancreatic ductal adenocarcinoma, where it was shown to enhance tumor growth via triggering of the complement cascade or IL-33 secretion and a type 2 immune response [97, 98]. Interactions of *M. globosa* with the host in a healthy state have not been investigated so far.

4.2.2.5 Malassezia restricta

Similar to *M. globosa*, *Malassezia restricta* is a skin commensal that is often detected in stool samples and only grows as yeast cells (**Figure 4**). It has also been detected in the colonic mucosa of Crohn's disease patients and associated with worsening of colitis in an IBD mouse model [99].

4.3 Tools for mycobiome research

While the mycobiome field is still in its infant state, many research tools could be adapted from microbiome research. Although they are still less developed and require more optimizations, progress has been slower due to the niche nature of the topic. However, advancements have been made in recent years.

4.3.1 Culturing

In vitro culturing has been the historic basis for microbiome research since it represents a relatively simple method. Isolating species through culturing remains a crucial aspect of research to confirm that the fungi are actually alive and thus abide to the adapted Koch's postulates [100]. However, a large percentage of fungi species remains unculturable, which renders any mechanistic studies impossible [101]. This so-called "dark matter" of the microbiome is thought to include many fungi species, with more to be identified. For example, a recent sequencing study of the deep ocean detected many previously unidentified fungi species [102]. The fungi that are possible to culture also differ in their growth requirements, with specific and complex media, vastly varying in growth speeds ranging from hours to weeks and a menagerie of morphologies. Consequently, there is a strong bias on a select few fungi species that are intensely studied, while the function of the majority remains unclear.

4.3.2 Next-generation sequencing methods

The advent of next-generation sequencing methods revolutionized the microbiome field and, consequently mycobiome research. The application of various methods significantly differ among researchers, leading to a lack of a uniform approach. This loss of consistency can bring challenges when interpreting and translating findings. While sequencing has the great advantage of being independent of the culturability of the species, it is unable to distinguish between living or dead organisms since its reliance on nucleic acids, and is therefore prone to environmental contaminations.

4.3.2.1 DNA extraction

DNA extraction methods vary greatly between labs and commercial kits used, but the choice of the right method is even more relevant for fungi, which require harsher approaches to disrupt the cell wall absent in bacteria. At the same time, the DNA should stay intact enough to allow sensible amplification for sequencing. Due to this discrepancy, the methods used are usually adapted to

the specific fungi strains of interest with no clear consensus, thereby creating potential biases in the resulting data. Morphology changes can create another layer of complexity by possibly changing the DNA extraction efficiency.

4.3.2.2 Internal transcribed spacer (ITS) sequencing

While 16S sequencing used to be the most commonly used method for bacterial microbiome analysis, it cannot be applied to detect fungi, since they are eukaryotes and therefore have different mitochondria. The parallel method to 16S sequencing that was developed for eukaryotes is 18S or Internal transcribed spacer (ITS) sequencing. It relies on the same principle as 16S sequencing, taking advantage of regions of mitochondrial DNA that are conserved at the start and end of it (allowing for universal primer binding), but diverse in the middle to enable species-level identification [103]. There are two regions, ITS1 or ITS2 that can be used with different sets of primers that are targeting either region (**Figure 5**). The ITS1 region is situated between the 18S and 5.8S genes, while the ITS2 region sits between the 5.8S and 28S genes. So far, there is no consensus on which of these two regions is best for sequencing, with both being used [104, 105]. However, unlike the 16S region, the size of the ITS region can be very variable, creating potential biases during amplification [103].

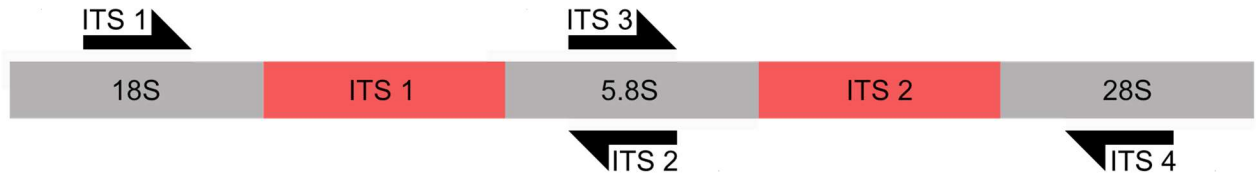

Figure 5: ITS sequencing principle. Structure of the ribosomal DNA with different genes and the four ITS primer binding sites, the amplicon length of the ITS1 or 2 structure can vary greatly between species. ITS: internal transcribed spacer.

ITS sequencing is advantageous as it can specifically detect fungi and some plants, thus not losing reads to host tissue or bacteria and being able to detect even less abundant species. It can therefore be applied to low biomass samples such as tumor tissues, although it is also prone to artifacts and environmental contaminations [77]. Since it is quite similar to 16S sequencing, some analysis tools have been adapted or developed, although the resolution of the sequencing is limited by the quality of databases, which are continuously improving but still troubled by wrongly assigned entries and limited reference genomes [103, 106]. Apart from the analysis or database biases, ITS or 18S sequencing can also be problematic due to differences in ITS and 18S gene copy numbers. The variance in gene copy numbers between fungi species is even more severe than for bacteria and can additionally be altered by environmental cues [107, 108]. This potential

bias or misrepresentation needs to be taken into account when analyzing the data although it is difficult to control for. Another disadvantage is the sole detection of fungi species, while it allows for better detection of low abundance fungi, it cannot integrate human or bacterial data, and if this is required, the method of choice should be Shotgun Metagenomic sequencing.

4.3.2.3 Shotgun Metagenomic sequencing

Shotgun sequencing is based on random cutting of the DNA into smaller pieces, thereby avoiding typical amplification biases. The lack of a specific target sequence has the advantage of allowing parallel sequencing of any DNA present, for example host, bacteria, and fungi, giving a community overview and showing potential associations. The lack of specificity on the other hand is also the main disadvantage of this method, requiring a very deep sequencing depth in order to detect less abundant species. This creates a financial barrier for these studies and was therefore used to a lesser extent in the past, but has become more popular in recent years, accelerating the study of transkingdom interactions [55, 109, 110]. So far, analysis tools for these studies are less developed relying on the adaptation of bacteria-based methods and requiring custom-built databases.

4.3.2.4 RNA sequencing

Up to date, parallel RNA sequencing of host and fungal RNA has not been done extensively and sometimes requires separate extraction protocols. Ideally, this would allow for the measurement of gene expression in both interaction partners at the same time, thus opening up new ways to gain mechanistic insights. However, it is still in its infancy and to date has only been investigated in an infectious disease context but not commensalism [111, 112]. Due to this, the database for fungal gene expression is very limited to a few model fungi like *C. albicans* or ecologically relevant fungi.

4.3.3 In vitro models: Cell lines, organoids, and organ-on-a-chips

Mechanistic studies require the controlled modeling of both interaction partners: the mammalian host and the microbe. Several reductionist models that focus on the gut epithelial-microbe interplay are available, each with different advantages and disadvantages that allow targeted manipulation of single components.

Immortalized cell lines have long been used as epithelial models and while they are readily available and easy to handle, they are transformed and can only represent a healthy epithelium to a certain degree. Cocultures have a limited duration of several hours, since the microbes can

overgrow. In order to maintain the viability of potentially anaerobic microbes and cell lines, compromises must be made regarding oxygen levels and growth media composition [113]. Fungi-cell line cocultures have been limited to infection models, using HeLa cells or oral epithelial cell lines to show the potential use of probiotic *Lactobacilli* species to reduce infectivity of *C. albicans* [114-116].

Organoids have recently emerged as versatile tools for studying microbe-host interactions [113]. There are two different types of intestinal organoids, which differ quite a lot in their strengths and handling:

Adult stem cell-derived organoids are established from stem cells at the bottom of the crypt from healthy, cancerous or other tissues and contain only epithelial cells [117]. The cells are embedded into an extracellular matrix, where they self-organize into a 3D structure that has a polarized monolayer with a fluid-filled lumen, mimicking the intestinal lumen. They can be further differentiated into various cell types or maintained in a stem-like state in culture with high genomic stability [117]. The presence of a closed luminal space allows for easier coculture also with anaerobic microbes that can last several days, until the need for passaging the organoids arises [113]. Exposure of the correct side of the epithelium to the microbes can be done through several ways (**Figure 6**).

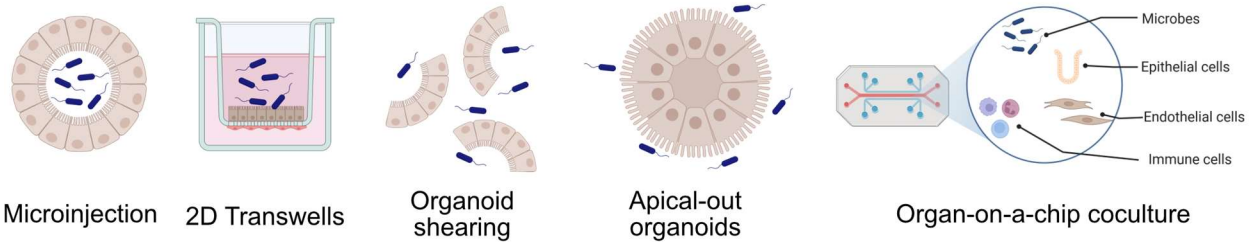

Figure 6: Strategies for organoid-microbe cocultures. From left to right the methods are the following: microbes can be microinjected inside the lumen of organoids or added to the top chamber of Transwells that were seeded with organoids dissociated into single cells to form a 2D organoid layer. Furthermore, microbe or metabolite exposure can occur during shearing of the organoids or through addition to the culture medium of organoids that were pretreated to reverse polarity. A different coculture strategy that allows for further increase of the coculture complexity is the use of organ-on-a-chips, where depending on the design other potential components such as immune or endothelial cells can be added. Created with biorender.

One option is via microinjection, which requires a more complex set-up and is technically more challenging but allows for several daylong exposure or even repeated exposures [118]. It is possible to seed organoids in a 2D layer onto transwells, which makes them however less stable and less differentiated, as previously demonstrated for stomach organoids and *Helicobacter* infection [119]. Alternatively, especially for virus or metabolite exposure, they can be mixed with the organoids during mechanical shearing to allow for exposure on both the basal and apical side

[120]. It is also possible to reverse polarity of the organoids but this often suffers from instability and incompleteness of the reversal [121, 122]. Potential readouts of these coculture settings are mutational signatures on the host DNA level, transcriptional or epigenetic changes, or functional readouts such as changes in barrier integrity, cell fate, or cytokine secretion [113, 123]. However, while there are ample examples of organoid cocultures with bacteria, viruses, and parasites, reports of fungus organoid cocultures are lacking.

Pluripotent stem cell-derived organoids on the other hand are generated from embryonic stem cells or induced pluripotent stem cells, and differentiated over weeks to months through exposure to different growth factors [124]. While this leads to 3D structures that can contain cell types of both the mesenchyme and epithelium, it is a slow process and less scalable. So far, no live fungi cocultures have been attempted, although heat-killed *Aspergillus fumigatus* was microinjected into both lung and intestinal organoids to study the inflammatory response [125].

Another upcoming model system that allows for a gradual increase in complexity are organ-on-a-chips, which are microfluidic devices that sometimes contain a flow and several chambers. They can be seeded with cell lines, organoids, or primary cells, and cocultured with endothelial cells, immune cells, and microbes (**Figure 6**) [113]. Due to the complexity of the setup and costs of the components, they have not been used for large studies yet. One study in 2019 used it to combine an intestinal Caco2 cell line, endothelial cells, and macrophages together with *Lactobacilli* colonization to model *C. albicans* infection [126]. *Lactobacilli* colonization was able to reduce *C. albicans* growth and translocation across the intestinal barrier in this model.

Apart from the intestine, cocultures with other organoid types to model the low biomass microbiome are rare and limited to tissue-trophic viral or parasitic infections such as Hepatitis B virus or *Plasmodium falciparium* infection of liver organoids [127, 128].

4.3.4 Mouse models

Mouse models are commonly used in microbiome research because they are mammalian and can model a whole organism with a complete blood circulation and immune system. Apart from differences in microbiome composition, which was discussed earlier (4.1), there are a few other key points that differ between mice and humans that can have an impact in microbiome research. While the layout of the GI tract follows the same pattern, the proportions are different, especially in case of the cecum that is much larger in mice and used for fermentation [12]. The pH of the stomach is higher in mice, potentially due to different dietary patterns, which influences the

microbial composition [12, 129]. Eating behavior, diet, and biorhythm are distinct between mice and humans, with some of the main differences being the herbivory, coprophagy, and nocturnal activity of mice [12, 130]. Most mouse strains used are inbred, such as C57BL/6 mice, while other strains that are outbred, for example Swiss-Webster mice, can have a different microbiome and mycobiome dependent on host genetics [49, 131].

4.3.4.1 The natural mouse mycobiome

Laboratory specific pathogen free (SPF) mice have been shown to have a low fungal burden, with usually no derivation of fungi by culturing [132]. Sequencing studies have reported the mycobiome to be highly dependent on vendor, research facility, and diet [133, 134]. So-called “wildling” mice that have a reconstituted natural microbiome from wild mice have a much higher fungi load with a more developed immune system [135]. Similarly, renaturing of mice into a wild habitat increased granulopoiesis, which was dependent on intestinal fungi and could be recapitulated through colonization with *C. albicans* [136]. Therefore, fungi play an important role also in mice immunity development, which cannot be detected using regular SPF mice. However, colonization with specific fungi species can be limited due to resistance of the bacterial microbiome, especially *Lactobacilli*, or other commensal fungi, as shown recently for *C. albicans* [137, 138]. In order to enable mechanistic studies to study a single fungi species, intervention is required to open up the ecological niche, usually achieved with antibiotics (ABX) treatment, or germ-free (GF) animals that are completely devoid of a microbiome [139].

4.3.4.2 Antibiotics (ABX)-treated mice

The standard way of breaking colonization resistance is with an ABX pretreatment that for fungi colonization can also be maintained along the experiment. The exact cocktail of ABX used varies throughout studies, but usually contains a mix that targets a broad spectrum of bacteria [140]. Occasionally anti-fungal drugs are also added to the mixture but it is not always necessary since SPF mice have usually low levels of intestinal fungi. Treatment with ABX has the advantage that it is cheap, easy to use and prepare, and can be applied to any mouse strain immediately. On the downside, most likely some resistant bacteria species will remain in the intestine, which can vary depending on the facility, making the results potentially less reproducible.

4.3.4.3 Germ-free (GF) mice

GF mice are the gold standard tool for microbiome research. These animals are kept in sterile isolators and have no remaining microbiome whatsoever. For experiments, they can be moved into isocages or into specific experimental isolators to reduce the risk of contaminating the entire colony. This allows the studying of the effect of the microbiome in an isolated manner; however, it

requires a dedicated GF facility that is expensive to maintain, with trained staff. Due to the important role of the microbiome, these mice while perfectly viable have some developmental defects such as a more immature immune system, among others [140].

4.4 Acute Liver Failure (ALF)

4.4.1 Background and mouse models of ALF

ALF is defined as a rapid decline in liver function in a person without a preexisting liver disease that can lead to multi-organ failure [141]. While rarely presented, it has high mortality and morbidity with an estimated incidence of 1-6 cases per million population in developed countries, and 2000-3000 cases per year in the US, although estimates might include wrongly diagnosed cases of acute on chronic liver failure [141-143]. Clinical symptoms of ALF are liver damage, increased intracranial pressure that leads to encephalopathy, and renal failure, among others [141]. ALF can be reversible, through intravenous or oral delivery treatment with *N*-acetylcysteine, however, liver transplantation remains the only alternative when treatment fails [141, 144]. It can be caused by viral Hepatitis A, B, or E, ischemic injury, or drug-induced liver injury (DILI) [145]. In developing countries and worldwide acute viral hepatitis is the predominant etiology, meanwhile in North America, Japan, and Europe DILI is the leading cause [141]. More specifically, Acetaminophen (N-acetyl-p-aminophenol or APAP), which is sold as the over-the-counter analgesic and antipyretic drug Paracetamol, toxicity is the main reason for DILI in Western countries, followed by idiosyncratic DILI [146-148]. One single intentional overdose with amounts greater than 10-15 g, mostly as a suicide attempt, or accidental overdoses over several days with lower amounts can induce ALF, while the latter is more difficult to treat, and can be worsened by fasting or alcohol intake [149, 150].

Mechanistically, under normal circumstances 90 % of APAP undergoes sulfation or glucuronidation and can be secreted through the urine as nontoxic metabolites, together with 2 % of APAP that is secreted without metabolization (**Figure 7**) [151]. Between 5-9 % of APAP undergoes Cytochrome P450 E21-mediated oxidation to N-acetyl-p-benzoquinoneimine (NAPQI) that can be detoxified by glutathione (GSH) binding. In case of an APAP overdose, the normal metabolization pathways get overwhelmed, leading to an accumulation of NAPQI, which depletes GSH levels. Highly reactive NAPQI forms adducts with cellular proteins, leading to oxidative stress and mitochondrial dysfunction, resulting in ATP depletion. Ultimately, this culminates in hepatocyte necrosis, triggering an inflammatory response.

ALF is characterized by an increase in the elevated international normalized ratio, aminotransferase levels in the serum, and liver necrosis measured through liver biopsies. Due to the fast disease progression it is difficult to study, making animal models highly relevant. Several mouse models have been established based on surgical resection of the liver, pharmacological DILI induction, or immunogenic models of viral hepatitis [152]. Among the pharmacological

models, the most popular includes injection of an overdose of APAP, Thioacetamide (TAA), or d-galactosamine, with the main readouts being elevation of transaminase levels and liver histology. In humans, ALF develops over several days, whereas in mouse models this is shortened to several hours to a few days, which corresponds to their shorter lifespan and higher metabolic rate [152]. Interestingly, female mice have been shown to be less susceptible to APAP induced ALF with a faster recovery of GSH levels. Clinically on the other hand, more women are diagnosed with ALF than men, which does not necessarily present a contradiction to the biological findings in mice, but potentially confounding factors that are specific to the complexity of human life [153, 154].

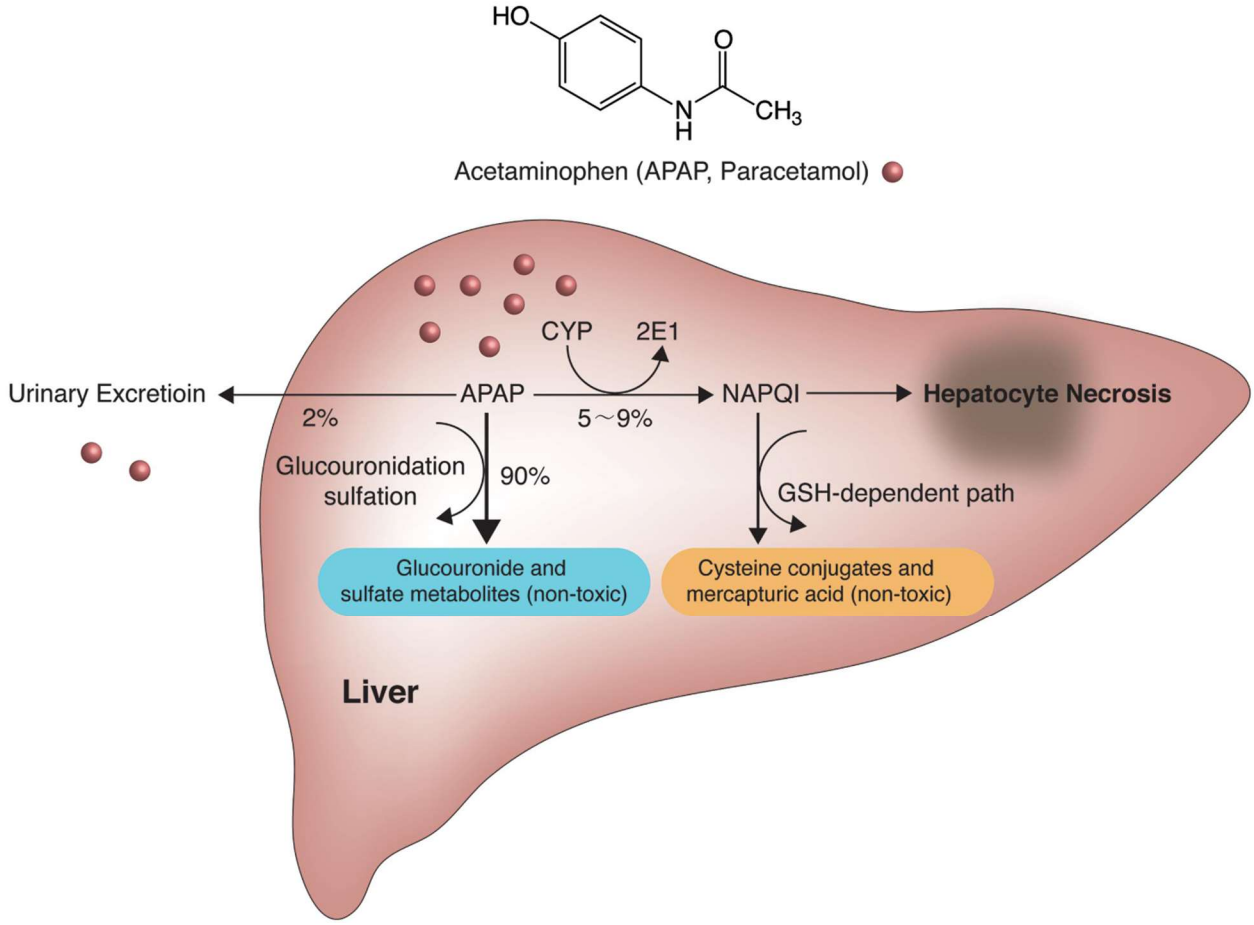

Figure 7: Liver metabolism of APAP. The majority of APAP undergoes detoxification via glucuronidation or sulfation, leading to secretion through the urine together with a small percentage that is secreted without further metabolization. 5-9 % is metabolized by CYP2E1 into the toxic NAPQI, which can cause hepatocyte necrosis if it is not detoxified by GSH. APAP overdose overwhelms the two detoxification mechanisms, resulting in massive hepatocyte cell death. APAP: Acetaminophen; CYP2E1: Cytochrome P450 E21; NAPQI: N-acetyl-p-benzoquinoneimine; GSH: glutathione. Adapted from [151].

4.4.2 The role of the microbiome in ALF

The gut-liver axis is connected through the portal vein, and the bile, which feedbacks to the intestine. Signals are modulated through immune-mediated antigens and metabolites, such as the well-known gut microbial metabolism of bile acids [6]. Acute liver failure has been associated with the microbiome through multiple studies, and coined the word “pharmacometabonomics”. In a human cohort, it was shown that the microbial metabolite *p*-cresol could compete with APAP for enzymatic sulfonation and be a urine indicator for APAP metabolism [155]. Additionally, patients that received proton pump inhibitors or ABX, which are known to cause intestinal dysbiosis, were more prone to ALF [156]. Nlrp6-/- mice as an intestinal dysbiosis model could confirm that APAP injection led to worse necrosis and higher ALT and AST levels. Further, the diurnal differences in APAP toxicity were reported to be microbiome-dependent, with APAP toxicity being worse at ZT12 than ZT0 only in SPF mice, while this was lost in GF or ABX-treated mice [157]. A later study confirmed this and pinpointed the effect to be solely dependent on one specific microbial metabolite, 1-phenyl-1,2-propanedione, which appeared to deplete GSH levels [158]. A single cell RNA sequencing study on the other hand, showed that the worsening of ALF with the microbiome was based on an interplay between damage-associated molecular patterns from the liver and MAMPS from the portal blood [159]. An increase in TLR and NOD agonists in the blood after ALF induction triggered TLR, MAPK, and MYC activation, which in turn activated a transcriptional program and increased monocyte infiltration, leading to more liver damage.

Several recent studies brought a more nuanced view by demonstrating the different roles of specific bacterial species. Interestingly, C57BL/6 mice from two different vendors that had the same genetic background but different microbiomes had varying susceptibilities to APAP [160]. Metabolomics of the portal serum detected differential levels of phenylpropionic acid that could alleviate APAP toxicity, however, it remained unclear which microbe produced it. In another study, *Lactobacillus vaginalis* could protect against APAP hepatotoxicity by liberating daidzein from the mouse diet and thus preventing ferroptosis [161]. Alternatively, *Bifidobacterium* could alleviate APAP toxicity, after oral magnesium supplementation, by increasing the production of indole-3-carboxylic acid, which inactivated CYP2E1 [162]. Further bacteria species have been associated with changes in susceptibility to ALF through various pathways, suggesting a potentially complex interplay that might be relevant for clinical purposes [163-165].

4.4.3 Fungi and ALF

To date, there are a few connections between fungi and ALF. It is well-known that mushroom poisoning, particularly of *Amanita* species can cause ALF, and that the patients are highly prone to deadly microbial infections, with fungal infections accounting for 32 % of the cases [166, 167]. However, intestinal fungi have not been the focus of much research, with one study showing that oral gavage with *S. cerevisiae* could alleviate APAP liver damage, which was hypothesized to be via detoxification of a bacterial metabolite [158]. Treatment of mice with the antifungal fluconazole worsened liver damage in a mouse model, although it remained unclear if this was a due to a protective effect by certain fungi species, changes in the bacterial community, or most likely, direct liver toxicity effects of the treatment by cytochrome P450 inhibition [168, 169].

Fungi and specifically *C. albicans* have been shown to have an influence on other liver diseases, such as for example alcohol-associated liver disease. Chronic ethanol exposure in mice increased the mycobiota population and the levels of β-glucan measured in the systemic circulation, which could signal via the C-type lectin-like receptor CLEC7A on Kupffer cells to exacerbate the disease [170]. Treatment with an antifungal reduced this effect in mice. ITS sequencing of a human cohort could reproduce the alcohol-mediated effects on the mycobiome, showing lower diversity and higher levels of *Candida* in the disease cohort [171]. On a mechanistic level, the exotoxin Candidalysin was shown to worsen the disease in a mechanism independent of CLEC7A, while additionally *C. albicans*-specific Th17 cells were increased in the circulation and liver and exacerbated the disease in a Kupffer cell-dependent way [172, 173]. Other liver diseases that have been associated with shifts in the mycobiome include Primary sclerosing cholangitis, liver fibrosis, and non-alcoholic fatty liver disease, highlighting the connection between liver and intestinal fungi [174-176].

4.5 Breast cancer

4.5.1 Breast cancer background & mouse models

The term breast cancer encompasses a heterogeneous group of malignancies originating from the mammary glands. The World Health Organization reported that 2.3 million women were diagnosed with breast cancer in 2022, and it was responsible for 670000 deaths globally [177]. On a molecular level, tumors can be categorized into three different subtypes based on their expression levels: Hormone receptor (HR) positive, epidermal growth factor 2 (ERBB2, formerly HER2) positive, or triple negative. HR positive tumors refer to the steroid hormone receptor and transcription factor estrogen receptor alpha (ERα), which triggers oncogenic signaling, or the closely related progesterone receptor (PR) [178]. ERBB2 is a transmembrane receptor tyrosine kinase that is overexpressed or amplified and regulates cell proliferation through several pathways. Triple negative breast cancer has no expression of ER, PR, or ERBB2, and is still poorly understood [179]. HR positive tumors can further be classified into Luminal A or Luminal B subtypes, with Luminal B cancers showing additional ERBB2 expression or having high levels of the proliferation marker Ki67 [179, 180]. All of the subtypes have a differing prevalence, prognosis, and therapy options some of them taking advantage of the molecular variations in a targeted way, making them quite distinct diseases [181].

Mouse models are commonly used for breast cancer research. Depending on the research question, different models can be applied to model different stages of tumorigenesis. In transplantable models, either a cell line or a patient-derived xenograft is transplanted. While the cell line cannot mimic the heterogeneity of tumors, it has the advantage that the tumors develop fast [182]. If a human cell line or a xenograft is transplanted, the mice require immune suppression, limiting the translatability. The transplantation could occur ectopically, facilitating tumor growth measurements over time. However, due to physiological positioning of the mammary glands, orthotopic transplantations are common, which have the benefit of providing the correct tumor microenvironment, and are conducted via injection into the mammary pad or intraductal injection [182, 183]. Carcinogen-induced breast cancer mouse models exist as well and can aid with the research on pathogenesis of breast cancer [184]. There are multiple genetically modified mouse models, which have the advantage of modeling more stages of tumorigenesis but take several months to develop. Typically they either express an oncogene under a site-specific promoter such as the mouse mammary tumor virus (MMTV) promotor, or contain conditional knock-outs of tumor suppressors [185]. However, most human breast cancers do not arise from hereditary mutations but rather spontaneous ones, which remains difficult to model.

The mouse model used in this study contains a human activated ERBB2 under the MMTV promoter on a FVB background, with tumors arising in hemizygous mice after a mean latency of 146 days that are histologically categorized as solid or nodular adenocarcinomas and molecularly resemble human luminal breast cancer [186].

4.5.2 The role of the microbiome in breast cancer

Shifts in the microbiome have been reported in breast cancer for both the gut and low-biomass tumor microbiome. Several studies detected microbial changes in the gut, in some studies according to clinical stages of the tumors, in others with differences also between pre- and post-menopausal women [187-190]. Additionally, breast tumors themselves were shown to have an intratumoral microbiome, for which breast tumors had the highest bacterial load and diversity compared to melanomas, pancreatic, ovarian, lung, brain, and bone tumors [191]. However, the accuracy of the analysis methods of this study remain contested to date [80].

On a mechanistic level, ABX-induced dysbiosis was demonstrated to increase the number of circulating tumor cells in a breast cancer mouse model and subsequent metastasis [192]. It has also been speculated that the capability of several intestinal bacteria species to deconjugate estrogens leading to their reabsorption into the circulation, could influence breast cancer progression, due to the estrogen-related cell proliferation effects [193]. Furthermore, colonization of the gut or the breast duct with *Bacteroides fragilis* species that have the ability to produce the enterotoxigenic BFT toxin was shown to enhance tumor growth and metastasis [194]. Intratumoral colonization with *Fusobacterium nucleatum* was similarly able to boost tumor growth and metastasis, in an immune-mediated way [195]. More recently, several bacteria species were demonstrated to invade tumor cells and promote metastasis by restructuring of the actin cytoskeleton in circulating tumor cells, and thus enhancing the ability of the cells to withstand mechanical stress [196].

4.5.3 Fungi in breast cancer

To date, not much is known about the influence of fungi on breast cancer onset and progression. Changes in fungal signals of the tumor microbiome have been reported to be distinct between cancer subtypes [197, 198]. Two studies profiled the tumor mycobiome across tumor types including breast cancer, both reporting the presence of a tumor mycobiome [76, 77]. One study found an enrichment in *Malassezia* species and *Yarrowia lipolytica* in breast tumors compared to other tumors [76]. The other study detected co-localization of fungal signals with cancer cells, as

well as more fungi-bacteria co-occurrences in breast tumors centered around the *Malassezia* and *Aspergillus* genus respectively [77]. Additionally, it showed the potential use of fungi as a biomarker for diagnosis, with increased levels of *M. globosa* associated with lower overall survival in breast cancer. These findings have been recently challenged, showing a strong contamination of the deposited genomes with human DNA, particularly for *M. globosa* and *C. albicans*, which might abolish some of the reported findings [80].

Mechanistic studies are largely missing so far and have mainly focused on infection models. Systemic infection with *C. albicans* could increase tumor growth in an ectopic breast cancer mouse model, which went along with an expansion of regulatory T cells in the tumor microenvironment [199]. Interestingly, invasive infection with *Aspergillus fumigatus* also enhanced tumor size in an ectopic model, which appeared to be dependent on regulatory T cell activation as well, and an increase of tissue inhibitor of metalloproteinase-1 levels in the serum that could impact metastasis [200].

Overall, the role of commensal fungi particularly in the gut is still unclear, meriting further studies.

5 Aims

While it is well known that fungi are an integral part of the microbiome, their role in interactions with the healthy host as well as under disease circumstances remains largely unclear. Therefore, the main aim of this dissertation was to characterize the interplay between commensal fungi species and their mammalian host. The focus was placed on five selected fungi species that are described above (4.2.2).

The purpose of this thesis can be separated into the following five main aims (**Figure 8**):

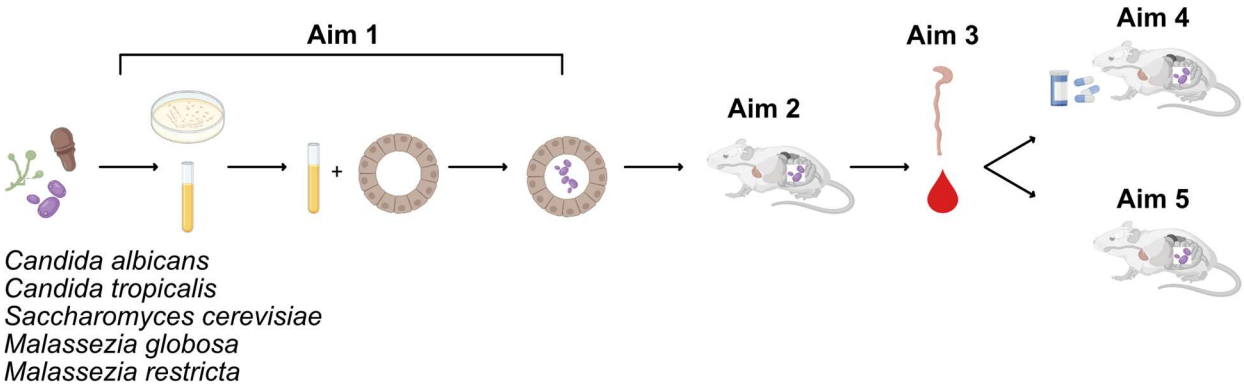

Figure 8: Graphical overview of the thesis aims. The five selected fungi species were evaluated regarding their interaction with a mammalian host. For this, different tools were developed, adjusted, and applied with an increasing level of complexity, starting with (Aim 1) in vitro cultures, to intestinal organoid exposures, the development of a live fungi coculture system. This was followed by the use of various mouse models to model commensalism in a healthy host by establishing intestinal colonization (Aim 2) and profiling the host intestinal mucosa transcriptome and serum metabolome (Aim 3), as well as characterizing the impact of fungi colonization in an acute liver failure model (Aim 4) and a breast cancer mouse model (Aim 5). Created with biorender.

Aim 1: Characterization of fungal growth in vitro and establishment of in vitro fungi-host epithelium interaction models

The first aim of my PhD thesis was to study the five selected commensal fungi in a reductionist way in vitro and to set up the necessary tools and methods in our lab. Specifically, this was separated into the following points:

- Evaluating fungal growth preferences in different media and oxygen atmospheres and profiling their respective metabolic outputs
- Testing the ability of fungal supernatants to change the growth of healthy and CRC-derived intestinal organoid lines or induce mutations
- Establishment of a live fungi-organoid coculture model over several days and determining effects on a transcriptional and functional level
- Investigating the application of the fungi-coculture model to study intracellular fungi

Aim 2: Establishment of long-term intestinal fungi colonization mouse models

Secondly, I determined under which circumstances different fungi species could maintain gut colonization over several weeks and optimized the methods to detect them, by:

- Optimizing DNA extraction, ITS sequencing, and metagenomic shotgun sequencing methods and analysis tools for highest fungal representation and accuracy
- Testing and improving colonization of the five selected fungi species in antibiotics-treated, germ-free, and isolator-housed mice

Aim 3: Profiling fungi-host interactions at the transcriptomic and metabolomic levels

To dissect the interplay between fungi and mammalian host under healthy steady-state conditions, I focused on two main points:

- The impact of sustained fungal colonization on the transcriptomic response of the host intestinal mucosa by RNA sequencing of two intestinal regions
- Metabolomics analysis of the host serum before and after liver metabolism to determine if fungal metabolites possess the ability to cross into the host circulation and to which extent this occurs

Aim 4: Investigating the influence of *C. albicans* gut colonization on an ALF mouse model

Applying the findings from above to a disease model that is related to the first-hit-organ, the liver, targeting the gut-liver axis and testing the effects on ALF severity using the APAP model, specifically:

- Determining the effects of gut colonization on liver damage
- Exploring the dependency of these effects on sex, T and B cells, and other microbial factors

Aim 5: Identifying the impact of *C. albicans* gut colonization on a breast cancer mouse model

Finally, I tested if fungal colonization can influence a disease that is physiologically distant from the intestine and has a long development period, through the following points:

- Evaluating the effects of intestinal *C. albicans* colonization on tumor growth as well as metastasis levels
- Defining the potential roles of interaction such as microbial translocation or metabolome changes

6 Materials and Methods

6.1 Fungi culture

The following fungi strains were used in this thesis (**Table 1**).

Table 1: Fungi strains

Species	CBS #	Vendor	Growth media
Candida albicans	8758	Westerdijk Fungal Biodiversity Institute	YPD, YM, Sabouraud
Candida albicans-RFP	-	Provided by Iliev lab, Weill Cornell Medicine	YPD, YM, Sabouraud
Candida tropicalis	94	ATCC	YPD, YM, Sabouraud
Saccharomyces cerevisiae	8803	Westerdijk Fungal Biodiversity Institute	YPD, YM, Sabouraud
Saccharomyces cerevisiae	2910	Westerdijk Fungal Biodiversity Institute	YPD, YM, Sabouraud
Malassezia globosa	7966	Westerdijk Fungal Biodiversity Institute	mDixon, MLNA
Malassezia restricta	7877	ATCC	mDixon, MLNA

The following fungi media were used in this thesis (**Table 2**).

Table 2: Fungi media

Name	Vendor	Medium protocol
YPD	Serva (#48507)	-
YM	NeoLab (M286-100G)	-
Sabouraud	Sigma Aldrich (#S3306)	-
mDixon	-	ATCC Medium 2693
MLNA	-	ATCC Medium 2737
CHROMagar/Sabouraud	BD (PA-254515.06)	-

Fungi were grown in the indicated medium supplemented with Chloramphenicol (50 µg/mL, VWR, ICNA0219032105) at 30 °C with 150 rpm shaking under aerobic conditions in an Innova 42 incubator (Eppendorf) or under anaerobic conditions in a Type B Vinyl anaerobic chamber (Coy

Lab Products). Liquid culture growth was assessed using an Ultrospec 10 Cell Density OD meter (biochrom). For supernatant derivation, fungi were grown in liquid culture for either 24 h under aerobic conditions or seven days under anaerobic conditions. Cultures were centrifuged at 1000 g for five minutes, supernatants were filtered under sterile conditions, aliquoted, and kept at -20 °C for further use. To generate the fungi mix for sequencing calibration, fungal cells were counted using a hemocytometer, and then mixed together at equal amounts.

For fungal growth with 4-way ABX exposure, metronidazole (1 g/L, LKT Laboratories Inc., M1977) was dissolved in MilliQ water (120 mL/1 L) with acetic acid added (0.2 mL/1L) and stirred for 30 min – 1 h. Ampicillin (1 g/L, Formedium, AMP25), neomycin (1 g/L, Sigma-Aldrich, N1876), and vancomycin (0.5 g/L, bioworld, 1404939) were added and topped up until the end volume with PBS or YPD medium.

6.2 Mouse models

6.2.1 Maintenance

The following mouse strains were used in this thesis (**Table 3**):

Table 3: Mouse strains

Strain	Microbiome	Supplier
C57BL/6	SPF	WIS: Harlan laboratories ENVIGO; DKFZ: Janvier
C57BL/6	GF	WIS GF facility
Swiss-Webster	GF	WIS GF facility
RAG1-/-	GF	WIS GF facility
FVB/N-Tg(MMTV-Erbb2*,-cre)1Mul/J	GF	JAX Stock No: 032576, WIS GF facility

Mouse experiments were approved by the respective authorities, the local institutional animal care and use committee for experiments at WIS or the Regierungspräsidium Karlsruhe for experiments at DKFZ (approval number G 81-21). Mice were housed in the animal facility under standard conditions (12 h light/dark cycle, 20-24 °C, 45-65 % humidity) with standard chow and water access ad libitum. GF mice were kept in sterile isolators or isocages.

6.2.2 Antibiotics treatment

The 4-way antibiotics cocktail was prepared as described above (6.1) and dissolved to the final volume with mouse drinking water. ABX were sterile filtered before administration. For experiments at DKFZ, mice were pre-treated with 4-way ABX for three to seven days, followed by pure Ampicillin (1 g/L) for the remainder of the experiment. For experiments at WIS, unless indicated otherwise, mice were pre-treated with 4-way ABX for five days and then maintained on 4-way ABX throughout the experiment.

6.2.3 Fungi colonization

C. albicans, *C. tropicalis*, and *S. cerevisiae* were grown in fresh YPD broth from an overnight culture until they reached an OD600 = 0.4-1 while *M. globosa* and *M. restricta* were grown for three days until the OD600 was reached. Cultures were centrifuged at 1000 g for 5 min and resuspended with 1X PBS to reach an inoculation dose of $5x10^7$ CFU/mL. 7-9 week old mice received 200 µL of the fresh fungal suspension or PBS as a control via oral gavage for three days in a row, unless otherwise indicated. For colonization inside an isolator, the same fungal suspension was used for all three doses.

Colonization was monitored by stool collection, the stool pellets of which were weighted, resuspended in 1 mL 1X PBS, and homogenized with a TissueLyser II (Qiagen, 85300) and one X50 Nucleospin bead Type G (Fisher Scientific, 15824044). The fecal suspension was serially diluted with 1X PBS, plated on YPD plates with chloramphenicol in a serial dilution, and incubated a 30 °C overnight. CFU counts the next day were normalized to the plating volume and fecal pellet weight.

6.2.4 Fecal microbiota transplantation

Stool pellets collected from SPF mice or ABX-treated SPF mice as indicated were transferred into a Type B Vinyl anaerobic chamber (Coy Lab Products), homogenized with 900 µL 1X PBS/fecal pellet, settled by gravity, and the supernatant was separated into aliquots for direct oral gavage or stored at -80 °C. Mice received 200 µL of the fecal slurry by oral gavage.

6.2.5 APAP model

To induce ALF, eight-week-old mice were intraperitoneally injected with Acetaminophen (APAP, Sigma-Aldrich, A5000) dissolved in PBS 1X at a dose of either 500 mg/kg body mass or 300 mg/kg body mass as indicated. If indicated, mice were fasted for 6 h with free access to water before injection. All injections were executed between 13:00 and 15:00 to avoid known circadian effects. Mice were sacrificed 20 h after the injection.

6.2.6 Blood and tissue collection

Mice were anesthetized with ketamine (100 mg/kg) and xylazine (10 mg/kg) by intraperitoneal injection and blood was collected from the portal vein and/or systemically by cardiac puncture or retroorbital bleeding. Organs were collected accordingly depending on the experimental setting, and included lung, liver, kidney, adrenal gland, heart, mesenteric lymph nodes (MLN), duodenum, jejunum, ileum, colon, and were collected in this order to avoid contaminations. If breast tumors were present, they were excised, measured with a caliper, counted, and weighted. Tumor volume was calculated with the following formula: Tumor volume = Tumor length x tumor width^2 x 0.5. Total tumor volume or weight is the sum of the volume or weight of tumors found in the mouse.

6.2.7 Serum enzymes

Serum alanine aminotransferase (COBAS C 111 ALT, Roche, 04718569190), aspartate aminotransferase (COBAS C 111 AST, Roche, 04657543190), gamma-glutamyl transferase 2 (COBAS C 111 GGT2, Roche, 05401461190), and bilirubin total gen. 3 (COBAS C 111 BILT3, Roche, 0579564819) level activity was measured with a Cobas 111 Serum analyzer (Roche), samples were diluted in MilliQ water 1:15 or higher if necessary.

6.2.8 Histology

Lung or the left lobe liver samples were fixed in 4 % formaldehyde overnight, and processed by the Weizmann Institute of Science Histology Unit. Briefly, samples were transferred to 70 % EtOH, embedded in paraffin blocks, and subsequently sectioned and stained with Hematoxylin/eosin (H&E). The slides were blindly scored by Alon Harmelin, veterinary pathologist. Liver samples were scored for hemorrhage and necrosis from 0 (healthy) to 5 (severe liver damage), and lung samples for the presence of metastasis (yes/no).

6.3 Organoid culture

6.3.1 Maintenance

The following organoid lines were used in this thesis (**Table 4**).

Table 4: Organoid lines

Organoid line	Origin	Tissue specifications	Provided by
T41	Colon	Tumor	EMIL/JP
72	Duodenum	Healthy	EMIL/JP
CJ wt	Colon	Healthy (wildtype)	EMIL/JP
CJ P	Colon	Healthy with CRISPR-induced p53 mutation	EMIL/JP
CJ KAPS	Colon	Healthy with CRISPR-induced Kras, APC, p53, and Smad4 mutations	EMIL/JP
CJ KAPS green	Colon	Healthy with CRISPR-induced Kras, APC, p53, and Smad4 mutations with genetically-labelled Emerald GFP nucleus stain	EMIL/JP
EL11T	Colon	Tumor	EMIL/JP
EL11M	Liver	Metastasis from colon tumor	EMIL/JP

Table 5: Organoid (hC) medium composition

Reagent	End concentration	Source	Identifier
Advanced DMEM/F12		Thermo Fisher Scientific	12634-010
HEPES	1 %	Thermo Fisher Scientific	15630080
Glutamax	1 %	Thermo Fisher Scientific	35050061
R-spondin conditioned medium	2 %	U-Protein Express	Custom order
Noggin UPE	1 %	U-Protein Express	Custom order
B27 without Vitamin A	1 x	Thermo Fisher Scientific	12587010
N-Acetyl-L-cysteine	1.25 mM	Sigma-Aldrich	A9165
Nicotinamide	10 mM	Sigma-Aldrich	N0636
Human EGF	50 ng/mL	Peprotech	AF-100-15
A83-01	0.5 mM	Tocris	2939
SB202190	10 µM	Sigma-Aldrich	S7076
Prostaglandin E2	1 µM	Tocris	2296
Wnt surrogate	0.5 nM	U-Protein Express	Custom order
Primocin	100 µg/mL	Invivogen	ant-pm-2

Organoids kindly provided by Dr. Jens Puschhof (EMIL/JP, Ethics protocol 2012-293N-MA) were thawed from cryostocks by quickly warming them up in a water bath at 37 °C, and then slowly adding cold Dulbecco's Modified Eagle Medium (DMEM, Thermo Fisher Scientific, 41965039). Organoids were centrifuged at 500 g for 3 min at 4 °C, supernatant was removed, and the organoids resuspended in ice cold Cultrex Basement Membrane Extract (BME, Growth Factor Reduced, Type 2, R&D Systems, Bio-Techne, 3533-001-02) with cold DMEM at a ratio of 4:1. The suspension was seeded as 10 µL domes in low adhesion plates, solidified upside down for ~30 min at 37 °C, then pre-warmed human colon (hC) medium (**Table 5**) was added to each well. Depending on the organoid line, medium was exchanged every three days and organoids were maintained by mechanical splitting every one to two weeks. In order to do so, medium was aspirated and organoids were resuspended in cold DMEM and centrifuged at 500 g for 3 min at 4 °C. Supernatant was removed and organoids mechanically sheared by forceful pipetting putting

a p10 tip on top of a p1000 tip in 1 mL DMEM. Organoids were topped up with DMEM and centrifuged at the same speed again. The supernatant was discarded and organoids plated as described before at a splitting ratio of 1:2 to 1:4 depending on the organoid line.

To generate single cells for homogeneous seeding or Flow cytometry analysis, organoids were harvested using cold DMEM and dissociated into single cells using TryplE (Thermo Fisher scientific, 12605010) at 37 °C for 7-15 min, supplemented with 10 µM Rho kinase inhibitor (Y-27632 dihydrochloride, Abmole, M1817). The reaction was stopped by adding cold DMEM, cells were centrifuged at 500 g for 5 min at 4 °C.

Organoids were stored for long-term storage in cryovials, by adding freezing medium (80 % DMEM, 10 % Fetal Bovine Serum, 10 % Dimethylsulfoxide) slowly to the organoids and storing them in a Mr. Frosty at -80 °C, before transferring them to liquid nitrogen after 24 h.

6.3.2 Fungi supernatant exposure

Fungi supernatants were derived as described above. For organoid exposure, pH was adjusted to pH 7 using a pH-meter (Mettler Toledo) if necessary, and the supernatants sterile filtered again.

6.3.3 Microinjection

Organoids were cultured without ABX overnight before injection to detect potential contamination. Fungi were grown until OD600 = 0.4, 2 mL of the culture was washed with 1X PBS and resuspended in 200 µL 1X Fast green injection dye (Sigma-Aldrich, F7252). Heat-killed fungi were inactivated by heating them to 99 °C for 5 min. To stain fungi with a fluorescent dye, fungi cells were washed twice with 1X PBS, incubate for 45 min at 37 °C with 20 µM eBiosciences Cell Proliferation Dye eFluor 450 (Thermo Scientific, 65084285) in 1X PBS. Afterwards, the fungi cells were washed twice with 1X PBS and mixed with injection dye. Microinjection was executed by loading glass needles with 10 µL of the fungal suspension using Microloader tips (Sigma-Aldrich, EP5242956003), and injecting with the FemtoJet 4i microinjector (Eppendorf, 5252 000.013). After injection, organoid medium was changed to fresh hC medium with or without the indicated concentration of amphotericin B (Sigma-Aldrich, A9528) and gentamycin (5 µg/mL, Sigma-Adrich, G1397).

To quantify fungal survival inside the organoids, one dome of organoids was harvested in 1 mL cold DMEM, and centrifuged at 500 g for 3 min at 4 °C. The organoid pellet was resuspended in 200 µL DMEM with 0.5 % saponin, and incubated at room temperature for 10 min to lyse the organoid cells. Following that, the sample was centrifuged at 500 g for 3 min at 4 °C, resuspended

in 100 µL YPD, and plated in serial dilution on YPD plates, followed by overnight incubation at 30 °C.

To measure single cell outgrowth, organoids were harvested in cold DMEM after overnight fungi-organoid coculture as described above, and incubated with DMEM with primocin at 500 µg/mL. for 20 min at room temperature to kill any remaining fungi. Following that, organoids were dissociated to single cells and cultured as described above with Rho kinase inhibitor.

6.3.4 Transmission Electron Microscopy (TEM)

For TEM, the fungi-microinjected organoids were mechanically dissected with a spatula following overnight coculture, and embedded in Epoxy-resin according to standard procedures by the Electron Microscopy Core Facility at DKFZ. This included primary fixation in buffered aldehyde (4 % Formaldehyde, 2 % Glutaraldehyde, 1 mM $CaCl_2$, 1 mM $MgCl_2$ in 40 mM cacodylate-buffer, pH 7.1), post-fixation in buffered 1 % osmium tetroxide and en-block staining in 1 % uranyl acetate. Following dehydration in graded steps of ethanol, samples were embedded in Epoxide (Glycidether, NMA, DDSA: Serva). From the polymerized Epon-blocs, ultrathin sections were prepared at nominal thickness 50 nm (UCT, Leica), contrast-stained with lead-citrate and Uranylacetate, and observed in a Zeiss EM 910 at 80kV (Carl Zeiss). Micrographs were taken using a slow scan CCD camera (TRS).

6.3.5 Microscopy

Organoids were imaged live with the Eclipse i2-U light/fluorescence microscope (Nikon), Durchlichtmikroskop OBL137 trinokular microscope (Kern), or EVOS M7000 Imaging System (Invitrogen, Thermo Fisher) using the magnifications indicated. For confocal microscopy, organoids were fixed with 4 % formaldehyde for 30 - 60 min at room temperature. Organoids were washed with washing buffer (1X PBS, 0.1 % Triton X 100) three times, resuspended in blocking buffer (1X PBS, 0.2 % BSA) for 1 h at room temperature, and incubated overnight with 1:500 rabbit anti-*C. albicans* primary antibody (Abcam, AB-ab53891) at 4 °C. Subsequently, organoids were washed thrice with washing buffer, and incubated with 1:1000 donkey anti-rabbit Alexa Fluor 647-conjugated antibody (Invitrogen, A31573) for 2 h at room temperature. Organoids were washed three more times with washing buffer, transferred in 1X PBS to a black glass bottom plate, and imaged with the Olympus FluoView FV1000 confocal microscope (Olympus Life Science, Evident).

6.3.6 Cell Titer Glo Assay

To quantify total organoid mass by proxy of ATP content, organoids were dissociated into single cells as described above and cells were counted using the Vi Cell XR Counter (Beckman Coulter).

Cells were then seeded at a concentration of ~4000 to 10000 cells/well depending on the cell line with great care being taken to keep the mixture homogeneous by regular mixing through pipetting up and down. After solidification, medium supplemented with Rho kinase inhibitor was added together with the fungal supernatants at various dilutions. Organoids were cultured for eleven to twelve days with a medium change after one week. Cell Titer Glo Assay (Promega, G7571) was used according to manufacturer's instructions. Briefly, plates and reagents were equilibrated to room temperature for 30 min, the medium was aspirated and 100 µL Cell Titer Glo reagent was added to each well and the BME dome solubilized by pipetting. The solution was transferred to a black assay 96 well plate (costar, 137101), kept on a shaker in the dark for 30 min and then luminescence was recorded on a FLUOstar Omega plate reader (BMG Labtech) adjusting the settings so that the measurements would be in the medium range. Empty wells with just the reagent were used as a negative control and subtracted from all the values.

6.3.7 FACS and ImageStream

Organoids were dissociated into single cells as described above. Cells were fixed using the BD Cytofix/Cytoperm kit (BD, 554714) at manufacturer's instructions. Briefly, cells were resuspended in 900 µL Perm/Fix solution and incubated for 20 min at 4 °C. Afterwards, cells were washed twice with 1 mL Wash/Perm buffer, resuspended in 200 µL Wash/Perm buffer with Alexa Fluor 488 anti-yH2AX Phospho (Ser139) antibody (1:40) (BioLegend, 613406) and incubated in the dark for 30 min at 4 °C. Cells were washed again two times with 1 mL Wash/Perm buffer, resuspended in 200 µL PBS and filtered through a Cell Strainer into Falcon 5 mL Round Bottom Polystyrene Test Tubes (NeoLab, 352235). Samples were analyzed with a FACSymphony A3 machine (BD Biosciences). Subsequent analysis was performed with FlowJo version 10.7.1 (BD Biosciences).

For ImageStream analysis, organoids were additionally stained with anti-*C. albicans* FITC antibody (Abcam, ab21164) after single cell dissociation at 1:200 in DMEM with Rho kinase inhibitor supplementation for 45 min in the dark. Afterwards, cells were fixed and as described above, and analyzed at the DKFZ FACS core facility with an ImageStream X Mark II machine (Amnis, Cytek Biosciences) at 40x with the channels Brightfield, FITC, and RFP. Data was analyzed with IDEAS Image Analysis software (Amnis, Cytek Biosciences) and gated based on cells, focused cells, FITC, and RFP.

6.4 Sequencing

6.4.1 RNA sequencing

6.4.1.1 RNA extraction

Organoids were collected in RLT buffer and subsequently extracted using the RNeasy Mini kit (Qiagen, 74104). Tissues were collected in RNAlater (Rhenium, am7021), and stored at -80 °C until extraction using the RNeasy Mini kit. DNA depletion was performed using the RNase-free DNase Set (Qiagen, 79256) according to manufacturer's instructions. RNA concentration was determined using a Nanodrop One (Thermo Scientific) or Qubit RNA HS or BR Assay kit (Thermo Fisher Scientific, Q32855 and Q10211).

6.4.1.2 Quantitative PCR (qPCR)

The following qPCR primers were used in this thesis (**Table 6**).

Table 6: qPCR primer

Name	Sequence (5`-3`)	Type	Vendor	Source
C. albicans fw	GGGTTTGCTTGAAAGACGGTA	Taqman	Thermo Scientific	[201]
C. albicans rv	TTGAAGATATACGTGGTGGACGTTA			
C. albicans probe	ACCTAAGCCATTGTCAAAGCGATCCCG			
M. globosa fw	GGCCAAGCGCGCTCT	Taqman	Thermo Scientific	[202]
M. globosa rv	CCACAACCAAATGCTCTCCTACAG			
M. globosa probe	ATCATCAGGCATAGCATG			
M. restricta fw	GGCGGCCAAGCAGTGTTT	Taqman	Thermo Scientific	[202]
M. restricta rv	AACCAAACATTCCTCCTTTAGGTGA			
M. restricta probe	TTCTCCTGGCATGGCAT			
16S fw	ACTCCTACGGGAGGCAGCAGT	SybrGreen		[203]

16S rv	ATTACC GCGGCTGCTGGC		Sigma-Aldrich	
18S fw	ATTGGAGGGCAAGTCTGGTG	SybrGreen	Sigma-Aldrich	[203]
18S rv	CCGATCCCTAGTCGGCATAG			
ITS fw	CTTGGTCATTTAGAGGAAGTAA	SybrGreen	Sigma-Aldrich	[203]
ITS rv	GCTGCGTTCTTCATCGATGC			
GAPDH fw	ACAACTTTGGTATCGTGGAAGG	SybrGreen	Sigma-Aldrich	Harvard primer bank 378404907c2
GAPDH rv	GCCATCACGCCACAGTTTC			
FN 1 fw	CGGTGGCTGTCAGTCAAAG	SybrGreen	Sigma-Aldrich	Harvard primer bank 47132556c1
FN 1 rv	AAACCTCGGCTTCCTCCATAA			
CDKN2A fw	GATCCAGGTGGGTAGAAGGTC	SybrGreen	Sigma-Aldrich	Harvard primer bank 17738298a1
CDKN2A rv	CCCCTGCAAACTTCGTCCT			
SMAD6 fw	CCTCCCTACTCTCGGCTGTC	SybrGreen	Sigma-Aldrich	Harvard primer bank 236465444c1
SMAD6 rv	GGTAGCCTCCGTTTCAGTGTA			
TP53 fw	CAGCACATGACGGAGGTTGT	SybrGreen	Sigma-Aldrich	Harvard primer bank 371502118c1
TP53 rv	TCATCCAAATACTCCACACGC			
SAGE1 fw	TGGCCTGATGCTACCATCG	SybrGreen	Sigma-Aldrich	Harvard primer bank 145580596c2
SAGE1 rv	AGACTTTGTCAGTTCGAGATTGG			
PTK2B fw	CCCCTGAGTCGAGTAAAGTTGG	SybrGreen	Sigma-Aldrich	Harvard primer bank 325651912c1
PTK2B rv	GATACGCACGTCCTCCTTTTC			
BMP15 fw	TGTGAACTCGTGCTTTTCATGG	SybrGreen	Sigma-Aldrich	Harvard primer bank 257743453c1
BMP15 rv	CTCAATCAGGGGCAAAGTAGG			

qPCRs using Taqman were prepared using the Applied Biosystems TaqMan Fast Advanced Master Mix (Thermo Scientific, 4444963) and Custom TaqMan Gene Expression Assay (Thermo

Scientific, 4331348) and run according to manufacturer's protocol on an Applied biosystems QuantStudio 7 Flex qPCR machine (Thermo Fisher Scientific).

Reverse transcription was performed with a High-Capacity cDNA Reverse Transcription Kit (Thermo Fisher Scientific, 4368814) according to manufacturer's protocol on a Mastercycler nexus GSX1 (Eppendorf).

qPCR using SybrGreen was performed using Applied Biosystems PowerUp SYBR Green Master Mix (Thermo Fisher Scientific, A25776) according to manufacturer's instructions on a applied biosystems QuantStudio 7 Flex qPCR machine (Thermo Fisher Scientific).

6.4.1.3 RNA sequencing library preparation and analysis

RNA sequencing libraries were prepared as in Zmora et al. [204]. Libraries (2 pM) were sequenced on a NextSeq 2000 (Illumina). Raw files were converted to FASTQ file with bcl2fastq software (Illumina, v2.20.0.422), filtered with Fastp with default parameters [205], and reads were aligned with Gencode annotation (GRCm38p6) and STAR (v2.7.11a) [206]. For subsequent analysis DESeq2 (v1.40.2) was applied with default parameters [207]. Enrichment analysis was performed with fgsea (v1.26.0), and Venn diagrams were generated with https://bioinformatics.psb.ugent.be/webtools/Venn/.

6.4.2 Metagenomic sequencing

6.4.2.1 DNA extraction

DNA of stool samples or the Zymobiomics Microbial Community Standard (Zymo Research, D6300) was performed with the DNeasy PowerSoil Pro Kit (Qiagen, 47014), Invitrogen PureLink Microbiome DNA Purification kit (A29789), or QIAmp Fast DNA Tissue Kit (Qiagen, 51404) according to manufacturer's protocol with or without the mentioned adjustments. For lyticase treatment, samples were mixed with lyticase (Sigma-Aldrich, SAE0098) at 200U/reaction in 500 µL 1X PBS, and incubated at 30 °C for 30 min. After centrifugation for 2 min at 15000 g, the pellet was further processed for DNA extraction as described above. DNA concentrations were measured with dsDNA HS or BR Assay Kit (Thermo Fisher Scientific, Q33231 or Q32853).

6.4.2.2 ITS sequencing

The following primers were used for the ITS region in ITS sequencing (**Table 7**).

Table 7: ITS region primers for sequencing from Illumina

Name	Sequence Adaptor + Primer (5`-3`)
ITS fw 1	TCGTCGGCAGCGTCAGATGTGTATAAGAGACAGCTTGGTCATTTAGAGGAAGTAA
ITS fw 2	TCGTCGGCAGCGTCAGATGTGTATAAGAGACAGCTCGGTCATTTAGAGGAAGTAA
ITS fw 3	TCGTCGGCAGCGTCAGATGTGTATAAGAGACAGCTTGGTCATTTAGAGGAACTAA
ITS fw 4	TCGTCGGCAGCGTCAGATGTGTATAAGAGACAGCCCGGTCATTTAGAGGAAGTAA
ITS fw 5	TCGTCGGCAGCGTCAGATGTGTATAAGAGACAGCTAGGCTATTTAGAGGAAGTAA
ITS fw 6	TCGTCGGCAGCGTCAGATGTGTATAAGAGACAGCTTAGTTATTTAGAGGAAGTAA
ITS fw 7	TCGTCGGCAGCGTCAGATGTGTATAAGAGACAGCTACGTCATTTAGAGGAAGTAA
ITS fw 8	TCGTCGGCAGCGTCAGATGTGTATAAGAGACAGCTTGGTCATTTAGAGGTCGTAA
ITS rv 1	GTCTCGTGGGCTCGGAGATGTGTATAAGAGACAGGCTGCGTTCTTCATCGATGC
ITS rv 2	GTCTCGTGGGCTCGGAGATGTGTATAAGAGACAGGCTGCGTTCTTCATCGATGG
ITS rv 3	GTCTCGTGGGCTCGGAGATGTGTATAAGAGACAGGCTACGTTCTTCATCGATGC
ITS rv 4	GTCTCGTGGGCTCGGAGATGTGTATAAGAGACAGGCTGCGTTCTTCATCGATGT
ITS rv 5	GTCTCGTGGGCTCGGAGATGTGTATAAGAGACAGACTGTGTTCTTCATCGATGT
ITS rv 6	GTCTCGTGGGCTCGGAGATGTGTATAAGAGACAGGCTGCGTTCTTCATCGTTGC
ITS rv 7	GTCTCGTGGGCTCGGAGATGTGTATAAGAGACAGGCGTTCTTCATCGATGC

For ITS sequencing, libraries were prepared according to the Illumina protocol (Illumina, Document #1000000064949v01) with the primer mix mentioned above and a DNA starting concentration of 5 ng/µL according to manufacturer's recommendations and accordingly scaled volumes. Final libraries were compiled by diluting libraries to 10 nM and mixing at equal amounts, libraries were sequenced on a MiSeq (Illumina). Demultiplexing to FASTQ files was done with bcl2fastq Conversion Software (Illumina) based on their associated IDT barcode sequence. Analysis was performed using QIIME2 v2021.2 [208], ITSxpress [209], and Dada2 [210] with default parameters.

6.4.2.3 Shotgun sequencing

For Shotgun sequencing, libraries were prepared using the Nextera XT DNA Library Preparation Kit (Illumina, FC-131-1096) according to manufacturer's protocol. Final libraries were compiled by diluting libraries to 10 nM and mixing at equal amounts, libraries were sequenced on a NextSeq

2000 (Illumina) at a read depth of 10 million reads/sample for pure strains and 40 million reads/sample for stool samples. Demultiplexing to FASTQ files was done with bcl2fastq Conversion Software (Illumina) based on their associated IDT barcode sequence. Human or mouse reads were removed with KneadData v0.1.4 (https://github.com/biobakery/kneaddata), and subsequent analysis performed with HUManN3 [211], or Kraken2 [212] and Bracken [213].

6.5 Metabolomics

6.5.1 Untargeted metabolomics and metabolic profiling

Polar metabolite analysis and extraction was performed by the WIS Metabolomics Facility, following a protocol previously outlined [214], with slight adaptations: Serum samples (100 µL) were mixed with 1 mL of a homogenous mix of pre-cooled (-20 °C) methanol (MetOH):methyl-tert-butyl-ether (MTBE) 1:3 (v/v) and subjected to vortexing and sonication for 30 min in an ice-cold sonication bath. Subsequently, a solution of UPLC-grade water and methanol (3:1, v/v) (0.5 ml) containing the internal standards (^{13}C- and ^{15}N-labeled amino acids standard mix, Sigma-Aldrich, 767964) was added to the samples, which was followed by centrifugation. The upper organic phase was transferred to a 2 ml Eppendorf tube. The polar phase underwent reextraction with 0.5 ml of MTBE following the same procedure. The combined organic phases were dried using a speedvac and then stored at -80°C. The lower polar phase, intended for polar metabolite analysis, was lyophilized, dissolved in 150 µL of a 1:1 solution of UPLC-grade water and methanol (v/v), and centrifuged at 20000 g for 5 minutes. The supernatant was transferred to a new tube, centrifuged again, and 80 µL was transferred into HPLC vials for subsequent analysis.

Metabolic profiling of the polar phase was conducted as described previously [215], with minor modifications. Briefly, analysis was performed using an Acquity I class UPLC System combined with mass spectrometer Q Exactive Plus Orbitrap™ (Thermo Fisher Scientific) operated in a negative ionization mode. The LC separation was performed using the SeQuant Zic-pHilic (150 × 2.1 mm) with the SeQuant guard column (20 × 2.1 mm, Merck). The mobile phase B consisted of acetonitrile, the mobile phase A consisted of acetonitrile and 20 mM ammonium carbonate with 0.1 % ammonium hydroxide in DDW:acetonitrile (80:20, v/v), respectively. The flow rate was set at 200 µL/min, and the gradient profile was as follows: 0-2 min 75 % of B, 14 min 25 % of B, 18 min 25 % of B, 19 min 75 % of B, for 4 min. Data processing was performed using TraceFinder (Thermo Fisher Scientific). Compounds were identified based on accurate mass, retention time, isotope pattern, and fragments, and verification was conducted using an in-house generated mass

spectra library. Peaks were quantified by calculating the area under the curve (AUC) and then normalized against the AUC values of internal standards and original sample volume.

Further analysis was performed using MetaboAnalyst 6.0 [216] with sample normalization by median, data transformation by log transformation (base 10), and no further data scaling or filtering.

6.5.2 Targeted metabolomics

Targeted metabolomics was performed by the WIS Metabolomics Facility.

Analysis of indole-3-propionic acid and daidzein

Sample preparation

Serum (50 uL) was incubated with indole-3-propionic-2,2-d2 acid (10 uL of 1 ug/mL in 20 %-aqueous methanol) as internal standard (IS; C.D.N. Isotopes) for 2 min. Methanol (250 uL) was added, and the mixture was incubated in a shaker (Thermomix C, Eppendorf, 2000 rpm, 23 °C, 10 min), then centrifuged (14000 g, 5 min). The obtained supernatant was collected and dried in a speedvac, then in a lyophilizer. The residue was dissolved in a mixture of methanol (10 uL) and water (40 uL), followed by centrifugation (21000 g, 5 min) to remove insoluble material. The soluble fraction was then transferred into an insert of a LC-MS vial for injection.

LC–MS/MS analysis

For LC–MS/MS analysis, samples were analyzed using an Acquity I-class UPLC system (Waters) and Xevo TQ-S triple quadrupole mass spectrometer (Waters), equipped with an electrospray ion source and operated in positive ion mode. MassLynx and TargetLynx software (v.4.1, Waters) were employed for data acquisition and analysis. Chromatographic separation was carried out on a BEH C18AX column (100 × 2.1 mm, 1.7-µm Atlantis Premier, Waters) using mobile phase A (20 mM ammonium formate, pH 3.0) and phase B (acetonitrile) at a flow rate of 0.3 mL/min and a column temperature of 25 °C. The gradient profile was as follows: initially the column was held at 20 % B for 0–0.5 min, followed by a linear increase to 90 % B over 0.5–6 min, holding at 90 % B for 6–6.5 min, returning to 20 % B for 6.5–7 min, and equilibrating at 20 % B for 2 min. Samples maintained 8 °C were automatically injected in a volume of 1 µL. For mass spectrometry (MS), argon was utilized as the collision gas with a flow rate of 0.20 mL/min. The capillary voltage was set at 1.00 kV, with a source temperature of 150 °C, desolvation temperature of 550 °C, cone gas flow at 200 L/h and desolvation gas flow at 1100 L/h. Concentration was determined using standard curves spanning concentration from 0–10 µg/mL of the two compounds. Analytes were detected in positive mode using multiple-reaction monitoring (MRM) transitions (collision energy,

eV): 190.0>55.0 (17), 190.0>130.1 (12), 190.0>172.1 (9) for indole-3-propionic acid, 255.0>137.0 (20), 255.0>227.0 (20) for daidzein, and 192.1>56.0 (12), 192.1>130.1 (14), 190>174.1 (14) for IS.

Analysis of hydroquinone

Sample preparation

Serum (5 uL) was incubated with hydroquinone bis(2-hydroxyethyl) ether (5 uL of 20 ug/mL in methanol) as internal standard (IS, Merck) for 2 min. Then, a mixture of ethyl acetate – isobutanol – isopropanol was added (60:30:13, 100 uL) and incubated in a shaker (Thermomix C, Eppendorf, 1200 rpm, 30 °C, 10 min), then centrifuged (21000 g, 10 min). The obtained supernatant was collected and dried in a speedvac, then in a lyophilizer. The residue was derivatized with acetonitrile (50 uL) and N-Methyl-N-(trimethylsilyl)trifluoroacetamide (MSTFA, 50 uL), and placed in an insert of GC-MS vial for injection.

GC–MS analysis

The GC-MS system utilized for analysis included an Agilent 7890A gas chromatograph equipped with a split/splitless injector, coupled with a LECO Pegasus HT Time-of-Flight Mass Spectrometer (TOFMS). GC was conducted on a 30 m × 0.25 mm × 0.25 µm Rxi-5Sil MS column (Restek). Samples were analyzed under splitless mode conditions; with injector and transfer line temperatures set at 250 °C. Analytes, introduced by a 1 µL injection, underwent separation using the following chromatographic parameters: Helium served as the carrier gas at a flow rate of 1.0 mL/min. The thermal gradient initiated at 170 °C, maintained for 1 min, followed by a ramp to 300 °C at a rate of 30 °C/min and held at 300 °C for 3.0 min. Eluents were fragmented in the electron impact mode at an ionization voltage of 70 eV. MS analysis covered a mass range of 50-500 m/z at an acquisition rate of 20 spectra per second. The ion source chamber operated at 250 °C, while the detector voltage was set to 1650 V. Hydroquinone concentration was calculated using standard curve, ranging from 0.01–0.25 µg ml−1. Analytes were detected using characteristic masses 239+254 m/z for hydroquinone and 239+254+342 m/z for hydroquinone bis(2-hydroxyethyl) ether.

6.5.3 Data visualization and statistical analysis

Unless otherwise stated, data was analyzed and visualized with GraphPad Prism v9.0.2.

7 Results

7.1 Chapter 1: In vitro characterization of commensal fungi species

7.1.1 Going solo: Fungi cultures on their own

7.1.1.1 Establishing fungi culture growth in vitro

As a first step, and in order to increase the chances for successful growth, I attempted to grow the selected fungi using different media according to the suppliers' indications. As a result, I was successfully able to grow them all, observing species-dependent differences in growth rates, preferred medium, and morphology (**Figure 9**).

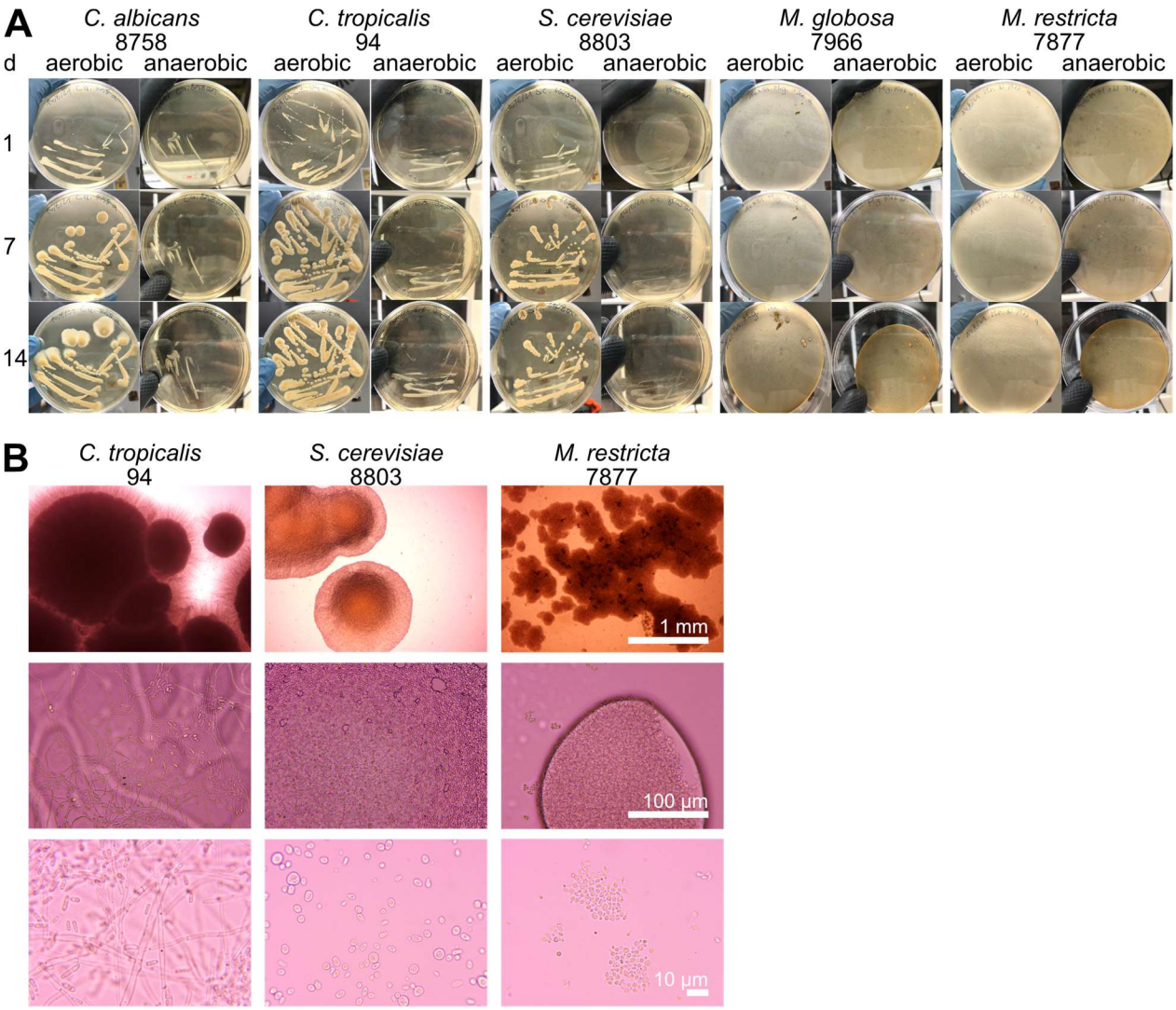

Figure 9: Fungi growth in vitro. A) Representative agar plate images showing the growth of five fungi strains over time, under aerobic or anaerobic conditions. *C. albicans*, *C. tropicalis* and *S. cerevisiae* grown on YPD agar, *M. globosa* and *M. restricta* on MLNA. **B)** Representative bright field microscopy images of fungi strains in different magnifications. d: day; YPD: yeast extract peptone dextrose; MLNA: modified Leeming and Notman agar.

Colony size varied across species. While *C. albicans*, *C. tropicalis* and *S. cerevisiae* displayed similar sized, creamy colonies on all agar types (YPD, YM and Sabouraud medium) (**Figure 9A-B**). *M. globosa* and *M. restricta* formed clusters that did not allow distinction of colonies and could only be grown on dedicated agar types rich in fatty acids (mDixon and MLNA) (**Figure 9A-B**). As the intestinal tract, particularly the colon, contains lower levels of oxygen, I cultured the fungi under anaerobic conditions using an anaerobic chamber [217]. Even though anaerobic conditions decreased growth rates, all species were still able to grow (**Figure 9A**).

The *Candida* species grew in single yeast cell morphology as well as multicellular hyphae and pseudohyphae shapes, depending on the growth medium used, while *S. cerevisiae* displayed the classical yeast-cell shape, and the yeast cell size was smallest for the *Malassezia* species (**Figure 9B**).

By comparing the growth rates using OD measurements of liquid cultures of the different fungi species across various growth media, I could observe that *C. tropicalis* showed the fastest growth, followed by *C. albicans*, and *S. cerevisiae*, in YPD medium (**Figure 10A**). They all grew at comparable rates in a matter of hours, whereas *Malassezia* species required several days (**Figure 10E-F**). When plotted by species, *C. albicans*, *C. tropicalis*, and *S. cerevisiae* grew at similar paces in YPD and YM medium, and at a slightly slower pace in Sabouraud medium (**Figure 10B-D**). This might be due to the more neutral pH of the Sabouraud medium compared to the higher acidity of YPD and YM. This difference in pH may induce a shift towards hyphae growth (data not shown), which could impact both the growth rate and the accuracy of the OD measurements. Both *Malassezia* species displayed much slower growth, especially when starting from a low initial OD, taking several days of no measurable increase in growth (**Figure 10E-F**). Importantly, due to the inherent aggregation properties of the fungi, measurements of low OD levels were unreliable, therefore measurement curves with a higher starting OD were used to get a more concise picture of the growth behavior.

Overall, successful growth was achieved for all five selected fungi candidates, with two different strains available per species (data not shown) and identity confirmation by metagenomic sequencing (data not shown).

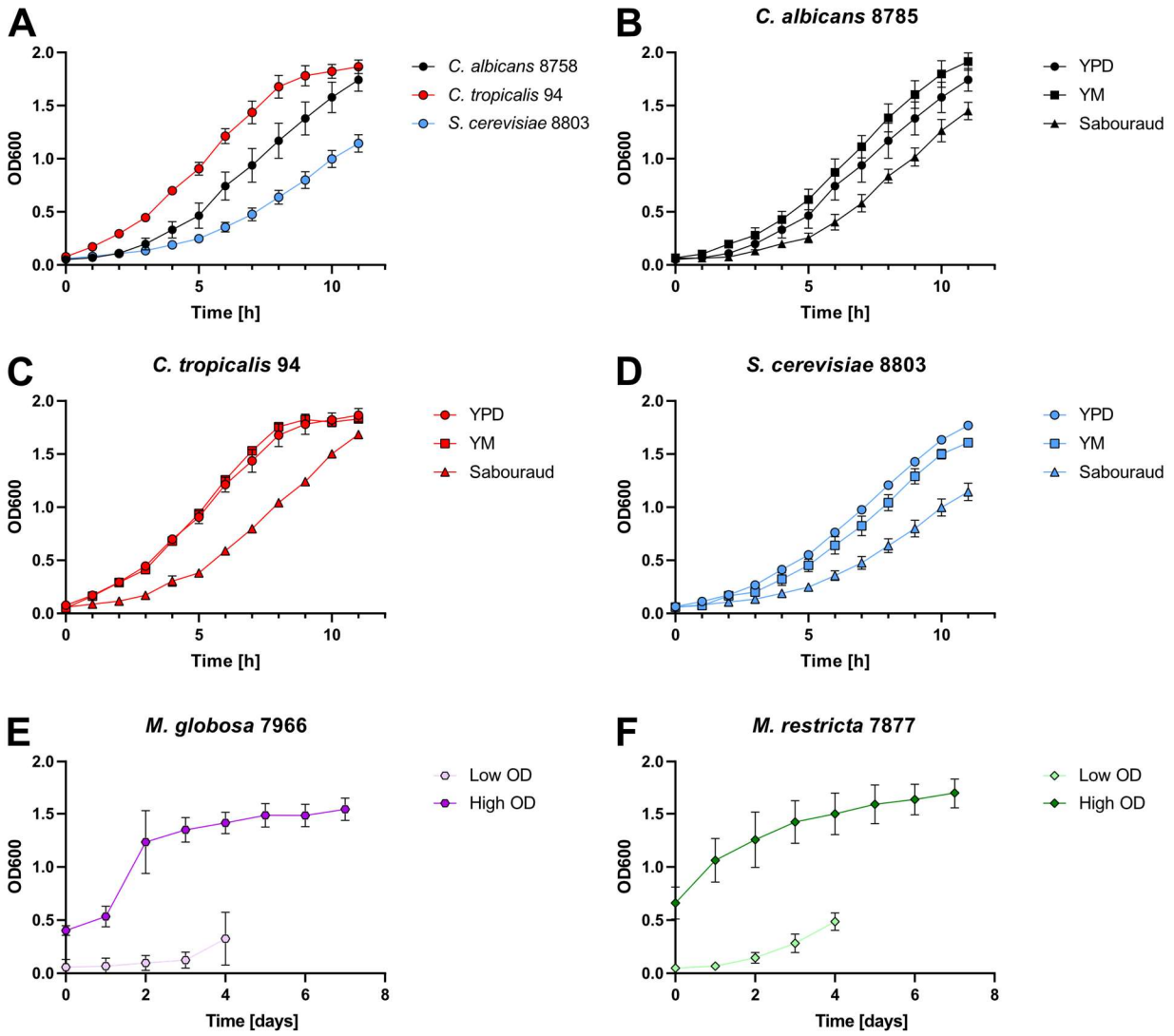

Figure 10: Growth curves of fungi measured by OD meter. A) Growth curve of three fungi in YPD broth. **B)** Growth curve of *C. albicans* CBS 8785 in YPD, YM, and Sabouraud medium **C)** Growth curve of *C. tropicalis* CBS 94 in YPD, YM, and Sabouraud medium. **D)** Growth curve of *S. cerevisiae* CBS 8803 in YPD, YM, and Sabouraud medium. **E)** Growth curve of *M. globosa* CBS 7966 in mDixon broth with a low or high initial OD. **F)** Growth curve of *M. restricta* CBS 7877 in mDixon broth with a low or high initial OD. YPD: yeast extract peptone dextrose; YM: yeast extract malt extract; mDixon: modified Dixon broth.

7.1.1.2 Metabolic profiling of fungi supernatants

In order to understand the functional differences between the fungi species, metabolic profiling of the supernatants derived from the in vitro growth of the fungi species was performed. The sample processing and measurement, as well as the initial analysis were conducted with the support of the metabolomics unit at the Weizmann Institute of Science in Israel. For this, I selected the three fastest growing fungi: *C. albicans*, *C. tropicalis*, and *S. cerevisiae*, and put them to grow at 30 °C under different conditions. I used two different media, YPD, a typical yeast medium, as well as DMEM with 10 % FCS as a medium that is more closely related to mammalian cell culture

conditions. Additionally, and in order to study the influence of the different oxygen atmospheres, I grew the fungi under aerobic and anaerobic conditions, which required two different time points of measurement: after 24 h for aerobic conditions and after seven days for anaerobic conditions due to the slower growth in general (**Figure 9A**). The obtained supernatants were sterile-filtered and send to the metabolomics unit without pH adjustment.

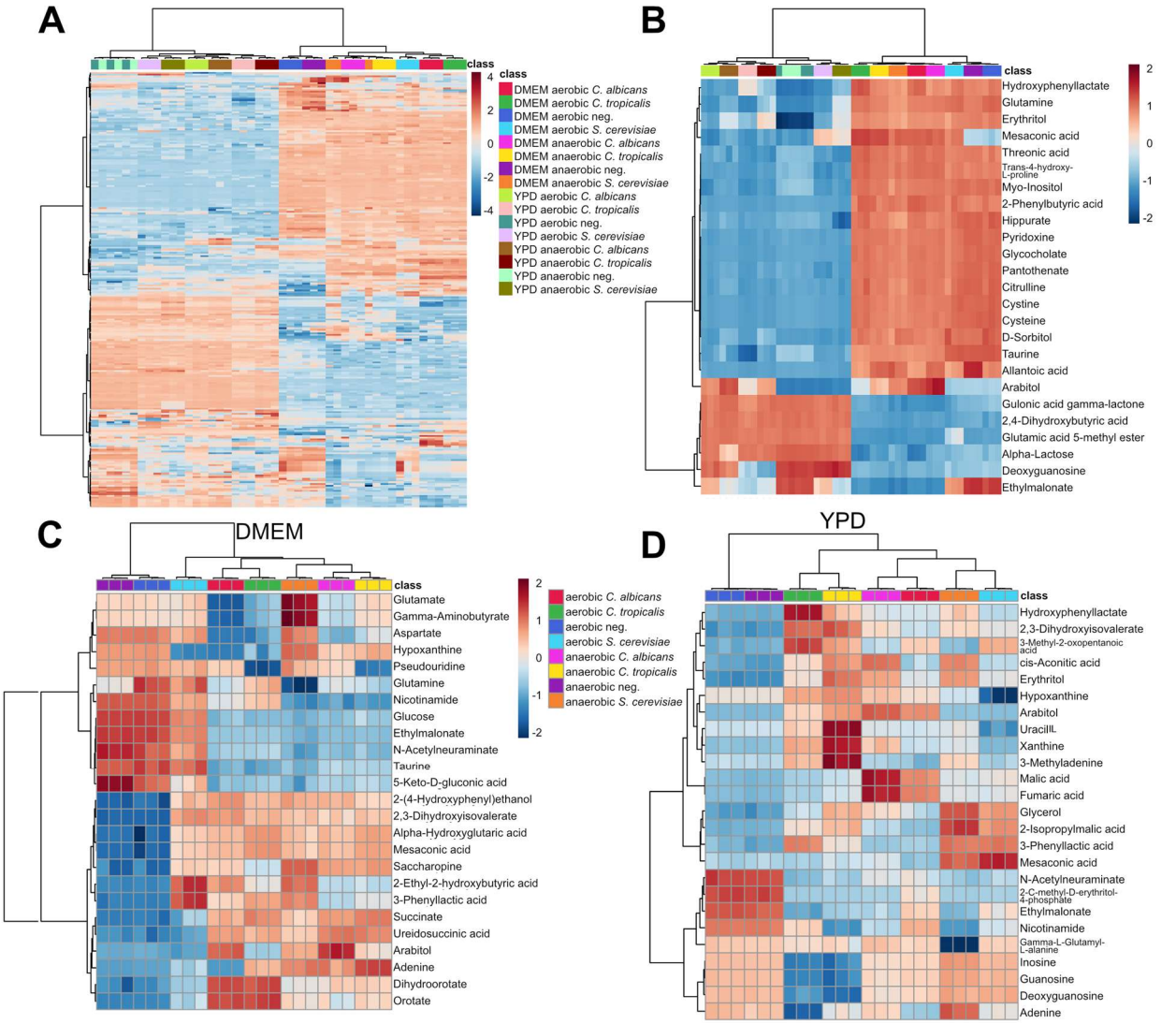

Figure 11: Metabolic profiling of supernatants derived from in vitro fungi growth. A) Heatmap displaying all metabolites. **B)** Heatmap showing the top 25 significantly different metabolites. **C-D)** Heatmap of the top 25 significantly different metabolites of **C)** DMEM supernatants, or **D)** YPD supernatants. YPD: yeast extract peptone dextrose; DMEM: Dulbeccos modified Eagle medium; neg.: negative.

The *Malassezia* species were excluded from this experiment since they grew at a much slower pace, even slower under anaerobic conditions, and did not grow in DMEM since they require additional supplementation of lipids [95]. Analysis of the metabolic profiling results indicated a

distinct clustering of the conditions based on medium type: YPD or DMEM (**Figure 11A**). For the growth in YPD, species clustered together initially, followed by a secondary distinction based on oxygen atmosphere, with the triplicates clustering closely except for the mixed controls. This suggests that there were minimal differences in the controls or the fungi based solely on the atmosphere. For the growth in DMEM, the fungi initially clustered based on atmosphere, and then by species with the triplicates clustering close together. Since the controls were separated by atmosphere, it seems that either the atmosphere or the later time point had a stronger influence on DMEM as opposed to YPD. This could be due to the potential degradation of sensitive components in such a complex medium.

The top 25 differentially detected metabolites also showed that the main differences were driven by inherent metabolite abundance differences between the two media, for example a higher glutamine content in DMEM or a higher amount of gulonic acid gamma-lactone in YPD medium (**Figure 11B**). Interestingly, mesaconic acid was produced by all fungi grown in DMEM, but only by *S. cerevisiae* in YPD (**Figure 11B**). Generally, it was striking but not surprising that the main driver in metabolic output was the nutrient availability. Therefore, I decided to analyze the two media separately so I could be able to detect trends more clearly.

When comparing only the metabolic profiling of the DMEM-grown supernatants and examining the top 25 differentially abundant metabolites, there were some that were consistently produced by all fungi, such as 2-(4-hydroxyphenyl)ethanol or alpha-hydroxyglutaric acid among others (**Figure 11C**). *S. cerevisiae* growth under aerobic conditions presented a more diverse metabolite profile in DMEM than all the other conditions. Even under anaerobic conditions, *S. cerevisiae* produced some specific metabolites such as glutamate and gamma-aminobutyarate. There were some metabolites specific to *Candida* that were produced only under aerobic conditions, such as orotate and dihydroorotate but also some that were specific for each *Candida* species, such as arabitol, produced by *C. albicans* only, or pseudouridine, found to be lower in *C. tropicalis* supernatants only. Similar trends emerged with the YPD-grown supernatants, where metabolites like N-acetylneuraminate were consumed by all fungi (**Figure 11D**). However, none of the top 25 metabolites were consistently produced by all fungal species (**Figure 11D**). In addition, each fungi had some specific metabolites that were produced only by this species in YPD medium, with mesaconic acid by *S. cerevisiae*, malic and fumaric acid by *C. albicans*, and uracil and xanthine by *C. tropicalis*, which also specifically consumed inosine and guanosine.

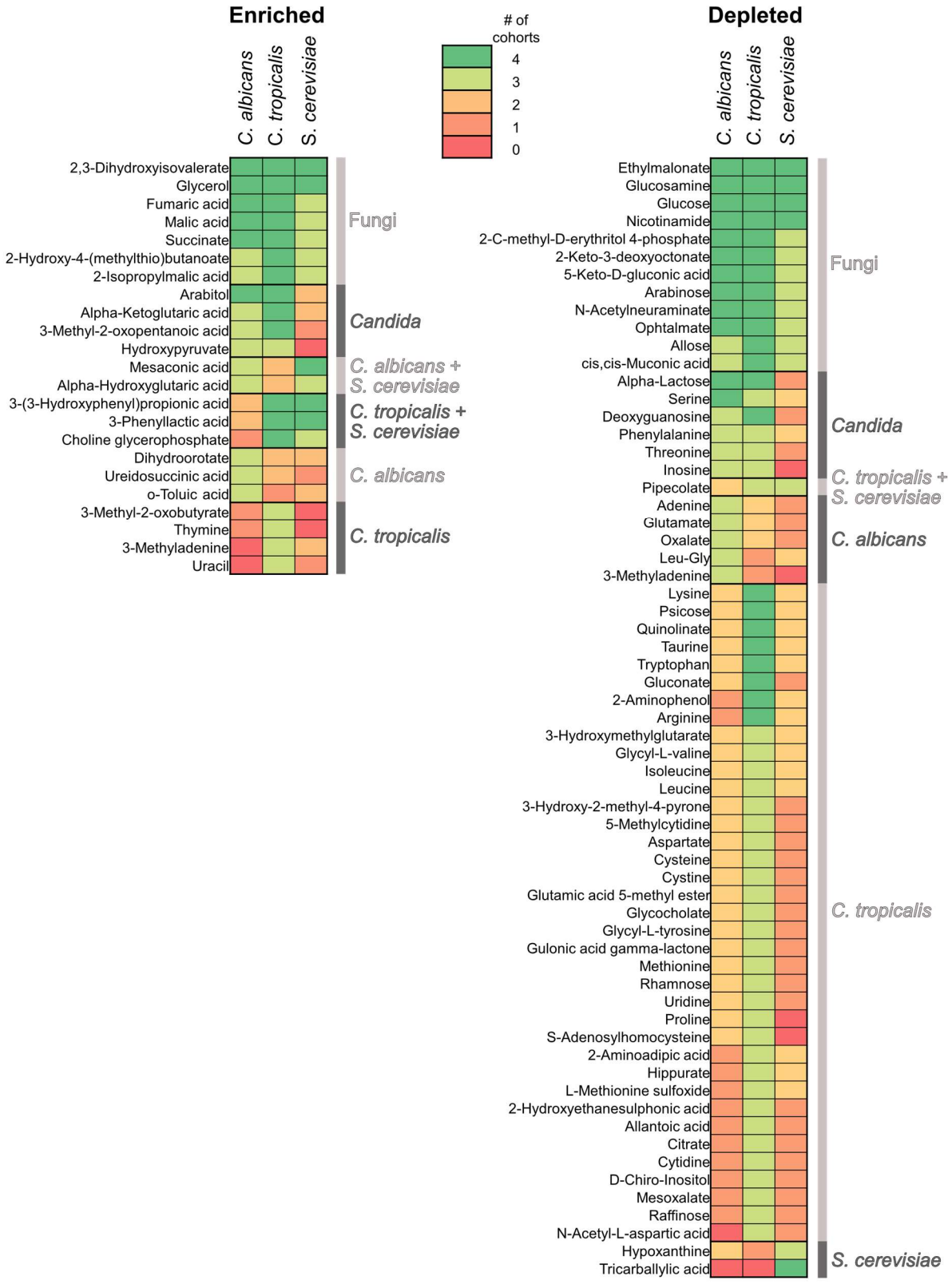

Figure 12: Analysis of metabolic profiling of fungi supernatants across in vitro growth conditions. Heatmaps of metabolites that were significantly (p.adj < 0.05) enriched or depleted by fungi strains compared to their respective experimental controls. Showing number of cohorts in which they were significant, grouped by trends across species.

To compare these trends across all growth conditions, the metabolite levels for each fungus were compared to their experimental controls; this analysis was performed by a postdoctoral fellow at WIS, Dr. Rafael Valdés-Mas. The metabolites that were significantly different (p.adj < 0.05) and changed in the same direction across at least three different cohorts for the same fungi were considered to be "conserved". These criteria were met by more metabolites that were depleted with the fungi compared to the enriched ones (**Figure 12**). To see how common these metabolites were across fungi species, they were segmented into several groups, based on their significance under the different conditions/cohorts. Seven metabolites were significantly enriched for all three fungi species ("Fungi"), many of which were associated with the tricarboxylic acid (TCA) cycle (**Figure 12**). In contrast, twelve metabolites were consistently depleted across conditions and species, which included mostly sugars such as glucose and glucosamine (**Figure 12**). A few metabolites were significantly enriched or depleted across several conditions for both *Candida* species but not *S. cerevisiae* ("*Candida*") such as arabitol or lactose, similarly some were consistently enriched or depleted for *S. cerevisiae* with one of the other fungi (**Figure 12**). Looking for "signature" metabolites that would be unique for a specific species, there was only one metabolite for *S. cerevisiae* that was significantly different in all cohorts for that species and for none of the others (**Figure 12**). Therefore, metabolites that were consistently significant in at least three cohorts for one species and less in the other two were considered specific. *C. albicans* produced three metabolites that fell into this category and five depleted, with no clear pathways that connected these metabolites (**Figure 12**). *C. tropicalis* on the other hand, produced five "specific" metabolites that belonged to the group of nucleobases and derivatives (**Figure 12**). One in particular, 3-methyladenine was "specifically" produced by *C. tropicalis*, but depleted by *C. albicans*, highlighting the different metabolic preferences for these strains (**Figure 12**). Interestingly, there were 37 metabolites that were "specifically" depleted by *C. tropicalis*, which spanned different categories such as amino acids, sugars, nucleosides, and organic acids (**Figure 12**). *S. cerevisiae* did not produce any "specific" metabolites, but two metabolites which it consumed, one of which, tricarballylic acid was truly unique to it (**Figure 12**). Overall, the different fungi species did appear to have specific metabolic preferences and outputs, even if they were mostly capable of producing the same metbolites under some conditions. While the metabolic profile was greatly dependent on the growth medium used, as well as the oxygen atmosphere under which the fungi was grown, some metabolites remained consistent across conditions and sometimes also across fungi species.

7.1.2 Impact of fungi supernatants on human gut epithelial organoids

In order to check whether the fungi-produced and consumed metabolites had an influence on the gut epithelium, I exposed human intestinal organoids to the fungi supernatants and measured the effects on the organoid growth using the Cell Titer Glo assay. This method allows the determination of viable cell mass by proxy of ATP abundance. Since the mDixon medium used for the growth of the *Malassezia* species had a toxic effect on the organoids on its own (data not shown), I only profiled the supernatants of *C. albicans*, *C. tropicalis* and *S. cerevisiae* grown in DMEM under aerobic conditions, which were pH-adjusted if necessary and sterile filtered before use. To maximize any potential growth effects, the organoids were dissociated into single cells, allowing exposure on both the apical and the basal side of the organoids, and subjected to different concentrations of the fungi supernatants over a period of eleven to twelve days until the control organoids had grown to a medium size. Since *C. albicans* specifically has been associated with colorectal cancer (CRC) [56, 76], I used the CRC-derived organoid line T41 for an initial experiment. Interestingly, all three fungi supernatants significantly increased the total organoid mass compared to the DMEM controls when added at the highest concentration (1:10) but not at the lower concentrations (1:100 or 1:1000) after eleven days of exposure (**Figure 13A**). To determine if this growth effect was specific to the derived-tissue location, disease state, or organoid line, a different organoid line derived from healthy duodenum tissue (line 72) was exposed to the fungal supernatants for a similar time. Not only did this effect vanish but was instead reversed, especially for *C. albicans* independently of the concentration and for *S. cerevisiae* at the highest concentration (**Figure 13B**). To profile this in a more systematic way, I used a healthy colon-derived organoid line (CJ wt) as well as two sub-lines derived from CJ wt, in which specific mutations to p53 (CJ P) and Kras, APC, p53, and SMAD4 (CJ KAPS), had been previously introduced by CRISPR-Cas9 gene editing, mimicking an early CRC state [218, 219]. In both CJ wt and CJ KAPS, there was no organoid growth effect by either *Candida* species, however, *S. cerevisiae* had a toxic effect that had not been seen with the previous lines (**Figure 13C, E, G**). Surprisingly, this effect was not visible for the CJ P line, which showed a large variability between the replicates, suggesting some technical issues rather than organoid-line specific effects (**Figure 13D**). To validate the previously observed growth effect, which we had only seen with the T41 line and to understand if this was CRC-specific, the experiment was repeated but the growth effect could not be reproduced. Instead the toxicity effect with the *S. cerevisiae* supernatant at the highest concentration appeared in this line as well (**Figure 13F**).

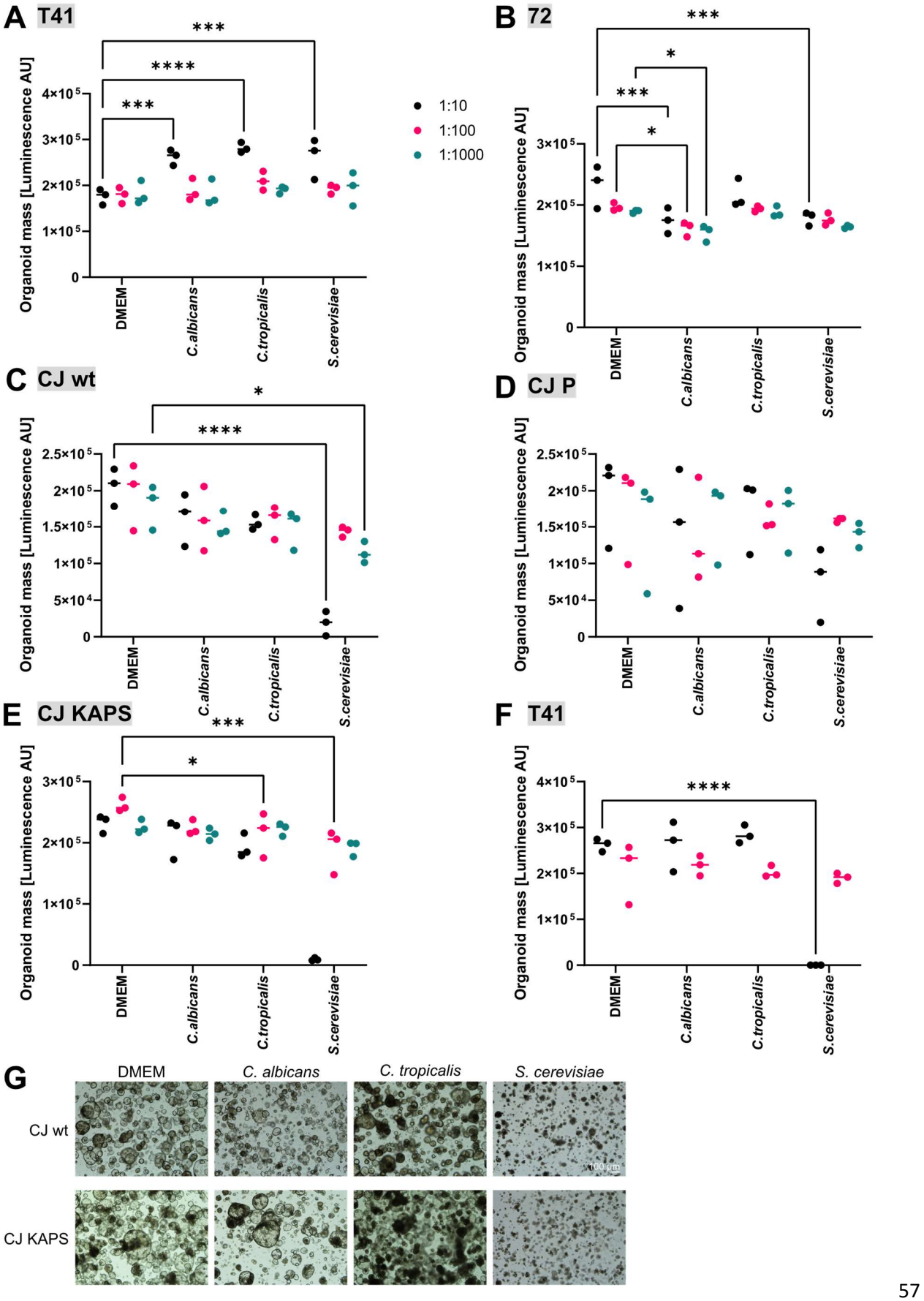
A T41
B 72
C CJ wt
D CJ P
E CJ KAPS
F T41
G
Organoid mass [Luminescence AU]
1:10
1:100
1:1000
DMEM
C.albicans
C.tropicalis
S.cerevisiae
DMEM
C. albicans
C. tropicalis
S. cerevisiae
CJ wt
CJ KAPS

Figure 13: Effect of fungi supernatants on the growth of intestinal human organoids measured by Cell Titer Glo Assay. A-F) Quantification of ATP using Cell Titer Glo assay of organoid line seeded as single cells, and exposed to fungi supernatants grown in DMEM medium. Three biological repetitions, statistical significance tested with 2-way ANOVA, only significant pairwise comparisons shown. **A)** Quantification of assay of CRC-derived organoid line T41 after eleven days exposure to fungal supernatants. **B)** Quantification of assay of duodenum-derived organoid line 72; **C)** colon-derived organoid line CJ wt; **D)** colon-derived organoid line with p53 mutation CJ P; **E)** colon-derived organoid line with Kras, APC, p53 & SMAD4 mutations after twelve days exposure to fungi supernatants. **F)** Quantification of assay of CRC-derived organoid line T41 with a different supernatant batch after eleven days exposure to fungi supernatants. **G)** Representative brightfield images are shown. DMEM: Dulbeccos modified Eagle medium; AU: artificial units; ANOVA: analysis of variance; CRC: colorectal cancer.

Since the growth effects were variable and with no consistent pattern, it seems that there might be batch effects between the collected supernatants, which together with organoid growth effects based on culture plate location in this assay makes it difficult to interpret.

One direct way in which metabolites can influence cancer development is through DNA damage, such as causing DNA double strand breaks [220]. To check whether any of the metabolites produced or altered by the fungi could cause DNA double strand breaks, I exposed the healthy duodenal organoid line 72 to the highest concentration of the fungi supernatants (1:10) for 12 h while breaking the organoids through mechanical shearing. This way, access of the supernatant to the apical and basal side of the epithelium was possible, while at the same time a relevant time period where these effects could be measured was maintained. Subsequently, organoids were dissociated into single cells, fixed, and stained for a DNA double strand marker (yH2AX) for subsequent FACS analysis (**Figure 14A-C**) [221, 222]. After gating out debris and doublets, as expected, only a low number of cells were positive for yH2AX in the stained negative control (**Figure 14A, D**), however, a clearly evident shift was observed in the positive control (**Figure 14B, D**). Exposure to *C. albicans*, *C. tropicalis* or *S. cerevisiae* supernatants did not induce an increase in DNA double strand breaks (**Figure 14C-D**), suggesting that at least the metabolites produced under these specific conditions (grown in DMEM under aerobic conditions) were not responsible for DNA double strand breaks.

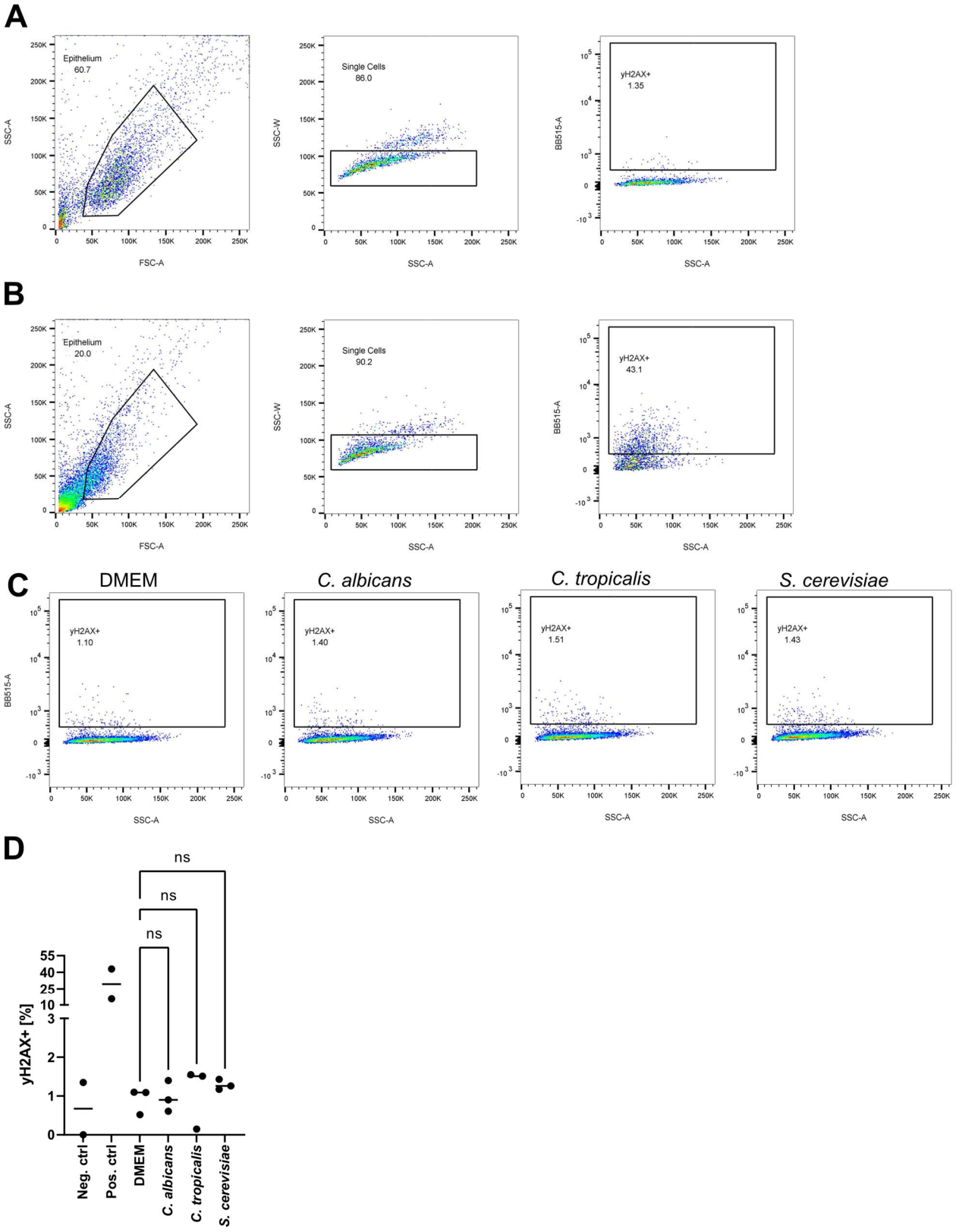

Figure 14: DNA damage of intestinal human organoids after fungi supernatant exposure by yH2AX FACS. A-D) Duodenal organoid line 72 exposed to fungi supernatant (1:10 dilution) for twelve hours; data combined from two separate experiments. Representative FACS plots for **A)** the negative control; **B)** positive control (Mitomycin C treatment

at 150 µM end concentration) and **C)** experimental conditions. **D)** Quantification of yH2AX positive cells as a percentage of the parent population (single cells); statistical significance determined with Kruskal-Wallis test. yH2AX: gamma Histone H2AX; FACS: fluorescence activated cell sorting; DMEM: Dulbecco's modified Eagle medium; ns: non-significant; ANOVA: analysis of variance.

7.1.3 It takes two: Establishment and characterization of fungi-organoid cocultures

7.1.3.1 Fungi-organoid coculture establishment

Since there were no clear or consistent effects of the in vitro produced fungal metabolites (**7.1.2**), I decided to increase the complexity of the system by modeling the direct interaction of live fungi with the intestinal epithelium. To address this, I established the first-ever fungi-organoid coculture system with the goal to avoid overgrowth of the fungi and ensure exposure to the apical organoid side. This had been previously achieved through microinjection of microbes into the organoids but had never been applied to fungi [118, 123]. Initially, I attempted to establish the optimal antifungal concentration that would prevent any fungal growth outside the organoids but allow the growth of the fungi inside the organoids. Amphotericin B (AmpB) was established as a suitable antifungal since it is known to have low permeability from the gastrointestinal tract in humans [223]. Thus, it was speculated that the epithelial barrier of the organoids could prevent it from entering the lumen. The three different fungi species *C. albicans*, *C. tropicalis* and *S. cerevisiae*, each able to grow in mammalian cell culture medium, were microinjected into the lumen of healthy duodenum-derived human organoid line 72, or the injection dye as a control. AmpB was also added at two different concentrations: 250 and 25 ng/mL. The growth was monitored by imaging across time (**Figure 15A**), as well as culturing of the medium and the organoids without the medium at day two and five respectively (**Figure 15B**). It was possible to maintain the coculture for several days and fungal growth was observed inside the organoids as seen by the number of fungal colonies detected at day five with the lower AmpB concentration (**Figure 15B**). However, it is important to note that under low dose of AmpB there was still fungal growth detected outside of the organoids, such was the case for *C. tropicalis* and *S. cerevisiae* (**Figure 15A-B**). *C. albicans* also grew outside of the organoids, as visible by microscopy, but since it is known for its ability to adhere and form biofilms, it could have stuck to the plate when harvesting the media for subsequent culturing, which could explain why it did not regrow on the agar plate [224, 225] (**Figure 15A-B**). On the other hand, at a higher dose of AmpB, the fungal growth inside of the organoids was limited, inhibiting its growth but not killing the fungi since they could regrow when cultured (**Figure 15A-B**). Overall, there was a lower amount of fungi growth observed in the medium compared to the organoids during culturing. It is important to note that only approximately half of the culture medium was utilized from one well, in contrast to all of the organoids being cultured. Additionally,

the time points of collection differed, with the medium being collected on day two and the organoids on day five. Remarkably, the organoids were able to withstand severe fungal overgrowth in the coculture, demonstrating their resilience even in challenging conditions.

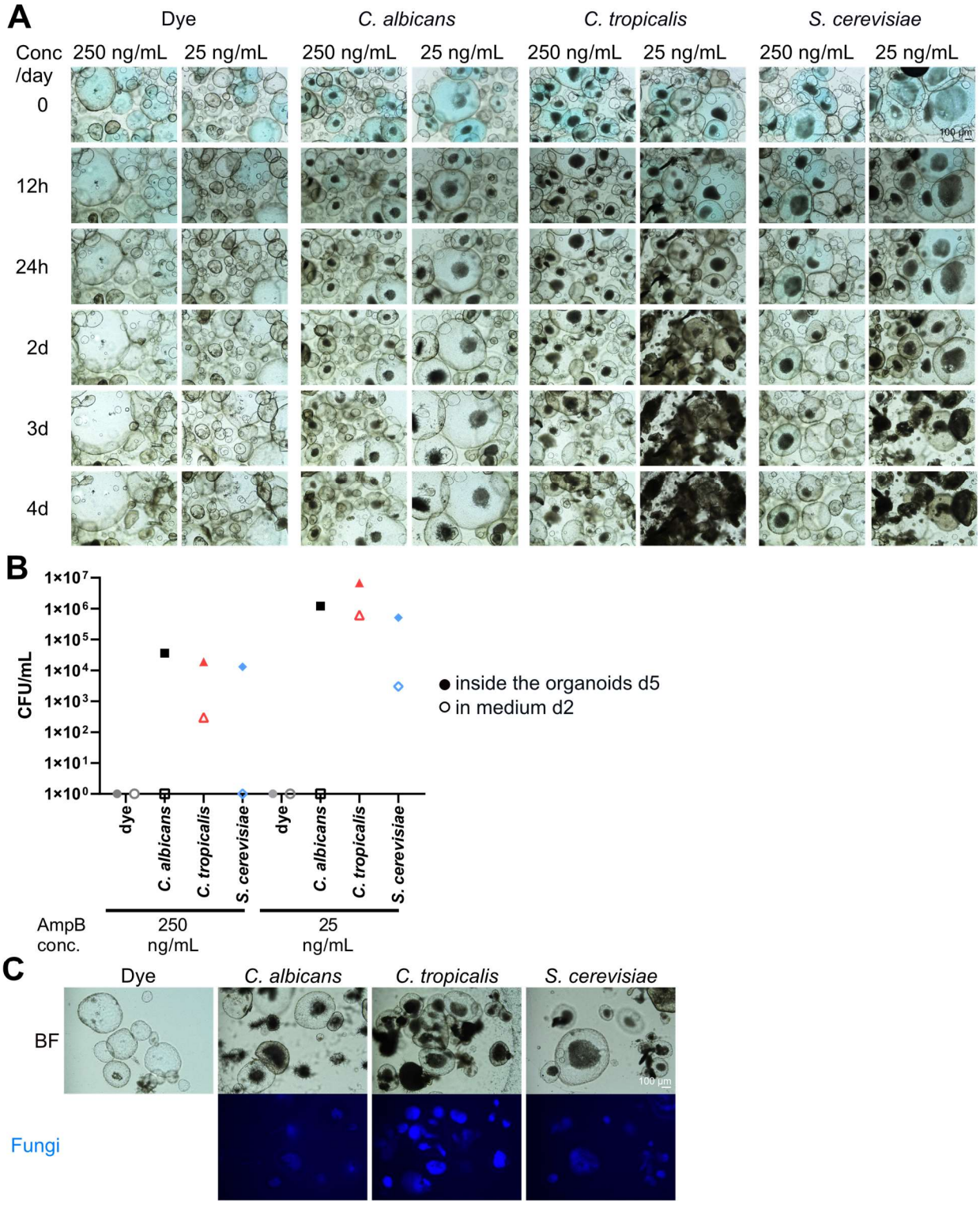

Figure 15: Establishment of fungi-organoid cocultures. A) Representative images of coculture time course in the presence of Amphotericin B at two different concentrations, organoid line 72. **B)** Quantification of amount of fungi after coculture in the organoids at d5 (data points with filling) and in 100 µL medium at d2 (data points empty). **C)** Representative images of coculture with fungi stained with cell proliferation dye (blue), and BF after 12 h coculture without antifungal, organoid line 72. Conc: concentration; BF: bright field; CFU: colony forming units; AmpB: amphotericin B.

It is worth mentioning that, even though together with my mentee master student, Ms. Jasmin Zech, we attempted to find an optimal AmpB concentration, or to use another antifungal to avoid overgrowth outside of the organoids without inhibiting the inside growth, we did not succeed (data not shown). Therefore, I decided to limit the fungi-organoid coculture to 12 h only, without using any antifungal since the active growth of the fungi was considered the most important factor to study the interactions as long as the organoids survived. To better visualize the fungi inside the organoids, I stained them using a live cell membrane marker, used for bacterial injections into organoids [123]. Without any antifungal treatment, the fungi successfully grew inside the organoids as visible by the mix of yeast and hyphae cells, characteristics of the *Candida* species, whereas *S. cerevisiae* was visible in its yeast form, as expected (**Figure 15C**). The switch towards hyphae morphologies is triggered by the organoid medium (data not shown), potentially due to the neutral pH and different nutrient availability [33]. While the cell dye stained the yeast cells well, any hyphae structures did not retain the dye, potentially because the hyphae are the site where the majority of proliferation is happening in organoid medium, which might dilute the dye (**Figure 15C**).

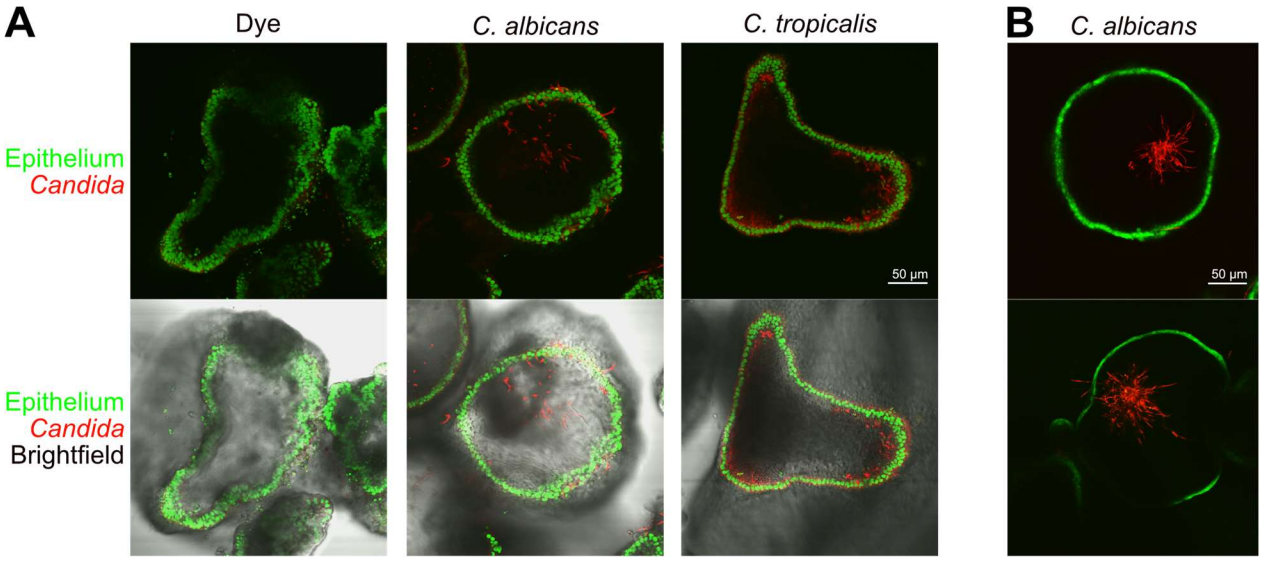

Figure 16: Visualization of fungi-organoid cocultures using confocal microscopy. Confocal images of **A)** coculture, fungi stained with *Candida* antibody, Brightfield, organoid line CJ-KAPS green, and **B)** *C. albicans* – organoid coculture with *C. albicans* – RFP strain, organoid line CJ KAPS green.

Since the hyphae formation is only occurring in the *Candida* species, Ms. Jasmin Zech and I used a *Candida*-specific antibody to stain the fungi after the overnight coculture and visualized it by using confocal microscopy (**Figure 16A**). The *Candida* antibody stained also hyphae cells, but could not properly permeate the organoid membrane, showing unspecific staining of the epithelial cells even after protocol optimization. To circumvent this problem, the Iliev lab at Weill Cornell Medicine kindly provided us with a genetically RFP-labelled *C. albicans* strain, which was used, with the support of Ms. Jasmin Zech, to microinject and imaged by confocal microscopy (**Figure 16B**). This demonstrated that some of the *C. albicans* hyphae were interacting with the epithelium, and sometimes even penetrated the membrane, which made me wonder if this could be a suitable model system to study intracellular fungi behavior.

7.1.3.2 Modeling intracellular fungi

Two recent publications showed the presence of intracellular fungi in various tumor types [76, 77], challenging the previous belief that this was a phenomenon only possible for immune cells or during infections [78, 79]. To test if the established microinjection coculture system also lead to the presence of intraepithelial fungi and its morphology, I partnered with the DKFZ Electron Microscopy Facility who processed and captured images of the fungi-microinjected organoids with Transmission Electron Microscopy (TEM) after overnight exposure (**Figure 17A-B**). Using a biopsy-derived CRC tumor organoid line (EL11T) and after coculture with *C. albicans*, most fungi cells were visible within the organoid lumen and some outside of the organoids due to either overgrowth during the culture or sample processing. Interestingly, there were fungi also present inside the epithelial cells (**Figure 17A**). The fungi cells could be distinguished by their thick white cell wall, which prevented the penetration of the fixative, leading to black unresolved intracellular matter. The intracellular fungi cells appeared to be inside a vacuole with an enrichment of cytoskeletal filaments around it (**Figure 17A-B**). To see if this was specific to this organoid line, I used a metastasis-derived organoid line from the same patient (EL11M) and cocultured it with *C. albicans*, *C. tropicalis* or *S. cerevsisiae*. Using TEM, it was possible to observe intracellular events for *C. albicans*, much fewer for *C. tropicalis*, which had not been present in the primary tumor-derived line, and none for *S. cerevsisiae* (**Figure 17B**). Since the number of events seen was small and the process of TEM laborious, time-intensive, and non-quantitative, another method was selected to quantify and further characterize the presence of intracellular fungi. For this purpose, I used Imagestream, which is a combination of FACS and fluorescence microscopy, available at the DKFZ FACS facility. I microinjected RFP-labelled *C. albicans* into the EL11M organoid line since this combination had shown the highest number of intracellular events.

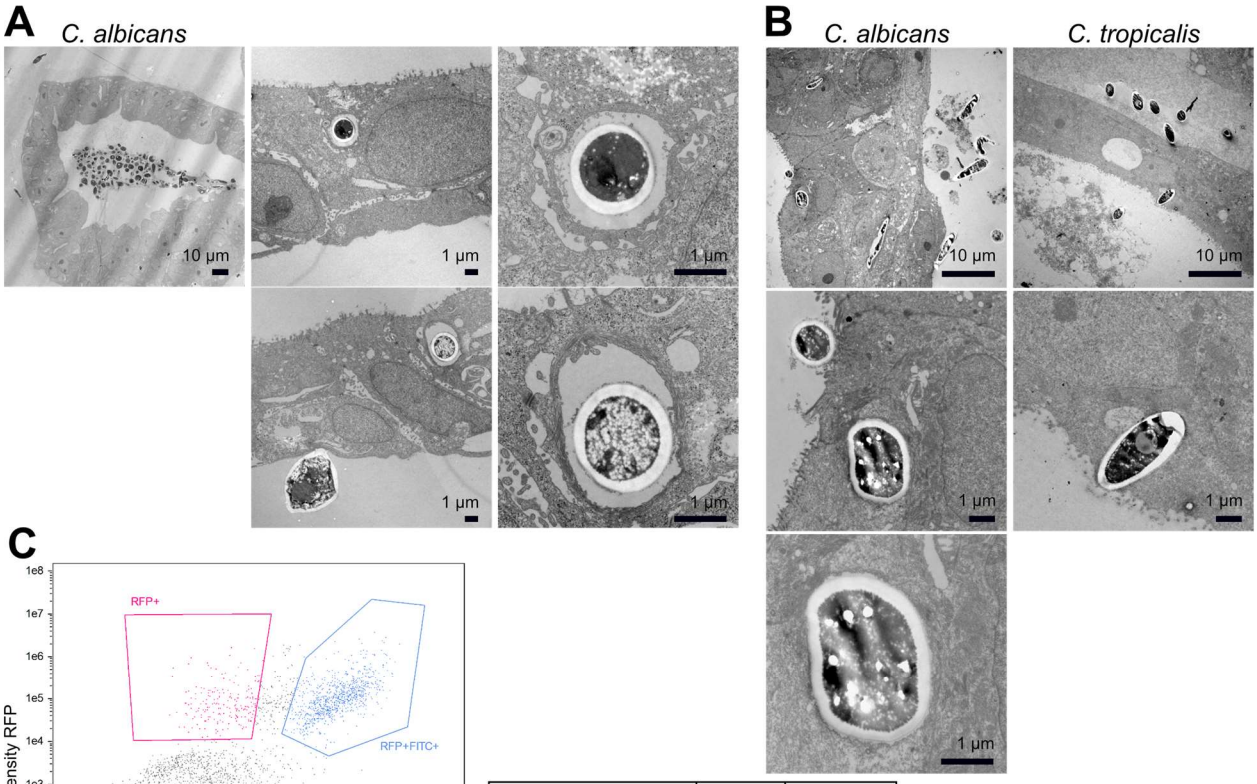

C

Population	Count	%Gated
Epithelial cells	2395	100
RFP+	197	8.23
RFP+ FITC+	916	38.2
FITC+	76	3.17

D

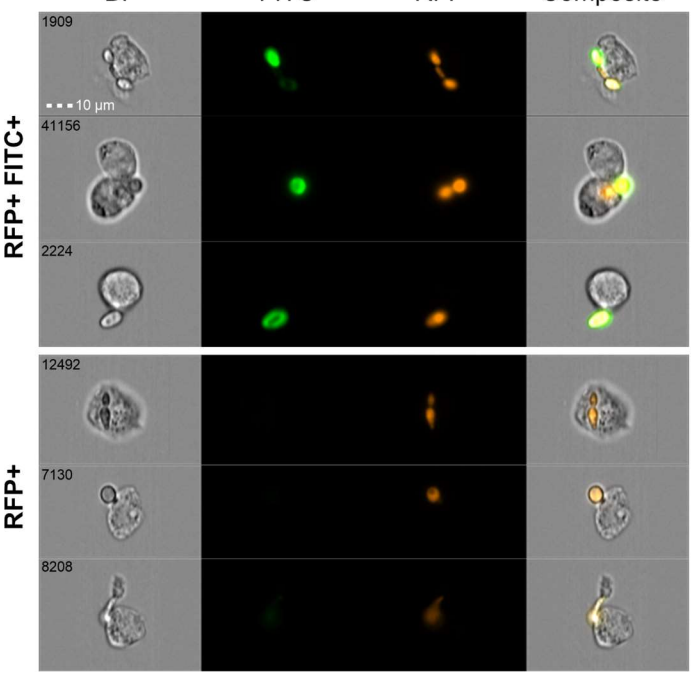

Figure 17: Determination of intracellular fungi after fungi-organoid cocultures. TEM images of **A)** *C. albicans* and EL11T or **B)** *Candida* species and EL11M. **C-D)** Imagestream analysis of EL11M organoids injected with *C. albicans*-RFP and stained for extracellular fungi with anti-*Candida*-FITC antibody. **C)** FACS plot displaying the populations and percentage table; **D)** Representative microscopy images of the respective populations. TEM: transmission electron microscopy; EL11T: CRC-derived organoid line; EL11M: metastasis-derived organoid line; BF: brightfield; FITC: fluorescein isothiocyanate; RFP: red fluorescent protein; FACS: fluorescence activated cell sorting.

In order to distinguish between intra- and extracellular fungi that might be attached to the epithelial cells, an additional *Candida* staining with a FITC-labelled antibody was used before fixation. Therefore, only extracellular fungi were stained but not intracellular ones. The majority of the cells were not stained at all, meaning they were not associated with fungi (in grey) (**Figure 17C**). Out of the fungi-associated cells, the largest percentage, 38.2 %, were double-positive cells (in blue), suggesting that the associated fungi were attached outside of the cell or partially penetrating them, which was also visible in the microscopy pictures (**Figure 17C-D**). A small percentage, 3.17 %, was only positive for FITC, which was due to background noise, since the fungi strain was genetically labelled with RFP (**Figure 17C**). The most interesting population were the cells that were positive for RFP but not for FITC, since they had to be intracellular at least at the time point of the extracellular FITC staining. 8.23 % of cells fell into this category, however, analysis of the corresponding microscopy images showed that not all fungi were truly intracellular (**Figure 17D**). While some fungal cells still appeared to be completely engulfed by the epithelial cell, others were partially inserted or next to it, suggesting that they were expelled from the epithelial cells or had been protected from the FITC staining (**Figure 17D**). I thus concluded that at least in the organoid coculture setting, while we could detect intracellular fungi at low numbers, this stage might only be of a transient nature. Whether this reflects also what is happening in vivo or if organoids are not a suitable model system for this phenomenon remains open.

7.1.3.3 Downstream effects of fungi-organoid cocultures

It has long been speculated that *Candida* species might have a tumor-promoting effect [56]. In order to test the effect of commensal fungi on several aspects of carcinogenesis, I used the coculture system described in the previous section. To profile DNA double strand breaks after overnight coculture with *C. albicans*, *C. tropicalis*, or *S. cerevisiae*, I used γH2AX FACS. As a result, no DNA damage was shown in two independent experiments (**Figure 18A-B**). It has been shown that CRC tumors that were enriched with *Candida* species had an upregulation of metastasis-associated genes [76]. Therefore, I tested if the overnight fungi coculture had an influence on the single cell outgrowth when the organoids were dissociated, reseeded, and followed by imaging monitoring. No notable differences were seen after organoid exposure, however, since the seeding densities were not normalized, no quantitative measure was taken to compare it (**Figure 18C**).

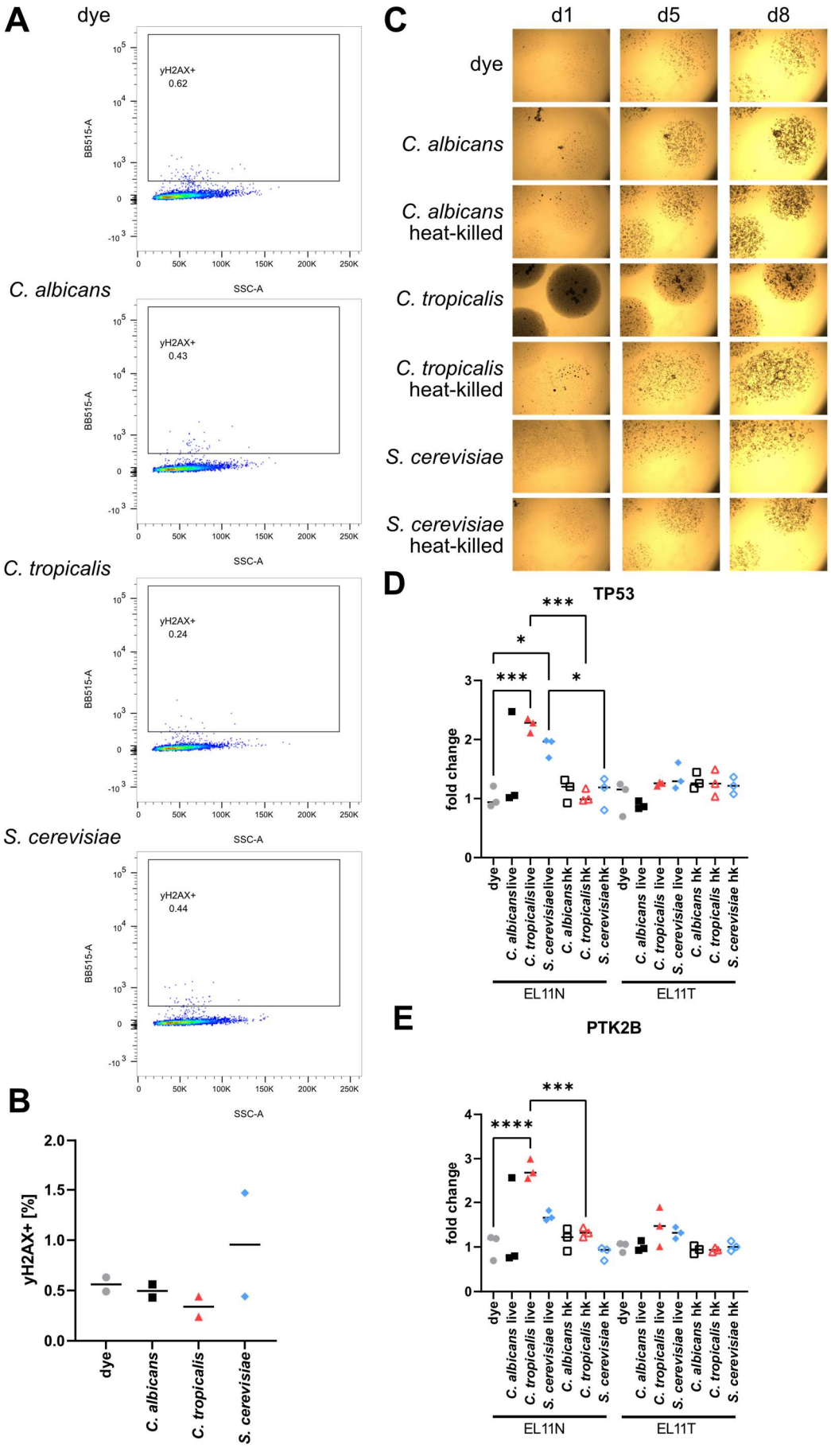
A
dye
yH2AX+
0.62
BB515-A
SSC-A
C. albicans
yH2AX+
0.43
C. tropicalis
yH2AX+
0.24
S. cerevisiae
yH2AX+
0.44
B
yH2AX+ [%]
dye
C. albicans
C. tropicalis
S. cerevisiae
C
d1
d5
d8
dye
C. albicans
C. albicans heat-killed
C. tropicalis
C. tropicalis heat-killed
S. cerevisiae
S. cerevisiae heat-killed
D
TP53
fold change
dye
C. albicans live
C. tropicalis live
S. cerevisiae live
C. albicans hk
C. tropicalis hk
S. cerevisiae hk
EL11N
EL11T
E
PTK2B
fold change
EL11N
EL11T

Figure 18: Impact of fungi-organoid cocultures. A) Representative γH2AX FACS plots after overnight coculture; organoid line 72. **B)** Quantification of γH2AX positive cells as a percentage of the parent population (single cells). **C)** Representative images of single cell outgrowth after overnight coculture; organoid line CJ wt red. **D-E)** qPCR results after overnight coculture for organoid lines EL11N and EL11T, statistical significance tested with 1-way ANOVA, only significant pairwise comparisons shown. hk: heat-killed; γH2AX: gamma Histone H2AX; FACS: fluorescence activated cell sorting.

The fungi had been killed with primocin treatment after the coculture but for some conditions, especially for *C. tropicalis* exposure, there were still remains of dead fungi present in the BME domes despite the washing steps. This might explain the slight reduction in growth, especially, since this was not present after heat-killed *C. tropicalis* exposure. With these specific experimental conditions and organoid line, there were no clear effects on organoid outgrowth. Continuous fungi exposure would be potentially required, which was not possible to model under this set-up. Additionally, this might also be specific to this organoid line, which originates from healthy colon tissue, and might be different with lines originating from tumor or metastatic tissue.

Next, I used two organoid lines derived from healthy and CRC tumor tissue of the same donor (EL11N & EL11T) and after overnight fungi coculture, candidate genes that had been associated to be differentially expressed with high or low *C. albicans* abundance in colon, stomach or head-neck cancers were profiled by qPCR [76]. The genes to be determined were TP53, SMAD6, FN1, SAGE1, PTK2B, CKDN2A, and BMP15, some of which are associated with metastasis-related pathways such as epithelial-mesenchymal transition, or general carcinogenic processes like cell cycle or differentiation [76]. Out of all, TP53 was significantly upregulated in the healthy line after live *C. tropicalis* or *S. cerevisiae* exposure, but not heat-killed ones (**Figure 18D**), and PTK2B displayed the same pattern as TP53 in the healthy and tumor line for *C. tropicalis*, but was not significant for *S. cerevisiae* (**Figure 18E**). *C. albicans* did not cause significant effects, and the patterns found were in the opposite direction to what had been reported in the literature [76], and might therefore be more of an immediate damage or infection response to pathogen exposure. This, combined with the observed morphology switch of the *Candida* species to hyphae, considered an infection-associated morphology [33], suggested that the tested fungi-organoid cocultures might not be the ideal system to model commensal fungi exposure, but rather an infection phenotype. The lack of the immune system in this simplified organoid setting might change the behavior of both the fungi and the epithelial cells response, compared to what might happen in vivo, requiring careful consideration when interpreting results. Therefore, I decided to move to an in vivo set up, which could certainly model the complexity required to study potential physiological aspects that could contribute to the host-fungi interactions.

7.2 Chapter 2: Colonization patterns of different fungi in the mouse intestine

In this chapter, I adapted and established methods for the detection of the mycobiome in our lab, and characterized the intestinal colonization behaviors of different fungi in various mouse models.

7.2.1 Adaptation of mycobiome detection methods

7.2.1.1 DNA extraction optimization

Unlike bacteria, fungi have a thick cell wall, which requires harsher conditions to break and extract the DNA. Therefore, I tested which extraction method yielded the highest amount of DNA. I started by using three different commercial kits and a commercially available mock community that contains two fungi species: *S. cerevisiae* and *Cryptococcus neoformans,* and eight bacteria. Using the Qiagen Power Soil Pro kit (QP) and variations of the extraction parameters, a longer beating time and an additional heating step, the amount of total DNA extracted was increased (**Figure 19A**). Using the Invitrogen PureLink DNA extraction kit, the DNA yield was low, never exceeding 1.5 ng/µL. There were small differences induced by parameter variations but a trend towards less total DNA amount with a longer beating time (**Figure 19B**). This could potentially be due to fragmentation of the DNA, while with the QP kit the yield was always above 40 ng/µL (**Figure 19A**). A third commercial kit, the Qiagen FastTissue kit (QF), reached a yield of 34 ng/µL total DNA, which is in between the other two kits (data not shown).

Under these conditions QP had the best results, but the mock community has a very limited amount of species, therefore, I tested the kits on stool samples from three human donors. The biggest variation with all three kits was between donors, with stool ID#3 yielding the highest amount of total DNA in most cases (**Figure 19C-E**). With the stool samples, increasing the beating time or the additional heating step in the QP kit protocol did not improve the total DNA yield in a drastic way, consequently, the original protocol was chosen as the default (**Figure 19C**). For the other two kits, the total DNA yield was much lower when extracted with the Inv or QF kit than with the QP kit (**Figure 19D-E**). Some studies use pretreatment with the enzyme lyticase to lyse the cell wall to enhance DNA yield [226]. In my hands, pretreatment with lyticase did not increase the DNA amount but rather slightly reduced it, hence this was not further used (**Figure 19F**). In conclusion, extraction with the QP kit yielded the highest amount of total DNA, but it was unclear if this would also give the best representation in species abundance, therefore, the most promising conditions were subjected to sequencing.

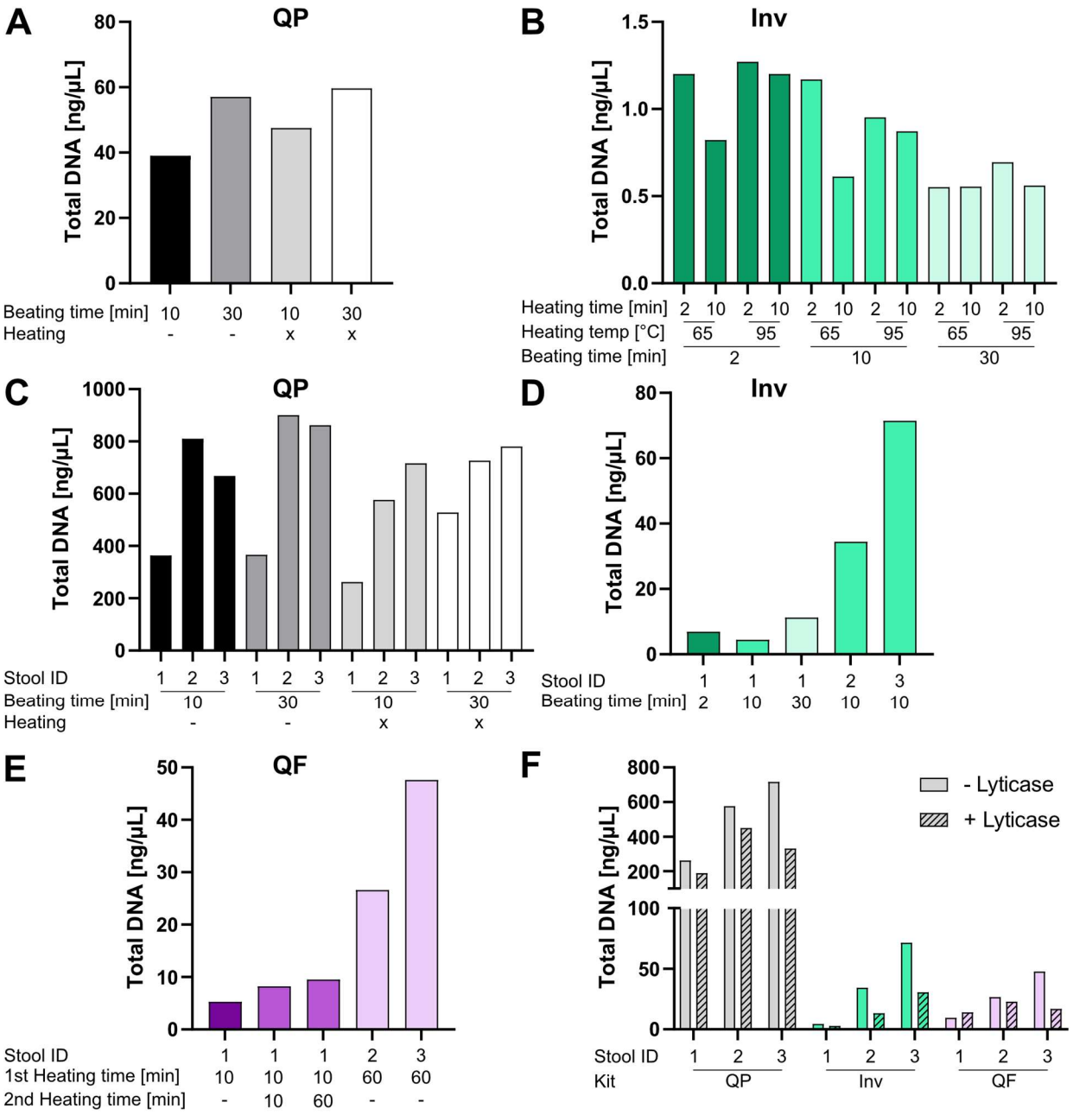

Figure 19: DNA extraction optimization for mycobiome detection. A-B) Extraction of Zymo mock community using **A)** the Qiagen Power Soil Pro kit; heating step was 65 °C when indicated or **B)** the Invitrogen PureLink DNA isolation kit. **C-F)** Extraction of three human stool samples using **C)** the Qiagen Power Soil Pro kit; **D)** the Invitrogen PureLink DNA isolation kit, all samples were heated to 95 °C for 10min; or **E)** the Qiagen FastTissue kit, the beating time for all samples was 4 min. **F)** Extraction with all three kits with or without lyticase pretreatment with the following extraction parameters for each kit: QP: 10 min beating and heating; Inv: 10 min beating and heating to 95 °C; QF: 4min beating, 1st heating step for 5 min, 2nd heating step for 60 min at 56 °C and 1000 rpm. Temp: temperature; QP: Qiagen Power Soil Pro kit; Inv: Invitrogen PureLink DNA isolation kit; QF: Qiagen FastTissue kit.

7.2.1.2 ITS sequencing optimization

Together with our lab sequencing specialist, Ms. Sabine Schmidt, I applied the Illumina ITS sequencing protocol to the mock community and stool samples extracted above. This protocol uses a mix of eight forward and seven reverse ITS primers that amplify the ITS1 region to capture the widest fungal diversity, which is expected to result in varied amplicon lengths depending on the taxa. First, I tested the sensitivity of the 1st ITS PCR by titrating the amount of mock DNA that contained two fungi species: *S. cerevisiae* and *C. neoformans*, among eight bacteria. After the PCR, the samples were run on a Tapestation gel and bands for both fungi were clearly visible and distinguishable based on their amplicon size: 308 bp for *C. neoformans* and 580 bp for *S. cerevisiae* based on the expected amplicon length by Primer blast and the added overhang from the primers (**Figure 20A**). Both fungi could be detected even at low concentrations but *S. cerevisiae* was always detected in higher amounts, which could be due to a higher primer affinity, or, more likely, a difference in ITS gene copy number (**Figure 20B**). *S. cerevisiae* has an expected 18S gene copy number of 109, whereas *C. neoformans* has 60 (see product information), which could explain the varying amounts.

Next, I aimed to study if and how DNA extraction with the three different kits had an influence on the species distribution. For the QP and Inv kits, this species distribution bias was even enhanced by the extraction, with the band for *C. neoformans* not even visible after extraction with the Inv kit after the 1st ITS PCR step, which was not the case for the QF kit (**Figure 20C**). Analysis of the ITS sequencing with the ITSxpress tool could detect the correct and expected fungi species and showed an even higher level of *S. cerevisiae* (**Figure 20D**). Since this was the case for all extraction conditions, even with the QF kit, it could also be a mapping or database bias, in that *S. cerevisiae* might be better represented in the database. Adjusting the different extraction parameters with the QP kit (heating and beating time) did not seem to make a difference, therefore the shortest method was used, which included no heating step and 10 min of bead beating.

Since the mock community included only two fungi species, I used human stool samples from three volunteers as representatives of complex microbial communities. Comparing the extraction efficiency of the three DNA extraction kits for all three stool samples, stool ID #2 had less bands visible on the Tapestation gel after the 2nd ITS PCR step compared to stool ID #1 and #3, independent of the extraction method (**Figure 20E**). Interestingly, taxonomic analysis still showed several fungi species to be present also in stool ID #2, whereas stool ID #3 mainly consisted of *Saccharomyces*, which potentially overshadowed the presence of any other taxa (**Figure 20F**). Comparing between the different kits, the QP kit could clearly extract the highest diversity of fungi, as visible by both the number of bands on the gel and by taxonomic analysis (**Figure 20E-F**).

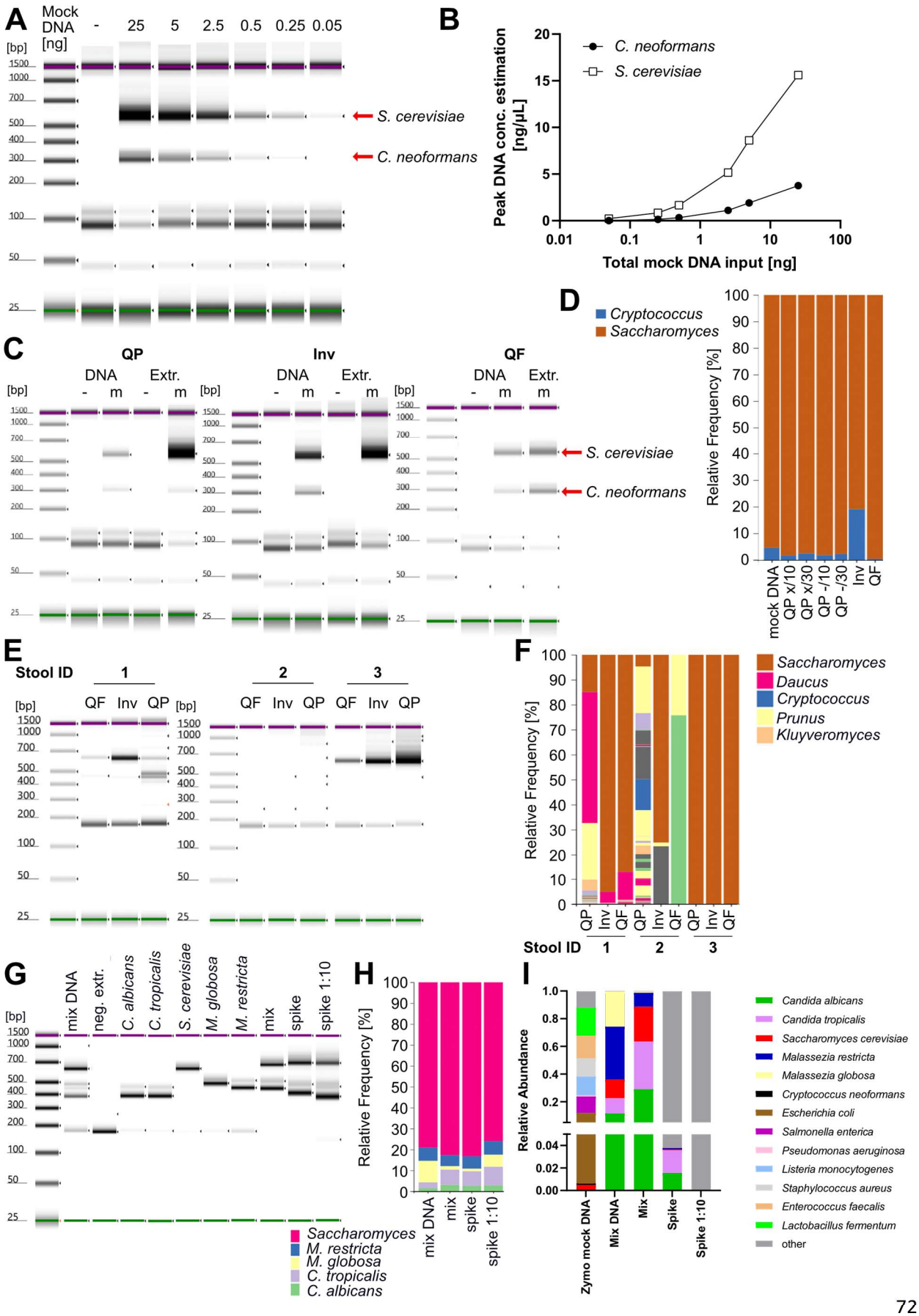
A
Mock DNA [ng]
- 25 5 2.5 0.5 0.25 0.05
[bp]
1500
1000
700
500
400
300
200
100
50
25
S. cerevisiae
C. neoformans
B
Peak DNA conc. estimation [ng/µL]
C. neoformans
S. cerevisiae
Total mock DNA input [ng]
C
QP
Inv
QF
DNA
Extr.
S. cerevisiae
C. neoformans
D
Cryptococcus
Saccharomyces
Relative Frequency [%]
mock DNA
QP x/10
QP x/30
QP -/10
QP -/30
Inv
QF
E
Stool ID
1
2
3
QF Inv QP
F
Saccharomyces
Daucus
Cryptococcus
Prunus
Kluyveromyces
Relative Frequency [%]
Stool ID
G
mix DNA
neg. extr.
C. albicans
C. tropicalis
S. cerevisiae
M. globosa
M. restricta
mix
spike
spike 1:10
Saccharomyces
M. restricta
M. globosa
C. tropicalis
C. albicans
H
Relative Frequency [%]
mix DNA
mix
spike
spike 1:10
I
Relative Abundance
Zymo mock DNA
Mix DNA
Mix
Spike
Spike 1:10
Candida albicans
Candida tropicalis
Saccharomyces cerevisiae
Malassezia restricta
Malassezia globosa
Cryptococcus neoformans
Escherichia coli
Salmonella enterica
Pseudomonas aeruginosa
Listeria monocytogenes
Staphylococcus aureus
Enterococcus faecalis
Lactobacillus fermentum
other

Figure 20: ITS and Shotgun sequencing optimization. A-B) Titration of input DNA (Zymo mock community) into ITS PCR. **A)** Tapestation gel image after 1st ITS PCR; red arrows indicate expected fungi bands. **B)** Quantification of Tapestation band intensities of each fungi. **C-D)** 1st PCR and ITS sequencing of Zymo mock community after DNA extraction with three different kits. **C)** Tapestation gel images after 1st ITS PCR. **D)** Taxonomic distribution after ITS sequencing. **E-F)** 2nd PCR and ITS sequencing of stool samples after DNA extraction with three different kits. **E)** Tapestation gel images after 2nd ITS PCR. **F)** Taxonomic distribution after ITS sequencing, top 5 genera described. **G-H)** 2nd PCR and ITS sequencing of pure fungi strains, a mixed consortium, and the mix spiked into a stool sample (spike: 10^7 fungi cells). **G)** Tapestation gel images after 2nd ITS PCR. **H)** Taxonomic distribution after ITS sequencing. **I)** Taxonomic distribution after Shotgun sequencing of the Zymo mock community, mix of fungi strains, and the mix spiked into a stool sample. QP: Qiagen Power Soil Pro kit; Inv: Invitrogen PureLink DNA isolation kit; QF: Qiagen FastTissue kit; Extr: extraction; bp: base pairs; m: mock; x/10: heating, 10 min beating; x/30: heating, 30 min beating; -/10: no heating, 10 min beating; -/30: no heating, 30 min beating.

Some of the taxa detected even belonged to the kingdom of plants, suggesting that the QP kit can also extract DNA from food components. Based on this, the QP kit emerged as the best fit for fungal community DNA extraction, and was used as the standard from hereon.

As a next step, I aimed to test whether the fungi species of interest could be detected, and to which capacity. Therefore, I sequenced each of them separately, mixed together at equal numbers of cells (mix), or amount of DNA (mix DNA), and finally spiked the mix into a stool sample at two different concentrations for extraction. The five fungi had different amplicon lengths as visible by the bands of the Tapestation gel (**Figure 20G**), and could all be correctly identified alone, in the mix, and in the spikes at a species-level resolution except for *S. cerevisiae*, which only reached genus level identification. (**Figure 20H**). However, there was considerable bias visible already in the mix DNA with an overrepresentation of *Saccharomyces*, which counted for up to 80 % of the relative frequency. In the extracted mix less *M. globosa* could be detected compared to the mix DNA, suggesting an extraction bias, which was also visible in the spiked samples, where still all species could be detected at both dilutions (**Figure 20H**). In conclusion, ITS sequencing allowed sensitive detection of fungi species and identified many species in the stool samples that might have been present only in low amounts. However, there was a bias towards certain species that could be a result of varying gene copy numbers, extraction efficiency, primer affinity, and database representation, which could skew community composition results severely and needs to be taken into consideration for further analysis.

7.2.1.3 Shotgun metagenomic sequencing

Shotgun metagenomic sequencing has the major advantage that fungi, bacteria and host features can be detected at the same time. Therefore, I tested the detection of the commercial mock community, the fungi mix, and spiking of the stool sample with the fungi mix at two concentrations by Shotgun sequencing. Analysis of the commercial mock community showed that it was possible to detect the bacteria as well as the fungi, although the fungi were detected at low percentages (**Figure 20I**). In the fungi mix, all five fungi could be detected and identified correctly at a species level, with less *M. globosa* detected after extraction compared to the DNA mix, similar to what was

observed with ITS sequencing, suggesting that it might indeed be harder to extract DNA from it under the currently used conditions. Apart from this bias, the distribution between the species was much more even compared to the ITS sequencing analysis (**Figure 20H, I**). Detection of fungi after spiking of the mix into the stool sample was only possible at the higher concentration, where four of the five fungi could still be detected at low abundances around 0.11 % to 2.03 % while *M. restricta* was not detectable (**Figure 20I**). This demonstrated the detection limit of this method, that is dependent on the sequencing depth used, since no other non-spiked fungi were detected in the stool, even though ITS sequencing could detect several species (**Figure 20F, I**). Shotgun sequencing although convenient for unbiased whole community detection is limited by its sequencing depth, which can be adjusted depending on the specific focus of the investigation.

7.2.2 Brief characterization of the SPF mice mycobiome in the DKFZ mouse facility

Before colonizing SPF mice, I tested the fungi baseline levels to assess if it would be necessary to administer an antifungal pretreatment. For this purpose, I collected several tissues and stool contents from four untreated SPF mice housed in the animal facility of the DKFZ with different cleanliness states, from the kidney and liver to different gastrointestinal tract tissues and stool contents. The DNA was extracted and qPCR was used to discern the levels of colonization in each tissue and stool contents. Bacterial colonization, as measured by 16S, was as expected present in samples from stool content, small intestine content, and to a lesser extent in the stomach, the colon and small intestinal mucosa, but absent in the liver and kidney (**Figure 21A**). Primers for both 18S or ITS were used to check for the presence of any eukaryotes or fungi specifically, but there was no signal in any mouse for any of the tissues (**Figure 21B-C**). This was also confirmed by culturing, where no fungi colonies grew out from fecal pellets on Chromagar/Sabouraud plates (data not shown). Since it is known that fungi can overgrow in the intestine of humans after antibiotics exposure [73-75], stool samples of SPF mice that had been treated with a four-way antibiotics mix for one week were also cultured, to check if there was a fungal bloom. No growth could be detected under the specific growth conditions (Chromagar/Sabouraud plates under aerobic conditions; data not shown). Selected stool samples were then subjected to ITS sequencing, and while there were a few bands visible on the Tapestation gel, they remained faint even after the second PCR (**Figure 21D**) and taxonomic analysis showed a large variety of fungi, suggesting that many of them might be environmental contaminants rather than gut colonizers (**Figure 21E**). Wildling mice have been specifically designed to have a more “natural” and diverse microbiome [135], therefore, I also sequenced one wildling stool sample. The bands on the Tapestation gel were much more intense and taxonomic analysis revealed a specific fungi: *Kazachstania pintolopesii* (**Figure 21D-E**), which was previously reported to be present in mice

[227]. The detection of a feasible fungi species with our processing pipeline in the wildling mouse strengthens our finding of no or low amounts of fungi in the antibiotics-treated SPF mice that could interfere with our colonization attempts.

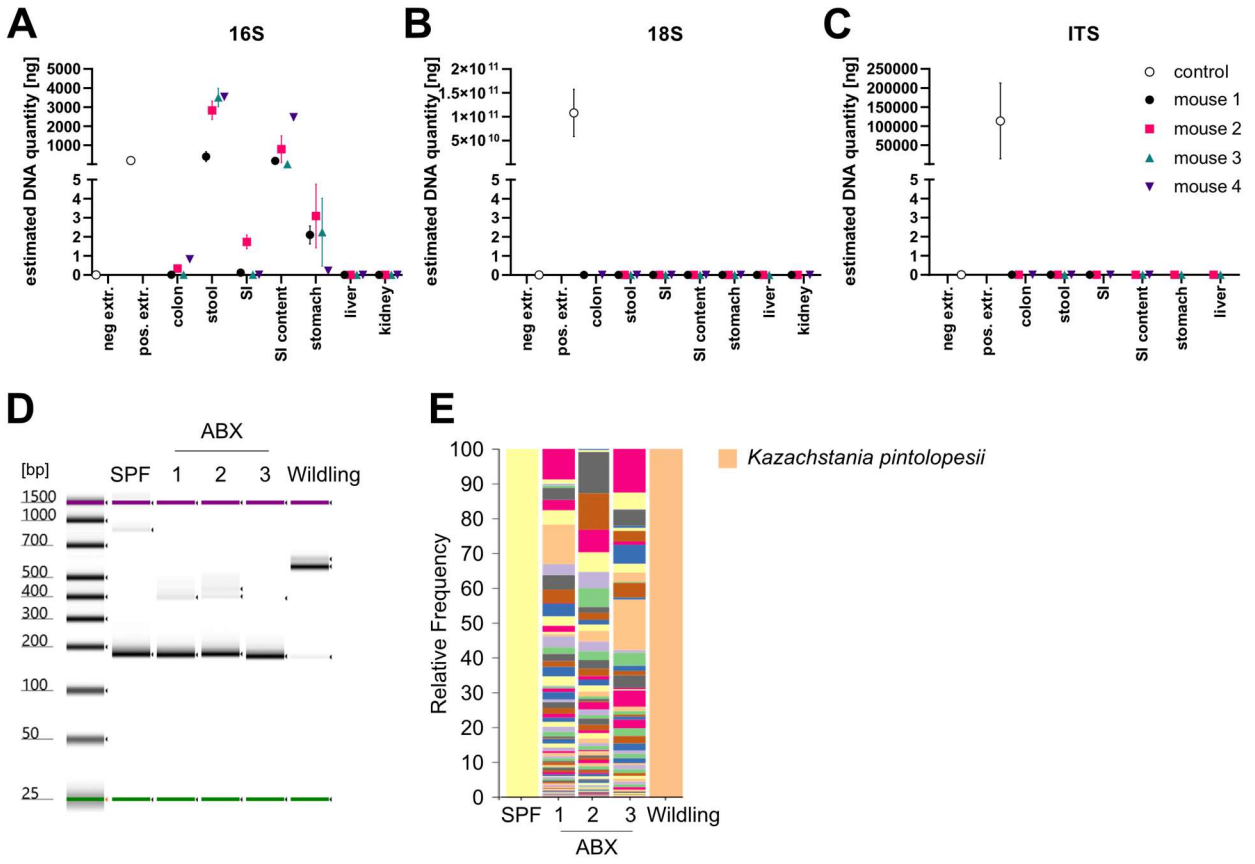

Figure 21: Background mycobiome in SPF mice of the DKFZ mouse facility. A-C) qPCR on DNA extracted from four different SPF mice using **A)** 16S primers with DNA extracted from *Fusobacterium nucleatum* as the positive control; **B)** 18S and **C)** ITS primers with DNA extracted from *C. albicans* as the positive control. **D-E)** ITS sequencing of stool samples from mice treated with 4-way ABX for one week (Metronidazole 0.25 g/L, Vancomycin 0.5 g/L, Ampicillin and Neomycin 1 g/L). **D)** Tapestation gel image after 2nd ITS PCR. **E)** Taxonomic distribution after ITS sequencing. SI: small intestine; extr: extraction; ABX: antibiotics; SPF: specific pathogen free.

7.2.3 *Candida albicans*: successful colonization

The first fungi species chosen for initial colonization tests was *Candida albicans*. The following experiments in this chapter that were conducted at the Weizmann Institute of Science (WIS) were performed together with Dr. Sara Federici, Dr. Denise Kviatcovsky, and Dr. Dragos Ciocan. Regular SPF mice were pretreated with a 4-way ABX mix for three days (DKFZ) or six days (WIS) respectively, followed by three days of oral gavage with the fungi suspension, while maintaining the ABX treatment. Colonization was monitored by stool collection and subsequent culturing,

allowing assessment of the fungi load in the intestine by proxy. *C. albicans* successfully colonized over a period of eight weeks in the mouse facilities of two different institutes, DKFZ and WIS (**Figure 22A**). After eight weeks, mice were sacrificed and tissues were collected and cultured to assess the extent of fungal colonization or infection. The entire intestine from the duodenum to the colon was successfully colonized at the mucosal and the intestinal content levels of these tissues with an increase in fungal load along the progression of the intestine, and in the content versus the mucosa (**Figure 22B-C**). Other organs, such as liver, kidney, adrenal gland, heart, lung, or mesenteric lymph nodes, did not show any fungi growth (data not shown). This confirmed that *C. albicans* could successfully colonize ABX-treated SPF mice independently of the vivarium without culminating in a systemic infection, but remaining in a commensal state along the gastrointestinal tract.

To test the colonization behavior of *C. albicans* in other conditions, germ-free (GF) mice that were transferred to the biosafety level 2 (BSL2) room were colonized by either three or one time oral gavage in both males and females. Results pooled from four independent experiments showed that *C. albicans* could colonize for an eight-week period the entire intestinal tract without causing a systemic infection, with no difference between males or females or the number of initial gavages (**Figure 22D-F**). However, three initial gavages remained as the default for further experiments.

To ensure that this was not specific to the particular mouse strain used (C57BL/6), GF Swiss-Webster mice, an outbred mouse strain, were colonized with *C. albicans*. The overall colonization levels were lower compared to the GF C57BL/6 mice, and required an additional gavage during the experiment (**Figure 23A**). At the endpoint, all mice except for one still had *C. albicans* present in the intestinal content of at least one section of the intestine even if it could not be detected in the mucosal tissue (**Figure 23B-C**).

Finally, another mouse strain, FVB, was used in an extremely controlled isolator environment to analyze the colonization capabilities with no other bacteria present. For this, GF mice in a dedicated GF isolator were colonized with *C. albicans* via oral gavage. *C. albicans* remained at high colonization levels over a period of twelve weeks and was present in both the mucosa and the intestinal content along the entire intestine (**Figure 23D-F**). In conclusion, *C. albicans* successfully and consistently colonized at various levels of background microbiomes, from ABX-treated SPF mice to GF isolator-housed mice, and in different mouse strains.

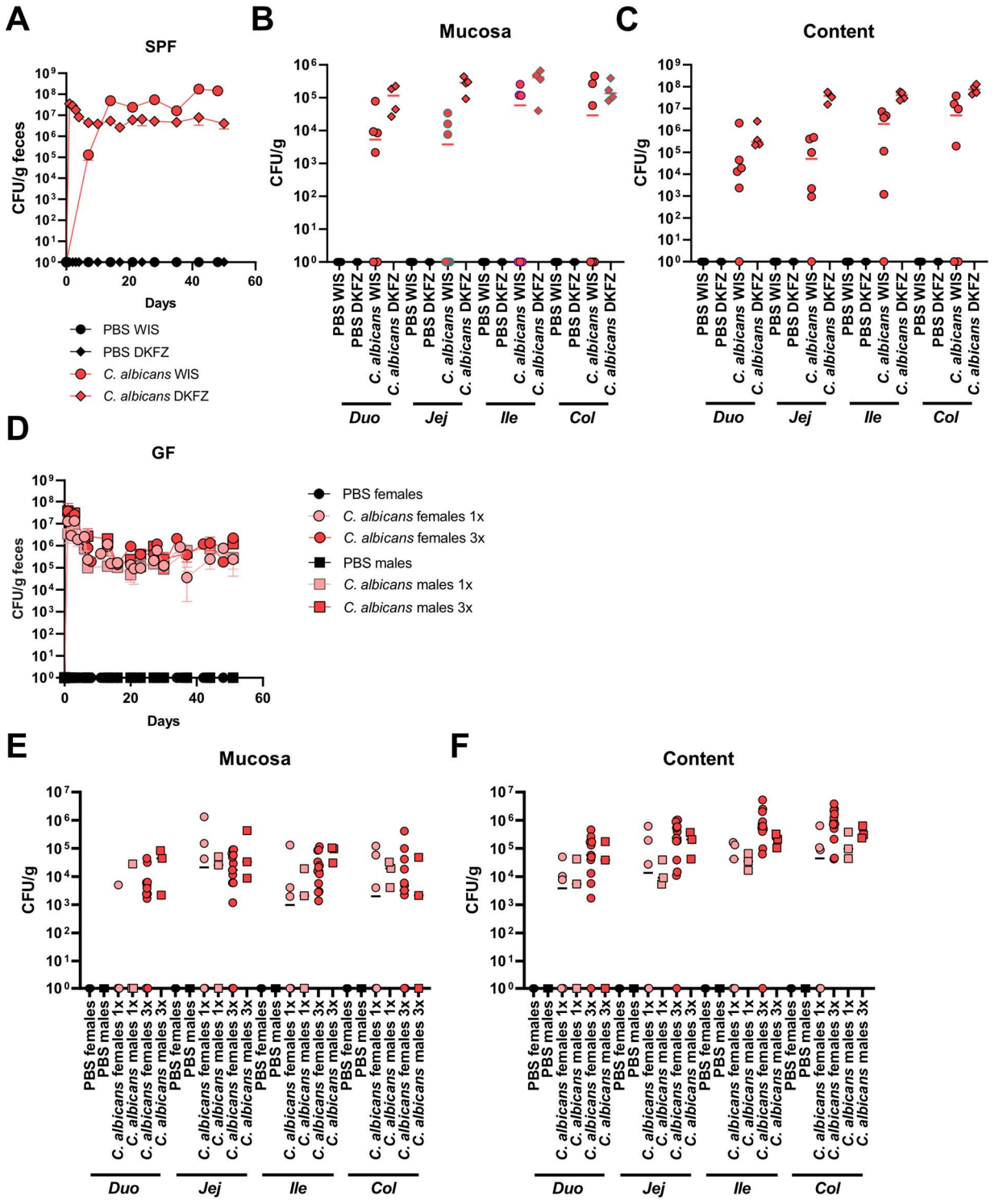

Figure 22: *Candida albicans* colonization in ABX-treated SPF and GF C57BL/6 mice. A-C) Colonization of ABX-treated SPF female mice housed in two different vivaria (n=5-6). **A)** CFU counts over time. **B-C)** Colonization of various regions of the GI tract at the time point of sacrifice (8 weeks) in the **B)** mucosa and **C)** intestinal content. **D-F)** Colonization of GF mice, males and females, with 1x or 3x initial *C. albicans* gavage. Pooled from four independent experiments (n=3-16). **D)** CFU counts across time. **E-F)** Colonization of various regions of the GI tract at the time point of sacrifice (8 weeks) in the **E)** mucosa and **F)** content. ABX: antibiotics; SPF: specific pathogen free; GF: germ-free; WIS: Weizmann Institute of Science, Israel; DKFZ: German Cancer Research Center, Germany; CFU: colony forming units; Duo: duodenum; Jej: jejunum; Ile: ileum; Col: colon; GI: gastrointestinal; BL6: C57BL/6 mice.

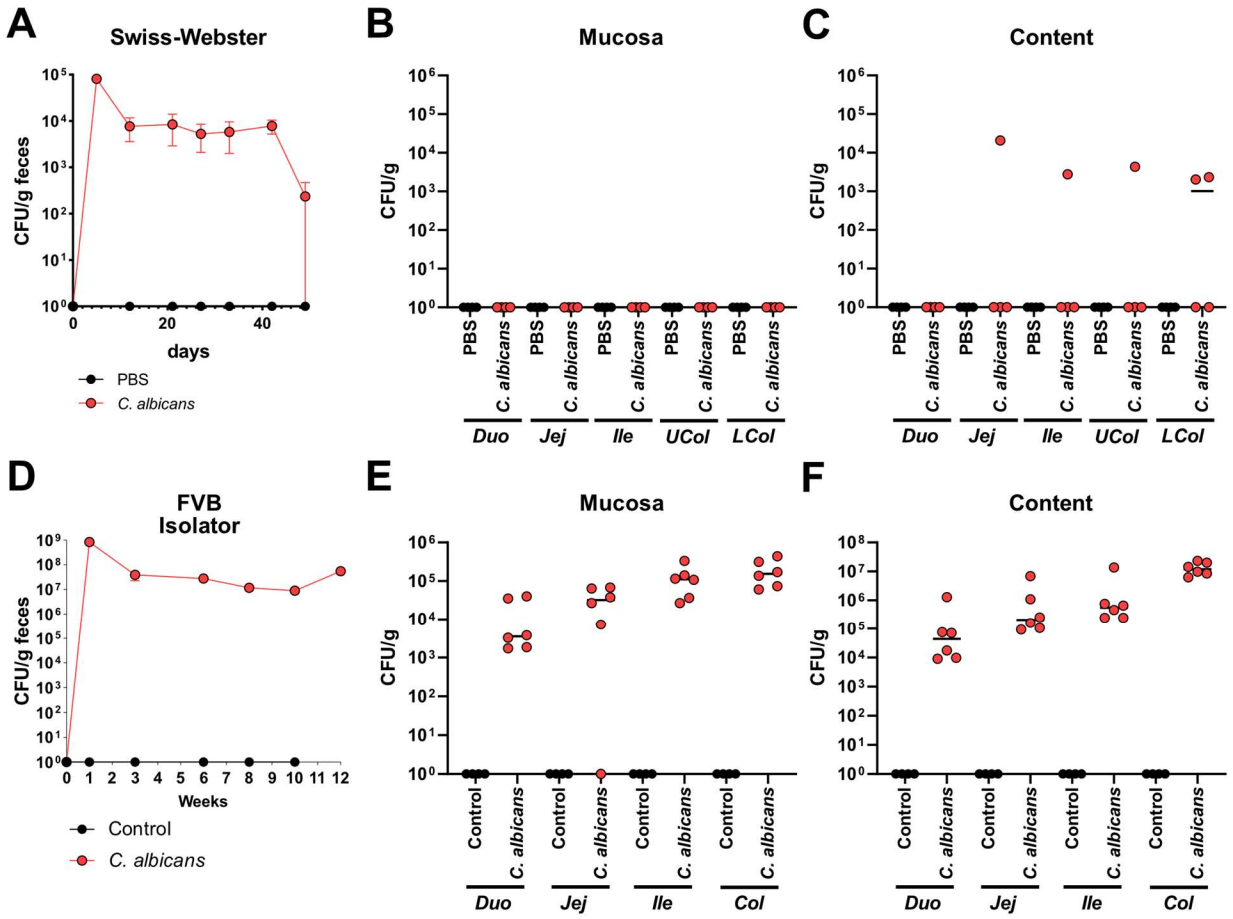

Figure 23: *Candida albicans* colonization in Swiss-Webster GF and isolator-housed mice. A-C) Colonization of Swiss-Webster GF female mice (n=4). **A)** CFU counts over time. **B-C)** Colonization of various regions of the GI tract at the time point of sacrifice (8 weeks) in the **B)** mucosa and **C)** content. **D-F)** Colonization of isolator-housed FVB female mice (n=4-7). **D)** CFU counts over time. **E-F)** Colonization of various regions of the GI tract at the time point of sacrifice (8 weeks) in the **E)** mucosa and **F)** content. GF: germ-free; CFU: colony forming units; Duo: duodenum; Jej: jejunum; Ile: ileum; Col: colon; UCol: upper colon; LCol: lower colon; GI: gastrointestinal.

7.2.4 *Saccharomyces cerevisiae*, *Malassezia globosa* and *Malassezia restricta*: examples of non-successful colonization

Since colonization with *C. albicans* proved successful, the same colonization scheme was applied to the remaining selected fungi species. An initial three times oral gavage with *S. cerevisiae* in ABX-treated SPF mice was performed as a first colonization attempt. Monitoring the colonization by culturing revealed that the fungi was lost within seven days and no fungi could be recovered from the intestine at the experimental endpoint after 14 days (**Figure 24A**). To check whether this was also the case in a cleaner setting, together with Dr. Sara Federici and Dr. Denise Kviatcovsky, we aimed to colonize GF mice that were moved to the BSL2 room, with *S. cerevisiae*.

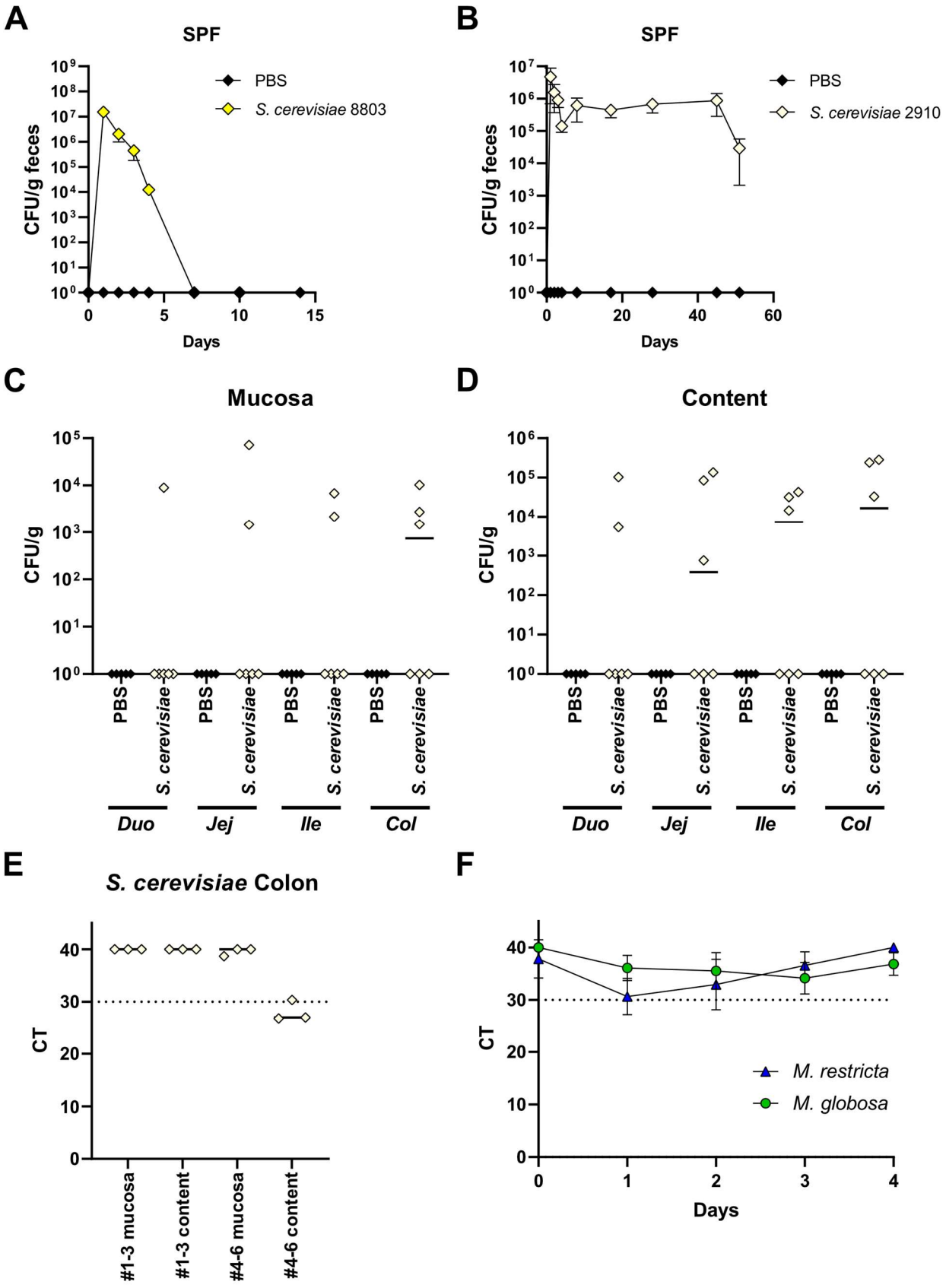
A
SPF
PBS
S. cerevisiae 8803
CFU/g feces
Days
B
SPF
PBS
S. cerevisiae 2910
CFU/g feces
Days
C
Mucosa
CFU/g
PBS
S. cerevisiae
Duo
Jej
Ile
Col
D
Content
CFU/g
PBS
S. cerevisiae
Duo
Jej
Ile
Col
E
S. cerevisiae Colon
CT
#1-3 mucosa
#1-3 content
#4-6 mucosa
#4-6 content
F
CT
M. restricta
M. globosa
Days

Figure 24: *Saccharomyces cerevisiae*, *Malassezia globosa* and *Malassezia restricta* colonization trials. A-B) CFU counts over time of ABX-treated SPF female mice at DKFZ **A)** *S. cerevisiae* strain 8803 (n=6) and **B)** *S. cerevisiae* strain 2910 (n=6). **C-E)** Colonization of various regions of the GI tract at the time point of sacrifice (8 weeks) as measured by **C-D)** plating in the **C)** mucosa and **D)** content and **E)** by qPCR of the colon mucosa and content (n=6, housed in two cages). Undetermined values set to CT 40. **F)** qPCR of *M. globosa* and *M. restricta* levels in stool samples after oral gavage of ABX-treated SPF female mice, n=6. Undetermined values set to CT 40. ABX: antibiotics; SPF: specific pathogen free; DKFZ: German Cancer Research Center, Germany; CFU: colony forming units; Duo: duodenum; Jej: jejunum; Ile: ileum; Col: colon; CT: cycle threshold.

The colonization capacity was also rapidly lost as measured by colony growth from stool samples (data not shown). The strain of *S. cerevisiae* used in these experiments (#8803) is a reference laboratory strain that might not be adapted to the gut growth conditions, therefore, I used a different strain, #2910, which was originally isolated from human feces. ABX-treated SPF mice receiving this strain could retain it longer, with levels dropping only after seven weeks (**Figure 24B**). At the eight weeks endpoint, fungal growth was evident only in the stool content and mucosa of three mice from the same cage, confirmed by culturing and qPCR (**Figure 24C-E**). While the second *S. cerevisiae* strain showed better colonization behavior initially, it still could not consistently colonize the mouse gut and had cage-dependent effects, therefore it did not act as a true commensal under these circumstances.

Additionally, I also tested the gut-colonization capacity in ABX-treated SPF mice of two other fungi: *Malassezia globosa* and *Malassezia restricta*. Since these two fungi species do not grow as single colonies, qPCR in addition to culturing was used to monitor colonization with species-specific primers. Cycle threshold (CT) values were over 30 even one day after gavage (**Figure 24F**), suggesting that there was no fungal signal and the fungi were not colonizing but immediately excreted. In line with this, no fungal outgrowth was observed after plating during the experiment (data not shown) and at the eight weeks endpoint no fungal signal was detected in neither the stool content nor the mucosa in any of the intestinal regions in (data not shown because CT values were undetermined). Since the fungi appeared to be excreted immediately after oral gavage and it is unclear also in humans if they are intestinal commensals or only transient, no further colonization attempts were undertaken.

7.2.5 *Candida tropicalis*: a curious case

Out of all of the fungi species tested, *C. albicans* was the most successful one, therefore I aimed to test if other *Candida* strains, such as *Candida tropicalis* would also present similar colonization behavior. All the following experiments in this chapter were conducted in collaboration with Dr. Sara Federici, Dr. Denise Kviatcovsky, and Dr. Dragos Ciocan, unless specified to have been conducted at the DKFZ. Similar to previous experiments, SPF mice were pre-treated for either

three days or six days with 4-way ABX in two different mouse facilities at the DKFZ in Germany or the WIS in Israel, respectively. The mice were orally gavaged with the fungal suspension for three consecutive days over a period of eight weeks with continuous ABX exposure. Colonization was monitored via culturing of fecal pellets across time. In both vivaria, mice were successfully colonized throughout this time period and along the entire GI tract (**Figure 25A-C**).

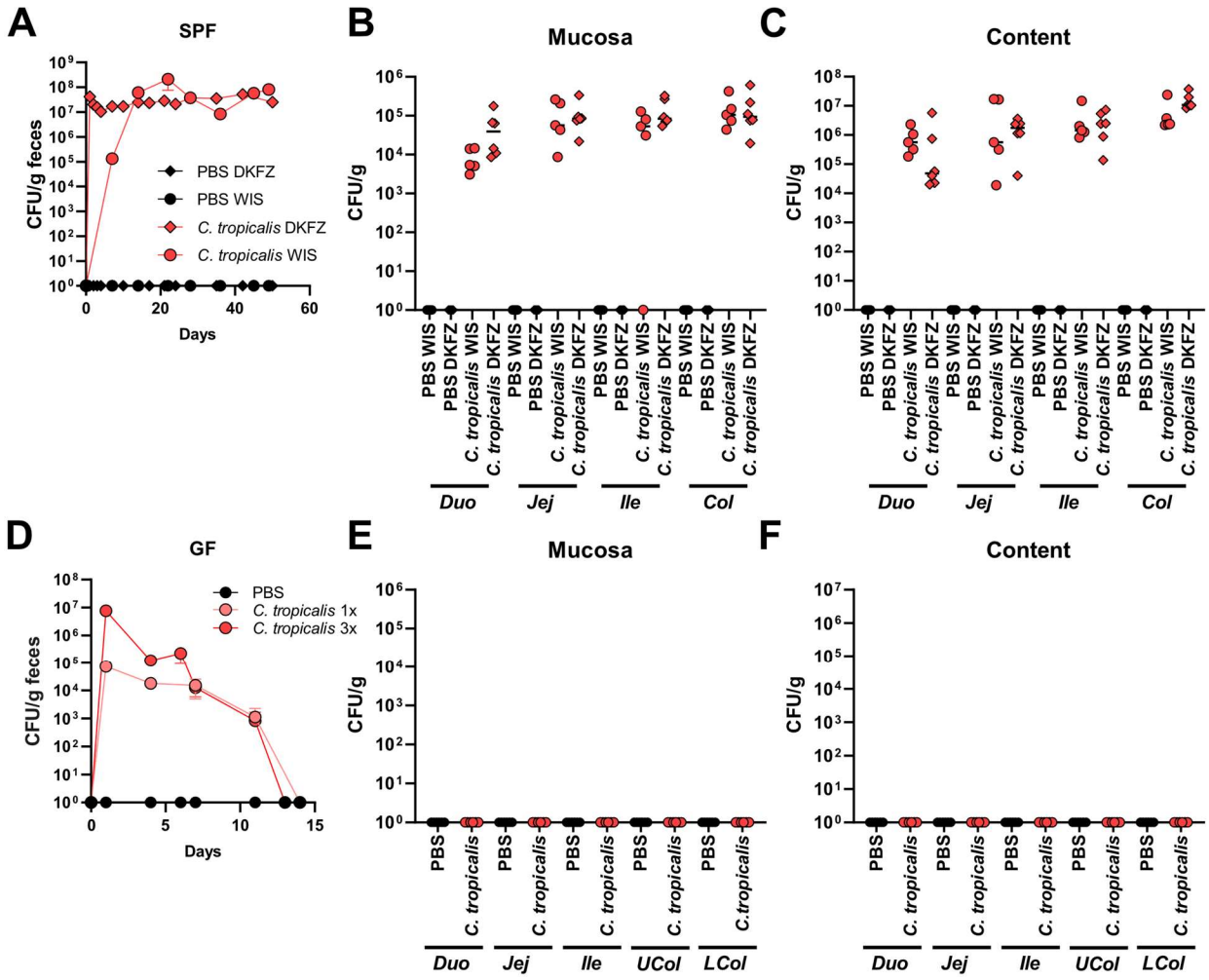

Figure 25: *Candida tropicalis* colonization in ABX-treated SPF and GF C57BL/6 mice. A-C) Colonization of ABX-treated SPF female mice housed in two different vivaria (n=5-6). **A)** CFU counts over time. **B-C)** Colonization of various regions of the GI tract at the time point of sacrifice (8 weeks) in the **B)** mucosa and **C)** content. **D-F)** Colonization of GF mice in males and females with 1x or 3x initial gavage. **D)** CFU counts over time. Pooled from three independent experiments (n=3-13). **E-F)** Colonization of various regions of the GI tract at the time point of sacrifice (8 weeks) in the **E)** mucosa and **F)** content. ABX: antibiotics; SPF: specific pathogen free; GF: germ-free; WIS: Weizmann Institute of Science, Israel; DKFZ: German Cancer Research Center, Germany; CFU: colony forming units; Duo: duodenum; Jej: jejunum; Ile: ileum; Col: colon; UCol: upper colon; LCol: lower colon; GI: gastrointestinal.

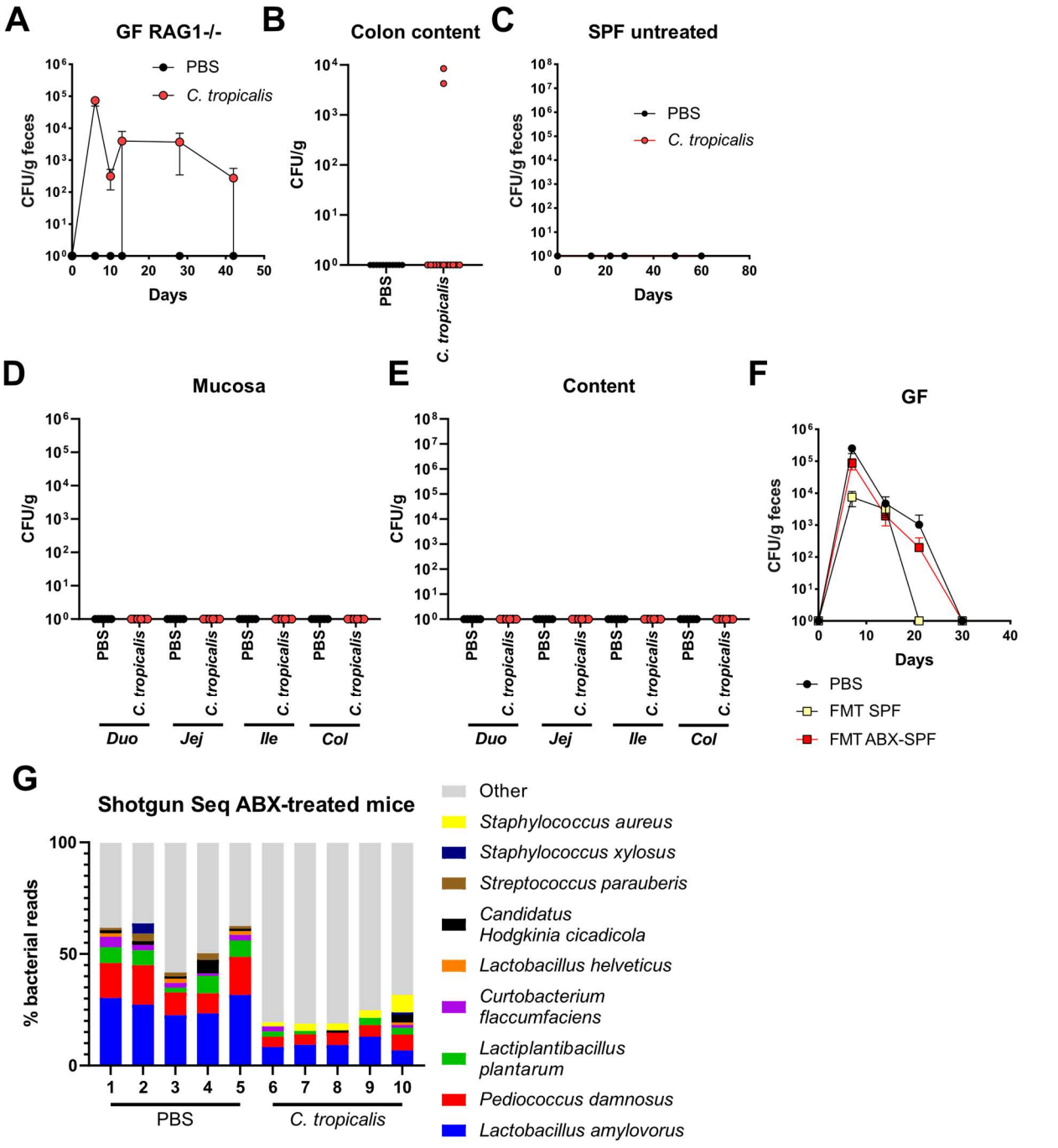

Figure 26: *Candida tropicalis* colonization in GF RAG1-/-, untreated SPF and GF C57BL/6 mice with FMT. A-B) Colonization of GF RAG1-/- male and female mice. Pooled from three independent experiments (n=12-13). **A)** CFU counts over time. **B)** Colonization of colon content at the time point of sacrifice (8 weeks). **C-E)** Colonization of untreated SPF female mice (n=6). **C)** CFU counts over time. **D-E)** Colonization of various regions of the GI tract at the time point of sacrifice (8 weeks) in the **D)** mucosa and **E)** content. **F)** CFU counts across time of GF C57BL/6 mice colonized with *C. tropicalis* after FMT from untreated or ABX-treated SPF mice (n=6-7). **G)** Taxonomic distribution after Shotgun metagenomic sequencing of ABX-treated SPF mice. Species depicted had an abundance of over 1 % of the total bacterial reads and were present in two or more samples. ABX: antibiotics; SPF: specific pathogen free; GF: germ-free; CFU: colony forming units; Duo: duodenum; Jej: jejunum; Ile: ileum; Col: colon; GI: gastrointestinal; RAG1: recombination-activating gene 1; FMT: fecal microbiota transplantation.

The success of this colonization encouraged the use of GF mice that were transferred to the BSL2 room, and immediately colonized with *C. tropicalis*. Surprisingly, the colonization was lost after a maximum of 14 days, independently of an initial one or three times gavage (**Figure 25D**). Three independent experiments were performed and the results were consistent across repeats. After eight weeks, no fungal outgrowth could be detected at any section of the intestine, neither the mucosa nor the stool content (**Figure 25E-F**). Such results were unexpected considering that the colonization in ABX-treated mice prevailed.

To evaluate if the adaptive immune system, which is developed differently in GF mice [140] might play a role in preventing colonization, GF RAG1-/- mice that lack functional T and B cells were used to colonize with *C. tropicalis*. After oral gavage with the fungi, no consistent colonization could be achieved in three independent experiments. Across the eight week time period, two single mice retained the fungi in the colon content, showing high levels of colonization, the remaining animals lost it completely (**Figure 26A-B**). These results suggest that the main driver of this effect was not the adaptive immune system.

Another hypothesis was that *C. tropicalis* actually requires a background microbiome to support colonization. Therefore, SPF mice that were not treated with ABX were orally gavaged with *C. tropicalis*. *C. tropicalis* could not colonize, as visible by the lack of colonies in stool over time and in tissue and content at the end time-point (**Figure 26C-E**). This is in line with other studies reporting that colonization with *Candida* strains in mice requires some type of clearing of the microbial niche for an advantageous growth [228]. Considering that ABX treatment changes the ecological niche not only by affecting the bacterial number, but also composition [229, 230], the colonization of *C. tropicalis* might depend on the presence of certain bacterial species in ABX-treated mice. Therefore, one day before *C. tropicalis* colonization, GF mice received a fecal microbiota transplantation (FMT) from either ABX-treated or untreated SPF mice, to establish a different background microbiome. Despite of this pretreatment, *C. tropicalis* colonization was also lost over time (**Figure 26F**). To understand which species are present in ABX-treated SPF mice that would support *C. tropicalis* colonization, stool samples from ABX-treated SPF mice that were colonized or not with *C. tropicalis* were analyzed by Shotgun sequencing. As a result, stool composition was shifted by the presence of *C. tropicalis*, giving raise to new species like *Staphylococcus aureus* (**Figure 26G**). Therefore, I speculated that continuous ABX exposure might be necessary to maintain the right bacterial composition that would enable *C. tropicalis* colonization.

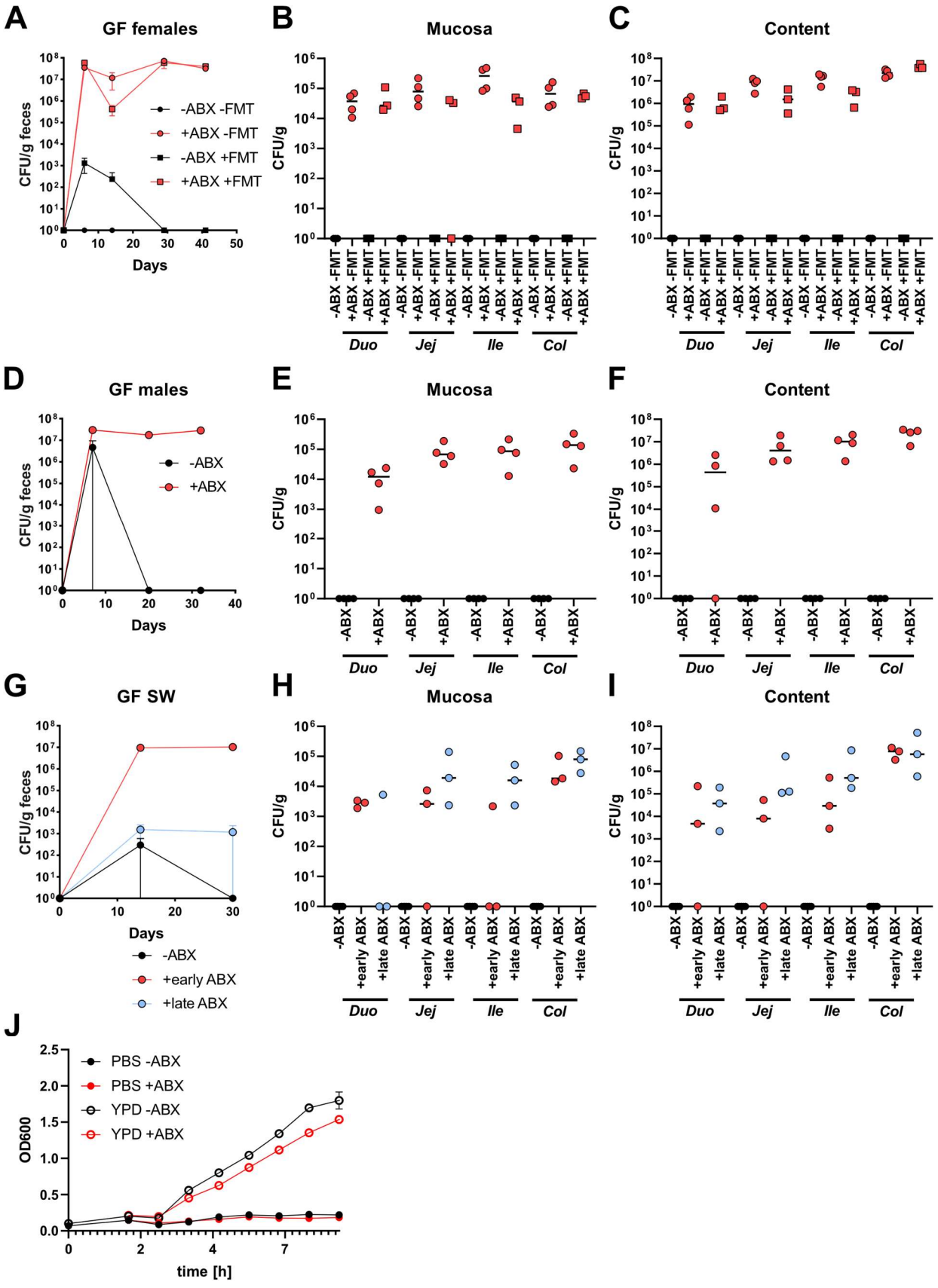
A
GF females
CFU/g feces
Days
-ABX -FMT
+ABX -FMT
-ABX +FMT
+ABX +FMT
B
Mucosa
CFU/g
C
Content
CFU/g
-ABX -FMT
+ABX -FMT
-ABX +FMT
+ABX +FMT
Duo
Jej
Ile
Col
D
GF males
CFU/g feces
Days
-ABX
+ABX
E
Mucosa
CFU/g
F
Content
CFU/g
-ABX
+ABX
Duo
Jej
Ile
Col
G
GF SW
CFU/g feces
Days
-ABX
+early ABX
+late ABX
H
Mucosa
CFU/g
I
Content
CFU/g
-ABX
+early ABX
+late ABX
Duo
Jej
Ile
Col
J
OD600
time [h]
PBS -ABX
PBS +ABX
YPD -ABX
YPD +ABX

Figure 27: *Candida tropicalis* colonization in ABX-treated GF C57BL/6 mice. A-C) Colonization of GF female mice with or without ABX treatment with or without FMT (n=3-5). **A)** CFU counts over time. **B-C)** Colonization of various regions of the GI tract at the time point of sacrifice (8 weeks) in the **B)** mucosa and **C)** content. **D-F)** Colonization of GF male mice with or without ABX treatment (n=4). **D)** CFU counts over time. **E-F)** Colonization of various regions of the GI tract at the time point of sacrifice (8 weeks) in the **E)** mucosa and **F)** content. **G-I)** Colonization of SW GF mice with or without ABX treatment from the start (early) or late (after four weeks) time-point (n=3-5). **G)** CFU counts over time. **H-I)** Colonization of various regions of the GI tract at the time point of sacrifice (8 weeks) in the **H)** mucosa and **I)** content. **J)** In vitro growth curves of *C. tropicalis* in PBS or YPD medium with or without ABX (n=3). ABX: antibiotics; SPF: specific pathogen free; GF: germ-free; CFU: colony forming units; Duo: duodenum; Jej: jejunum; Ile: ileum; Col: colon; GI: gastrointestinal; FMT: fecal microbiota transplantation; SW: Swiss-Webster; PBS: phosphate-buffered saline; YPD: yeast peptide dextrose.

Thus, as a next step, female C57BL/6 GF mice transferred to the BSL2 room received a FMT from ABX-treated SPF mice, followed by oral gavage with *C. tropicalis*. These mice were separated into two groups that did or did not receive continuous ABX administration. In order to allow the bacterial community from the FMT to stabilize after administration to the mice, five days were maintained between FMT and *C. tropicalis* inoculation with or without ABX treatment. Strikingly, *C. tropicalis* could colonize in mice receiving ABX, independently of the FMT, for an eight-week period (**Figure 27A**) and throughout the entire intestine in both, the mucosa and content (**Figure 27B-C**). To determine if this was reproducible and sex-independent, male GF C57BL/6 mice were orally inoculated with *C. tropicalis* and maintained with or without ABX. ABX treatment allowed *C. tropicalis* colonization also in males over the extended period, and across the GI tract (**Figure 27D-F**). Finally, to check whether this was specific to the C57BL/6 strain, SW mice were treated as previously described, and similarly ABX treatment was the determining factor for successful *C. tropicalis* colonization (**Figure 27G-I**). Additionally, another factor was considered, instead of immediate and continuous ABX exposure, mice started to be treated with ABX four weeks after *C. tropicalis* inoculation, a time point where they had most likely lost the colonization (**Figure 27G**). Upon ABX treatment, *C. tropicalis* levels raised back again with no difference in intestinal colonization levels between early and late ABX exposure after eight weeks (**Figure 27H-I**). This suggests, that *C. tropicalis* colonization is not completely lost but could be present either at very low levels making its detection by culturing unlikely, in another intestinal compartment like the cecum that was not tested by culturing, or recovered through coprophagy.

To explain this striking phenotype, I tested if the ABX used have a direct effect on the growth of *C. tropicalis* in an in vitro culture experiment. *C. tropicalis* was grown either in a nutrient free or rich environment, PBS or YPD broth respectively, with or without the addition of ABX mixture. The ABX mix did not exert a direct growth-promoting effect on the fungus when grown in YPD broth, but rather a slight inhibitory effect, and the same effect was observed when inoculated in PBS (**Figure 27J**). I concluded that the observed effect in the in vivo setting could be due to an indirect cause.

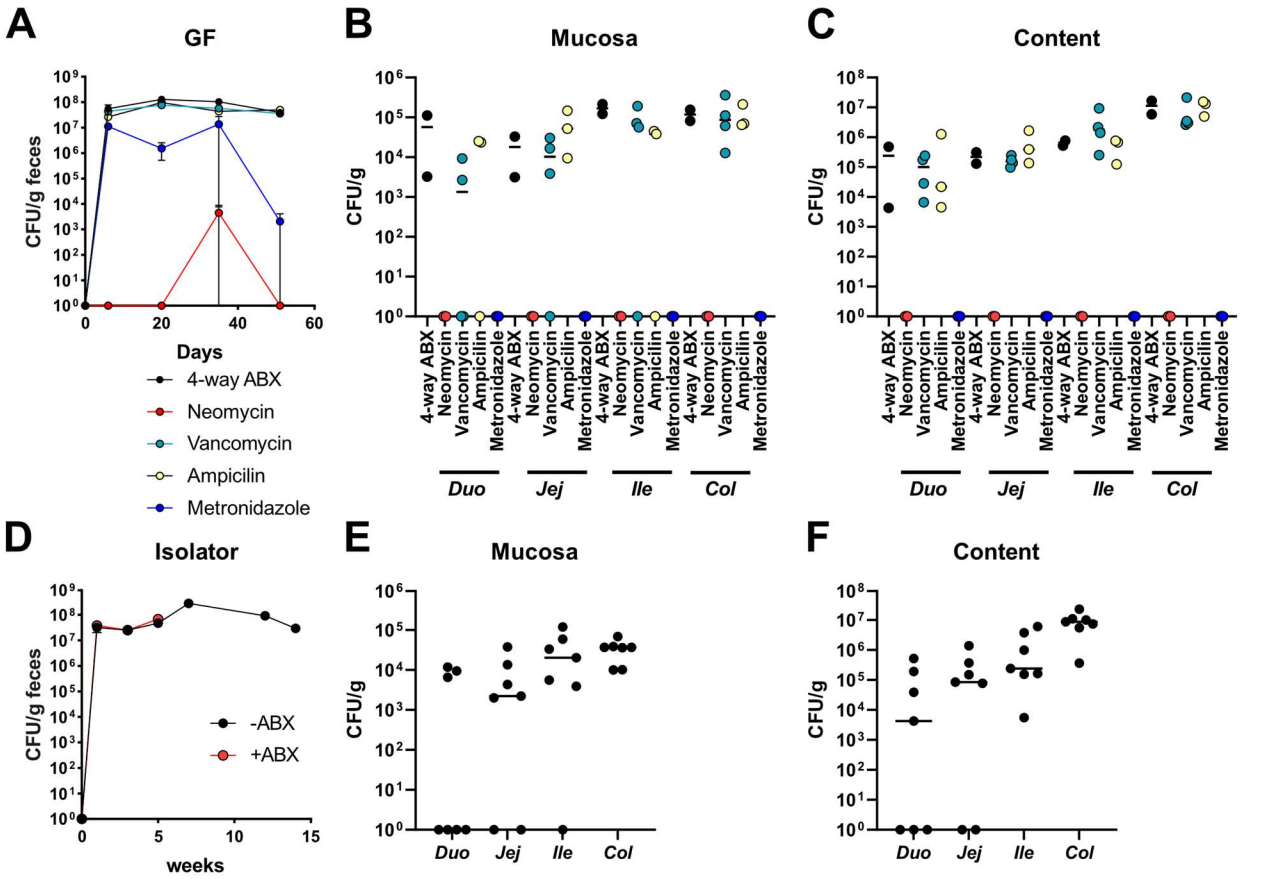

Figure 28: *Candida tropicalis* colonization in single ABX-treated GF or isolator-housed C57BL/6 mice. A-C) Colonization of GF female mice with 4-way or single ABX treatment (n=2-4). **A)** CFU counts over time. **B-C)** Colonization of various regions of the GI tract at the time point of sacrifice (8 weeks) in the **B)** mucosa and **C)** content. **D-F)** Colonization of Isolator-housed GF female mice with or without ABX treatment (n=7-10). **D)** CFU counts over time. **E-F)** Colonization of various regions of the GI tract at the time point of sacrifice (14 weeks) in the **E)** mucosa and **F)** content. ABX: antibiotics; GF: germ-free; CFU: colony forming units; Duo: duodenum; Jej: jejunum; Ile: ileum; Col: colon; GI: gastrointestinal.

Since the ABX cocktail used is a combination of four different compounds that target a broad spectrum of bacteria, I tested if and which of these ABX individually could affect the colonization on its own. In order to do so, mice were pretreated with either the 4-way ABX mix or individual ABX for one week before *C. tropicalis* administration, while being continuously treated with the respective ABX. Interestingly, treatment with Ampicillin or Vancomycin alone was sufficient to maintain *C. tropicalis* colonization, while colonization was immediately lost with Neomycin treatment and over time with Metronidazole (**Figure 28A**). After eight weeks, at the end point of the experiment, only mice that had received the 4-way mix, Ampicillin, or Vancomycin had stable levels of *C. tropicalis* in the intestinal mucosa and content (**Figure 28B-C**). The specificity of this, combined with the previous results, such as the reemergence of the colonization even after late ABX treatment, suggested that the GF mice were naturally colonized in the BSL2 room, acquiring a background microbiome. To validate this hypothesis or test if other off-target ABX effects were

responsible, a novel colonization set-up was used. GF mice were inoculated with *C. tropicalis* inside the isolator, ensuring that no background microbiome is present. The GF mice received the fungus by oral gavage and also treated with or without ABX inside the isolator. In this clean environment, the ABX were not necessary to enable *C. tropicalis* colonization, it remained high even without ABX for a 14-week period and throughout the GI tract (**Figure 28D-F**). The previously observed phenotype was thus most likely due to contamination of the ex-GF mice in the BSL2 room with a background microbiome that outcompeted *C. tropicalis*. While this was a laborious, time-consuming, and tedious process, successful *C. tropicalis* was possible, requiring an environment without certain background bacteria.

7.3 Chapter 3: Profiling Fungi-Host Interactions

7.3.1 Host intestine transcriptional response to fungi colonization

After establishing successful colonization of the mouse intestine with two different *Candida* species, I investigated the host response to this colonization by bulk RNA sequencing of the gut mucosa. The two regions that were furthest apart from each other, duodenum and colon, were profiled under varying experimental conditions with different background microbiomes. The sequencing data was analyzed in collaboration with Dr. Rafael Valdés Mas at WIS. Data from four independent experiments was analyzed separately, as well as integrated for potential overlapping features that might show a distinct response to the fungal colonization.

7.3.1.1 Antibiotics-treated SPF mice

The first RNA sequencing batch included an experiment performed at the DKFZ, with mice that were pretreated with 4-way ABX for three days, followed by colonization with either *C. albicans* or *C. tropicalis* while maintained on Ampicillin (see **Figure 22A-C** and Methods). Principal Component Analysis (PCA) of the sequencing dataset showed significant clustering firstly by tissue type and only secondly by group, with PC1 describing the separation between duodenum and colon samples (**Figure 29A**). When analyzing the samples of each type of tissue separately, most of the *Candida* samples clustered together for both the colon and the duodenum with PC2 showing a cage effect for the colon samples (**Figure 29B-C**). In the colon samples, PBS and *C. albicans* samples significantly clustered separate, whereas in the duodenum, a similar trend was observed for PBS and *C. tropicalis* samples. Comparison of differential gene expression in the colon between *C. albicans*-colonized to PBS-control mice, showed that *C. albicans* induced a downregulation of most of the genes (**Figure 29D**). Around tenfold less genes were differentially expressed in the duodenum compared to the colon (4599 in the colon vs 30 in the duodenum) following the same trend of downregulation with *C. albicans* colonization (**Figure 29E**). Colonization with *C. tropicalis* showed the same pattern, with more downregulated genes compared to the control group in both tissues, and a lower number of differentially expressed genes (DEGs) for the colon and a higher number for the duodenum compared to *C. albicans* (**Figure 29F-G**). Downregulation of genes appeared to be a general response to *Candida* colonization. Comparing the DEGs between the two *Candida* species per tissue, in the colon *C. albicans* had 3665 unique DEGs, while *C. tropicalis* only had 58, with 934 DEGs overlapping (**Figure 29H**). In contrast, *C. tropicalis* had 478 unique DEGs in the duodenum, while *C. albicans* only had three with 27 DEGs overlapping (**Figure 29H**). Based on this, I concluded that *C. albicans* seems to elicit a much stronger response in the colon and *C. tropicalis* in the duodenum, suggesting species-specificity.

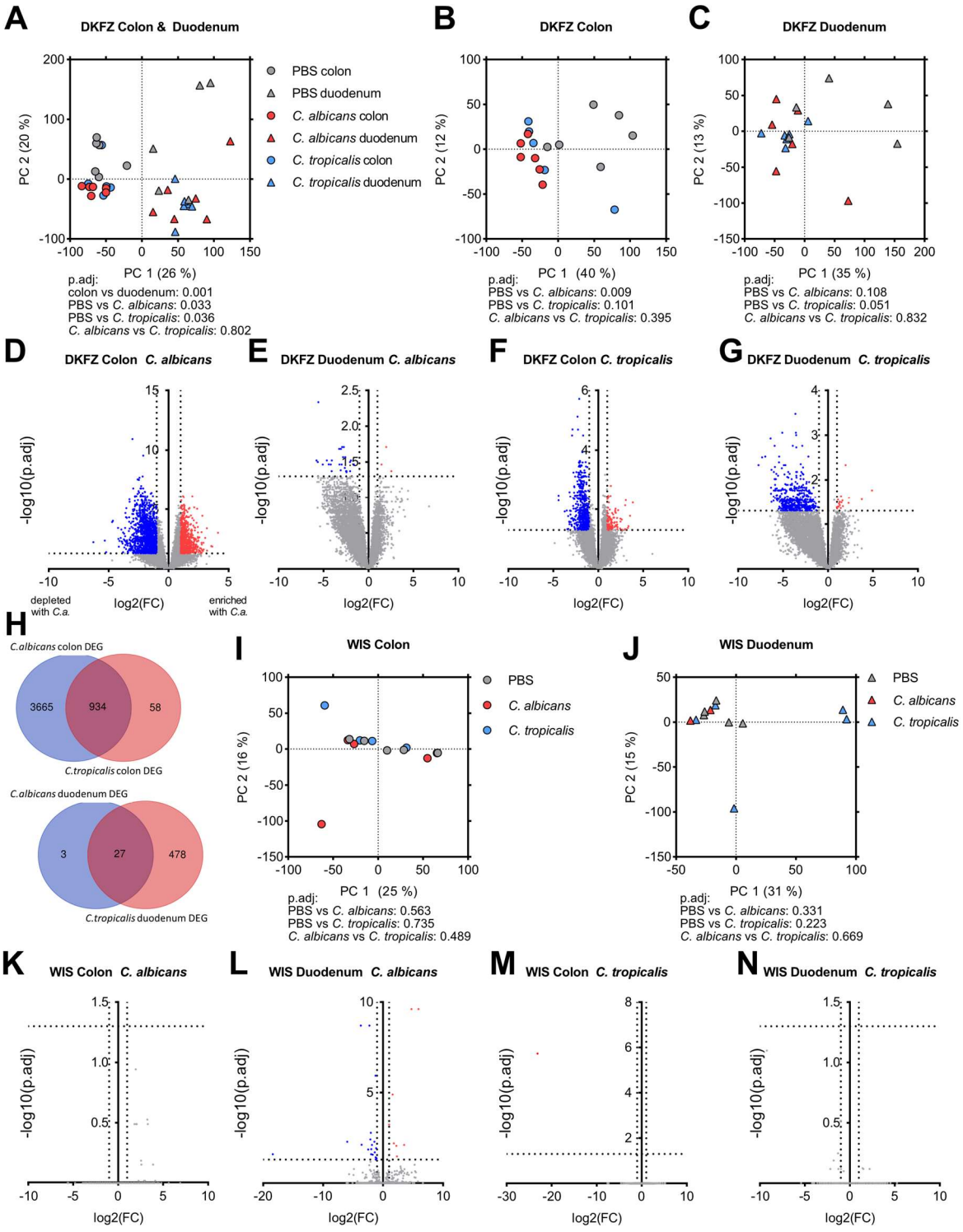

Figure 29: Host transcriptional response of the intestinal mucosa to *Candida* colonization in ABX-treated SPF mice. A-H) ABX-treated SPF mice at DKFZ. **A-C)** PCAs of **A)** all samples together, **B)** Colon and **C)** Duodenum samples analyzed separately; statistical testing between groups by PERMANOVA. **D-G)** Volcano plots after differential gene expression analysis comparing **D-E)** *C. albicans* colonized mice to controls or **F-G)** *C. tropicalis* colonized mice to controls in the **D & F)** colon, or **E & G)** duodenum. **H)** Venn diagrams of DEGs with *C. albicans* or *C. tropicalis* in the colon and duodenum. **I-N)** ABX-treated SPF mice at WIS. **I-J)** PCAs of **I)** Colon and **J)** Duodenum samples; statistical testing between groups by PERMANOVA. **K-N)** Volcano plots after differential gene expression analysis comparing **K-L)** *C. albicans* colonized mice to controls or **M-N)** *C. tropicalis* colonized mice to controls in the **K & M)** colon or **L &**

N) duodenum. ABX: antibiotics; SPF: specific pathogen free; DKFZ: German Cancer Research Center; WIS: Weizmann Institute of Science; PCA: principal component analysis; PERMANOVA: permutational multivariate statistical permutation test; DEG: differentially expressed gene.

In a separate experiment conducted at the WIS, mice were treated with 4-way ABX throughout the experiment while colonizing them with either *Candida* strain (see **Figure 22D-F**). PCA of neither the colon nor the duodenum samples showed a significant separation by experimental group (**Figure 29I-J**). Interestingly, while *C. albicans* colonization had previously elicited the strongest response in the colon, there were no significant DEGs compared to the PBS control in this experiment in the colon (**Figure 29K**), and only a few in the duodenum (**Figure 29L**). Similarly, *C. tropicalis* colonization only lead to one DEG in the colon and none in the duodenum (**Figure 29M-N**). While this is puzzling compared to the previous experiment, it is possible that differential gene expression analysis was limited in its statistical power by the low number of mice used per group (2-5 mice per group vs 6).

To see if there was still a common transcriptional signature between both experiments, I compared all the genes that had a fold change (FC) larger than 1.5 in the same direction, independent of their significance. For *C. albicans* in the colon, out of all the upregulated genes, 578 were common in both experiments, which is more than 10 %, whereas there were more than double that amount of common genes downregulated (1378) (**Figure 31A**). In the duodenum this effect was even more striking, with 306 common upregulated genes and 2598 common downregulated genes (**Figure 31E**). For *C. tropicalis* in the colon, the number of mutual up- and downregulated genes was similar with 544 upregulated and 686 downregulated ones (**Figure 31C**), while in the duodenum there were 305 common upregulated genes and 1128 common downregulated (**Figure 31G**). Overall, considering that the mice received different ABX treatment and were housed in two animal facilities with different baseline microbiomes and chows, it is not surprising that the transcriptional responses were different. The existence of an overlap of genes that were changed in the same direction despite not being necessarily significant, could be the starting point of discovering a general host response to the fungi colonization that was explored further below.

7.3.1.2 GF mice

To assess the mucosal transcriptional response to fungi in ex-GF mice that were transferred to the BSL2 room, the colon and duodenum mucosa of two independent experiments were subjected to RNA sequencing. One experiment comprised mice colonized with *C. albicans* or PBS as a control, the second experiment additionally included mice that had been colonized with *C. tropicalis* but lost colonization over time (see previous chapter). Despite having the same experimental setup, and only a few weeks passing between the two experiments, the PCAs of both tissues showed significant separation by experiment, even though they were sequenced in

the same batch (**Figure 30A, D**). When analyzing each experiment separately, the first one did show a non-significant trend towards a separation by group but was limited by the low number of mice per group (n = 3-4) (**Figure 30B, E**). For the second experiment, in the colon, *C. tropicalis* exposure induced significant separation of the samples from the other groups, whereas in the duodenum the PBS samples showed a trend towards separate clustering (**Figure 30C, F**). Differential gene expression analysis of the first experiment revealed a strong response to *C. albicans* in the colon but not in the duodenum with more downregulated genes, similar to what was shown in the first ABX-treated SPF mice cohort (**Figure 30G, H & Figure 29D, E**). The second cohort however, despite having a larger number of mice per group (n = 6) only had a small response in the colon with only five DEGs (**Figure 30I**) but a stronger response in the duodenum with more upregulated genes (**Figure 30J**).

In the same experiment, there was a significant transcriptional response to *C. tropicalis* in the colon mucosa despite the loss of colonization (**Figure 30K**) and a smaller response in the duodenum (**Figure 30L**). This was surprising since loss of the colonization had been confirmed by culturing of different compartments of the intestinal tract (**Figure 25D-F**). Enrichment analysis of the DEGs showed association of pathways with metabolic processes, stimulus, and stress (**Figure 30M**), which might be the response to the bacterial colonization that was most likely outcompeting the fungi. The background bacterial colonization could also be a possible explanation for the different transcriptional responses between the two cohorts of *C. albicans* colonization. The background microbiome that is acquired from the environment might vary based on the momentous conditions of the experiment.

To assess whether there is a consistent, fungi-dependent transcriptional response across different cohorts, I analyzed genes with a fold change greater than 1.5 that showed consistent directional changes in two cohorts with *C. albicans* colonization. This approach allowed me to account for potential differences in statistical power due to varying group sizes and identify a common transcriptional response to fungal colonization. While the majority of the genes did not overlap, there were 1238 genes in the colon commonly upregulated and 999 genes downregulated, in the duodenum 569 genes upregulated and 1637 genes downregulated (**Figure 31B, F**). Since the set-up between the two experiments was the same and the library preparation as well as the sequencing were part of the same batch, the only factor separating these experiments is most likely the acquisition of different background microbiomes due to the experiments being conducted a few weeks apart from each other. The huge impact of this on the transcriptional response is striking and concerning in regards to the reproducibility of experiments in general.

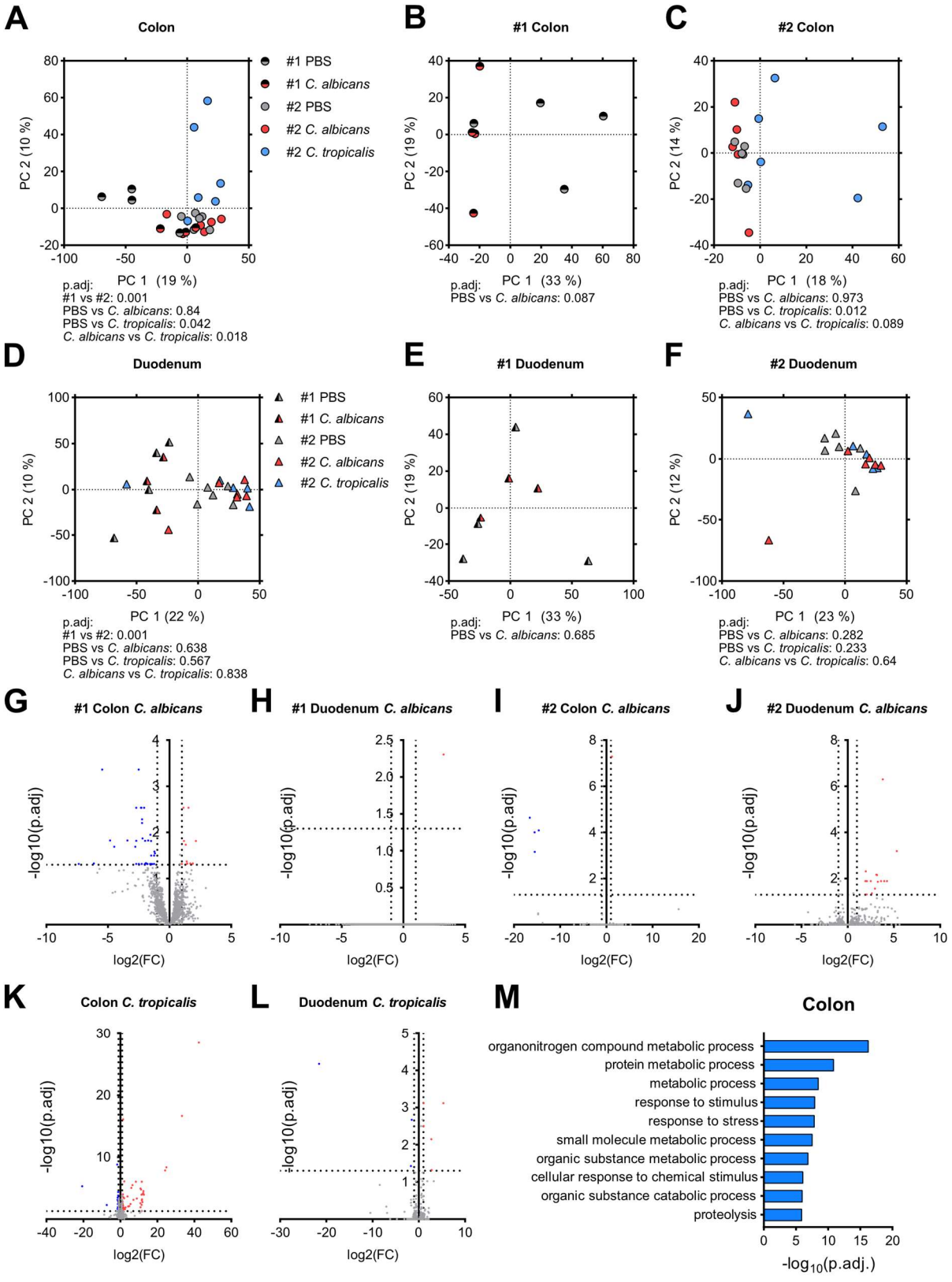

Figure 30: Host transcriptional response of the intestinal mucosa to *Candida* colonization in GF mice. A-F) PCAs of **A-C)** colon and **D-F)** duodenum samples of two cohorts analyzed **A & D)** together or separately with **B & E)** cohort #1 with PBS controls and *C. albicans* colonization and **C & F)** cohort #2 with PBS controls; *C. albicans* or *C. tropicalis*

colonization; statistical testing between groups by PERMANOVA. **G-L)** Volcano plots after differential gene expression analysis in two different cohorts **G-H)** cohort #1 and **I-L)** cohort #2, comparing **G-J)** *C. albicans* colonized mice to controls or **K-L)** *C. tropicalis* colonized mice to controls in the **G, I & K)** colon or **H, J & L)** duodenum. **M)** Pathway enrichment analysis of DEGs of colon samples of *C. tropicalis* colonized mice compared to controls. GF: germ-free; PCA: principal component analysis; PERMANOVA: permutational multivariate statistical permutation test; DEG: differentially expressed gene.

Nevertheless, I was curious to address the extent of this variability and if there was a core transcriptional response of the mucosa to the fungi colonization, that was conserved across experimental setups. Therefore, I compared the common genes from the two ABX and the two GF cohorts with each other, separated by the directionality of their FC. Out of this, in the colon only a small subset of 44 genes was mutually upregulated, and 87 genes downregulated (**Figure 31D**), while in the duodenum 26 genes were commonly upregulated and 341 genes downregulated (**Figure 31H**). To see, which were specific to the fungi species, I compared these genes to the ones with *C. tropicalis* colonization that were common in both ABX datasets. In the colon, among the upregulated genes, 16 were common for all *Candida* colonized mice, remaining 28 to be specific for *C. albicans*, and in the downregulated genes 26 as a common *Candida* response and 61 as *C. albicans* specific. Similarly in the duodenum, 6 were commonly upregulated with both *Candida* species, and 20 unique to *C. albicans*, 51 commonly downregulated and 290 *C. albicans*-specific (**Figure 31D, H**). Analysis for *C. tropicalis*-singularity was limited by their lack of colonization under GF conditions unless cultivated in a designated isolator, which was not subjected to RNA sequencing.

A robust fungi signal might be common between different areas of the intestine, so I compared if there were any common genes between the duodenum and the colon gene sets. None of the common *Candida*-response genes overlapped between the different tissues, while for the *C. albicans*-specific genes only one was commonly upregulated and two commonly downregulated (**Figure 31I**), suggesting a high degree of tissue specificity, as also observed before by separate PCA clustering (see **Figure 29A**). The one commonly upregulated gene was Immunoglobulin lambda variable 1 (Iglv1), which is suggested to be involved in an immune response [231, 232]. The two commonly downregulated genes were Sodium Voltage-Gated Channel Alpha Subunit 9 (SCN9A), involved in nociception signaling [233], and the uncharacterized gene Gm43795.

In conclusion, there are some genes that could be considered as a “core” response to fungal colonization. However, analysis is limited by the available comparable datasets, since the number of common genes was drastically reduced with every comparison. Apart from single genes, this also appears to be highly tissue-specific, and the commonality or specificity of each dataset has to be understood in the specific context of the available comparisons.

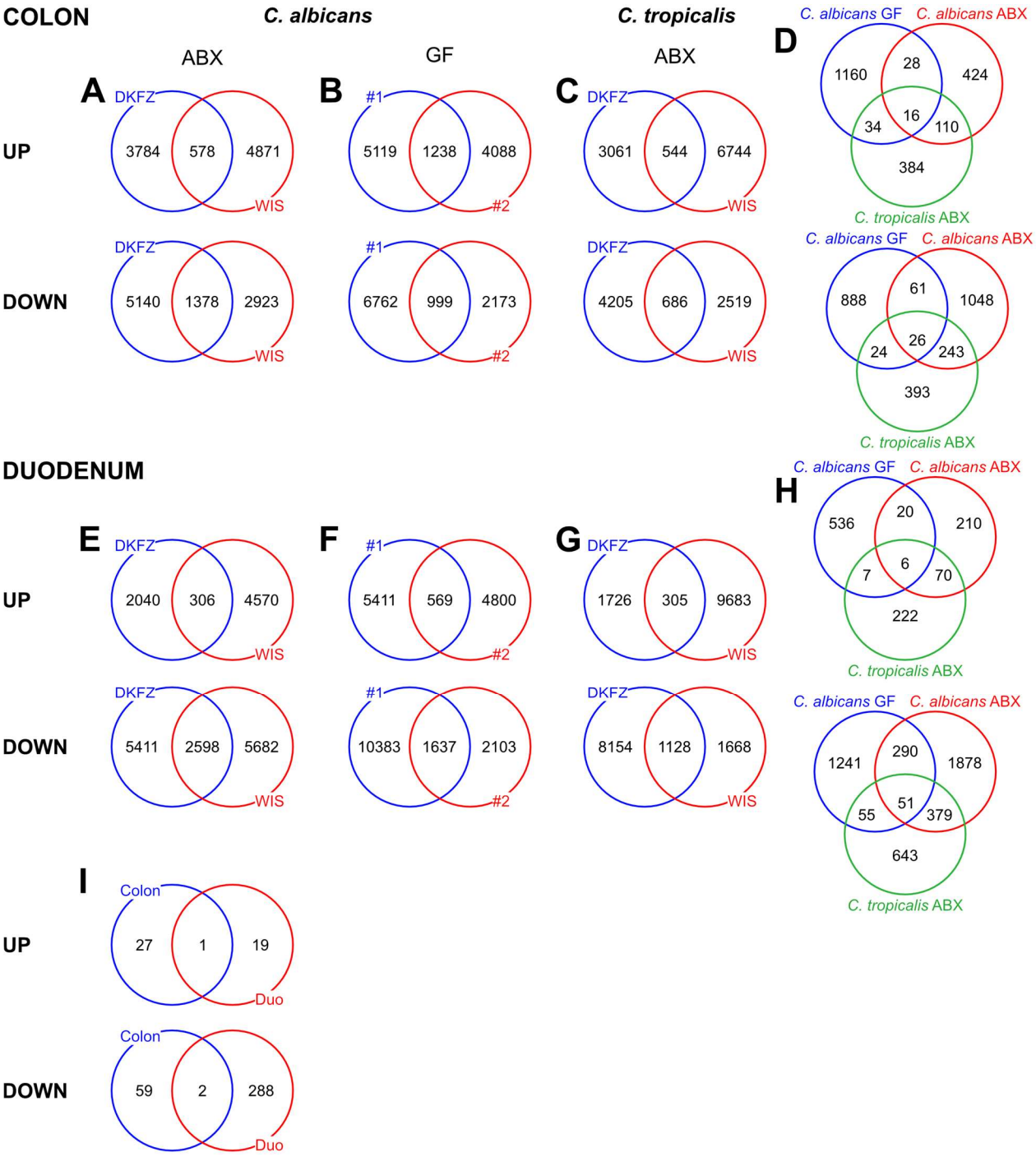

Figure 31: "Core" transcriptional response to *Candida* colonization across experimental conditions. Venn diagrams of genes with a FC > 1.5 separated by directionality of gene expression in the **A-D)** colon, or **E-H)** duodenum. Mice colonized with **A, B, E & F)** *C. albicans* vs healthy controls or **C & G)** *C. tropicalis* vs healthy controls comparing **A, C, E, G)** ABX-treated mice at DKFZ vs WIS, or **B & F)** GF mice from two cohorts. **D & H)** Overlap of genes that were common in A, B & C or E, F & G respectively. **I)** Overlap of genes that were specific for *C. albicans* and common in all experimental conditions in **D & H**. ABX: antibiotics; SPF: specific pathogen free; GF: germ-free; DKFZ: German Cancer Research Center; WIS: Weizmann Institute of Science; Duo: duodenum; FC: fold change.

7.3.2 Influence of fungi colonization on the mammalian host serum metabolome

As one of the main aims of this thesis, I wanted to test if commensal fungi species could produce metabolites in the gut that reach the bloodstream of the mammalian host, and thereby potentially have an influence on physiological processes or disease. To investigate this, I collected serum samples from mice successfully colonized for eight weeks with a fungus and performed metabolomics analysis. Serum was collected from the portal vein and systemically through retro-orbital or cardiac bleeding, in this way the metabolic profile could be determined before and after potential metabolization via the liver and assess the metabolic profile of the blood coming directly from the gut. Metabolomics profiling was performed by Dr. Sergey Malitsky and Dr. Maxim Itkin, while targeted metabolomics was done by Dr. Alexander Brandis at the WIS metabolomics core facility. Data analysis was performed by me. Metabolic profiling unlike untargeted metabolomics includes the co-injection of a library of standards together with the sample, which allows for higher confidence in the identification of metabolites, while limiting the number of metabolites that can be detected. Untargeted metabolomics relies on the retention time and fragment identification and was only developed at a later time point with the core facility, thus not being deployed in the first experiments. Targeted metabolomics uses a standard curve obtained from a pure metabolite, allowing the quantification of one specific metabolite and, therefore, is used for validation of metabolic profiling results.

7.3.2.1 Metabolic profiling in GF mice

Initial metabolic profiling was performed on GF mice that were colonized with *C. albicans* or PBS controls. This experiment included GF C57BL/6 male and female mice that were transferred to the BSL2 room where they received three consecutive initial oral gavages. Serum samples from portal and systemic blood were analyzed by metabolic profiling for both lipids and polar metabolites. While lipidomics did not show any significant hits (data not shown), the focus from hereon was set on the polar metabolites. PCA showed a significant clustering of samples by experimental group in the portal serum, with a trend also present in the systemic serum (**Figure 32A-B**). There were more significantly different metabolites in the portal than in the systemic serum, but strikingly three metabolites were significantly enriched with the *C. albicans* colonization in both: hydroquinone, 3-(1H-indol-3-yl)-propionic acid (IPA), and daidzein ((**Figure 32C-D**). The main focus of this analysis was on those potential metabolites enriched after fungi colonization, since they could be either produced by the fungi directly, or as a response to the fungal colonization. The top 25 differential metabolites were at similar levels across samples more so in the portal than in the systemic serum, but especially consistent for the three main common hits

(**Figure 32E-F**). This was also evident when plotting the three individual metabolites separately, showing no outliers and a clear separation by group (**Figure 32G-I**).

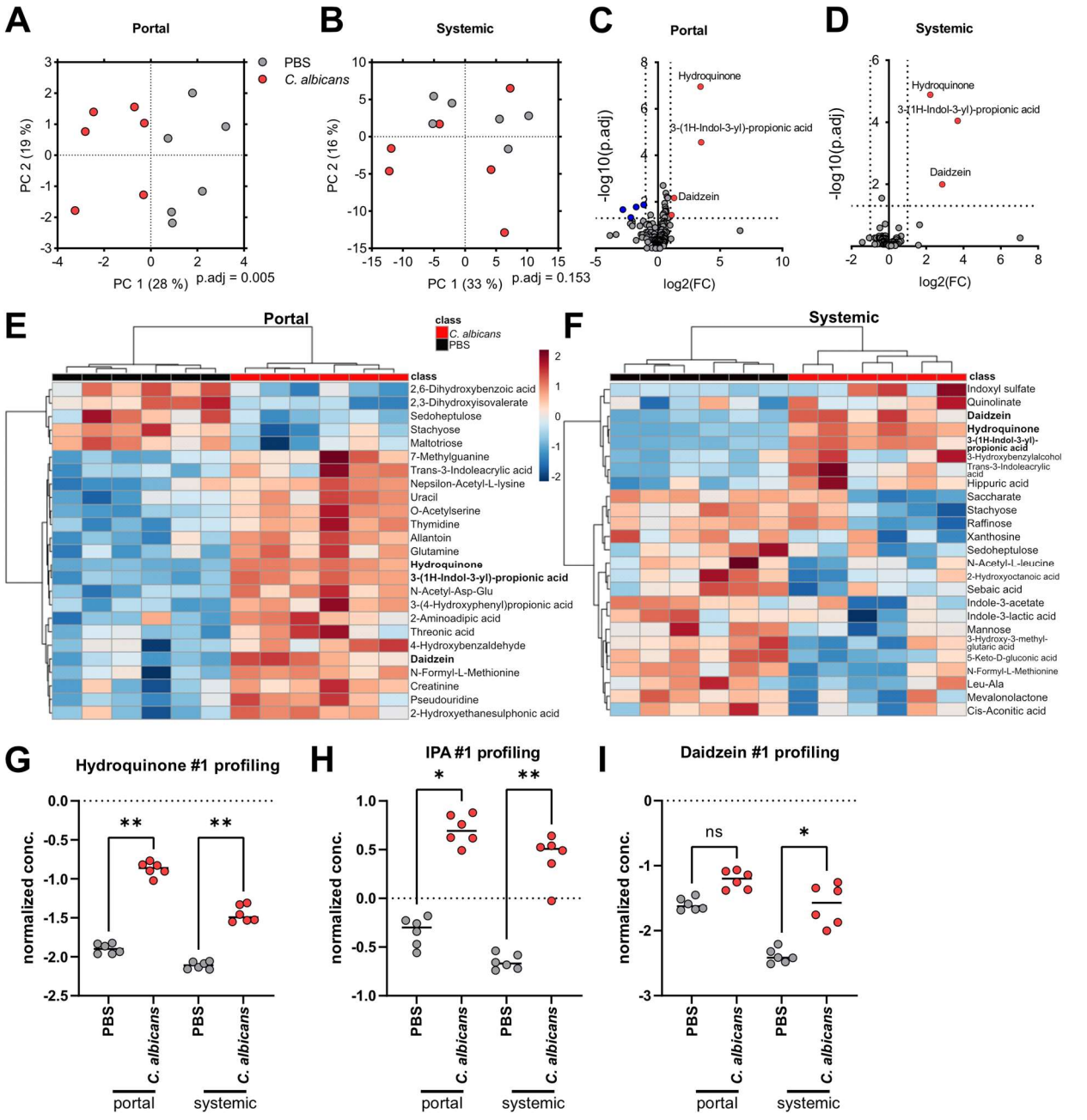

Figure 32: Host serum metabolic profiling of the first cohort of GF mice colonized with *C. albicans*. A-B) PCA of **A)** portal and **B)** systemic serum; statistical testing between groups by PERMANOVA. **C-I)** Differential metabolite analysis of *C. albicans* vs PBS control mice **C-D)** Volcano plots of **C)** portal and **D)** systemic serum; **E-F)** Heatmaps of top 25 significantly different metabolites in **E)** portal and **F)** systemic serum; **G-I)** Normalized concentrations of "hit" metabolites, statistical testing by Kruskal-Wallis test. PCA: principal component analysis; GF: germ-free; PERMANOVA: permutational multivariate statistical permutation test; ns: not significant; * p.adj. < 0.05; ** p.adj. < 0.01.

To validate these results and in order to quantify the levels of metabolites, the same samples were subjected to targeted metabolomics. Targeted metabolomics could confirm the presence of IPA and daidzein after *C. albicans* colonization, but no significant detection for hydroquinone in neither systemic nor portal serum (**Figure 33A-C**). This was surprising, suggesting potential mis-identification in the metabolic profiling by co-elution of similar compounds.

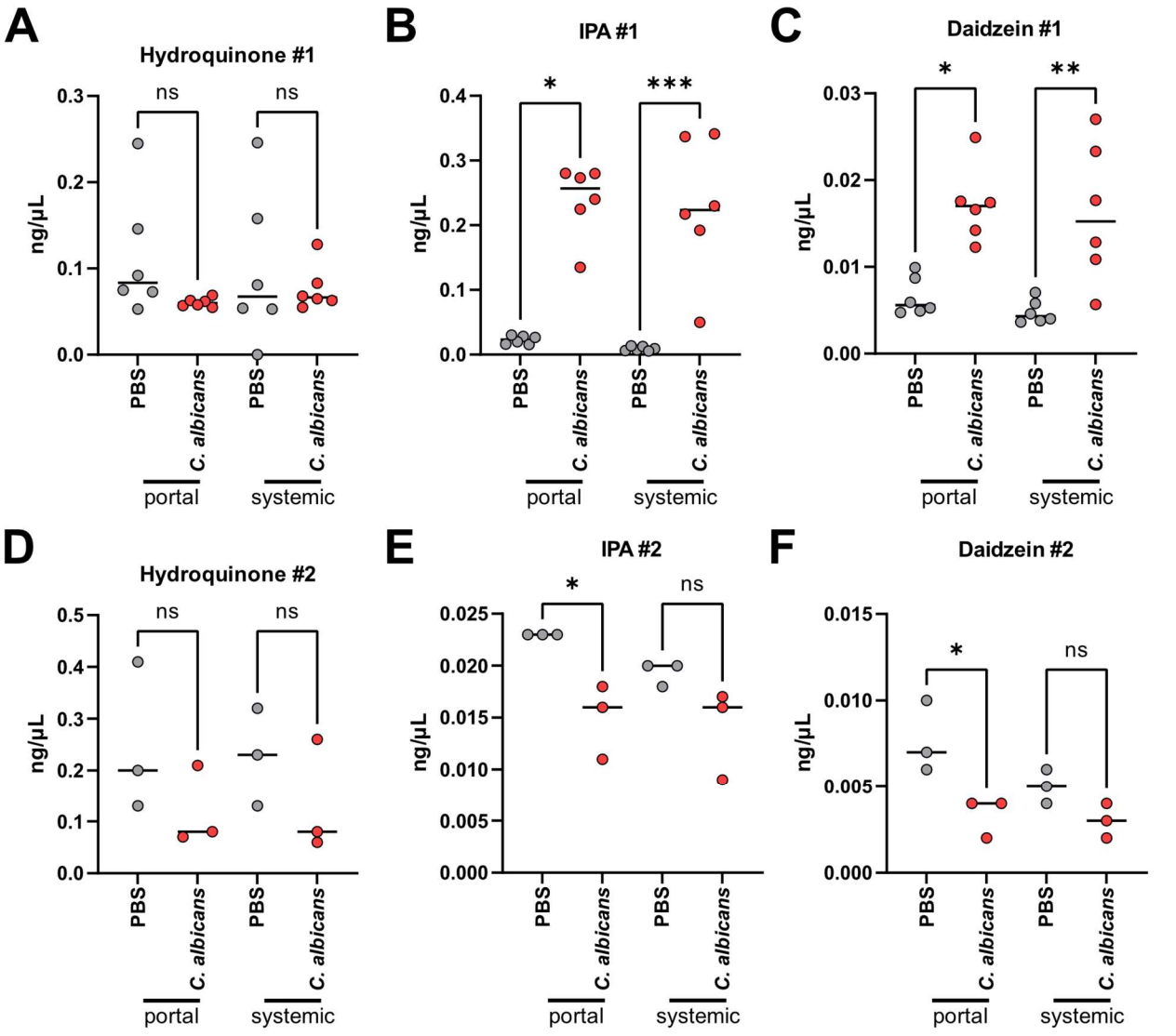

Figure 33: Validation of "hit" metabolites by targeted metabolomics. A-C) 1st cohort of GF mice colonized with *C. albicans*, 3x initial gavage. **D-F)** 2nd cohort of GF mice colonized with *C. albicans*, 1x initial gavage. Statistical testing by Kruskal-Wallis test. GF: germ-free; ns: not significant; * p.adj. < 0.05; ** p.adj. < 0.01; *** p.adj. < 0.001.

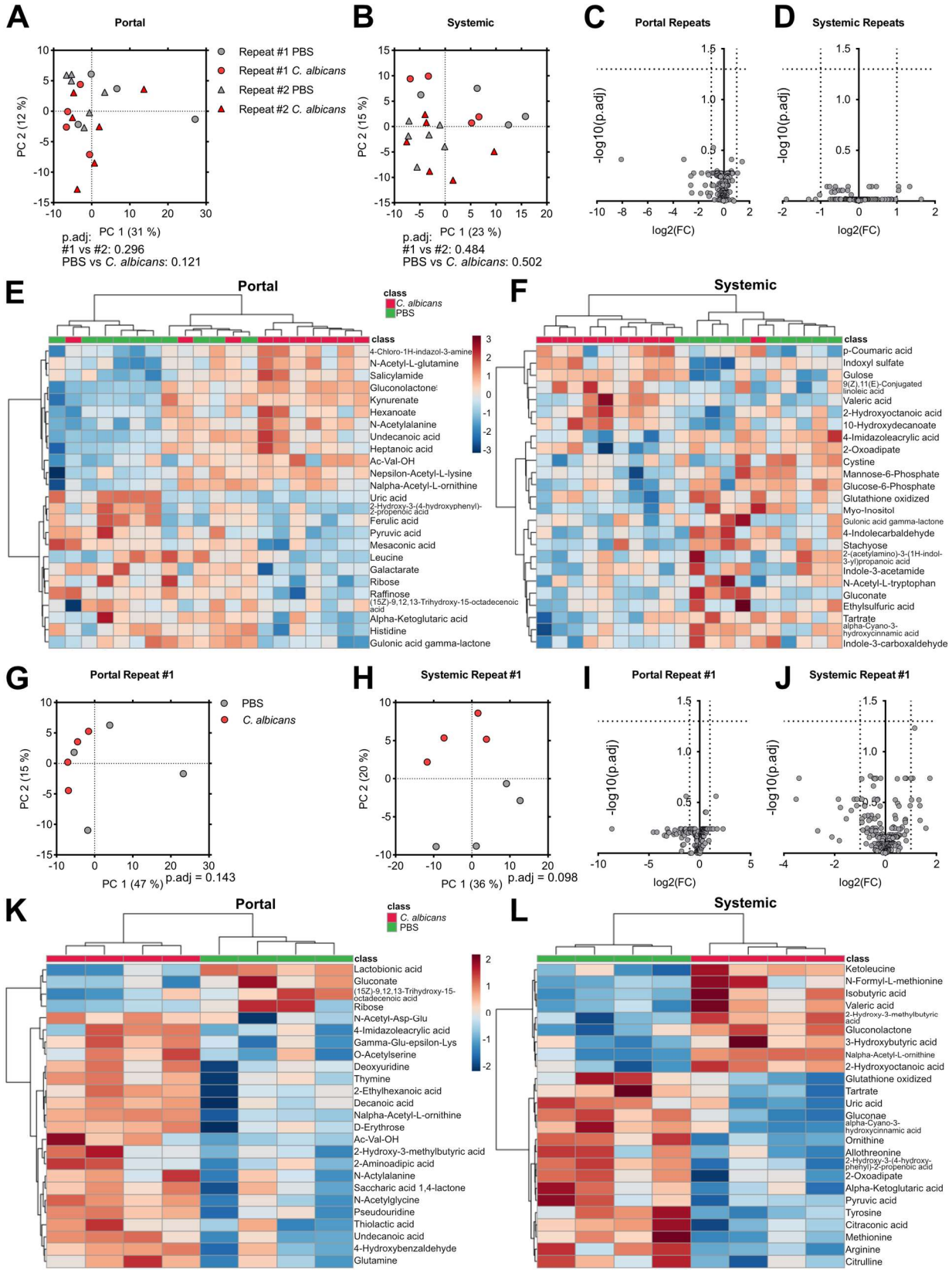

Figure 34: Host serum metabolic profiling of two repeat cohorts of GF mice colonized with *C. albicans*. A-F) Combined analysis of both repeat cohorts **A-B)** PCA of **A)** portal and **B)** systemic serum; statistical testing between

combined PBS and *C. albicans* groups by PERMANOVA. **C-F)** Differential metabolite analysis of *C. albicans* vs PBS control mice **C-D)** Volcano plots of **C)** portal and **D)** systemic serum; **E-F)** Heatmaps of top 25 significantly different metabolites in **E)** portal and **F)** systemic serum. **G-L)** Analysis of repeat cohort #1. **G-H)** PCA of **G)** portal and **H)** systemic serum; statistical testing between groups by PERMANOVA. **I-L)** Differential metabolite analysis of *C. albicans* vs PBS control mice **I-J)** Volcano plots of **I)** portal and **J)** systemic serum; **K-L)** Heatmaps of top 25 significantly different metabolites in **K)** portal and **L)** systemic serum. PCA: principal component analysis; GF: germ-free; PERMANOVA: permutational multivariate statistical permutation test.

To validate if these same metabolites would also be increased in a new sample set, targeted metabolomics of the three hit metabolites was repeated on samples from an independent experiment, where the only difference was that female mice had received only one initial gavage, but with no difference in colonization levels. Hydroquinone did not show an increase also in this dataset, but IPA and daidzein no longer increased after *C. albicans* colonization but rather decreased, with baseline levels being similar as in the first experiment (**Figure 33D-F**). This was unfortunate but could potentially be due to the slightly different experimental setup.

Hence, I repeated the original experiment with the initial three-time gavage twice, subjecting the serum samples to metabolic profiling. Since metabolic profiling was performed in the same batch, both experiments could be analyzed together for greater statistical power. The PCAs showed no significant clustering by experimental group, but did show a non-significant trend for separation by cohort for the systemic serum (**Figure 34A-B**). There were no significant metabolites between *C. albicans* or PBS controls despite the larger mice group size (**Figure 34C-D**). Even for the top 25 metabolites the levels were variable between samples (**Figure 34E-F**). Since the main separation in the PCA resulted to be by cohort, the cohorts were analyzed separately as well. While the first repeat cohort was particularly limited by small group sizes (n = 4), it did show a non-significant trend towards separate clustering in the portal and systemic serum (**Figure 34G-H**). None of the metabolites significantly differed between groups but were relatively consistent across samples (**Figure 34I-L**). The second repeat cohort (n=6 per group) displayed the same trend towards separate clusters by experimental group only in the portal serum samples, and not in the systemic ones (**Figure 35A-B**). None of the metabolites were significantly different between the groups and metabolite levels were quite inconsistent across samples (**Figure 35C-F**). Strikingly, none of the three previous candidate metabolites were significantly different in these cohorts, hydroquinone and daidzein were not detected, while IPA showed a trend in the opposite direction as reported before (data not shown). In conclusion, the metabolic profile was inconsistent across experiments, which could be the result of the different acquired background microbiomes. One argument that strengthens this hypothesis is that GF mice that were initially colonized with *C. tropicalis* and lost it over time (see **Figure 25D-F**) still showed distinct clustering in the metabolic profiling analysis, that was significantly different in the systemic serum, and even had one significantly different metabolite in the portal serum (**Figure 35G-L**).

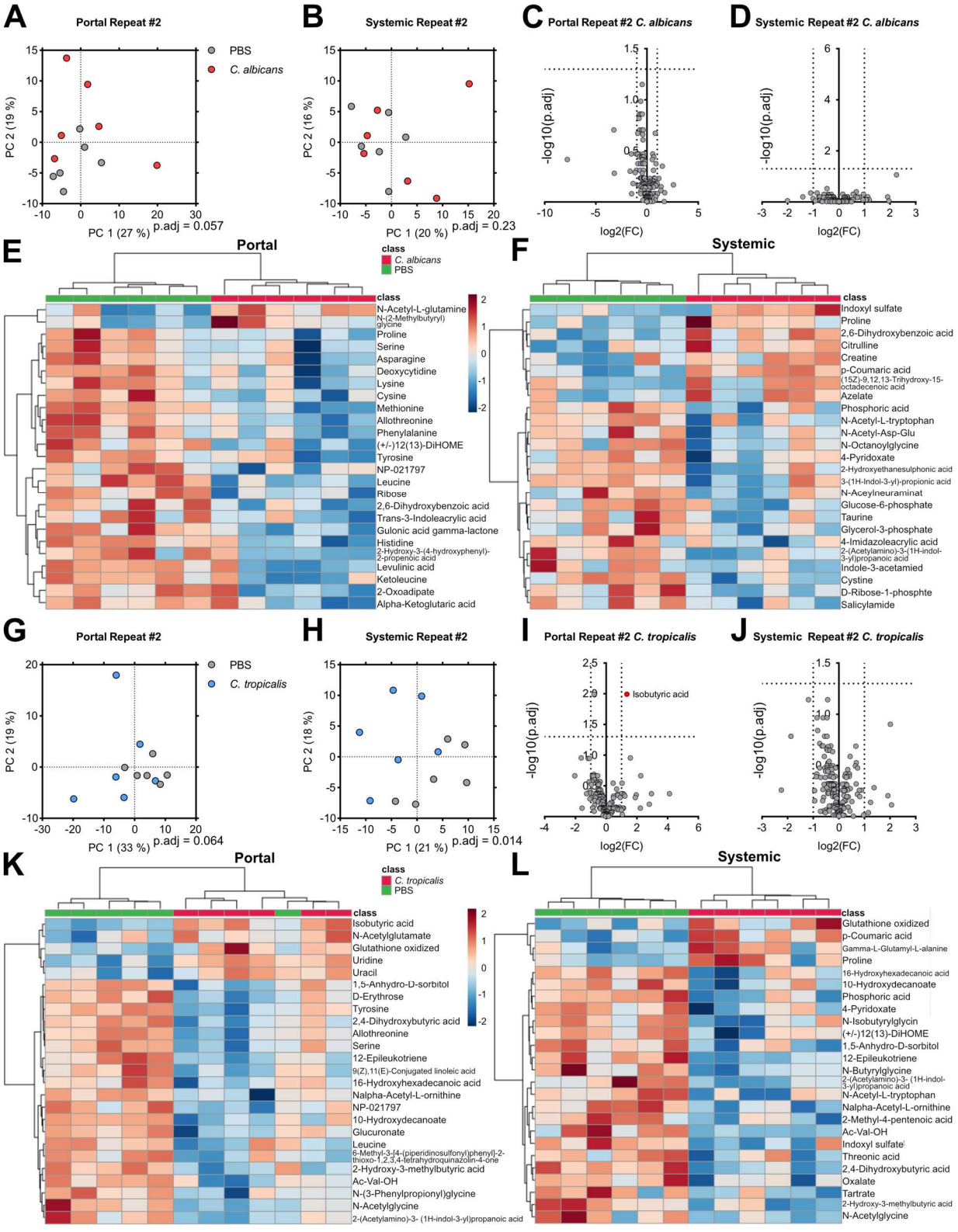

Figure 35: Host serum metabolic profiling of the second repeat cohort of GF mice colonized with *C. albicans* or *C. tropicalis*. A-F) Analysis of *C. albicans*-colonized vs PBS control mice. **A-B)** PCA of **A)** portal and **B)** systemic serum; statistical testing between groups by PERMANOVA. **C-F)** Differential metabolite analysis **C-D)** Volcano plots of **C)** portal and **D)** systemic serum; **E-F)** Heatmaps of top 25 significantly different metabolites in **E)** portal and **F)** systemic serum. **G-L)** Analysis of *C. tropicalis*-colonized vs PBS control mice. **G-H)** PCA of **G)** portal and **H)** systemic serum; statistical

testing between groups by PERMANOVA. **I-L)** Differential metabolite analysis **I-J)** Volcano plots of **I)** portal and **J)** systemic serum; **K-L)** Heatmaps of top 25 significantly different metabolites in **K)** portal and **L)** systemic serum. PCA: principal component analysis; GF: germ-free; PERMANOVA: permutational multivariate statistical permutation test.

Since colonization of the fungus was reportedly lost, it is possible that the initial colonization shaped the composition of the acquired bacterial microbiome community structure, which then remained different between the groups, thus influencing the serum metabolome. Since the acquired microbiome is naturally shaped by the environment, which might be affected by factors such as seasons, experimenters, caretakers, food chow, and other experiments performed in the same room, this could explain the variation between different cohorts. To test this, metabolic profiling was performed on serum samples of mice that are known to have a remnant bacterial background microbiome, namely SPF mice with ABX treatment.

7.3.2.2 Metabolic profiling in ABX-treated SPF mice

SPF mice at the WIS were treated with 4-way ABX and colonized with *C. albicans*, *C. tropicalis*, or PBS as previously described. These mice were housed in the BSL2 room and serum samples were collected and analyzed the same way as for the GF mice. PCAs showed significantly separate clustering between the PBS and *C. albicans* group, but not *C. tropicalis* in the systemic serum with a similar trend in the portal serum (**Figure 36A-B**). Interestingly, comparing the *C. albicans*-colonized group to the PBS controls, none of the metabolites were significantly different in the portal serum, while a few were significantly different in the systemic serum (**Figure 36C-D**). This could be due to the liver metabolism that could convert several different metabolites into a similar compound, which are only then significantly different. Variability of metabolite levels across samples within a group was also lower in the systemic serum than in the portal serum (**Figure 36E-F**). It was striking that under these conditions, IPA was significantly lower with *C. albicans* colonization, which was directly opposite to what was previously observed in the first GF mice cohort (see **Figure 32C-D**). This further encourages the suspicion, that some of the metabolites measured might be due to the presence of bacteria and not the fungi.

Comparing *C. tropicalis*-colonized mice to PBS controls, one metabolite was significantly lower in the portal serum, and four were lower and one higher in the systemic blood (**Figure 36G-H**). However, there was variability of the metabolite levels across the samples within a group (**Figure 36I-J**).

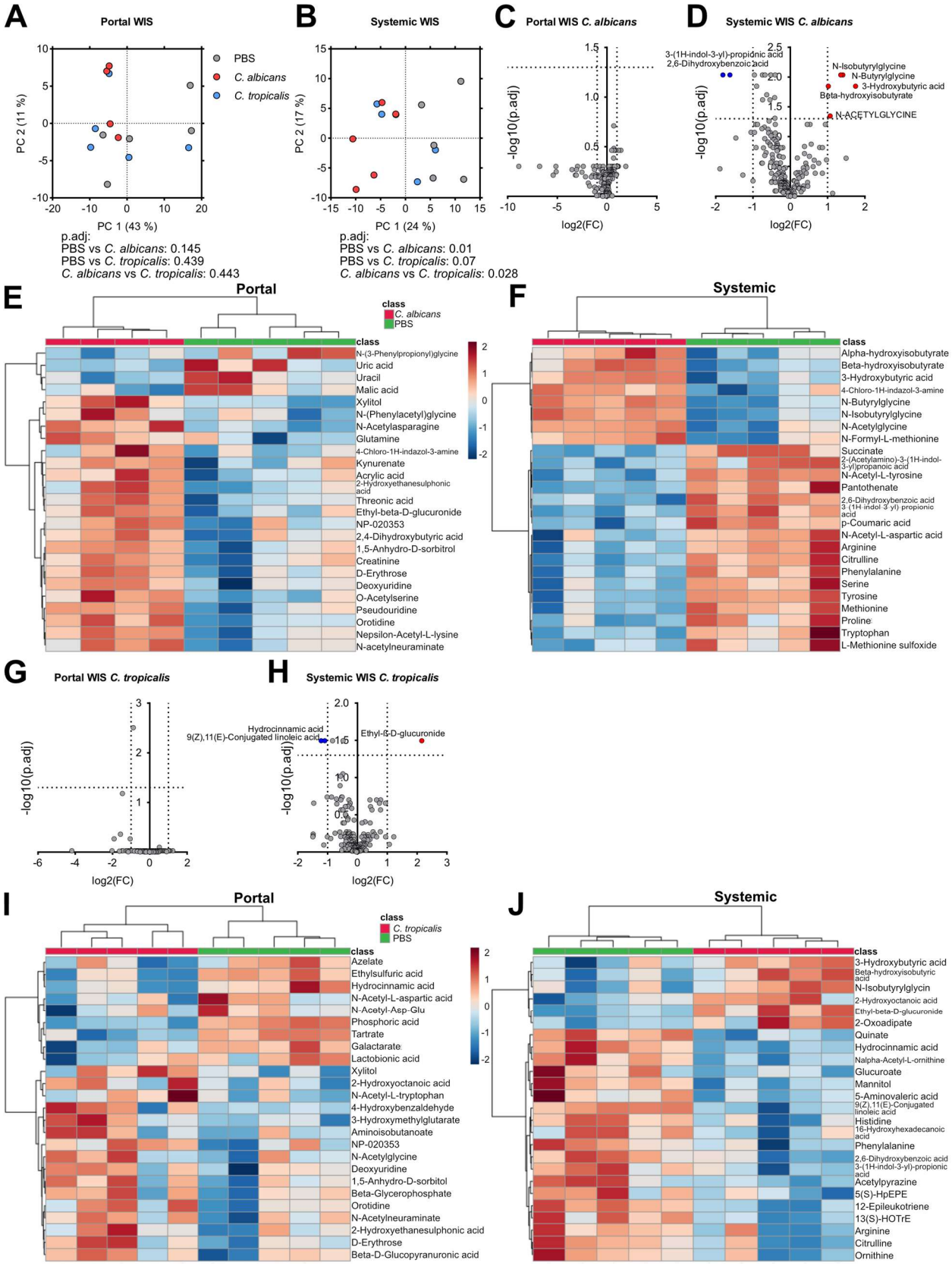

Figure 36: Host serum metabolic profiling of ABX-treated SPF mice at WIS colonized with *C. albicans* or *C. tropicalis*. A-B) PCA of **A)** portal and **B)** systemic serum; statistical testing between groups by PERMANOVA.

C-F) Differential metabolite analysis of *C. albicans*-colonized vs PBS control mice **C-D)** Volcano plots of **C)** portal and **D)** systemic serum; **E-F)** Heatmaps of top 25 significantly different metabolites in **E)** portal and **F)** systemic serum. **G-J)** Differential metabolite analysis of *C. tropicalis*-colonized vs PBS control mice **G-H)** Volcano plots of **G)** portal and **H)** systemic serum; **I-J)** Heatmaps of top 25 significantly different metabolites in **I)** portal and **J)** systemic serum. PCA: principal component analysis; PERMANOVA: permutational multivariate statistical permutation test; ABX: antibiotics; SPF: specific pathogen free; WIS: Weizmann Institute of Science.

A similar experiment was performed in SPF mice at the DKFZ with a different ABX treatment (see **6.2.2**), and serum samples were subjected to metabolic profiling. PCAs showed a non-significant separation between *C. albicans*-colonized samples and PBS but not *C. tropicalis* in portal and systemic serum (**Figure 37A-B**). No metabolites were significantly different between the groups, which might be also influenced by the low number of mice per group in some cases (n=3-6) (**Figure 37C-D, G-H**). The metabolite levels were more consistent across samples of one group for the *C. albicans*-colonized mice samples compared to the *C. tropicalis*-colonized mice samples (**Figure 37E-F, I-J**), suggesting a weaker metabolic output from *C. tropicalis* or less changes to the formation of the acquired bacterial community. In conclusion, metabolomics analysis was also influenced by the background microbiome, which could be different due to the distinct ABX treatment, vivaria, and even food chow. Therefore, comparison of these experiments is difficult, due to many varying factors.

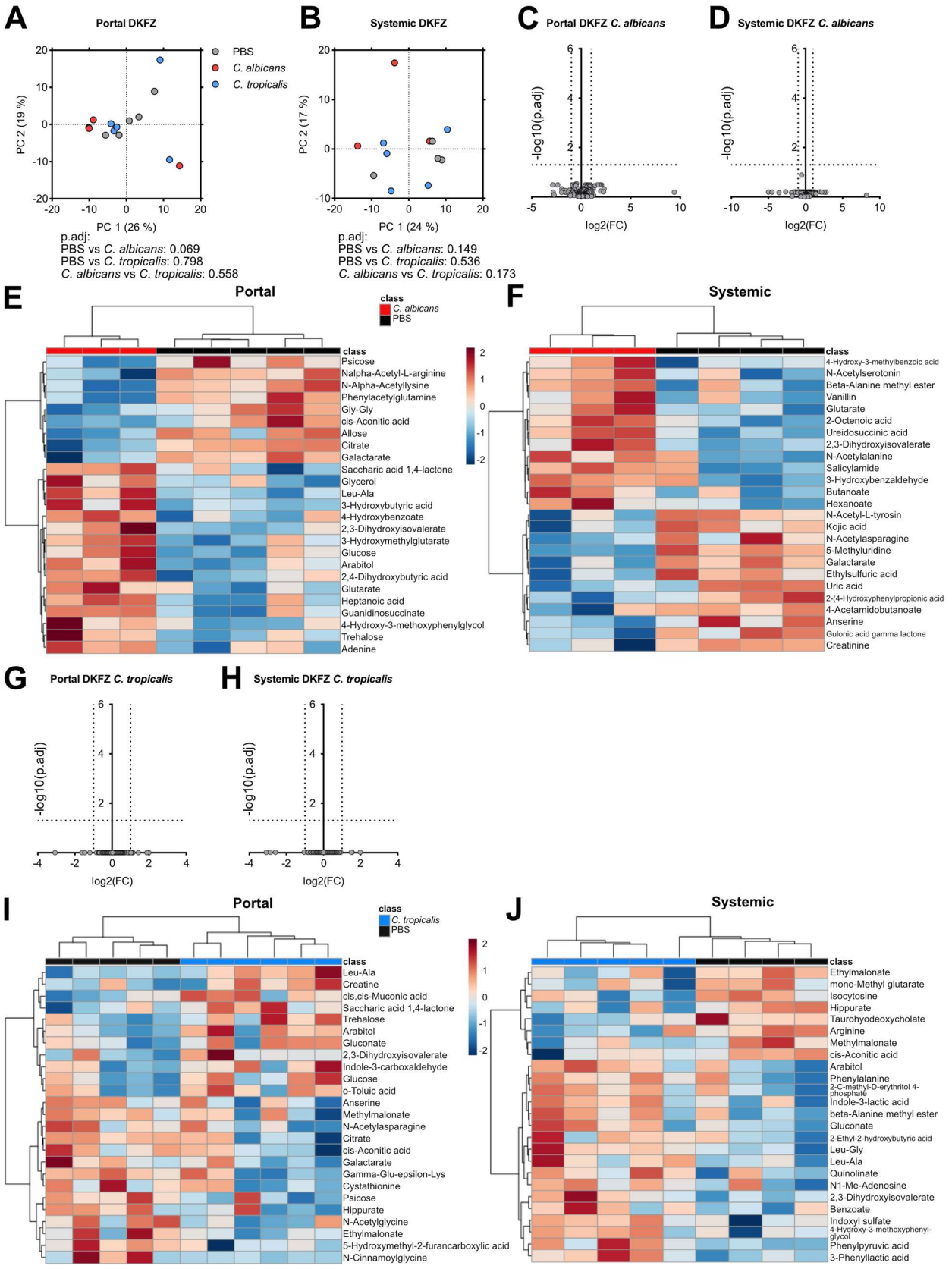

Figure 37: Host serum metabolic profiling of ABX-treated SPF mice at DKFZ colonized with *C. albicans* or *C. tropicalis*. A-B) PCA of **A)** portal and **B)** systemic serum; statistical testing between groups by PERMANOVA.

C-F) Differential metabolite analysis of *C. albicans*-colonized vs PBS control mice **C-D)** Volcano plots of **C)** portal and **D)** systemic serum; **E-F)** Heatmaps of top 25 significantly different metabolites in **E)** portal and **F)** systemic serum. **G-J)** Differential metabolite analysis of *C. tropicalis*-colonized vs PBS control mice **G-H)** Volcano plots of **G)** portal and **H)** systemic serum; **I-J)** Heatmaps of top 25 significantly different metabolites in **I)** portal and **J)** systemic serum. PCA: principal component analysis; PERMANOVA: permutational multivariate statistical permutation test; ABX: antibiotics; SPF: specific pathogen free; DKFZ: German Cancer Research Center.

7.3.2.3 Metabolomics of isolator-housed GF mice

After several different settings attempts, the only way of understanding which metabolites might be produced by a specific fungus that could be measured in the host blood stream, is by colonizing GF mice with one single fungi species and keeping them housed inside an isolator.

7.3.2.3.1 *C. albicans* isolator

GF isolator-housed FVB mice were colonized with *C. albicans,* while age-matched control mice remained in another isolator to avoid potential contamination. Unfortunately, some control mice unexpectedly died, reducing the group sizes (n=4 control and n=6 *C. albicans* mice), still metabolic profiling of the portal and systemic serum was performed. PCAs showed a significant clustering by experimental group for the portal samples, which was less present in the systemic ones (**Figure 38A-B**). There were no significantly different metabolites between the two groups in neither the portal nor the systemic blood (**Figure 38C-D**) and metabolic levels varied between the samples within the groups, for the systemic samples so much so that they did not even cluster together (**Figure 38E-F**). To see if there is a consistent *C. albicans* signature independent of significance, which is dependent on group sizes, I compared all metabolites that had a fold change of 1.5 in either direction from all datasets within their directionality. There were no metabolites overlapping in all datasets, or even in all GF datasets, suggesting that any fungal signal is changed or altered by the bacterial community.

Based on this, it appears that there is no significant fungal metabolic signal, which is surprising since the fungi survive in the gut and are expected to be metabolically active. Since it is possible that the potential fungal metabolites might not be part of the list of standards used in the metabolomics library, a true untargeted analysis (discovery mode) that relied on an algorithm rather than the standards was performed to detect metabolites of interest. Thus, a much larger number of metabolites could be detected (1182 metabolites) compared to what was measured with the polar library (218 metabolites). The downside of this method is that the identity of the metabolites is less clear and difficult to sometimes impossible to reveal. Using the discovery mode, the samples showed a non-significant but clear trend in their clustering by experimental group in the PCA (**Figure 38G-H**) and in the portal blood three metabolites were significantly higher in the *C. albicans* compared to the control samples, and five lower, while in the systemic serum five were significantly lower as well (**Figure 38I-J**).

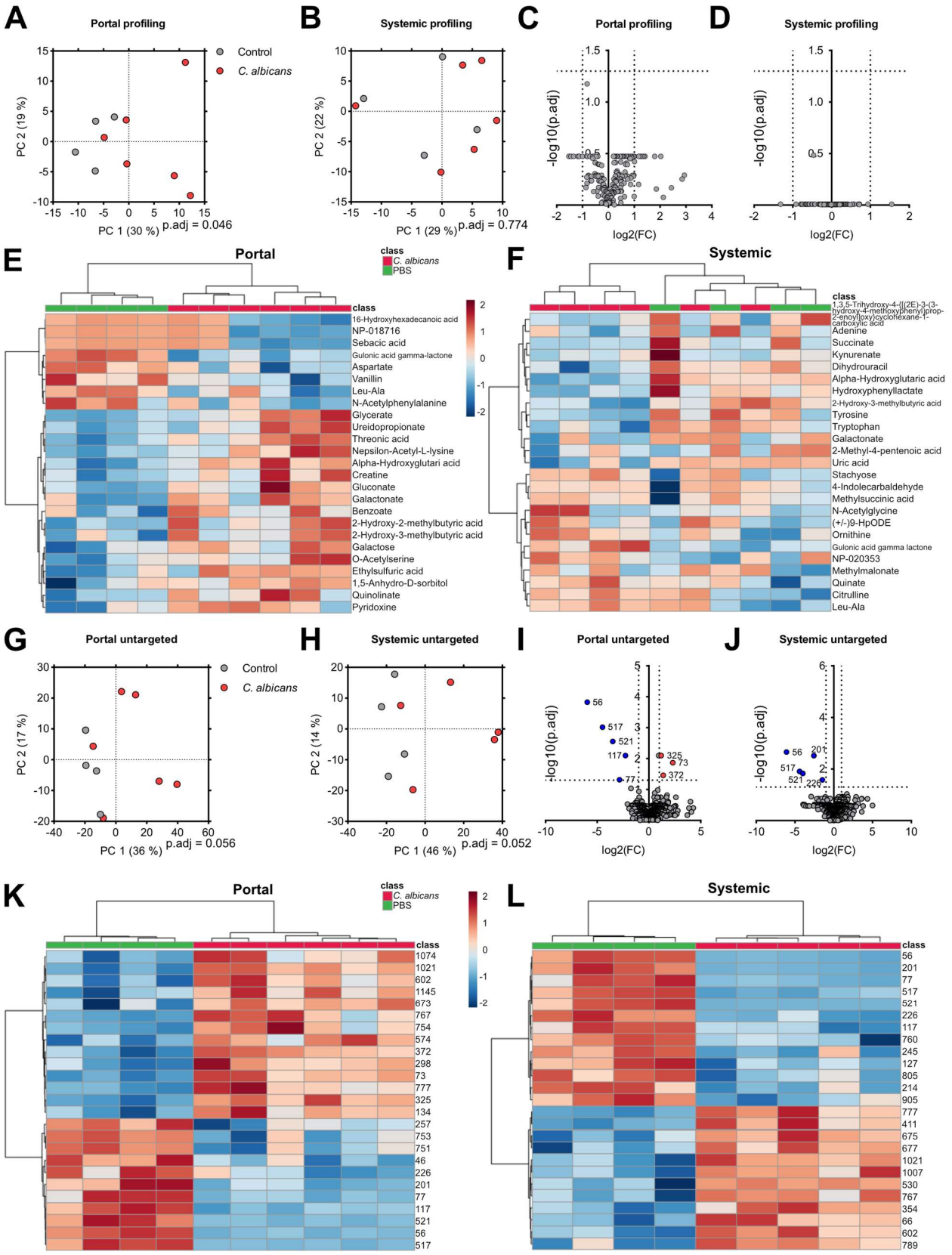

Figure 38: Host serum metabolic profiling and untargeted metabolomics of GF isolator-housed FVB mice colonized with *C. albicans*. A-F) Metabolic profiling **A-B)** PCA of **A)** portal and **B)** systemic serum; statistical testing

between groups by PERMANOVA. **C-F)** Differential metabolite analysis **C-D)** Volcano plots of **C)** portal and **D)** systemic serum; **E-F)** Heatmaps of top 25 significantly different metabolites in **E)** portal and **F)** systemic serum. **G-L)** Untargeted metabolomics **G-H)** PCA of **G)** portal and **H)** systemic serum; statistical testing between groups by PERMANOVA. **I-L)** Differential metabolite analysis **I-J)** Volcano plots of **I)** portal and **J)** systemic serum; **K-L)** Heatmaps of top 25 significantly different metabolites in **K)** portal and **L)** systemic serum. PCA: principal component analysis; GF: germ-free; PERMANOVA: permutational multivariate statistical permutation test.

Out of these, three were common for both blood sample locations, while the other two were different. The top 25 differential metabolites showed high in-group homogeneity for the metabolic levels and a larger fold change between the groups, signaling a much clearer difference compared to the metabolic profiling (**Figure 38K-L**). Based on this, I concluded that *C. albicans* does have an effect on the host metabolome, which is mainly through reduction of several metabolites, but the exact identity of these metabolites is unclear. This was further discussed in the discussion of this thesis (**8.5)**.

7.3.2.3.2 *C. tropicalis* isolator

Similar to the experiment above, GF C57BL/6 mice housed in an isolator were colonized with *C. tropicalis*, while the controls remained in a separate isolator. PCAs of both, portal and systemic serum showed a trend for separate clustering between the two experimental groups (**Figure 39A-B**). Accordingly, no metabolites were significantly different in the portal blood, however, in the systemic blood, ethylsulfuric acid was significantly higher in the *C. tropicalis* group (**Figure 39C-D**). The metabolite levels across the samples were inconsistent within a group, while ethylsulfuric acid showed a small fold change and was not significant when tested with the Kruskal-Wallis test (**Figure 39E-G**). This metabolite was not measured under in vitro conditions (**7.1.1.2**). With the untargeted discovery mode, there was significant clustering by group in the PCA for the portal serum but not for the systemic serum (**Figure 39H-I**). Accordingly, in the portal serum there were seven metabolites significantly increased and seven decreased, while in the systemic serum one increased and five decreased (**Figure 39J-K**). Out of these, three metabolites overlapped and were changed in the same direction, with two decreased (56 & 1030) and one increased (602) with *C. tropicalis* (**Figure 39L**). The heatmaps showed higher consistency of metabolite levels across groups compared to the metabolic profiling (**Figure 39M-N**). Overall, for both *Candida* species untargeted metabolomics could produce a stronger signal than the polar library of the metabolic profiling. Colonization with both species showed some specific metabolites that changed in the host blood stream, the identification of which was discussed further in the discussion (**8.5**).

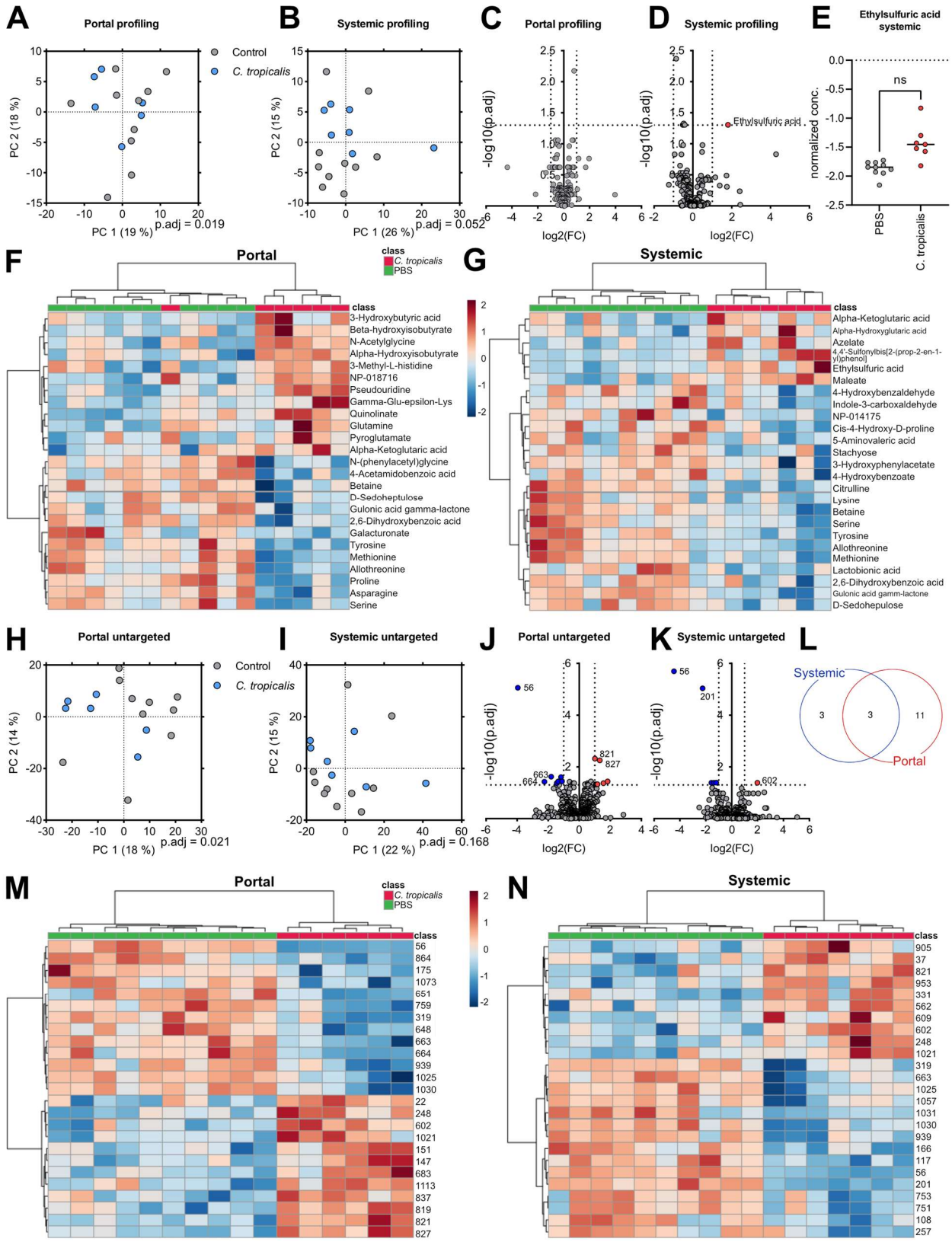

Figure 39: Host serum metabolic profiling and untargeted metabolomics of GF isolator-housed C57BL/6 mice colonized with *C. tropicalis*. A-G) Metabolic profiling **A-B)** PCA of **A)** portal and **B)** systemic serum; statistical testing between groups by PERMANOVA. **C-G)** Differential metabolite analysis **C-D)** Volcano plots of **C)** portal and **D)** systemic

serum; **E)** Normalized concentration of significant metabolite; **F-G)** Heatmaps of top 25 significantly different metabolites in **F)** portal and **G)** systemic serum. **H-N)** Untargeted metabolomics **H-I)** PCA of **H)** portal and **I)** systemic serum; statistical testing between groups by PERMANOVA. **J-N)** Differential metabolite analysis **J-K)** Volcano plots of **J)** portal and **K)** systemic serum; **L)** Venn diagram of significant metabolites in portal and systemic; **M-N)** Heatmaps of top 25 significantly different metabolites in **M)** portal and **N)** systemic serum. PCA: principal component analysis; GF: germ-free; PERMANOVA: permutational multivariate statistical permutation test.

7.3.2.3.3 Strain differences

The experiments performed inside the GF isolators were done using two different fungi strains and two different mouse strains (see **7.2**). Therefore, I wanted to test how similar the metabolome of untreated isolator-housed GF mice was compared to the respective control mice. The control mice of the *C. tropicalis* colonization were C57BL/6 mice, while the control mice of the *C. albicans* colonization were FVB mice and both experiments were age-matched and had been measured in the same batch, allowing direct comparison. PCAs of the metabolic profiling showed a significant clustering by mouse strain for both portal and systemic serum (**Figure 40A-B**), and many significant hits in both sera (**Figure 40C-D**), which were at consistent levels across samples within one group (**Figure 40E-F**). For the untargeted discovery mode, this was even more pronounced, with highly significant separate sample clusters (**Figure 40G-H**), even more significantly different metabolites (**Figure 40I-J**), and very strong FC differences and consistency across samples within one group (**Figure 40L-M**). To compare how many significantly different metabolites were measured in the two serum types and with the two measurement methods, I calculated how many metabolites had a p value smaller than 0.05 and a FC larger than two in either direction. For both, portal and systemic serum, about 10 times more metabolites fit these criteria with the untargeted measurement compared to the metabolic profiling, which is in line with a larger range of detection (**Figure 40K**). However, as a percentage of the total metabolites detected, untargeted metabolomics still had about twice as many significant hits than with metabolic profiling, pointing out the limitations of this particular library (**Figure 40K**). Interestingly, there were more significantly different metabolites detected in the systemic serum compared to the portal serum with both methods (**Figure 40K**). Overall, this comparison showed huge differences in the host serum metabolome between two age-matched mouse strains, which opens up questions about the applicability and transferability of serum metabolomics data between different mouse strains, let alone from mice to humans.

In this chapter, I discovered how the acquisition of a background microbiome has important implications also for further downstream readouts. Colonization success alone does not guarantee stable results, since there are many factors that influence downstream readouts, such as mouse strain differences, food chow, and vivaria, but also remaining bacterial microbiome signals that can differ between experiments.

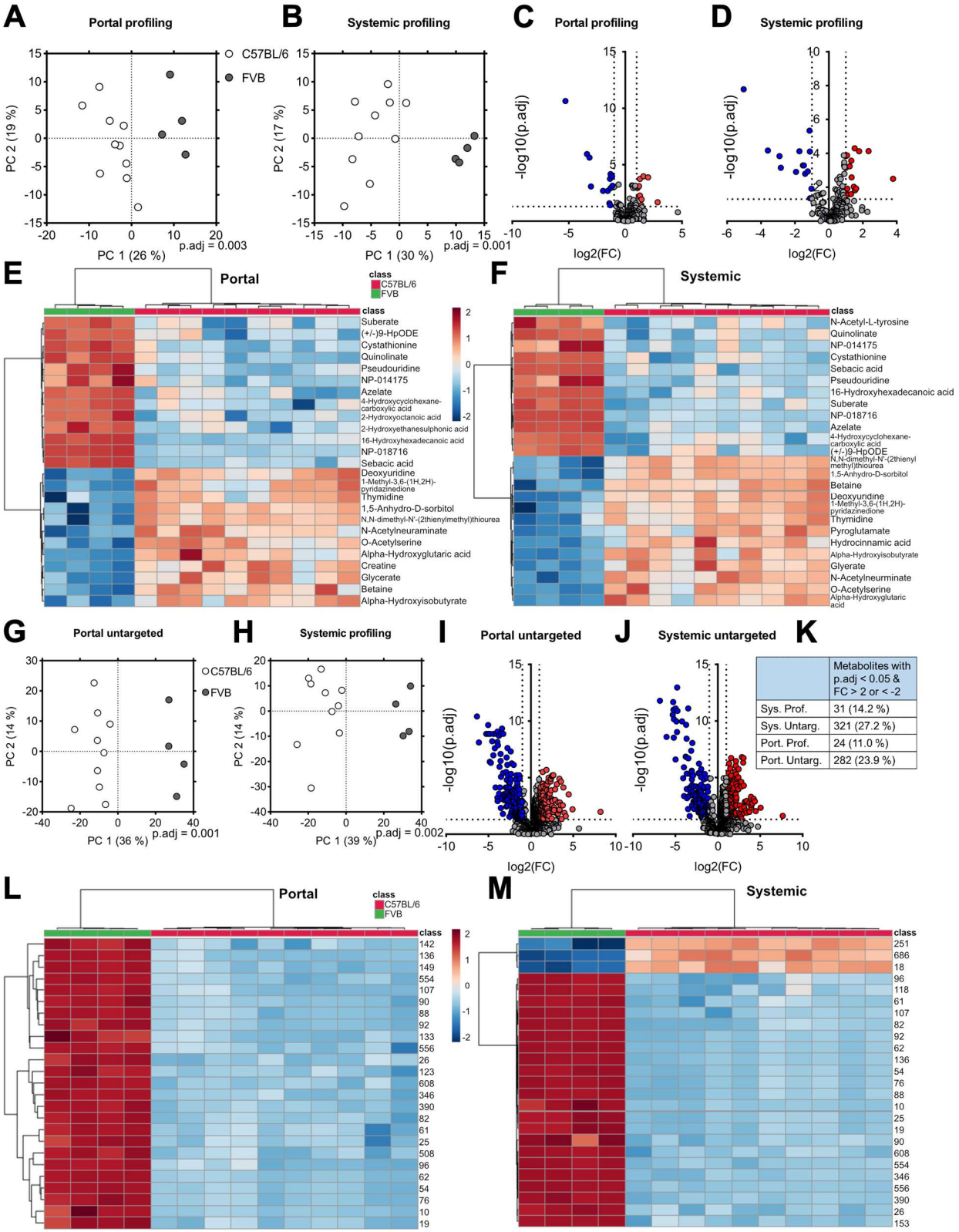

Figure 40: Host serum metabolic profiling and untargeted metabolomics of GF isolator-housed FVB mice vs. C57BL/6 mice. A-F) Metabolic profiling **A-B)** PCA of **A)** portal and **B)** systemic serum; statistical testing between groups by PERMANOVA. **C-F)** Differential metabolite analysis **C-D)** Volcano plots of **C)** portal and **D)** systemic serum; **E-F)** Heatmaps of top 25 significantly different metabolites in **E)** portal and **F)** systemic serum. **G-M)** Untargeted

metabolomics **G-H)** PCA of **G)** portal and **H)** systemic serum; statistical testing between groups by PERMANOVA. **I-M)** Differential metabolite analysis **I-J)** Volcano plots of **I)** portal and **J)** systemic serum; **K)** Table of significantly different metabolites as measured with different methods and in different sera, absolute number and as percentage of total metabolites detected; **L-M)** Heatmaps of top 25 significantly different metabolites in **L)** portal and **M)** systemic serum. PCA: principal component analysis; GF: germ-free; PERMANOVA: permutational multivariate statistical permutation test.

7.4 Chapter 4: Role of *C. albicans* in Acute Liver Failure

The presence of fungal metabolites that could only be detected in the portal blood encouraged the investigation of their potential effects on the liver in a disease context. Therefore, a well-established acute liver failure (ALF) model induced by acetaminophen was chosen. I chose to study the impact of *C. albicans* in this setting since it successfully colonized the mouse intestine. The advantage of such a model, apart from the quick turnaround time, was that it had been previously shown by our lab and others that the microbiome has an influence on the severity of the disease [158, 159, 162]. However, the impact of fungal colonization on ALF has not been investigated yet.

The general setup of the experiments consisted of colonization with *C. albicans* by three time oral gavage followed by a one-week waiting time for adjustment and establishment of a colonization equilibrium. One week after the first gavage, a weight-adjusted dose of acetaminophen (APAP, 300 or 500 mg/kg) was injected after 6 h fasting, and mice were sacrificed after 20 h. The extent of liver damage was assessed by measuring serum liver enzyme levels: ALT (alanine aminotransferase) and AST (aspartate aminotransferase). Moreover, blinded scoring of liver histology slides by a pathologist determined the extent of liver necrosis. The amount of *C. albicans* colonization was measured by culturing of colon content samples.

To address the direct effect of *C. albicans* on ALF under clean conditions, the mice were kept in a GF isolator where only *C. albicans* was used to colonize the mice, while the control mice remained in isocages. After one week, the colon was colonized as measured by high CFU counts in colonic stool samples, with no difference in the colonization levels between sexes (**Figure 41A**). The control males had high liver damage as measured by both, ALT and AST levels, indicating successful induction of ALF (**Figure 41B-C**). Colonization with *C. albicans* in males resulted in two subsets based on their liver damage response to APAP injection: one set with high enzyme levels, and one set that was completely protected from liver damage (**Figure 41B-C**). This was interesting and the existence of two subsets puzzling, since the mice were age-matched, had similar colonization levels, and no cage effect was observed. The lower amount of liver damage was also detectable by histology, although even the subset that had very low enzyme levels still had some extent of damage, suggesting differences in temporal resolution between enzyme measurements and tissue damage, which might take longer to recover (**Figure 41D**).

Females, on the other hand, were already protected without *C. albicans* colonization, except for two outliers of the control group, with no difference with or without *C. albicans* colonization (**Figure 41B-C**). The high resistance of female mice to APAP ALF induction compared to male mice has

been similarly described in the literature [153]. Interestingly, liver damage as scored by histology was only minimally lower compared to the males, showing that the APAP did manage to induce damage, but it had stabilized quicker on the serum enzyme level (**Figure 41D**).

To check whether this phenotype would still exist with a background microbiome present, the experiment was repeated using GF mice that were transferred to the BSL2 room, thus most likely naturally acquiring a basal microbiome in the process. GF Swiss-Webster (SW) mice were used for this experiment. Colonization levels with *C. albicans* were high and comparable between sexes, but lower than those determined inside the isolator (**Figure 41E**). Interestingly, higher liver enzyme levels in the males were observed (**Figure 41F-G**). The control mice that had received PBS showed extremely high liver enzyme levels, with one mouse even succumbing to the disease (**Figure 41F-G**). Compared to that, male mice colonized with *C. albicans* displayed lower enzyme levels, while the histology score was very variable (**Figure 41F-H**). In the female mice, the serum enzyme levels were low, except for one outlier in the *C. albicans* group, however, this was not reflected in the histology scores (**Figure 41F-H**). While the small group size and large variability makes conclusions difficult, it is possible that the divergent results of liver enzyme levels and histology reflect different temporal resolutions, with for example enzyme levels already decreasing while tissue damage was still visible. Therefore, it appears that males are more sensitive to APAP and *C. albicans* colonization can reduce the amount of liver damage in males, with the higher levels potentially being due to mouse strain differences or the presence of background bacteria.

It has been shown that colonization with *C. albicans* can exacerbate alcoholic liver disease in mice dependent on Th17 cell activation [173]. Thus, I wanted to test, if the decrease of ALF in males colonized with *C. albicans* was dependent on T and B cells. In order to do so, I repeated the same experiment in RAG1-/- mice that lack functional T and B cells [234]. Colonization levels in the colon content were high, with no difference between the sexes (**Figure 41I**). Strikingly, despite the lack of an adaptive immune system, the phenotype remained similar to the previous experiments, with very high liver enzyme levels in the PBS group in males and comparatively lower levels with *C. albicans* colonization (**Figure 41J-K**). The same trend was also visible for the liver damage as measured by histology, although it was not significant (**Figure 41L**). Analysis of the females was more limited due to a small group size (n=2 per group). Nevertheless, the females remained more protected from liver damage than males but with higher enzyme levels for the control mice than in the previous experiments. However, complete protection with *C. albicans* colonization was observed (**Figure 41J-K**). Histology scoring of the liver was very variable and limited by the small group sizes (**Figure 41L**). Based on these results, the observed phenotype is not mediated by the adaptive immune system, and unlike in alcoholic liver disease, not dependent on Th17 cells.

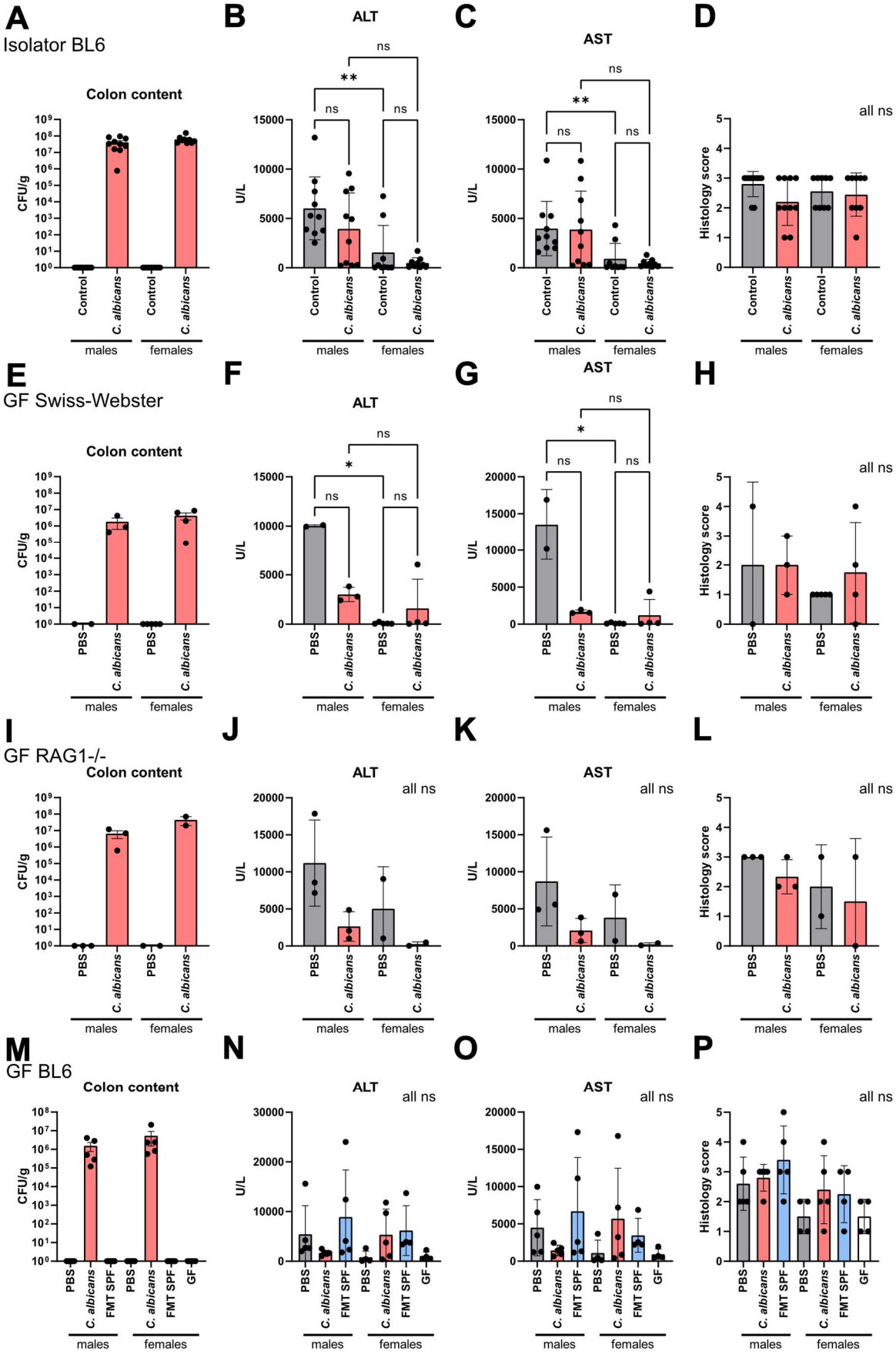
A
Isolator BL6
Colon content
CFU/g
B
ALT
U/L
C
AST
U/L
D
Histology score
all ns
E
GF Swiss-Webster
Colon content
CFU/g
F
ALT
U/L
G
AST
U/L
H
Histology score
all ns
I
GF RAG1-/-
Colon content
CFU/g
J
ALT
U/L
all ns
K
AST
U/L
all ns
L
Histology score
all ns
M
GF BL6
Colon content
CFU/g
N
ALT
U/L
all ns
O
AST
U/L
all ns
P
Histology score
all ns
Control
PBS
C. albicans
FMT SPF
GF
males
females
ns
*
**

Figure 41: Influence of *C. albicans* colonization on ALF in Isolator-housed or GF mice. A-D) Isolator-housed C57BL/6 mice treated with 300 mg/kg APAP after 6 h fasting. **A)** CFU counts of colon content. **B-C)** Portal serum **B)** ALT levels and **C)** AST levels. **D)** Histology score. **E-H)** GF Swiss-Webster mice treated with 300 mg/kg APAP after 6 h fasting. **E)** CFU counts of colon content. **F-G)** Portal serum, **F)** ALT levels and **G)** AST levels. **H)** Histology score. **I-L)** GF RAG1-/- mice treated with 300 mg/kg APAP after 6 h fasting. **I)** CFU counts of colon content. **J-K)** Portal serum, **J)** ALT levels and **K)** AST levels. **L)** Histology score. **M-P)** GF C57BL/6 mice treated with 500 mg/kg APAP without fasting. **M)** CFU counts of colon content. **N-O)** Portal serum **N)** ALT levels and **O)** AST levels. **P)** Histology score. Statistical testing by Kruskal-Wallis test; ns: not significant; * p.adj. < 0.05; ** p.adj. < 0.01; GF: germ-free; BL6: C57BL/6 mice; ALT: alanine aminotransferase; AST: aspartate aminotransferase; ALF: acute liver failure; APAP: acetaminophen; CFU: colony forming units; RAG1: recombination-activating gene 1; FMT: fecal microbiota transplantation; SPF: specific pathogen free.

Next, I wanted to confirm if this phenotype persisted in GF C57BL/6 mice that were moved to the BSL2 room, and if it would be possible to elicit a liver damage response at the enzyme level by increasing the used APAP dose from 300 mg/kg to 500 mg/kg without any prior fasting in female mice, serum analysis was done by Dr. Suhaib Abdeen. Colonization levels in the colon content were high with no difference between sexes, and there were no colonies detected from the liver (**Figure 41M**). Group sizes were smaller but there was still huge variability within a group, making it difficult to draw conclusions in some cases. In the male mice, the same trend as before could be observed, with decreased enzyme levels with *C. albicans* colonization (**Figure 41N-O**), which was not reflected in the histology score (**Figure 41P**). The enzyme levels in the male PBS group were lower than in the previous two experiments, and, despite a higher APAP dose being used, more similar to the isolator experiment, suggesting that mouse strain differences have an impact on liver enzyme levels. To elucidate any effect due to a basal microbiome in a more controlled fashion, I included another group in this experiment that orally received FMT from untreated SPF mice. Previous FMT treatment increased the serum enzyme levels in both males and females as well as the histology score (**Figure 41N-P**), confirming a general response to bacterial colonization. The female PBS control mice remained at low enzyme levels and a lower histology score despite the higher dose of APAP (**Figure 41N-P**). To rule out that this was not due to a bacterial effect, an additional group of female GF mice that remained inside isocages was tested. Encouragingly, this group exhibited the same pattern as the female PBS mice, confirming the lack of damage-reducing bacterial effects. Contrary to the male mice, female mice colonized with *C. albicans* had an increase in both serum enzyme levels and histology score. This effect had not been observed in the isolator experiment, suggesting that it was either the higher APAP dose used, or the assembly of *C. albicans*-associated bacteria that triggered the response (**Figure 41N-P**).

To test, which of these two potential causes was more likely, I used a different experimental set-up that included a more present bacterial microbiome. SPF mice were treated with ABX, resulting in a reduction of the microbiome but not complete removal. This was combined with the exact same conditions as in the isolator experiment, namely a lower APAP dose (300 mg/kg) preceded

by 6 h of fasting. To enable proper fungal colonization, SPF mice were pretreated with 4-way ABX for five days, followed by colonization, and after one week APAP was injected. Colonization of *C. albicans* was highly present in the colon content for both sexes (**Figure 42A**). In male mice, enzyme levels from the PBS controls were lower than in the isolator, which suggests that either some of the ABX-resistant bacteria have a protective effect, or the presence of bacteria during development shaped somehow the level of response compared to the GF mice (**Figure 42B-C**). Female control mice had lower enzyme levels compared to male mice (**Figure 42B-C**), which was also reflected in the histology scores (**Figure 42D**). Interestingly, *C. albicans* colonization increased the enzyme levels in both males and females but with great variability within the groups despite a large group size of 9-10 animals (**Figure 42B-C**), however, this was not reflected in the histology score (**Figure 42D**). The complete reversal of the *C. albicans* phenotype that had been observed in the GF isolator conditions in males, as well as the replication of the same trend in females, implies that the exacerbation of the liver damage visible in the liver enzyme levels is not a direct *C. albicans* but rather an indirect effect caused by *C. albicans*-associated bacteria.

To confirm this hypothesis and evaluate if it is dependent on the fasting condition, the experiment was repeated in female GF C57BL/6 mice moved to the BSL2 room. These mice were injected with the lower 300 mg/kg APAP dose but not subjected to prior fasting, therefore the glutathione levels were not depleted. This experiment was conducted together with Dr. Denise Kviatcovsky. Colonization levels were confirmed by plating duodenum and colon contents, showing high levels in the colon as seen before, and no fungal colonies detected in the liver except for one outlier, which might be due to experimental contamination during plating as no colonies were present in other experiments (**Figure 42E**). PBS control mice showed low ALT and AST levels, potentially due to the low APAP dose injected, together with the presence of glutathione (**Figure 42F-G**). These levels were significantly increased when the mice were colonized with *C. albicans*, which was also present in the histology score (**Figure 42F-G, J**). To ensure that the observed phenotype was due to acute liver failure and not caused by biliary duct damage, I additionally tested the BILT3 (bilirubin total gen. 3) and GGT2 (gamma-glutamyltransferase 2) levels. Serum levels for both markers were low and not significantly different between the groups, confirming the typical phenotype of ALF (**Figure 42H-I**).

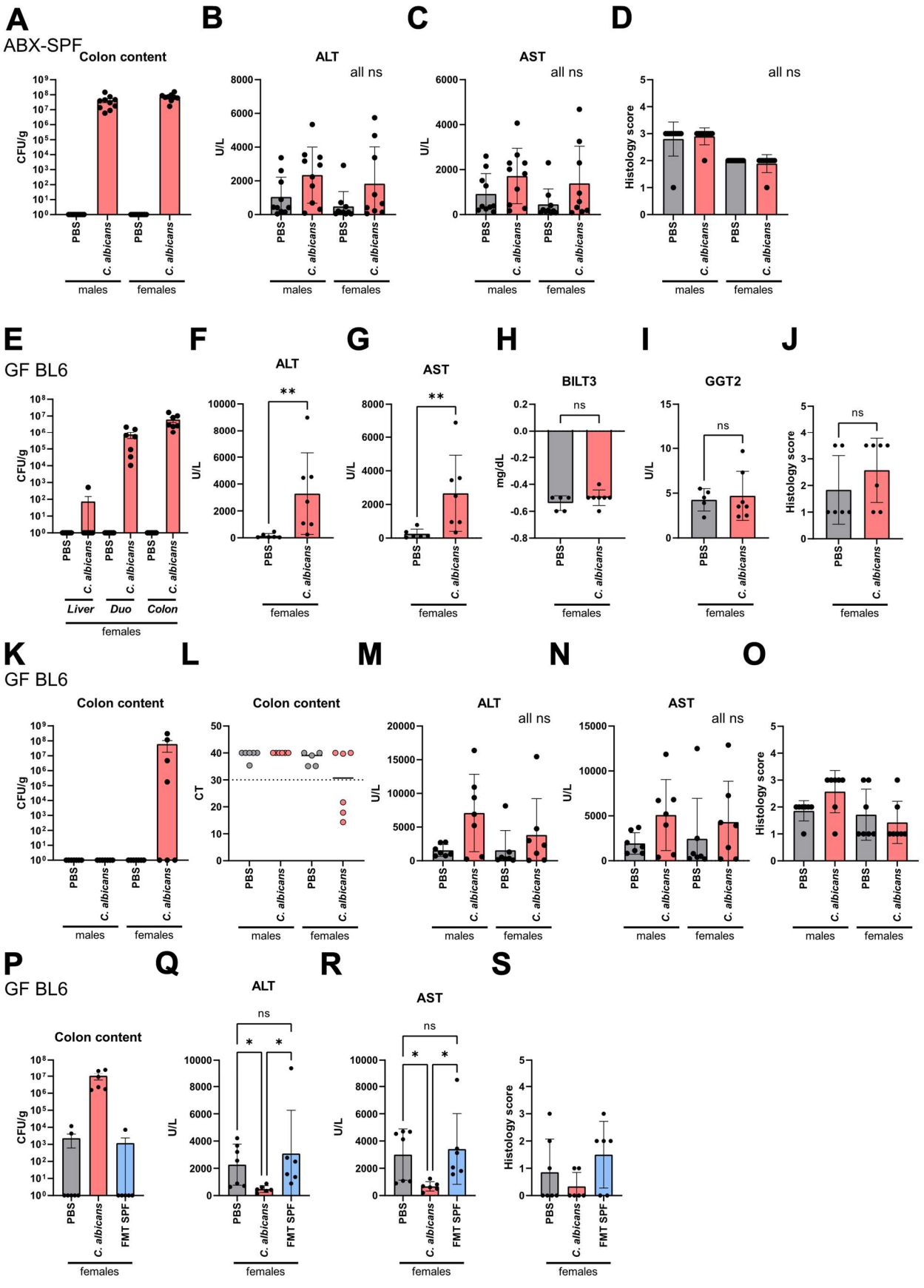
A
ABX-SPF
Colon content
CFU/g
PBS
C. albicans
males
females
B
ALT
all ns
U/L
C
AST
all ns
U/L
D
all ns
Histology score
E
GF BL6
CFU/g
Liver
Duo
Colon
females
F
ALT
**
U/L
G
AST
**
U/L
H
BILT3
ns
mg/dL
I
GGT2
ns
U/L
J
ns
Histology score
K
GF BL6
Colon content
CFU/g
L
Colon content
CT
M
ALT
all ns
U/L
N
AST
all ns
U/L
O
Histology score
P
GF BL6
Colon content
CFU/g
FMT SPF
Q
ALT
ns
*
*
U/L
R
AST
ns
*
*
U/L
S
Histology score

Figure 42: Influence of *C. albicans* colonization on ALF in ABX-treated SPF or GF mice. A-D) ABX-treated SPF C57BL/6 mice treated with 300 mg/kg APAP after 6 h fasting. **A)** CFU counts of colon content. **B-C)** Portal serum, **B)** ALT levels and **C)** AST levels. **D)** Histology score. **E-J)** GF C57BL/6 mice treated with 300 mg/kg APAP without fasting. **E)** CFU counts of liver, duodenum, and colon content. **F-I)** Systemic serum **F)** ALT, **G)** AST, **H)** BILT3, and **I)** GGT2 levels. **J)** Histology score. **K-O)** GF C57BL/6 mice treated with 500 mg/kg APAP without fasting. **K)** CFU counts of colon content. **L)** qPCR with *C. albicans*-specific primers of DNA extracted from colon content. Undetermined values were set to CT 40. **M-N)** Portal serum **M)** ALT levels and **N)** AST levels. **O)** Histology score. **P-S)** GF BL6 mice treated with 500 mg/kg APAP without fasting. **P)** CFU counts of colon content. **Q-R)** Portal serum **Q)** ALT levels and **R)** AST levels. **S)** Histology score. Statistical testing by Kruskal-Wallis test; ns: not significant; * p.adj. < 0.05; ** p.adj. < 0.01; GF: germ-free; BL6: C57BL/6 mice; ALT: alanine aminotransferase; AST: aspartate aminotransferase; ALF: acute liver failure; APAP: acetaminophen; CFU: colony forming units; FMT: fecal microbiota transplantation; SPF: specific pathogen free; ABX: antibiotics. BILT3: bilirubin total gen. 3; GGT2: gamma-glutamyltransferase 2.

Since the increase of ALT and AST levels appeared to be dependent on bacteria that co-occurred with *C. albicans*, I aimed to test if it would be possible to enhance the effect by lowering the *Candida* load present in the gut. This experiment was conducted in collaboration with Dr. Hagit Shapiro and serum enzyme levels measured by Dr. Suhaib Abdeen. The mice were colonized with a lower dose of *C. albicans* by restricting the fungal load to a 1000 fold lower single initial gavage. After one week, a 500 mg/kg dose of APAP was injected, and mice were not subjected to fasting conditions. Interestingly, low-level colonization led to either complete loss of live fungi in the colon content, or overgrowth to previous levels in a cage-dependent manner as measured by plating (**Figure 42K**), and confirmed by qPCR (**Figure 42L**). PBS control mice had slightly lower enzyme levels for the males compared to previous experiments, but not as low as in the ABX-treated SPF mice. On the other hand, female mice showed even lower enzyme levels except for one outlier (**Figure 42M-N**). Strikingly, independent of the levels of live *C. albicans* isolated from the colon content, male and female mice that had been initially exposed to *C. albicans* had higher serum enzyme levels, which was also visible in the histology score for the males as well (**Figure 42M-O**). The presence of this exacerbation phenotype despite the lack of live fungi cells in the colon content, unlike what happened in the GF isolator conditions, strongly suggests that it is mitigated not by *C. albicans* directly but by a naturally acquired bacterial community. This community appears to be specifically triggered by initial *C. albicans* colonization but not dependent on its continued presence.

While there are somewhat consistent visible trends, any experimental outcome that can be altered so strongly by the acquired microbiome is prone to non-consistency and chance. In a similar repeat experiment, performed in collaboration with Dr. Hagit Shapiro, and serum enzyme level measurements done by Dr. Suhaib Abdeen, the outcome was drastically altered. GF C57BL/6 female mice that were moved to the BSL2 room for colonization with *C. albicans* (at original high levels), or FMT derived from SPF mice, were injected with 500 mg/kg APAP without fasting. While there were a few mice in the PBS and FMT groups that appeared to be contaminated with *C. albicans* (**Figure 42P**), this was more likely a technical issue during the samples processing.

Serum enzyme levels of the PBS control group were consistently higher than in any other experiment, while the *C. albicans* group appeared to be completely protected from liver damage, as detected in both, serum enzyme levels (**Figure 42Q-R**) and liver histology score (**Figure 42S**). Liver damage was enhanced in mice that had received FMT to a similar extent as in the PBS group (**Figure 42Q-S**). In general, this experiment suggests that for a reason that needs to be further studied, the bacterial communities naturally acquired were shaped differently than in the other experiments, potentially triggering a disease exacerbating effect in the PBS group while the *C. albicans* group remained protected.

Overall, I could observe two main effects that were opposite to each other when inducing APAP-based ALF in *C. albicans* colonized mice. Firstly, *C. albicans* on its own seemed to have a direct protective effect in male mice. Due to the lower innate responsiveness to APAP of female mice, I could not assess if this was indeed sex-dependent or if it could be reproduced with a higher dose in females. This effect appeared to be independent of T and B cells and consistent across different mouse strains. Secondly, the presence of *C. albicans* could worsen liver damage in mice of both sexes by possibly shaping the composition of the microbial community, leading to an increase in harmful bacteria and exacerbating the damage. This effect however, was probably dependent on the bacterial species present, and could be changed in either direction. Taken together, this confirms that even in a short acute disease model like this one, the background microbiome can drastically alter the phenotype to the opposite direction, complicating the identification of any signal that would be applicable in a human disease scenario.

7.5 Chapter 5: *C. albicans* in Breast Cancer

Since analysis of the serum metabolome had shown that *C. albicans* could produce or trigger the production of certain metabolites that were measurable in the blood stream, I wanted to test if this could have an influence on a disease that was physically distant from the gut. One of the initial key hits of the previously described metabolomics dataset was hydroquinone (see **Figure 32G**). This compound is known to cause DNA double-strand breaks and has been linked to several different cancer types [235, 236]. Even though hydroquinone was not detected in further experiments, it led me to believe that a cancer model could be used to evaluate the effect of this fungus in a different disease context. I chose a breast cancer model because it produces tumors far from the gut, and a genetic mouse model, where the whole cascade of cancer development is available. Additionally, the specific mouse strain used, containing a copy of the human activated Erbb2 gene under control of the mammalian mammary tumor virus promoter, had the advantage of having been successfully established under GF conditions in our lab at the Weizmann Institute of Science already. Previous studies and internal results had shown an influence of the microbiome on breast cancer development but not in the context of gut colonization with *C. albicans*. Therefore, I colonized mice at the age of eight weeks with *C. albicans* and monitored their disease progression compared to non-colonized controls. This was driven by two potential hypotheses how an effect could be mediated, either from the intestinal fungi through for example, secreted metabolites, or through migration of fungi into the tumor tissue, potentially becoming intracellular.

7.5.1 Intestinal *C. albicans* colonization in ex-GF breast cancer mice

The two initial experiments were conducted together with Dr. Denise Kviatcovsky, Dr. Sara Federici, and Dr. Dragos Ciocan. Formerly GF mice were transferred to the BSL2 room for further colonization with *C. albicans*, and control mice were also housed in this environment. Mice were regularly monitored to assess colonization by stool sample collection and plating, and tumor growth. Once the tumors reached the predetermined endpoint size, mice were sacrificed. Colonization levels of *C. albicans* were high but additional dosages of *C. albicans* were required when the levels were dropping below 10^5 CFU/g feces (**Figure 43A**). This was most likely due to the natural acquisition of a microbiome during this long time period, which reduced the competitiveness of *C. albicans*. There was no significant difference between the survival of the mice with or without *C. albicans* colonization, with trends regarding the median survival going in opposite directions in the two experiments (**Figure 43B**). Upon sacrifice, the number of tumors per mouse was used to quantify tumor load since multiple tumors apart from the primary tumor could usually be detected, as well as two different metrics for tumor size: tumor volume and weight,

both plotted for each tumor separately and combined per mouse. There were no significant differences between the groups in any of these metrics, with the first experiment displaying a trend towards lighter and smaller tumors in *C. albicans*-colonized mice, while the second experiment showed the opposite trend for the volume (**Figure 43C-G**).

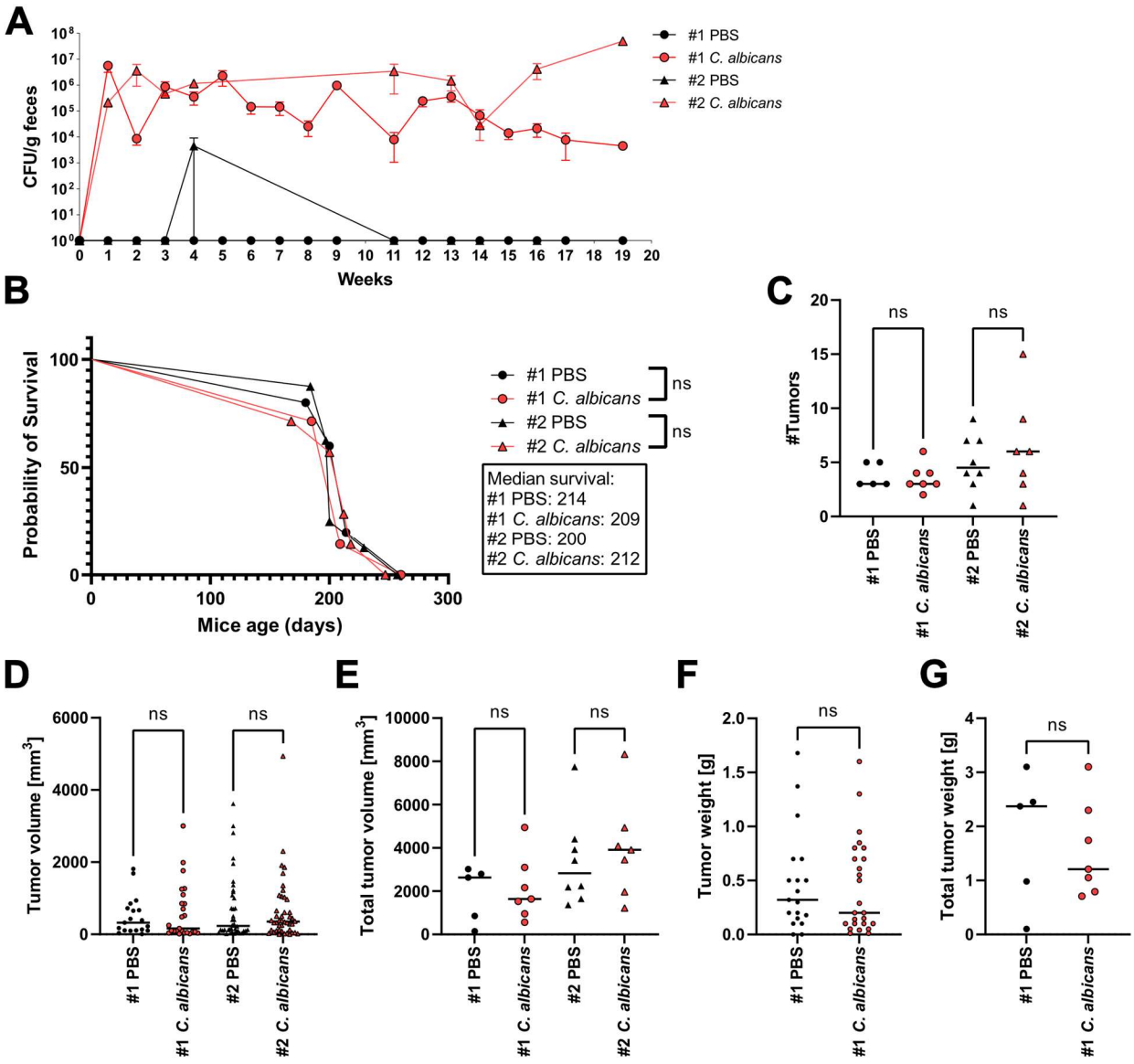

Figure 43: Effects of *C. albicans* colonization on breast cancer development in formerly GF mice. Two independent survival experiments (#1 & #2) of GF mice housed in the BSL2 room. **A)** CFU counts over time. **B)** Survival curves; significance tested by Log rank (Mantel-Cox) test. **C)** Number of tumors detected per mouse; significance tested by Kruskal Wallis test with pairwise comparison. **D)** Volume of the tumors; significance tested by Kruskal Wallis test with pairwise comparison. **E)** Total tumor volume per mouse; significance tested by ANOVA with pairwise comparison. **F)** Tumor weights; significance tested by Mann-Whitney test. **G)** Total tumor weights per mouse; significance tested by two-sided T test. GF: germ-free; CFU: colony forming units; ns: not significant.

In conclusion, there was no clear and common effect by *C. albicans* colonization on breast cancer development. Since I had previously seen that responses and downstream readouts under dirtier conditions in the BSL2 room could have huge fluctuations due to the uncontrolled nature of their potential microbiome acquisition, I repeated the same experiment under technically more challenging but cleaner conditions using a GF isolator.

7.5.2 Intestinal *C. albicans* colonization in isolators with breast cancer mice

This experiment was performed together with Dr. Denise Kviatcovsky and Dr. Dragos Ciocan. GF mice were moved to a GF isolator, and colonized with *C. albicans*, while the control mice remained in the original isolator. After the initial three-time gavage, mice maintained high *C. albicans* colonization levels for the entire five month period, suggesting that the dropping colony levels in the BSL2-housed GF mice experiment were indeed due to a naturally acquired microbiome (**Figure 44A, Figure 43A**). At the time of sacrifice, the entire intestinal tract was colonized, with an increase in colonization levels from duodenum to colon as expected from previous colonization experiments (**Figure 44C-D** and **7.2**). Interestingly, no live *C. albicans* could be isolated from the tumor tissues, similar to what had been observed in the previous experiments (data not shown), confirming that the live fungi did not translocate to the tumor tissue (**Figure 44E**). There was no significant difference in survival with or without *C. albicans* colonization, but a trend towards longer survival with *C. albicans* with a median survival of 214.5 days versus 206 days for the control group (**Figure 44B**). In line with this, mice colonized with *C. albicans* had significantly less tumors per mouse and lower tumor weight with all tumors separated or combined per mouse (**Figure 44F, I-J**). The same trend could be observed for the tumor volume, with *C. albicans*-colonized mice displaying smaller tumors, confirming a lighter tumor burden upon fungal colonization (**Figure 44G-H**). To see if *C. albicans* had an effect on advanced disease progression in the form of metastasis, histology of the lung was scored, since it is the primary tissue for breast cancer metastases. At least 75 % of the lungs showed metastases in both groups independently of the presence of *C. albicans* (**Figure 44K**). Based on this, *C. albicans* appeared to influence cancer development by reducing the tumor load.

To understand better if this was due to differences in tumor initiation or progression, another experiment was performed. In this case, instead of waiting until mice had reached the endpoint criteria according to tumor size, all mice were sacrificed once they had reached 206 days, the median survival age of the control group of the previous experiment (see **Figure 44B**). This

experiment was conducted in collaboration with Dr. Denise Kviatcovsky, Dr. Hagit Shapiro, and Dr. Suhaib Abdeen.

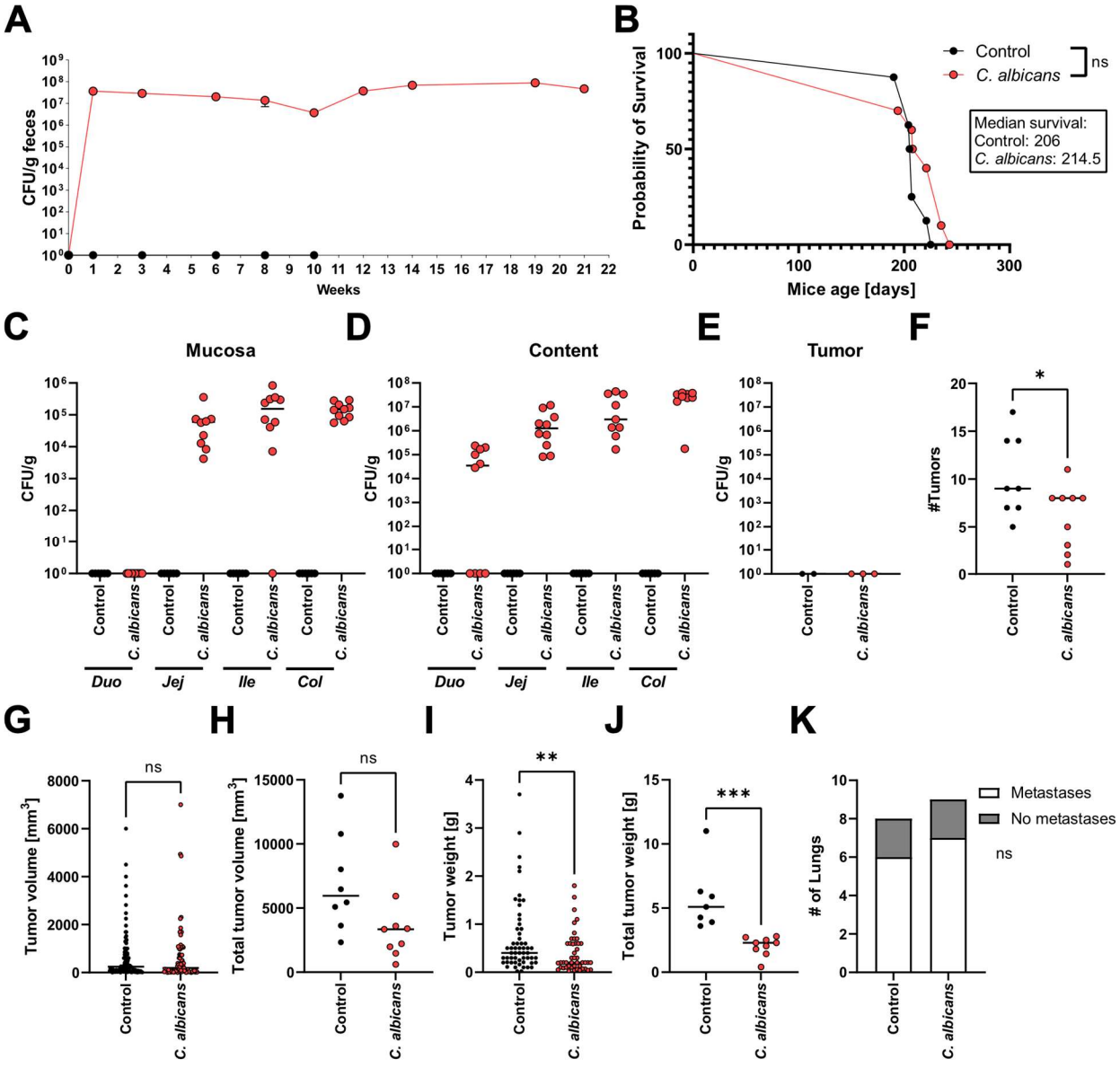

Figure 44: Effects of *C. albicans* colonization on breast cancer development in isolator-housed GF mice. Survival experiment. **A)** CFU counts over time. **B)** Survival curves; significance tested by Log rank (Mantel-Cox) test. **C-E)** CFU counts at sacrifice in **C)** intestinal mucosa, **D)** intestinal content, and **E)** tumors. **F)** Number of tumors detected per mouse; significance tested by two-sided T test. **G)** Volume of the tumors; significance tested by Mann-Whitney test. **H)** Total tumor volume per mouse; significance tested two-sided T test. **I)** Tumor weights; significance tested by Mann-Whitney test. **J)** Total tumor weights per mouse; significance tested by two-sided T test. **K)** Number of lungs scored as with or without metastases; significance tested by Fisher's exact test. GF: germ-free; CFU: colony forming units; ns: not significant; * p value < 0.05;** p value < 0.01; *** p value < 0.001.

Due to ethical animal-protection criteria, some mice needed to be sacrificed earlier because of their tumor size, which was the case for one mouse out of eight of the control group (12.5 %), and three mice out of eleven for the *C. albicans* group (27 %). All mice were included in the analysis

to avoid a bias (**Figure 45A-G**) but also additionally analyzed separately with only the mice that could be sacrificed at the correct time point included (**Figure 45H-K**).

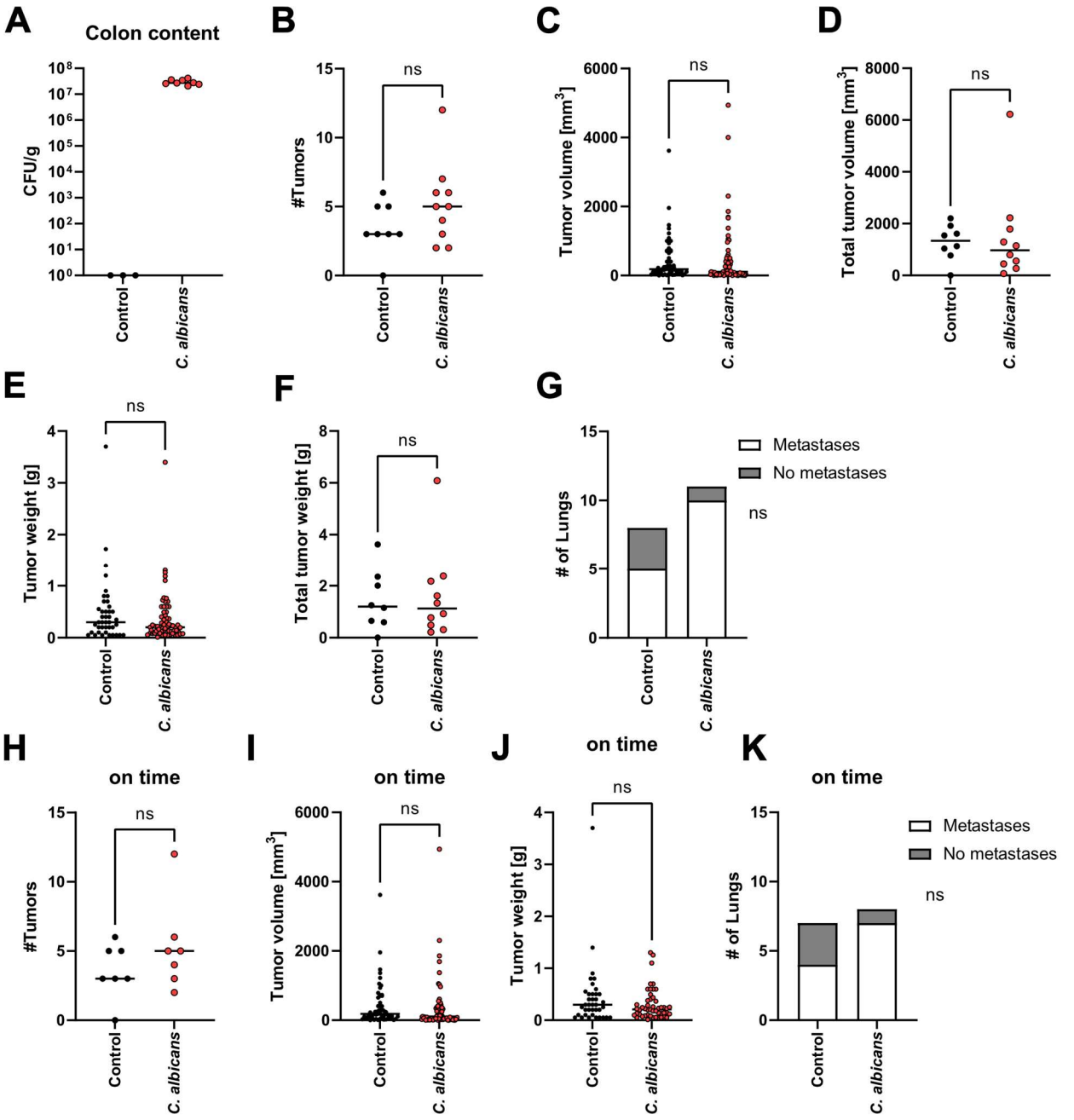

Figure 45: Effects of *C. albicans* colonization on breast cancer progression in isolator-housed GF mice. Fixed endpoint experiment. **A)** CFU counts in colon content at sacrifice. **B-G)** All mice included in the analysis; **B)** Number of tumors detected per mouse; significance tested by two-sided T test. **C)** Volume of the tumors; significance tested by Mann-Whitney test. **D)** Total tumor volume per mouse; significance tested two-sided T test. **E)** Tumor weights; significance tested by Mann-Whitney test. **F)** Total tumor weights per mouse; significance tested by two-sided T test. **G)** Number of lungs scored as with or without metastases; significance tested by Fisher's exact test. **H-K)** Only mice included in the analysis that were the exact same age and did not reach an endpoint sooner; **H)** Number of tumors detected per mouse; significance tested by two-sided T test. **I)** Volume of the tumors; significance tested by Mann-Whitney test. **J)** Tumor weights; significance tested by Mann-Whitney test. **K)** Number of lungs scored as with or without metastases; significance tested by Fisher's exact test. GF: germ-free; CFU: colony forming units; ns: not significant.

Colonization in a GF isolator had been previously shown to be stable over time, therefore, only the colon content at the time of sacrifice was assessed for *C. albicans* levels, which were indeed high as expected (**Figure 45A**). There was no significant difference for any of the tumor readouts, with a trend towards a higher number of tumors per mouse with *C. albicans* colonization, similar to what had been observed before (**Figure 45B**). However, fewer tumors per mouse were observed for both groups, which could be either due to the lower mice age on average at the time point of sacrifice, or due to a different operator's criteria for tumor detection. Interestingly, in regards to tumor size, the same trend was visible as in the previous experiment, with smaller and lighter tumors associated with *C. albicans* colonization (**Figure 45C-F**). Strikingly, mice colonized with *C. albicans* showed a non-significant trend towards more metastasis compared to the controls (**Figure 45G**). In the previous experiment, the levels of metastasis were high for both groups, while it was lower for the control group here, which might be due to the younger average age at sacrifice, allowing for the temporal resolution to catch this effect. To check that this was not biased by the inclusion of some mice that had to be sacrificed at a younger age, I also separately analyzed only the mice that had indeed reached the correct exact age at sacrifice. Encouragingly, the same trends were still visible as before, with no significant differences in terms of tumor number (**Figure 45H**), as well as smaller and lighter tumors present upon *C. albicans* colonization (**Figure 45I-J**), but an increased number of lungs with metastasis (**Figure 45K**).

Since this effect did not appear to be driven by translocation of *C. albicans* into the tumors, I hypothesized that it could be caused by metabolites secreted by *C. albicans* or produced as a response to colonization. To see, which metabolites were present at the late stage of tumor development and if any of them overlapped with the WT mice, I subjected serum samples from the portal blood and retroorbital bleeding of the isolator-housed survival experiment to metabolic profiling and untargeted metabolomics analysis.

7.5.2.1 Metabolomics of serum samples of isolator-housed GF mice colonized with C. albicans

Principal component analysis of metabolic profiling data for serum derived from both the portal and systemic blood showed significant clustering by experimental group, with or without colonization of *C. albicans* (**Figure 46A-B**). Interestingly, while there was only one metabolite significantly different for the portal blood, which was decreased, it was also reduced in the systemic serum, but additionally four metabolites were significantly enriched with *C. albicans* (**Figure 46C-D**). Similarly, metabolites clustered better together in the systemic compared to the portal serum samples, and metabolite levels appeared more consistent across samples within a group (**Figure 46E-F**).

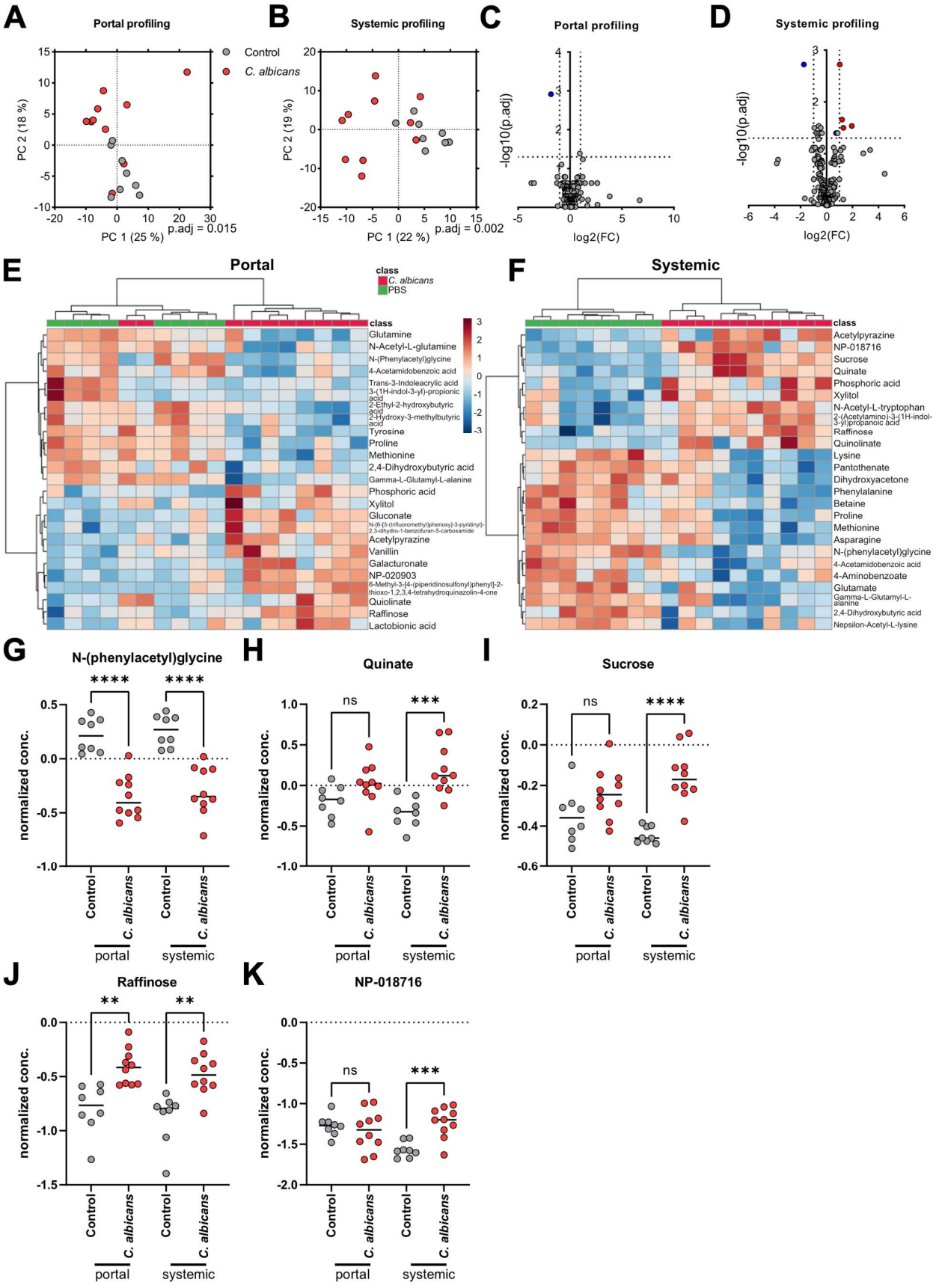
A
Portal profiling
Control
C. albicans
PC 2 (18 %)
PC 1 (25 %)
p.adj = 0.015
B
Systemic profiling
PC 2 (19 %)
PC 1 (22 %)
p.adj = 0.002
C
Portal profiling
-log10(p.adj)
log2(FC)
D
Systemic profiling
-log10(p.adj)
log2(FC)
E
Portal
class
C. albicans
PBS
Glutamine
N-Acetyl-L-glutamine
N-(Phenylacetyl)glycine
4-Acetamidobenzoic acid
Trans-3-Indoleacrylic acid
3-(1H-indol-3-yl)-propionic acid
2-Ethyl-2-hydroxybutyric acid
2-Hydroxy-3-methylbutyric acid
Tyrosine
Proline
Methionine
2,4-Dihydroxybutyric acid
Gamma-L-Glutamyl-L-alanine
Phosphoric acid
Xylitol
Gluconate
N-[6-[3-(trifluoromethyl)phenoxy]-3-pyridinyl]-2,3-dihydro-1-benzofuran-5-carboxamide
Acetylpyrazine
Vanillin
Galacturonate
NP-020903
6-Methyl-3-[4-(piperidinosulfonyl)phenyl]-2-thioxo-1,2,3,4-tetrahydroquinazolin-4-one
Quiolinate
Raffinose
Lactobionic acid
F
Systemic
class
Acetylpyrazine
NP-018716
Sucrose
Quinate
Phosphoric acid
Xylitol
N-Acetyl-L-tryptophan
2-(Acetylamino)-3-(1H-indol-3-yl)propanoic acid
Raffinose
Quinolinate
Lysine
Pantothenate
Dihydroxyacetone
Phenylalanine
Betaine
Proline
Methionine
Asparagine
N-(phenylacetyl)glycine
4-Acetamidobenzoic acid
4-Aminobenzoate
Glutamate
Gamma-L-Glutamyl-L-alanine
2,4-Dihydroxybutyric acid
Nepsilon-Acetyl-L-lysine
G
N-(phenylacetyl)glycine
normalized conc.
****
****
Control
C. albicans
Control
C. albicans
portal
systemic
H
Quinate
ns
***
I
Sucrose
ns
****
J
Raffinose
**
**
K
NP-018716
ns
***

Figure 46: Host serum metabolic profiling of GF isolator-housed breast cancer mice colonized with *C. albicans*. A-B) PCA of **A)** portal and **B)** systemic serum; statistical testing between groups by PERMANOVA. **C-F)** Differential metabolite analysis **C-D)** Volcano plots of **C)** portal and **D)** systemic serum; **E-F)** Heatmaps of top 25 significantly different metabolites in **E)** portal and **F)** systemic serum. **G-K)** Normalized concentrations of significant metabolites, statistical testing by G-I &K) One-way ordinary ANOVA or J) Kruskal-Wallis test. PCA: principal component analysis; GF: germ-free; PERMANOVA: permutational multivariate statistical permutation test; ns: not significant; * p.adj. < 0.05; ** p.adj. < 0.01; *** p.adj. < 0.001; **** p.adj. < 0.0001.

While there was the same trend in the portal blood for all significantly different metabolites except for NP-018716, the effect was larger in the systemic blood for quinate and sucrose (**Figure 46G-K**). This was quite striking and since the metabolite levels in the control group for quinate, sucrose, and NP-018716 were lower in the systemic than in the portal serum, one potential explanation could be that they were degraded or metabolized in the liver or reabsorbed along the way. This did not seem to happen in the same extent in the *C. albicans* group or was potentially more saturated due to a larger amount. However, none of these metabolites have a known association with breast cancer development in mice, which was further discussed in the next chapter (**8.5**).

Since I had previously seen that fungal metabolites or metabolites produced as a reaction to the colonization were better captured by untargeted metabolomics analysis, this was also performed here. For both the portal and systemic serum, the samples clustered significantly by experimental group as expected (**Figure 47A-B**). Many more metabolites compared to the metabolic profiling were significantly enriched or depleted and consistent across samples within one group, with more metabolites significantly different for the systemic serum (**Figure 47C-F**). Out of the significantly different metabolites, 24 overlapped between the portal and systemic serum, while 66 were specific for the systemic serum and only six were specific for the portal serum (**Figure 47G**). Since this was done by untargeted metabolomics analysis, the identity of the metabolites was unclear, and requires further investigation. To narrow down the list of potentially interesting metabolites, I wanted to see, which of these metabolites were the most consistent *C. albicans*-signature metabolites by comparing them to the metabolites measured in WT mice colonized with *C. albicans* (see **7.3.2.3.1**). These mice had the same genetic background, with only the breast cancer mice (“Hemi”) having an activated copy of the human Erbb2 gene under the expression of a mammary gland promotor. Since the WT mice do not develop tumors, they were sacrificed at an age of 20 weeks, while the “hemi” mice reached an age of about 30 weeks. Comparing the WT and “hemi” mice showed that between 18 and 32 % of the metabolites were significantly different as measured in portal and systemic serum, and with the two different metabolomics methods (**Figure 47H**). This big difference despite the clean isolator-housing and same genetic background could be due to either the age, genotype, or burden from the tumors. Despite these striking differences, I compared the metabolites that were significantly different with *C. albicans* colonization between both “hemi” and WT mice in serum collected from both the portal blood and

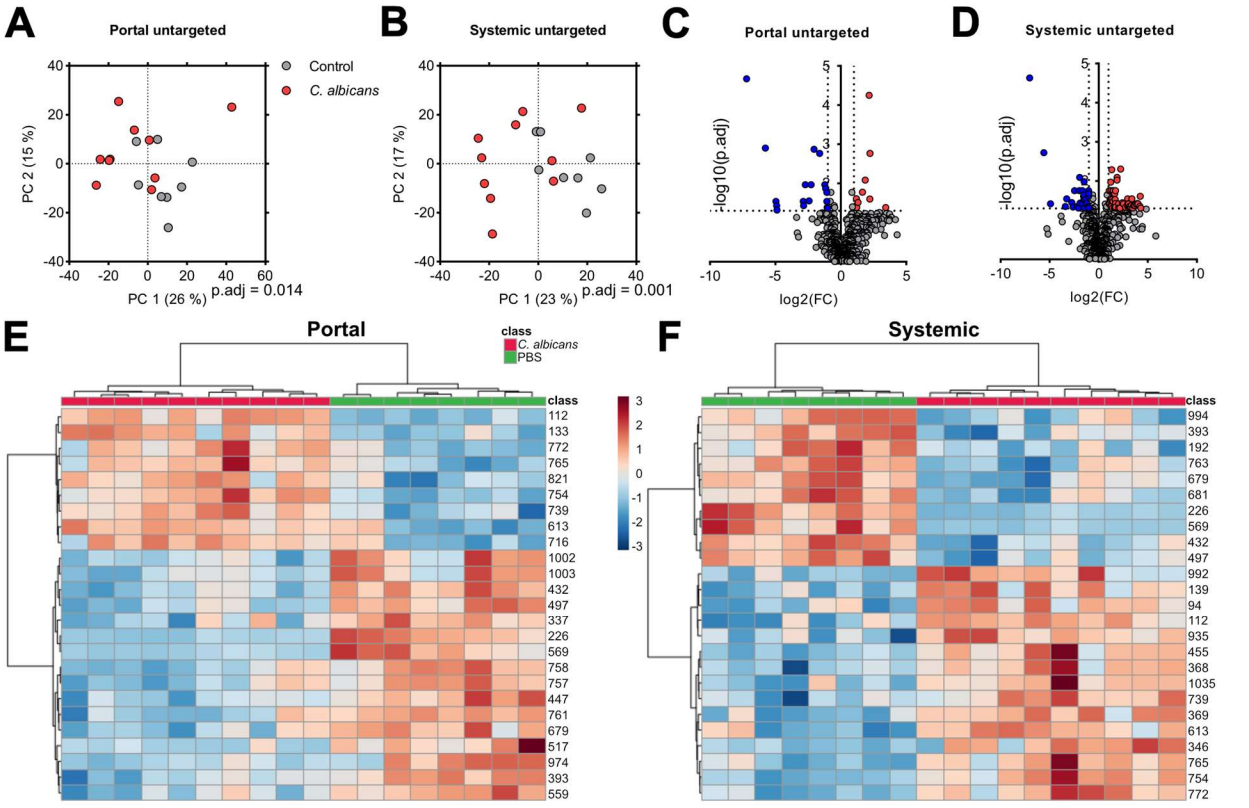

H

	Metabolites with p.adj < 0.05 & FC > 2 or < -2
Sys. Prof.	44 (20.2 %)
Sys. Untarg.	386 (32.7 %)
Port. Prof.	40 (18.3 %)
Port. Untarg.	353 (29.9 %)

J

Compound	Putative formula	ID	WT		Hemi		BL6	
			Sys log2(FC)	Port log2(FC)	Sys log2(FC)	Port log2(FC)	Sys log2(FC)	Port log2(FC)
m/z: 170.0949	NA	517	-4.4076	-4.493	-3.2653	-2.8763		
m/z: 357.1922	C18 H30 O7	372	1.3484	1.3821	1.0909	1.2072		
m/z: 187.0071	C7 H8 O4 S	226	-1.4622	-1.1397	-7.0413	-7.2022		
m/z: 341.1969	C18 H30 O6	521	-3.9963	-3.4972	-2.7432	-2.1882		
m/z: 367.2853	C22 H40 O4	56	-6.0891	-5.968	-3.4004	-3.3834	-4.4608	-3.9553

Figure 47: Host serum untargeted metabolomics analysis of GF isolator-housed breast cancer mice colonized with *C. albicans*. A-B) PCA of **A)** portal and **B)** systemic serum; statistical testing between groups by PERMANOVA. **C-F)** Differential metabolite analysis **C-D)** Volcano plots of **C)** portal and **D)** systemic serum. **E-F)** Heatmaps of top 25 significantly different metabolites in **E)** portal and **F)** systemic serum. **G)** Venn diagram of significant metabolites in portal and systemic. **H)** Table of significantly different metabolites as measured with different methods and in different sera, absolute number and as percentage of total metabolites detected. **I)** Venn diagram of significant metabolites in portal

and systemic in breast cancer mice (Hemi) and wild type mice (WT). **J)** Table of significantly different metabolites that overlapped with FC, background color indicates direction, stripes indicate non-significance. PCA: principal component analysis; GF: germ-free; PERMANOVA: permutational multivariate statistical permutation test; ns: not significant; * p.adj. < 0.05; ** p.adj. < 0.01; *** p.adj. < 0.001; **** p.adj. < 0.0001; FC: fold change; Sys: systemic; Port: portal; WT: wild type; Hemi: breast cancer mice; BL6: C57BL/6; Prof: metabolic profiling; Untarg: untargeted metabolomics.

a systemic source. Out of all the metabolites measured, only one was common for all of them and four were common in at least three datasets (**Figure 47I**). Examining these five metabolites more closely revealed that across all conditions, the metabolites were always changed in the same direction: one metabolite was increased and four were decreased (**Figure 47J**). Interestingly, this was also the case for the four metabolites that were only significant in three out of the four datasets, with the same directionality of change displayed in the missing cohort despite not being significant (in stripes) (**Figure 47J**). Out of these five metabolites, one of them was additionally significantly depleted in C57BL/6 mice colonized with *C. tropicalis* (see **7.3.2.3.2**), appearing to be a common *Candida* or maybe even general microbe effect (**Figure 47J**). Unfortunately, with only the mass to charge ratio (m/z), and sometimes the putative formula at hand, it was very difficult to determine which exact metabolite these could be, since there are still many potential isomers with vastly different functions possible. Therefore, since this belongs more to the realm of speculation, it was moved to the discussion section. Overall, it is possible that the decrease in tumor burden seen with *C. albicans* colonization is due to fungal metabolite signaling since there are changes in the host serum metabolome. Either one of the compounds measured by the metabolic profiling or one of the unidentified metabolites measured by untargeted metabolomics could be responsible for this phenotype. However, more research is necessary to confirm any mechanistic links.

8 Discussion

Commensal fungi are often overlooked in microbiome studies, and their significant contributions and roles remain largely unexplored. While the majority reside in the gut, they have also been detected in many other parts of our body, and even intratumorally at low levels [44, 45, 56]. Fungi have historically been studied mainly in the context of infectious diseases, however, commensal species that naturally inhabit our gut can be opportunistic, thus contributing to disease development. Shifts in the mycobiome composition have been associated with a variety of diseases, such as IBD, CRC, or NAFLD [54, 55, 176]. Further research has identified that these effects are often mediated through the modulation of the immune system or the secretion of bioactive metabolites. In this thesis, I investigated the interplay of the mammalian host with five selected commensal fungi species. I discovered interactions not just at the site of colonization in the intestine, but also at more distant body sites that can be reached via the circulation under healthy conditions, as well as in the context of two different disease models ALF and breast cancer.

8.1 Aim 1: Commensal fungi effects in vitro

My first aim of my thesis was to establish the use of several tools to study the effects of commensal fungi in vitro. The starting point was to manage successful growth of the five selected fungi species, which was achieved both aerobically and anaerobically, further confirming that they have the potential to be natural gut commensals, surviving in an atmosphere similar to that of the colon, with lower oxygen levels (**Figure 9 - Figure 10**) [217]. The growth rate of fungi was much slower under anaerobic conditions, which was visible by colony growth on agar plates as previously reported for *C. albicans* [237, 238]. Unfortunately, I was unable to quantify anaerobic fungi growth in liquid cultures due to the slower growth rate. This led to excessive condensation of the medium, making it difficult to obtain precise OD measurements.

The metabolic response of *C. albicans*, *C. tropicalis*, and *S. cerevisiae* under aerobic and anaerobic conditions grown in different growth media was strongly dependent on the nutrient availability, and the different oxygen levels (**Figure 11**). Both, low oxygen levels and changes in nutrient availability, can trigger a switch from yeast to hyphae morphology, thus strong changes in the metabolism are not surprising, as it can also impact virulence [239]. Hypoxia changes the fungal metabolism from respiration to fermentation, which also alters the required nutrients. This phenomenon has been demonstrated in *C. albicans*, where supplementation of oleic acid and nicotinic acid under anaerobic conditions enhances resistance to certain antifungal agents [240].

Similarly, *S. cerevisiae* requires addition of ergosterol for anaerobic growth, which has been much studied due to potential transferability of solutions for bioconversion or the food industry, [241, 242].

Despite these key differences in metabolic output, based on growth medium and atmospheric environment, several patterns were consistent across the different conditions for all or some of the fungi species (**Figure 12**). All three fungi produced several metabolites associated with the TCA cycle, which is surprising, since metabolism was reported to switch to fermentation. The reported switch to fermentation was shown for *C. albicans*, however, the profiled time point was only after three hours, rather than seven days, which could explain the different outcome [243]. The consumption of glucose by all fungi on the other hand is expected, since it is their preferred source of carbon, and the use of alternative carbon sources can even affect cell wall composition [244-246]. Similar to my results, there are certain metabolic pathways that were reported to be commonly regulated in both *Candida* species and some that are different, resulting in the production of other metabolites under the same growth conditions [247]. Under the growth conditions used in the experiments described in this thesis, *C. tropicalis* in particular had a distinct "signature" of metabolites that were depleted under all growth conditions profiled by this fungus and not with the others. However, apart from species differences, also the possibility of strain differences needs to be taken into account, which was not tested here and by adding another layer of complexity would give more nuance to these findings. For example, in the case of *S. cerevisiae*, specific strains can be used for diverse applications, with vastly different metabolic outputs. Environmental niches including other microbes in the vicinity, can also strongly alter the metabolic response [248]. Herein, only secreted metabolites, relevant for host interaction, were considered and have been shown to be quite distinct from the intracellular metabolites in *Candida* species [249]. Recently, a study profiling the metabolic output of cultured human intestinal fungi similarly reported the strong dependence on culture conditions, and highlighted the potential of fungi in regards to secondary metabolism based also on their genome [250].

As a first model of fungi-host interaction, I exposed human intestinal organoids to fungi supernatants and measured effects on organoid growth. Since *C. albicans* has been linked to CRC, I tested this on organoid lines derived from a cancer patient, and some genetically engineered lines with different CRC mutations [56, 76]. Any growth effects visible appeared to be highly dependent on the batch of supernatant used, limiting reproducibility and interpretability of the results (**Figure 13**). Additionally, the supernatants did not induce DNA double-strand breaks in the organoids, suggesting that the fungi are not producing genotoxic metabolites under the specific growth conditions used (**Figure 14**).

Since the supernatants alone did not appear to have a strong effect in the measured readouts, I increased the experimental complexity by adding live fungi that could interact with the epithelium in more ways. This fungi-organoid coculture was achieved through microinjection of the fungi into the intestinal organoid lumen, an experiment that has never been reported before. Unfortunately, it was not possible to find an optimal antifungal concentration that would limit fungi growth only outside the organoids but not inside, since even AmpB, which is known for its poor oral absorption capability, appeared to be able to cross the epithelial layer that separates the organoid lumen (**Figure 15**) [223]. Other antifungal agents used had the same problem (data not shown), limiting the survival of the coculture to one day or allowing the fungal overgrowth. Different imaging methods used were hampered by selectivity of the staining dyes to only some morphologies of the fungi or inability to penetrate the organoids (**Figure 16**). Resorting to a genetically labelled strain narrowed down the fungi that can be used for cocultures.

Intratumoral fungi detected inside tumor cells were described in two separate studies for multiple cancer types [76, 77]. I investigated if it was possible to model this using tumor-derived organoid lines in a fungi coculture system and measured the intracellular fungi by TEM and Imagestream (**Figure 17**). There were few intracellular *Candida* cells visible by TEM, which looked similar to previous studies [251, 252]. To distinguish the intracellular and extracellular *C. albicans* cells, an additional antibody staining step was added for the extracellular cells, which had been previously applied to infection studies using macrophages [253]. My results indicated that while it was possible to detect intracellular fungi, it remained unclear if they had entered into the organoid cells from the apical or basal side, and several half-inserted cells raised the question if the intracellular state was merely transient. To study this phenomenon further, and test what kind of effect the intracellular fungi has on the host cell and which pathways are regulating such behavior, the intracellular fungi could be sorted with flow cytometry and analyzed by parallel RNA sequencing (fungi and host). This has not been applied to intracellular fungi to date, but only in an infectious disease context to profile the adaptations of the host and fungal pathogen to invasive disease [254]. The halfway insertion of fungal cells into epithelial cells is reminiscent of the ability of *Candida* to escape macrophages after phagocytosis in an infectious disease state through initiating filamentous growth [253, 255]. It is unclear therefore, if the coculture is a physiological model for intracellular fungi or if it rather reflects an infectious disease setting. Additionally, the abundance of intracellular fungi and microbes has been controversially discussed, due to reanalysis of previous datasets demonstrating that many of the detected signals were due to contamination of microbial databases with human reads and vector contamination from sequencing primers and adaptors [80]. In this reanalysis, *S. cerevisiae* remained as the most

abundant fungi, which was described to be likely a cross-contaminant acquired during sample processing. Doubts about analysis methods have also spread to bigger biomass datasets, where previously detected fungal dysbiosis in the pancreatic tissue and fecal samples of healthy and pancreatic-ductal adenocarcinoma bearing mice and humans was no longer present upon reanalysis [97, 256]. This sheds light on several issues with analysis methods, and the importance of public availability of datasets to allow for reanalysis by peers.

Finally, I measured further downstream effects of fungi-organoid cocultures on the host cells related to carcinogenesis. There was no influence on DNA double-strand break levels or single cell outgrowth potential, as a proxy for metastatic growth (**Figure 18**). However, single cell outgrowth was only measured with a healthy intestinal organoid line, and might show different results with a tumor- or metastasis-derived organoid line. Interestingly, gene expression patterns of several genes that had been associated with *C. albicans*-containing tumors showed opposite trends or no effect to what was previously reported in the literature [76]. This highlights the limitations of using microbe-organoid cocultures: while a reductionist approach can be useful to pinpoint molecular mechanisms, the lack of an immune system can alter responses. Moreover, several immune mechanisms are mediated by the microbiome, which closely interacts with our immune system, for example, changes in inflammation-induced CRC was associated with varying levels of *Candida* [91, 257]. It is therefore not surprising that this could not be accurately represented in the proposed coculture setup, requiring further research.

8.2 Aim 2: Establishment of long-term intestinal fungi colonization in mouse models

For the second aim of my thesis, I initially optimized fungi detection methods. In my hands, the Qiagen Power Soil Pro kit yielded the highest amount of DNA with the best fungi representation with standard kit parameters (**Figure 19**). This kit is also commonly used as the standard kit in other studies for fungi detection [45, 51]. ITS sequencing and Shotgun metagenomic sequencing were established and adapted to fungi in the lab, with the former demonstrating a detection bias for certain fungi species potentially based on amplicon length or gene copy number, and the latter hitting sequencing depth limits (**Figure 20**), both of which are known problems [108].

The SPF mice in the DKFZ mouse facility did not have a culturable mycobiome on the culture media used, and showed a large variety of fungi with ITS sequencing, which has been previously shown to be highly dependent on vendor and facility (**Figure 21**) [134]. No fungal overgrowth was measured in ABX-treated mice, however, a better way to assess this would be to perform qPCR before and after ABX treatment to see if they mimic the human phenotype of fungal bloom [73-75].

I could successfully colonize the GI tract of ABX-treated, GF, and isolator-housed mice of three different mouse strains with *C. albicans*, which is in line with literature reports of consistent colonization after initial clearance of the niche (**Figure 22**, **Figure 23**), [139].

Three of the other selected fungi, *S. cerevisiae*, *M. globosa*, and *M. restricta,* did not colonize the intestinal tract of ABX-treated SPF mice (**Figure 24**). However, I never attempted to colonize them in a technically challenging isolator setting, which would be the cleanest option to decipher if these fungi cannot colonize due to colonization resistance from residual bacteria or because they are not true commensals and do not possess the ability to colonize the mouse gut. Other studies orally gavage mice with these fungi daily or every few days, which suggests that stable colonization was not possible as well and repeated exposure is rather mimicking fungal uptake with food [93, 99].

Colonization with the other *Candida* species, *C. tropicalis*, presented several challenges by only colonizing in ABX-treated SPF mice and isolator-housed mice but not GF mice (**Figure 25**, **Figure 26**, **Figure 27**, **Figure 28**). After many attempts, it became clear that the GF mice did not stay GF upon relocation to the BSL2 room, which was necessary since the fungi strain was BSL 2, but rather acquired a background microbiome, that could confer resistance to *C. tropicalis*. ABX use suppressed this but the microbiome acquisition was never visible by culturing, since the fungi culture plates contain the ABX chloramphenicol. As a final proof that bacterial colonization

prevented *C. tropicalis* colonization and which bacteria are responsible for this effect, qPCR and sequencing of stool samples before and after transfer to the BSL2 room could be performed, to see if the 16S load increases and which species appear. However, based on the previous experiments it is possible to speculate which bacteria species are the culprits, based on their ABX susceptibilities: the bacteria were susceptible to Ampicillin and Vancomycin but resistant to Metronidazole and Neomycin (**Figure 28**). Ampicillin is a beta-lactam antibiotic, acting against Gram-positive and -negative bacteria, while Vancomycin is a glycopeptide antibiotic mainly effective against Gram-positive bacteria [258, 259]. Meanwhile, Neomycin acts as an aminoglycoside antibiotic on Gram-negative bacteria, and Metronidazole targets anaerobic bacteria, therefore, Gram-positive bacteria that are aerobic such as for example *Enterococcus* or *Staphylococcus* species might fit this specific profile [260, 261]. While nothing is known about growth inhibition of bacteria on *C. tropicalis*, several bacteria like *Lactobacilli* and *Streptococci* have been shown to inhibit *C. albicans* in vitro and in vivo [262].

This adds to the puzzle of why the acquired microbiome only impacted *C. tropicalis* but not *C. albicans* colonization, although previous metabolic profiling of the supernatants of cultures grown in vitro had already revealed different metabolic outputs, perhaps pointing towards different growth requirements. In line with this, a recent study revealed the importance of the hyphal toxin Candidalysin for *C. albicans* to increase fitness and outcompete bacteria in the intestinal tract [263]. While *C. tropicalis* has the gene for Candidalysin, it appears to be under different regulatory elements, which might explain why it cannot compete well with the bacteria under these specific circumstances [90].

C. tropicalis has been much less investigated compared to *C. albicans*, therefore reports of successful mouse gut colonization are rare. One study repeated oral gavages with *C. tropicalis* twice a week despite the mice being GF, indicating similar issues, and highlighting the difficulty to judge what is inferred by a GF status in different studies [91]. The far-reaching consequences of this are further discussed in the next chapter.

8.3 Aim 3: Profiling fungi-host interactions at the transcriptomic and metabolomic levels

8.3.1 Transcriptome

To investigate the impact of fungal colonization on the host at different gut locations, I performed RNA sequencing on the mucosa of two distant areas – the duodenum and the colon – both known to be colonized by fungi. The mice had either received ABX treatment or were formerly GF mice, transferred to the BSL2 room, and colonized with *C. albicans* or *C. tropicalis* (**Figure 29**, **Figure 30**, **Figure 31**). Generally, there was high tissue specificity in the host response, which has been similarly reported for the response to high fat diets [264]. The transcriptional reaction to colonization with *Candida* included a stronger downregulation than upregulation of genes, which has not been reported before due to a surprising lack of transcriptional studies.

Strikingly, there was a distinct difference in gene expression response to *C. albicans* colonization between two repetitions of an identical GF experiment, suggesting that this response was strongly influenced by the acquired background microbiome. I attempted to determine a core response to the fungi that would be consistent across experimental conditions and not skewed by the diverging bacterial microbiomes. Each comparison narrowed down the common gene response further and "specific" responses to fungi species. However, the number of datasets available and the lack of other fungi or bacteria colonization datasets, to differentiate between a general host response to colonization and species-specific responses, limited this comparison. In order to prove if any specific response is due to the fungi itself or the associated bacterial community, a sequencing dataset of mice colonized with the fungus in an isolator setting would be necessary. After comparing all datasets and conditions, three genes were specific for *C. albicans* colonization, with one being uncharacterized. Iglv1, which is a region of the variable domain of immunoglobulin light chains, was upregulated upon *C. albicans* colonization, and could be relevant for an antibody response against *C. albicans* [231, 232]. This could be in line with reports profiling the rise of *C. albicans*-specific antibodies after colonization that help maintain commensalism and can be cross-reactive against other pathogens [38, 265, 266]. SCN9A on the other hand, was downregulated with *C. albicans* colonization, which is an important subunit of a sodium channel in nociception signaling [233]. Rodents with a knockout of this gene show pain insensitivity, therefore, downregulation by *C. albicans* allows speculation of a changed sense of pain in these animals, which was never reported before [267]. Interaction of any microbial member with this channel has never been disclosed and is a very surprising finding that could be interesting regarding novel analgesic research.

Unfortunately, it was not possible to detect fungal RNA reads from the same sequencing run (data not shown), even though *C. albicans* is expected to reside in the mucosa, which would have been an interesting insight into the regulation of commensalism in the fungi in vivo [268]. Potentially, separate RNA extraction protocols of neighboring regions would have been necessary to solve this issue, as was previously applied to infectious disease studies [111].

The strong influence of the acquired microbiome despite a high fungal load in the intestine implies that issues with "monocolonization" of formerly GF animals translate to downstream readouts, such as the host transcriptional response.

8.3.2 Metabolome

Apart from the direct interaction in the gut, the site of colonization, I aimed to investigate the potential impact of fungi on the host serum metabolome by producing or stimulating the production of bioactive molecules. Therefore, metabolomics analysis was performed on mice serum samples from the portal vein and a systemic source. In GF mice that were transferred to the BSL2 room, the influence of the naturally acquired bacterial microbiome was apparent through huge variations of the measured metabolites between experiments (**Figure 32**, **Figure 33**, **Figure 34**, **Figure 35**). Not only could the initial hits not be reproduced in other datasets but *C. tropicalis* colonization, which was lost in the first weeks, induced metabolite changes, indicating that it had a role in shaping the bacterial community. While the acquisition of the bacterial community under these circumstances was not measured, it is the most likely explanation given the previous experiments. Technically the colonization resistance and influence on downstream effects could also be due to another fungi species, but the presence of other fungi is rare in mouse facilities and might have been easily detected on the growth plates.

Comparison of two experiments with fungi colonization of ABX-treated SPF mice was difficult due to a simultaneous change of multiple important factors at once, such as vivaria and protocol of ABX treatment. These factors can have a strong influence on the bacterial background microbiome, which could explain the great variation in serum metabolomics between experiments (**Figure 36**, **Figure 37**). Metabolomics analysis of isolator-housed mice that were monocolonized only with *C. albicans* or *C. tropicalis* revealed that there were almost no significant metabolites even under these clean circumstances (**Figure 38**, **Figure 39**). In the case of *C. albicans* colonization this analysis was limited by the group size, therefore, I attempted to test if there were common "signature" metabolites changed in all experiments even if they were not significant in every single experiment analyzed on its own. However, comparing all metabolites with the same

change in directionality regardless of their significance among experiments did not reveal a “signature”. This suggests only a weak metabolic output as measured using the polar library, with a strong influence by not only the bacterial community but also batch effects between metabolomics runs, which were tried to minimize by combining experiments in runs. Interestingly, untargeted metabolomics analysis rather than metabolic profiling uncovered some significantly different metabolites with or without *Candida* colonization, suggesting that the polar library does not properly capture fungal metabolites. Use of a semipolar library would have been an alternative approach, although it is unclear if that would results in better capture of fungal metabolites. A previous study had similarly reported, that *C. albicans* infection had only little influence on the metabolome of the cecum, although this was hampered by low *C. albicans* growth [269]. Furthermore, metabolomics of the plasma of mice colonized with *C. albicans* showed downregulation of several metabolites and the importance of amino acid and TCA cycle pathways, although the consequences of this were not further assessed [270]. Another study reported an increase in sterols, endocannabinoids, and lipid compounds in the cecum upon *C. albicans* colonization, which was related to increased anxiety behavior [271]. On a broader scope, the human mycobiome was previously shown to be associated with fatty acids, in a metabolomics and metagenomics fecal sample correlation study [272]. These studies are in contrast to the absence of any significant changes measured with lipidomics, however, this could also be due to the difference in sample type: fecal or cecum content and serum.

When comparing the age- and sex-matched control mice of the respective isolator experiments, which belonged to two different mouse strains C57BL/6 and FVB, the serum metabolome contained many significantly different metabolites (**Figure 40**). This is in line with previous studies that have determined similar differences in metabolite levels in various tissues of other mouse strains, which raises questions regarding the transferability of metabolomics results between different mouse strains or even applicability to more genetically diverse humans [273-275].

The sensitivity of metabolomics serum analysis to mouse genetic and microbiome background, chow, and detection method makes the untangling of fungal effects difficult. Unless the common signal is very strong, it can be easily masked by confounders, which can be misinterpreted as the “true” signal. This has important implications for many mechanistic microbiome studies, not just in fungi research, with potential misassignment of effects to other microbial members that are not detectable unless specifically searched for. The microbe-free status of GF mice is not maintained unless they remain in designated isolators, which makes true “GF” studies technically challenging and limited by facility capacities. A lack of awareness of this issue can have far-reaching

consequences in regards to the experimental interpretation of results, as it affects every aspect of microbiome research.

Additionally, even when a pure monocolonization can be achieved, it remains unclear how parameters such as gene expression, metabolite secretion or even morphology would change with the addition of a specific community. Bacteria-fungi interaction studies have so far been either focused on sequencing composition studies or reduced to in vitro mechanistic setups, which cannot fully model the complexity of community structures but has shown a manifold of interactions [272, 276, 277]. How this common issue in microbiome research will be solved in the future remains to be addressed.

8.4 Aim 4: Investigating the influence of *C. albicans* gut colonization on an ALF mouse model

The liver is closely connected to the gut via the portal vein, thus many liver diseases have been associated with changes in the mycobiome, such as alcoholic liver disease, NAFLD or PSC [170, 174, 176, 278]. One liver disease that is strongly influenced by the microbiome is ALF, characterized by rapid multi-organ failure and oftentimes induced through an APAP overdose [142, 159, 162]. For this aim, I investigated the influence of *C. albicans* colonization on an APAP-induced ALF mouse model. Severity of the disease was measured by enzyme levels (ALT, AST), and scoring of liver necrosis. The two main seemingly contrary effects observed included a direct protection of liver damage in a subset of male mice colonized with *C. albicans*, and the increase of ALF severity in mice that had been exposed to *C. albicans* but assumedly accumulated a natural microbiome. Additionally, female mice were consistently more protected against ALF than male mice. This phenomenon has long been known, and has been described to be mediated by glutamate-cysteine ligase, the enzyme responsible for the rate-limiting first step of GSH biosynthesis [279-281]. Even though GSH was depleted at the same speed in males and females, it recovered at a 2.6 fold faster pace in female mice compared to male mice [153]. This study observed a decrease in both ALT levels and liver necrosis in females, although I had noted it primarily in enzyme levels and only occasionally in liver histology.

Colonization with *C. albicans* had a strong protective effect on APAP-induced liver damage not in all but in a subset of male mice that were housed in an isolator, suggesting a direct fungi effect since the mice were otherwise sterile (**Figure 41**). It was puzzling that this was only affecting a subset, since these mice were age-matched, cohoused, and treated the same way. Apart from an experimental mishandling, another explanation could be that the six-hour fasting period before the APAP injection was too short to deplete the GSH homogeneously, and some mice that happened to eat right before the fasting period would be more protected than others that did not. This could be possible, since the fasting period was during the morning, which is at the end of the active phase for mice, so not all mice might be adhering to the same feeding behavior [282]. For that reason, it is suggested to fast the mice overnight. This was unfortunately not possible in this case since I did not want to alter the time of injection (performed early in the afternoon), due to known circadian effects [157, 283]. However, ex-GF male mice colonized with *C. albicans* and transferred to the BSL2 room were also more protected than controls in three independent experiments: an outbred mouse strain (Swiss-Webster), a mouse strain without B and T cells (RAG1-/-), and the same mouse strain, C57BL/6. Interestingly, the basal enzyme levels for the other two mouse strains were much higher than for the C57BL/6 strain, which could be due to a predominance of

anti-inflammatory gene expression in C57BL/6 mice [284]. Most studies have employed male C57BL/6 mice for APAP toxicity studies, with other strains or females requiring potential dose adjustments [283]. It was encouraging that the enzyme levels in the controls were similar between the isolator and GF experiment of the same mouse strain, despite the use of a different protocol, with a higher dose and no fasting for the GF mice, showing a certain consistency. The reduction in ALF was not T and B cell dependent, unlike the *C. albicans*-induced exacerbation of alcoholic hepatitis, where Th17 cells contributed to this effect [173]. This partial liver damage protection of *C. albicans* colonized mice was mainly visible in the enzyme levels but was not reflected in the histological necrosis score of the liver, suggesting differences in temporal resolution. Since this was similar to the variation between males and females, the phenomenon could also be due to a differing regulation of GSH, although nothing is known about *C. albicans* ability to regulate this in the host. While in an infectious disease context, phagocytosed *C. albicans* upregulates its GSH pathways to counteract the oxidative stress, it seems unlikely that this would be applicable to an ALF setting [285]. Another alternative explanation could be the potential detoxification or accumulation of APAP by *C. albicans* directly, which has not been shown to date for fungi or APAP. However, it is well-known that members of the bacterial microbiome can have direct effects on drug efficacy through drug's metabolism or bioaccumulation [286, 287]. For APAP, it was previously reported that certain soil but not gut bacteria have the ability to metabolize APAP [288]. Additionally, bacterial metabolites could compete with APAP metabolism enzymes and thus alter pharmacokinetics [155].

Overall, before attempting to understand this phenomenon by, for example, metabolomics of the serum and sequencing of the liver before APAP injection, the isolator experiment should be repeated to rule out any technical experimental errors and confirm this phenotype. *C. albicans* colonization was shown previously to change transcription in the liver, therefore, it would be interesting to check whether any of these changes predispose the liver to be more protected against APAP, which could also be through activation of the immune system [271].

Some bacterial species have been shown to alleviate APAP liver toxicity, for example *L. vaginalis*, which produced β-galactosidase that could free daidzein from the diet, allowing the prevention of ferroptosis in liver cells [161]. Although daidzein was elevated in the first serum metabolomics analysis performed, it could never be validated in follow-up experiments, and no β-galactosidase activity has been described for *C. albicans* to date, suggesting that daidzein was not produced by *C. albicans,* and its phenotype was not mediated via the same mechanism. Similarly, another study showed microbiome-mediated alleviation through production of phenylpropionic acid, which

lowered CYP2E1 levels, however, this metabolite was not elevated in the serum metabolomics dataset from this thesis, and has not been reported to be produced by *C. albicans* [160].

While my findings highlight the impact of the isolated *C. albicans*, it is crucial to also consider the effects of the whole bacterial community. The acquisition of a bacterial background microbiome that was shaped by even a fleeting presence of *C. albicans,* worsened liver damage in both male and female mice (**Figure 42**). Interestingly, mice that had grown in the presence of a normal microbiome, which was later depleted by ABX administration, presented lower enzyme levels than mice that developed as GF and repopulated by receiving a FMT, highlighting the important role of the microbiome during development. The increase in liver damage appears to be mediated not directly through *C. albicans* colonization but rather the microbial communities associated with the fungi, since this effect was absent in the isolator experiment. Additionally, liver damage was pronounced in ABX-treated mice, as well as in mice that had received only a low, initial dose of *C. albicans* and had lost colonization at the time point of sacrifice, two conditions with higher expected bacterial levels. This indirect community effect seemed to overrule any “direct” *C. albicans* impact, whether it was mediated through a metabolite or regulation of the innate immune system. However, the reversal of this phenotype in another experiment showed that this community acquisition is fickle and can probably highly depend on the current environment, e.g. the season, or other ongoing experiments in the same room.

It has been previously reported that the microbiome has a strong influence on the APAP response, even the same mouse strain obtained from different vendors had varying levels of hepatotoxicity [160]. *C. albicans* has been shown to not just interact with bacteria in many ways but also to drive community assembly, such as after ABX treatment in the mouse gut, where it changed relative abundance and shifts in genera [289, 290]. Similarly, I had shown for *C. tropicalis*, that colonization of ABX-treated SPF mice changes the background bacterial microbiome (**Figure 26G**). It therefore seems possible that *C. albicans* could shift the microbial community assembly in formerly GF mice, which could induce a stronger APAP effect through e.g. production of pro-inflammatory metabolites. The striking difference between the effect of *C. albicans* on isolator-housed and ABX-treated SPF mice with the same protocol, shows that there is an interesting and novel possibility for a new fungi-bacterial interaction that appears to be sex-, and T and B cell-independent.

To further deepen our understanding of this effect, the next steps could involve conducting sequencing and comparison of stool samples to definitively confirm the presence of a *C. albicans*-associated bacterial community that potentially contributes to disease exacerbation. By analyzing the bacterial species or common bacterial functions present during periods of heightened liver

damage compared to periods of stability, we can pinpoint potential factors that may be driving this phenomenon. These findings could be validated through co-colonization models or FMT of the *Candida*-shaped bacterial community, allowing for a more targeted investigation into the mechanisms at play. Additionally, single cell RNA sequencing of the liver combined with multiplex ELISA could elucidate the inflammatory response on a transcriptional and protein level. The specificity of the effect to *C. albicans* and APAP could be further validated through the utilization of alternative ALF models, such as TAA injection. Additionally, testing the effect with other species of fungi may be necessary, which may involve modifying colonization models. Furthermore, the mechanism can be narrowed down by using knockout strains of the fungi involved. The deletion of specific genes that can also affect the fungal growth morphology and thus strongly shape their interaction with bacteria could be highly interesting, like the toxin Candidalysin that was implicated in alcoholic hepatitis [172, 263]. Finally, any potential *C. albicans*-associated bacterial community combinations relevant for humans should be confirmed by analysis of a clinical dataset with proper Shotgun metagenomic sequencing depth, which does not exist yet to my knowledge.

8.5 Aim 5: Identifying the impact of *C. albicans* gut colonization on a breast cancer mouse model

As a final aim, I investigated if intestinal *C. albicans* colonization could influence breast cancer progression in a genetic mouse model, potentially via metabolites, since significantly different metabolites were found in the systemic serum. While there were no significant differences in tumor development when formerly GF mice were housed in the BSL2 room, in a controlled isolator-housing, *C. albicans* colonization led to two contrasting effects (**Figure 43**, **Figure 44**, **Figure 45**). On the one hand, colonizing mice with *C. albicans* lowered the tumor burden of the mice compared to GF controls; on the other hand, it seemed to trigger earlier metastasis. *C. albicans* did not translocate from the intestine to the tumors and is thus unlikely to be present in the metastases, which was the proposed mechanism for bacteria in a different genetic breast cancer mouse model [196]. The reduction in tumor burden due to *C. albicans* colonization was found to be statistically significant in only one of the two isolator experiments, despite both experiments showing similar trends. This discrepancy may be attributed to potential temporal effects, as the mice in the second experiment were younger on average and were sacrificed at a predetermined age, rather than when their tumor burden reached a critical threshold. Tumor weight was occasionally impossible to measure when the scale was not sensitive enough for small tumors. It would be ideal if metastasis could be scored in a more quantitative way that takes into account the whole lung rather than a representative histology section, this could potentially be achieved via FACS analysis using an antibody against human activated Erbb2.

Since tumor burden and metastasis load are usually correlated but inverse in this case, it seems more likely that these are two separate effects driven by two concurring causes. It remains unclear if either of these two effects are specific to *C. albicans* colonization, as it could also be a general *Candida*, fungi, or even microbe colonization effect. This could be evaluated by monocolonization of the isolator-housed mice with a different species or strain to see if the effects persist, or by using other breast cancer mouse models to validate these findings. Furthermore, the relevance of these findings is also uncertain since the lightening of the tumor burden was absent in the GF mice that were transferred to the BSL2 room upon *C. albicans* colonization, suggesting that the acquisition of a bacterial community might overshadow these effects, which questions translatability into more complex human settings. Similar trends towards a lower tumor burden were visible in one of these experiments, but in the opposite direction in a repeat cohort. Additionally, intestinal mycobiome dysbiosis has not been described in breast cancer patients to date, therefore it remains unclear if this would have clinical relevance. A dataset of human breast

cancer patient stool samples would be required to perform deep Shotgun metagenomic sequencing to enable fungal detection.

On the other hand, intratumoral *C. albicans* in intestinal cancers has been described to have a pro-metastatic effect associated with a higher expression of metastasis-related genes [76]. However, it is uncertain if that would be applicable in a breast cancer setting without translocation of the fungi to the tumor site. Similarly, *C. albicans* was described to stimulate the production of MMPs that can drive metastasis and other oncometabolites in oral squamous carcinoma cell lines [89]. Since metabolites possess the ability to translocate and travel via the bloodstream, they could potentially have an impact on breast cancer development.

Accordingly, metabolic profiling analysis of the portal and systemic serum from breast cancer-bearing mice revealed five polar metabolites that significantly differed, one reduced and four enriched after *C. albicans* colonization in comparison to the control group (**Figure 46**). Although there are no established links between breast cancer and four of these metabolites, research has shown that sucrose is linked to accelerated tumor growth and heightened lung metastasis in different mouse models of breast cancer [291]. This contradicts the reduction in tumor burden but may offer an explanation for the earlier onset of lung metastasis observed in cases of *C. albicans* colonization.

Untargeted metabolomics analysis of the same serum samples could detect more significantly different metabolites that were both enriched or depleted after *C. albicans* colonization (**Figure 47**). Since their identity is unclear from this data, I compared these hits to the ones derived from wild type mice of the same mouse strain in both the portal and systemic serum. This analysis aimed to uncover the core *C. albicans* response that may warrant further investigation. Most metabolites were different between the wild type and breast cancer mice, which could be due to age, genotype or tumor burden. Another study previously showed that the serum metabolome can be strongly dependent on the mouse age, therefore it is possible that the different ages of the mice could be the main driver [292]. There were, however, five metabolites, one of which was common for all, and four were common in three of the four datasets (portal and systemic for wild type and breast cancer mice). Strikingly, they consistently exhibited changes in the same direction, even if the changes were not statistically significant. Additionally, one particular metabolite was found to be downregulated in C57BL/6 mice colonized with a different fungi, *C. tropicalis*, indicating a potential broad impact of fungi or other microbes. However, identification of these metabolites is challenging due to limited information, with only the mass-to-charge ratio and, in some instances, a putative formula available for analysis.

The one enriched metabolite with the ID 372 and putative formula C18H30O7 could potentially be the naturally occurring lipophilic antioxidant ascorbyl laurate. It is synthesized through the transesterification of ascorbic acid (vitamin C) and lauric acid, a reaction that interestingly can be catalyzed by a lipase isolated from another *Candida* species, *Candida antarctica* [293]. This enzyme, also known as Novozym 435, highly relevant for the food and cosmetics industry, has not been reported to be present in *C. albicans*. Additionally, a short search using NCBI Blast of the gene (GenBank Z30645.1) and amino acid (P41365.1) sequence did not find a similar sequence in the *C. albicans* genome making this route more unlikely.

Another potential method of synthesizing C18H30O7 involves starting with the metabolite with the ID 521 and putative formula C18H30O6, which was significantly decreased under the same conditions that caused the other metabolite to increase. Unfortunately this does not significantly contribute to the identity search, as similar oxidation reactions have been observed in monoterpenes, which are secondary organic aerosols, that have not been proven to be generated within the human body [294].

There are several possibilities for the identity of the depleted metabolite with the ID 226 and the putative formula C7H8O4S, but one stands out for its interesting link to ALF: p- or o-cresol sulfate. In a previous study p-cresol sulfate was described as a biomarker for ALF severity, and the intestinal bacteria-produced precursor p-cresol speculated to interfere with the detoxification process of APAP [155]. Significantly lower doses of the sulfate with *C. albicans* could correlate with the partial protective effect of *C. albicans* towards APAP-induced liver injury, possibly by lowering the levels of some precursor metabolites, enabling the enzymes to detoxify more APAP. This might also explain the microbiome-dependent reversal of the *C. albicans* direct effect, since p-cresol production and detoxification was shown to be highly dependent on certain bacteria [295, 296]. It would be interesting to investigate the serum metabolome of C57BL/6 mice after one week of colonization, the time point used for the ALF experiments, to test if this metabolite is also present in this experimental setup.

Finally, the metabolite that was commonly decreased with both *Candida* strains in two mouse strains, ID 56 with the putative formula C22H40O4 appears to be a long chain fatty acid or derivative. It could potentially be octadecyl fumarate, which is predicted to naturally occur in the human body according to the Human Metabolome Database, but is otherwise uncharacterized with no link to diseases. Interestingly, fatty acids were previously correlated with the mycobiome in humans, suggesting a broader fungi effect [272].

Targeted metabolomics analysis would be necessary to confirm the metabolite identity. If the identity and concentration of the metabolite can be confirmed, experiments could be conducted to determine the effects of controlled metabolite supplementation through osmotic pumps directly into the bloodstream on breast cancer progression. This could help to understand if the metabolite plays a role in tumor growth and metastasis. A similar scenario would be possible for the metabolites detected by metabolic profiling, particularly sucrose. Since the genetic breast cancer mouse model has a long latency, it could be interesting to use faster orthotopic models to investigate the validity of the metabolite effects. Additionally, it could be possible to test these effects and applicability to humans using mouse and human breast cancer organoids exposed to these metabolites. In order to test whether the transcriptional profile is different with or without *C. albicans* intestinal colonization, RNA sequencing of the tumors could be used to achieve further mechanistic insights. Given the genetic nature of the mouse model, multiple tumors at different levels of progression and morphologies can arise, bringing significant variation.

Finally, it is also possible that these effects are not mediated by metabolites directly but rather via the immune system, which was not investigated here. Indeed, systemic *C. albicans* infection has been described to increase tumor size dependent on regulatory T cells, which is opposite to the reduction in tumor load in the model tested in this thesis [199]. The metastasis effect may also be influenced by alterations in the immune system. Specifically the lung immune system undergoes specific changes that promote the formation of metastatic niches, while studies have demonstrated that intestinal fungi can impact the lung immune microenvironment, particularly in the progression of asthma [51, 297].

Two studies have shown the impact of *C. albicans* on the gut-brain axis, with anxiety being linked to elevated levels of sterols, endocannabinoids, and lipids in the cecum, and social behavior being influenced by mucosal colonization via Th17 cells [271, 298]. This research highlights the crucial role of the immune system and the secretion of bioactive metabolites as potential pathways through which intestinal fungi can affect behavior and disease in distant part of the body.

9 References

1. Sender, R., S. Fuchs, and R. Milo, *Revised Estimates for the Number of Human and Bacteria Cells in the Body.* PLOS Biology, 2016. **14**(8): p. e1002533.
2. Nelson, K.E., et al., *A catalog of reference genomes from the human microbiome.* Science, 2010. **328**(5981): p. 994-9.
3. Grice, E.A. and J.A. Segre, *The human microbiome: our second genome.* Annu Rev Genomics Hum Genet, 2012. **13**: p. 151-70.
4. Cho, I. and M.J. Blaser, *The human microbiome: at the interface of health and disease.* Nature Reviews Genetics, 2012. **13**(4): p. 260-270.
5. Natalini, J.G., S. Singh, and L.N. Segal, *The dynamic lung microbiome in health and disease.* Nat Rev Microbiol, 2023. **21**(4): p. 222-235.
6. Tilg, H., T.E. Adolph, and M. Trauner, *Gut-liver axis: Pathophysiological concepts and clinical implications.* Cell Metabolism, 2022. **34**(11): p. 1700-1718.
7. Peters, B.A., et al., *The Breast Microbiome in Breast Cancer Risk and Progression: A Narrative Review.* Cancer Epidemiology, Biomarkers & Prevention, 2024. **33**(1): p. 9-19.
8. Bäckhed, F., et al., *Dynamics and Stabilization of the Human Gut Microbiome during the First Year of Life.* Cell Host Microbe, 2015. **17**(5): p. 690-703.
9. Dong, T.S. and A. Gupta, *Influence of Early Life, Diet, and the Environment on the Microbiome.* Clin Gastroenterol Hepatol, 2019. **17**(2): p. 231-242.
10. Rothschild, D., et al., *Environment dominates over host genetics in shaping human gut microbiota.* Nature, 2018. **555**(7695): p. 210-215.
11. Huttenhower, C., et al., *Structure, function and diversity of the healthy human microbiome.* Nature, 2012. **486**(7402): p. 207-214.
12. Hugenholtz, F. and W.M. de Vos, *Mouse models for human intestinal microbiota research: a critical evaluation.* Cell Mol Life Sci, 2018. **75**(1): p. 149-160.
13. Krych, L., et al., *Quantitatively different, yet qualitatively alike: a meta-analysis of the mouse core gut microbiome with a view towards the human gut microbiome.* PLoS One, 2013. **8**(5): p. e62578.
14. Kieser, S., E.M. Zdobnov, and M. Trajkovski, *Comprehensive mouse microbiota genome catalog reveals major difference to its human counterpart.* PLOS Computational Biology, 2022. **18**(3): p. e1009947.
15. Xiao, L., et al., *A catalog of the mouse gut metagenome.* Nature Biotechnology, 2015. **33**(10): p. 1103-1108.
16. Cullin, N., et al., *Microbiome and cancer.* Cancer Cell, 2021. **39**(10): p. 1317-1341.
17. Kolodziejczyk, A.A., D. Zheng, and E. Elinav, *Diet-microbiota interactions and personalized nutrition.* Nat Rev Microbiol, 2019. **17**(12): p. 742-753.
18. Blacher, E., et al., *Microbiome-Modulated Metabolites at the Interface of Host Immunity.* J Immunol, 2017. **198**(2): p. 572-580.
19. Shan, Y., M. Lee, and E.B. Chang, *The Gut Microbiome and Inflammatory Bowel Diseases.* Annu Rev Med, 2022. **73**: p. 455-468.
20. Jie, Z., et al., *The gut microbiome in atherosclerotic cardiovascular disease.* Nat Commun, 2017. **8**(1): p. 845.
21. Blacher, E., et al., *Potential roles of gut microbiome and metabolites in modulating ALS in mice.* Nature, 2019. **572**(7770): p. 474-480.
22. Alli, S.R., et al., *The Gut Microbiome in Depression and Potential Benefit of Prebiotics, Probiotics and Synbiotics: A Systematic Review of Clinical Trials and Observational Studies.* Int J Mol Sci, 2022. **23**(9).
23. Kolodziejczyk, A.A., et al., *The role of the microbiome in NAFLD and NASH.* EMBO Mol Med, 2019. **11**(2).

24. Hufnagl, K., et al., *Dysbiosis of the gut and lung microbiome has a role in asthma.* Semin Immunopathol, 2020. **42**(1): p. 75-93.
25. Tian, L., et al., *Deciphering functional redundancy in the human microbiome.* Nature Communications, 2020. **11**(1): p. 6217.
26. Berg, G., et al., *Microbiome definition re-visited: old concepts and new challenges.* Microbiome, 2020. **8**(1): p. 103.
27. Zhang, C., C.L. Franklin, and A.C. Ericsson, *Consideration of Gut Microbiome in Murine Models of Diseases.* Microorganisms, 2021. **9**(5).
28. Ooijevaar, R.E., et al., *Clinical Application and Potential of Fecal Microbiota Transplantation.* Annu Rev Med, 2019. **70**: p. 335-351.
29. Salminen, S., et al., *The International Scientific Association of Probiotics and Prebiotics (ISAPP) consensus statement on the definition and scope of postbiotics.* Nat Rev Gastroenterol Hepatol, 2021. **18**(9): p. 649-667.
30. Suez, J., et al., *Post-Antibiotic Gut Mucosal Microbiome Reconstitution Is Impaired by Probiotics and Improved by Autologous FMT.* Cell, 2018. **174**(6): p. 1406-1423.e16.
31. Suez, J., et al., *The pros, cons, and many unknowns of probiotics.* Nat Med, 2019. **25**(5): p. 716-729.
32. Garcia-Rubio, R., et al., *The Fungal Cell Wall: Candida, Cryptococcus, and Aspergillus Species.* Frontiers in Microbiology, 2020. **10**.
33. Noble, S.M., B.A. Gianetti, and J.N. Witchley, *Candida albicans cell-type switching and functional plasticity in the mammalian host.* Nature Reviews Microbiology, 2017. **15**(2): p. 96-108.
34. Gladfelter, A.S. and P. Sudbery, *Septins in Four Model Fungal Systems: Diversity in Form and Function*, in *The Septins*. 2008. p. 125-146.
35. Sudbery, P.E., *Growth of Candida albicans hyphae.* Nature Reviews Microbiology, 2011. **9**(10): p. 737-748.
36. Logan, C., I. Martin-Loeches, and T. Bicanic, *Invasive candidiasis in critical care: challenges and future directions.* Intensive Care Med, 2020. **46**(11): p. 2001-2014.
37. Underhill, D.M. and I.D. Iliev, *The mycobiota: interactions between commensal fungi and the host immune system.* Nature Reviews Immunology, 2014. **14**(6): p. 405-416.
38. Doron, I., et al., *Mycobiota-induced IgA antibodies regulate fungal commensalism in the gut and are dysregulated in Crohn's disease.* Nature Microbiology, 2021. **6**(12): p. 1493-1504.
39. Huffnagle, G.B. and M.C. Noverr, *The emerging world of the fungal microbiome.* Trends in Microbiology, 2013. **21**(7): p. 334-341.
40. Ghannoum, M.A., et al., *Characterization of the oral fungal microbiome (mycobiome) in healthy individuals.* PLoS Pathog, 2010. **6**(1): p. e1000713.
41. Jo, J.-H., E.A. Kennedy, and H.H. Kong, *Topographical and physiological differences of the skin mycobiome in health and disease.* Virulence, 2017. **8**(3): p. 324-333.
42. Kalia, N., J. Singh, and M. Kaur, *Microbiota in vaginal health and pathogenesis of recurrent vulvovaginal infections: a critical review.* Annals of Clinical Microbiology and Antimicrobials, 2020. **19**(1): p. 5.
43. Drell, T., et al., *Characterization of the Vaginal Micro- and Mycobiome in Asymptomatic Reproductive-Age Estonian Women.* PLOS ONE, 2013. **8**(1): p. e54379.
44. Hallen-Adams, H.E. and M.J. Suhr, *Fungi in the healthy human gastrointestinal tract.* Virulence, 2016. **8**(3): p. 352-358.
45. Nash, A.K., et al., *The gut mycobiome of the Human Microbiome Project healthy cohort.* Microbiome, 2017. **5**(1): p. 153.
46. Sun, Y., et al., *Population-level configurations of gut mycobiome across six ethnicities in urban and rural China.* Gastroenterology, 2020.
47. Nel Van Zyl, K., et al., *Fungal diversity in the gut microbiome of young South African children.* BMC Microbiology, 2022. **22**(1): p. 201.

48. Szóstak, N., et al., *Host Factors Associated with Gut Mycobiome Structure.* MSystems, 2023. **8**(2).
49. Gupta, Y., et al., *Impact of diet and host genetics on the murine intestinal mycobiome.* Nature Communications, 2023. **14**(1): p. 834.
50. Fiers, W.D., I. Leonardi, and I.D. Iliev, *From Birth and Throughout Life: Fungal Microbiota in Nutrition and Metabolic Health.* Annual Review of Nutrition, 2020. **40**(1): p. 323-343.
51. van Tilburg Bernardes, E., et al., *Intestinal fungi are causally implicated in microbiome assembly and immune development in mice.* Nature Communications, 2020. **11**(1): p. 2577.
52. van der Velden, W.J., et al., *The incidence of acute graft-versus-host disease increases with Candida colonization depending the dectin-1 gene status.* Clin Immunol, 2010. **136**(2): p. 302-6.
53. Alonso, R., et al., *Identification of Fungal Species in Brain Tissue from Alzheimer's Disease by Next-Generation Sequencing.* J Alzheimers Dis, 2017. **58**(1): p. 55-67.
54. Sokol, H., et al., *Fungal microbiota dysbiosis in IBD.* Gut, 2017. **66**(6): p. 1039-1048.
55. Coker, O.O., et al., *Enteric fungal microbiota dysbiosis and ecological alterations in colorectal cancer.* Gut, 2019. **68**(4): p. 654-662.
56. Saftien, A., J. Puschhof, and E. Elinav, *Fungi and cancer.* Gut, 2023. **72**(7): p. 1410-1425.
57. Jacobsen, I.D., *The Role of Host and Fungal Factors in the Commensal-to-Pathogen Transition of Candida albicans.* Curr Clin Microbiol Rep, 2023. **10**(2): p. 55-65.
58. Visconti, A., et al., *Interplay between the human gut microbiome and host metabolism.* Nature Communications, 2019. **10**(1): p. 4505.
59. Wikoff, W.R., et al., *Metabolomics analysis reveals large effects of gut microflora on mammalian blood metabolites.* Proceedings of the National Academy of Sciences, 2009. **106**(10): p. 3698-3703.
60. Pickova, D., et al., *Aflatoxins: History, Significant Milestones, Recent Data on Their Toxicity and Ways to Mitigation.* Toxins, 2021. **13**(6): p. 399.
61. McGlynn, K.A. and W.T. London, *Epidemiology and natural history of hepatocellular carcinoma.* Best Practice & Research Clinical Gastroenterology, 2005. **19**(1): p. 3-23.
62. Marchese, S., et al., *Aflatoxin B1 and M1: Biological Properties and Their Involvement in Cancer Development.* Toxins, 2018. **10**(6): p. 214.
63. Himmelreich, U., et al., *Rapid etiological classification of meningitis by NMR spectroscopy based on metabolite profiles and host response.* PLoS One, 2009. **4**(4): p. e5328.
64. Vidal-García, M., et al., *Clinical validity of bis(methylthio)gliotoxin for the diagnosis of invasive aspergillosis.* Appl Microbiol Biotechnol, 2016. **100**(5): p. 2327-34.
65. Brandt, P., E. Garbe, and S. Vylkova, *Catch the wave: Metabolomic analyses in human pathogenic fungi.* PLOS Pathogens, 2020. **16**(8): p. e1008757.
66. Plato, A., S.E. Hardison, and G.D. Brown, *Pattern recognition receptors in antifungal immunity.* Semin Immunopathol, 2015. **37**(2): p. 97-106.
67. Gutierrez, M.W., et al., *"Molding" immunity—modulation of mucosal and systemic immunity by the intestinal mycobiome in health and disease.* Mucosal Immunology, 2022.
68. Main, J., et al., *Antibody to Saccharomyces cerevisiae (bakers' yeast) in Crohn's disease.* Bmj, 1988. **297**(6656): p. 1105-6.
69. Duarte-Silva, M., et al., *Reappraisal of antibodies against Saccharomyces cerevisiae (ASCA) as persistent biomarkers in quiescent Crohn's disease.* Autoimmunity, 2019. **52**(1): p. 37-47.
70. Standaert–Vitse, A., et al., *Candida albicans Is an Immunogen for Anti–Saccharomyces cerevisiae Antibody Markers of Crohn’s Disease.* Gastroenterology, 2006. **130**(6): p. 1764-1775.

71. Anju, V.T., et al., *Polymicrobial Infections and Biofilms: Clinical Significance and Eradication Strategies.* Antibiotics, 2022. **11**(12): p. 1731.
72. Azzam, S.Z., G.J. Cayme, and L.R. Martinez, *Polymicrobial interactions involving fungi and their importance for the environment and in human disease.* Microbial Pathogenesis, 2020. **140**: p. 103942.
73. Samonis, G., et al., *Prospective evaluation of effects of broad-spectrum antibiotics on gastrointestinal yeast colonization of humans.* Antimicrob Agents Chemother, 1993. **37**(1): p. 51-3.
74. Dollive, S., et al., *Fungi of the Murine Gut: Episodic Variation and Proliferation during Antibiotic Treatment.* PLOS ONE, 2013. **8**(8): p. e71806.
75. Seelbinder, B., et al., *Antibiotics create a shift from mutualism to competition in human gut communities with a longer-lasting impact on fungi than bacteria.* Microbiome, 2020. **8**(1): p. 133.
76. Dohlman, A.B., et al., *A pan-cancer mycobiome analysis reveals fungal involvement in gastrointestinal and lung tumors.* Cell, 2022. **185**(20): p. 3807-3822.e12.
77. Narunsky-Haziza, L., et al., *Pan-cancer analyses reveal cancer-type-specific fungal ecologies and bacteriome interactions.* Cell, 2022. **185**(20): p. 3789-3806.e17.
78. Romani, L., *Immunity to fungal infections.* Nature Reviews Immunology, 2004. **4**(1): p. 11-24.
79. Sprenger, M., et al., *Metabolic adaptation of intracellular bacteria and fungi to macrophages.* Int J Med Microbiol, 2018. **308**(1): p. 215-227.
80. Ge, Y., et al., *Comprehensive analysis of microbial content in whole-genome sequencing samples from The Cancer Genome Atlas project.* bioRxiv, 2024: p. 2024.05.24.595788.
81. Ponde, N.O., et al., *Candida albicans biofilms and polymicrobial interactions.* Crit Rev Microbiol, 2021. **47**(1): p. 91-111.
82. Moyes, D.L., et al., *Candidalysin is a fungal peptide toxin critical for mucosal infection.* Nature, 2016. **532**(7597): p. 64-68.
83. Kasper, L., et al., *The fungal peptide toxin Candidalysin activates the NLRP3 inflammasome and causes cytolysis in mononuclear phagocytes.* Nature Communications, 2018. **9**(1): p. 4260.
84. Ho, J., et al., *Candidalysin activates innate epithelial immune responses via epidermal growth factor receptor.* Nature Communications, 2019. **10**(1): p. 2297.
85. Allert, S., et al., *Candida albicans-Induced Epithelial Damage Mediates Translocation through Intestinal Barriers.* mBio, 2018. **9**(3): p. e00915-18.
86. Alnuaimi, A.D., et al., *Candida virulence and ethanol-derived acetaldehyde production in oral cancer and non-cancer subjects.* Oral Dis, 2016. **22**(8): p. 805-814.
87. Hsia, C.-C., et al., *Enhancement of formation of the esophageal carcinogen benzylmethylnitrosamine from its precursors by Candida albicans.* Proceedings of the National Academy of Sciences, 1981. **78**(3): p. 1878-1881.
88. Krogh, P., B. Hald, and P. Holmstrup, *Possible mycological etiology of oral mucosal cancer: catalytic potential of infecting Candida albicans and other yeasts in production of N-nitrosobenzylmethylamine.* Carcinogenesis, 1987. **8**(10): p. 1543-8.
89. Vadovics, M., et al., *Candida albicans Enhances the Progression of Oral Squamous Cell Carcinoma In Vitro and In Vivo.* mBio, 2022. **13**(1): p. e0314421.
90. Richardson, J.P., et al., *Candidalysins Are a New Family of Cytolytic Fungal Peptide Toxins.* mBio, 2022. **13**(1): p. e03510-21.
91. Wang, T., et al., *The Adaptor Protein CARD9 Protects against Colon Cancer by Restricting Mycobiota-Mediated Expansion of Myeloid-Derived Suppressor Cells.* Immunity, 2018. **49**(3): p. 504-514.e4.
92. Di Martino, L., et al., *Candida tropicalis Infection Modulates the Gut Microbiome and Confers Enhanced Susceptibility to Colitis in Mice.* Cellular and Molecular Gastroenterology and Hepatology, 2022. **13**(3): p. 901-923.

93. Chiaro, T.R., et al., *A member of the gut mycobiota modulates host purine metabolism exacerbating colitis in mice.* Science Translational Medicine, 2017. **9**(380).
94. Sivananthan, K. and A.M. Petersen, *Review of Saccharomyces boulardii as a treatment option in IBD.* Immunopharmacol Immunotoxicol, 2018. **40**(6): p. 465-475.
95. Xu, J., et al., *Dandruff-associated Malassezia genomes reveal convergent and divergent virulence traits shared with plant and human fungal pathogens.* Proceedings of the National Academy of Sciences, 2007. **104**(47): p. 18730-18735.
96. Prohic, A., et al., *Malassezia species in healthy skin and in dermatological conditions.* Int J Dermatol, 2016. **55**(5): p. 494-504.
97. Aykut, B., et al., *The fungal mycobiome promotes pancreatic oncogenesis via activation of MBL.* Nature, 2019. **574**(7777): p. 264-267.
98. Alam, A., et al., *Fungal mycobiome drives IL-33 secretion and type 2 immunity in pancreatic cancer.* Cancer Cell, 2022.
99. Limon, J.J., et al., *Malassezia Is Associated with Crohn's Disease and Exacerbates Colitis in Mouse Models.* Cell Host & Microbe, 2019. **25**(3): p. 377-388.e6.
100. Neville, B.A., S.C. Forster, and T.D. Lawley, *Commensal Koch's postulates: establishing causation in human microbiota research.* Current Opinion in Microbiology, 2018. **42**: p. 47-52.
101. James, T.Y., et al., *Toward a Fully Resolved Fungal Tree of Life.* Annual Review of Microbiology, 2020. **74**(1): p. 291-313.
102. Laiolo, E., et al., *Metagenomic probing toward an atlas of the taxonomic and metabolic foundations of the global ocean genome.* Frontiers in Science, 2024. **1**.
103. Tang, J., et al., *Mycobiome: Approaches to analysis of intestinal fungi.* J Immunol Methods, 2015. **421**: p. 112-121.
104. Yang, R.-H., et al., *Evaluation of the ribosomal DNA internal transcribed spacer (ITS), specifically ITS1 and ITS2, for the analysis of fungal diversity by deep sequencing.* PLOS ONE, 2018. **13**(10): p. e0206428.
105. Blaalid, R., et al., *ITS1 versus ITS2 as DNA metabarcodes for fungi.* Mol Ecol Resour, 2013. **13**(2): p. 218-24.
106. Kauserud, H., *ITS alchemy: On the use of ITS as a DNA marker in fungal ecology.* Fungal Ecology, 2023. **65**: p. 101274.
107. Lofgren, L.A., et al., *Genome-based estimates of fungal rDNA copy number variation across phylogenetic scales and ecological lifestyles.* Molecular Ecology, 2019. **28**(4): p. 721-730.
108. Lavrinienko, A., et al., *Does Intraspecific Variation in rDNA Copy Number Affect Analysis of Microbial Communities?* Trends in Microbiology, 2021. **29**(1): p. 19-27.
109. Lin, Y., et al., *Altered Mycobiota Signatures and Enriched Pathogenic Aspergillus rambellii Are Associated With Colorectal Cancer Based on Multicohort Fecal Metagenomic Analyses.* Gastroenterology, 2022.
110. Liu, N.-N., et al., *Multi-kingdom microbiota analyses identify bacterial–fungal interactions and biomarkers of colorectal cancer across cohorts.* Nature Microbiology, 2022.
111. Hebecker, B., et al., *Dual-species transcriptional profiling during systemic candidiasis reveals organ-specific host-pathogen interactions.* Sci Rep, 2016. **6**: p. 36055.
112. Muñoz, J.F., et al., *Coordinated host-pathogen transcriptional dynamics revealed using sorted subpopulations and single macrophages infected with Candida albicans.* Nat Commun, 2019. **10**(1): p. 1607.
113. Puschhof, J., C. Pleguezuelos-Manzano, and H. Clevers, *Organoids and organs-on-chips: Insights into human gut-microbe interactions.* Cell Host Microbe, 2021. **29**(6): p. 867-878.
114. Carmo, M.S.d., et al., *Lactobacillus fermentum ATCC 23271 Displays In vitro Inhibitory Activities against Candida spp.* Frontiers in Microbiology, 2016. **7**.

115. Mailänder-Sánchez, D., et al., *Antifungal defense of probiotic Lactobacillus rhamnosus GG is mediated by blocking adhesion and nutrient depletion.* PLoS One, 2017. **12**(10): p. e0184438.
116. Rizzo, A., A. Losacco, and C.R. Carratelli, *Lactobacillus crispatus modulates epithelial cell defense against Candida albicans through Toll-like receptors 2 and 4, interleukin 8 and human β-defensins 2 and 3.* Immunol Lett, 2013. **156**(1-2): p. 102-9.
117. Pleguezuelos-Manzano, C., et al., *Establishment and Culture of Human Intestinal Organoids Derived from Adult Stem Cells.* Current Protocols in Immunology, 2020. **130**(1): p. e106.
118. Pleguezuelos-Manzano, C., et al., *Mutational signature in colorectal cancer caused by genotoxic pks(+) E. coli.* Nature, 2020. **580**(7802): p. 269-273.
119. Boccellato, F., et al., *Polarised epithelial monolayers of the gastric mucosa reveal insights into mucosal homeostasis and defence against infection.* Gut, 2019. **68**(3): p. 400-413.
120. Fakhiri, J., et al., *Novel Chimeric Gene Therapy Vectors Based on Adeno-Associated Virus and Four Different Mammalian Bocaviruses.* Molecular Therapy Methods & Clinical Development, 2019. **12**: p. 202-222.
121. Co, J.Y., et al., *Controlling Epithelial Polarity: A Human Enteroid Model for Host-Pathogen Interactions.* Cell Rep, 2019. **26**(9): p. 2509-2520.e4.
122. Co, J.Y., et al., *Controlling the polarity of human gastrointestinal organoids to investigate epithelial biology and infectious diseases.* Nat Protoc, 2021. **16**(11): p. 5171-5192.
123. Puschhof, J., et al., *Intestinal organoid cocultures with microbes.* Nat Protoc, 2021. **16**(10): p. 4633-4649.
124. Spence, J.R., et al., *Directed differentiation of human pluripotent stem cells into intestinal tissue in vitro.* Nature, 2011. **470**(7332): p. 105-109.
125. Jose, S.S., et al., *Comparison of two human organoid models of lung and intestinal inflammation reveals Toll-like receptor signalling activation and monocyte recruitment.* Clin Transl Immunology, 2020. **9**(5): p. e1131.
126. Maurer, M., et al., *A three-dimensional immunocompetent intestine-on-chip model as in vitro platform for functional and microbial interaction studies.* Biomaterials, 2019. **220**: p. 119396.
127. De Crignis, E., et al., *Application of human liver organoids as a patient-derived primary model for HBV infection and related hepatocellular carcinoma.* Elife, 2021. **10**.
128. Yang, A.S.P., et al., *Development of Plasmodium falciparum liver-stages in hepatocytes derived from human fetal liver organoid cultures.* Nat Commun, 2023. **14**(1): p. 4631.
129. Schwarz, R., et al., *Gastrointestinal transit times in mice and humans measured with 27Al and 19F nuclear magnetic resonance.* Magn Reson Med, 2002. **48**(2): p. 255-61.
130. SAKAGUCHI, E., *Digestive strategies of small hindgut fermenters.* Animal Science Journal, 2003. **74**(5): p. 327-337.
131. Lundberg, R., et al., *Human microbiota-transplanted C57BL/6 mice and offspring display reduced establishment of key bacteria and reduced immune stimulation compared to mouse microbiota-transplantation.* Sci Rep, 2020. **10**(1): p. 7805.
132. Yeung, F., et al., *Altered Immunity of Laboratory Mice in the Natural Environment Is Associated with Fungal Colonization.* Cell host & microbe, 2020. **27**(5): p. 809-822.e6.
133. Mims, T.S., et al., *The gut mycobiome of healthy mice is shaped by the environment and correlates with metabolic outcomes in response to diet.* Communications Biology, 2021. **4**(1): p. 281.
134. Doron, I., I. Leonardi, and I.D. Iliev, *Profound mycobiome differences between segregated mouse colonies do not influence Th17 responses to a newly introduced gut fungal commensal.* Fungal Genetics and Biology, 2019. **127**: p. 45-49.

135. Rosshart, S.P., et al., *Laboratory mice born to wild mice have natural microbiota and model human immune responses.* Science, 2019. **365**(6452).
136. Chen, Y.-H., et al., *Rewilding of laboratory mice enhances granulopoiesis and immunity through intestinal fungal colonization.* Science Immunology, 2023. **8**(84): p. eadd6910.
137. Kralova, J.S., et al., *Competitive fungal commensalism mitigates candidiasis pathology.* bioRxiv, 2024: p. 2024.01.12.575358.
138. Zangl, I., et al., *The role of Lactobacillus species in the control of Candida via biotrophic interactions.* Microb Cell, 2019. **7**(1): p. 1-14.
139. Pérez, J.C., *Candida albicans dwelling in the mammalian gut.* Current Opinion in Microbiology, 2019. **52**: p. 41-46.
140. Kennedy, E.A., K.Y. King, and M.T. Baldridge, *Mouse Microbiota Models: Comparing Germ-Free Mice and Antibiotics Treatment as Tools for Modifying Gut Bacteria.* Frontiers in Physiology, 2018. **9**(1534).
141. Shingina, A., et al., *Acute Liver Failure Guidelines.* Official journal of the American College of Gastroenterology | ACG, 2023. **118**(7): p. 1128-1153.
142. Bernal, W. and J. Wendon, *Acute liver failure.* N Engl J Med, 2013. **369**(26): p. 2525-34.
143. Stravitz, R.T. and W.M. Lee, *Acute liver failure.* Lancet, 2019. **394**(10201): p. 869-881.
144. Blieden, M., et al., *A perspective on the epidemiology of acetaminophen exposure and toxicity in the United States.* Expert Rev Clin Pharmacol, 2014. **7**(3): p. 341-8.
145. Sedhom, D., et al., *Viral Hepatitis and Acute Liver Failure: Still a Problem.* Clin Liver Dis, 2018. **22**(2): p. 289-300.
146. Ostapowicz, G., et al., *Results of a prospective study of acute liver failure at 17 tertiary care centers in the United States.* Ann Intern Med, 2002. **137**(12): p. 947-54.
147. Björnsson, E.S., et al., *Incidence, presentation, and outcomes in patients with drug-induced liver injury in the general population of Iceland.* Gastroenterology, 2013. **144**(7): p. 1419-1425. e3.
148. Sgro, C., et al., *Incidence of drug-induced hepatic injuries: a French population-based study.* Hepatology, 2002. **36**(2): p. 451-455.
149. Larson, A.M., *Acetaminophen hepatotoxicity.* Clinics in liver disease, 2007. **11**(3): p. 525-548.
150. Larson, A.M., et al., *Acetaminophen-induced acute liver failure: results of a United States multicenter, prospective study.* Hepatology, 2005. **42**(6): p. 1364-1372.
151. Yoon, E., et al., *Acetaminophen-Induced Hepatotoxicity: a Comprehensive Update.* Journal of Clinical and Translational Hepatology, 2016. **4**(2): p. 131-142.
152. Hefler, J., et al., *Preclinical models of acute liver failure: a comprehensive review.* PeerJ, 2021. **9**: p. e12579.
153. Du, K., et al., *Lower susceptibility of female mice to acetaminophen hepatotoxicity: Role of mitochondrial glutathione, oxidant stress and c-jun N-terminal kinase.* Toxicol Appl Pharmacol, 2014. **281**(1): p. 58-66.
154. Rubin, J.B., et al., *Acetaminophen-induced Acute Liver Failure Is More Common and More Severe in Women.* Clin Gastroenterol Hepatol, 2018. **16**(6): p. 936-946.
155. Clayton, T.A., et al., *Pharmacometabonomic identification of a significant host-microbiome metabolic interaction affecting human drug metabolism.* Proc Natl Acad Sci U S A, 2009. **106**(34): p. 14728-33.
156. Schneider, K.M., et al., *Intestinal Dysbiosis Amplifies Acetaminophen-Induced Acute Liver Injury.* Cellular and Molecular Gastroenterology and Hepatology, 2021. **11**(4): p. 909-933.
157. Thaiss, C.A., et al., *Microbiota Diurnal Rhythmicity Programs Host Transcriptome Oscillations.* Cell, 2016. **167**(6): p. 1495-1510.e12.
158. Gong, S., et al., *Gut microbiota mediates diurnal variation of acetaminophen induced acute liver injury in mice.* Journal of Hepatology, 2018. **69**(1): p. 51-59.

159. Kolodziejczyk, A.A., et al., *Acute liver failure is regulated by MYC- and microbiome-dependent programs.* Nature Medicine, 2020. **26**(12): p. 1899-1911.
160. Cho, S., et al., *Phenylpropionic acid produced by gut microbiota alleviates acetaminophen-induced hepatotoxicity.* Gut Microbes, 2023. **15**(1): p. 2231590.
161. Zeng, Y., et al., *Liberation of daidzein by gut microbial β-galactosidase suppresses acetaminophen-induced hepatotoxicity in mice.* Cell Host & Microbe, 2023. **31**(5): p. 766-780.e7.
162. Li, D., et al., *Oral magnesium prevents acetaminophen-induced acute liver injury by modulating microbial metabolism.* Cell Host & Microbe.
163. Xia, J., et al., *Akkermansia muciniphila Ameliorates Acetaminophen-Induced Liver Injury by Regulating Gut Microbial Composition and Metabolism.* Microbiol Spectr, 2022. **10**(1): p. e0159621.
164. Saeedi, B.J., et al., *Gut-Resident Lactobacilli Activate Hepatic Nrf2 and Protect Against Oxidative Liver Injury.* Cell Metab, 2020. **31**(5): p. 956-968.e5.
165. Li, S., et al., *Bifidobacterium longum R0175 protects mice against APAP-induced liver injury by modulating the Nrf2 pathway.* Free Radic Biol Med, 2023. **203**: p. 11-23.
166. Escudié, L., et al., *Amanita phalloides poisoning: reassessment of prognostic factors and indications for emergency liver transplantation.* J Hepatol, 2007. **46**(3): p. 466-73.
167. Rolando, N., J. Philpott-Howard, and R. Williams, *Bacterial and fungal infection in acute liver failure.* Semin Liver Dis, 1996. **16**(4): p. 389-402.
168. He, Z., et al., *Gut Commensal Fungi Protect Against Acetaminophen-Induced Hepatotoxicity by Reducing Cyp2a5 Expression in Mice.* Frontiers in Microbiology, 2022. **13**.
169. Sanglard, D., *Clinical relevance of mechanisms of antifungal drug resistance in yeasts.* Enfermedades Infecciosas y Microbiología Clínica, 2002. **20**(9): p. 462-470.
170. Yang, A.-M., et al., *Intestinal fungi contribute to development of alcoholic liver disease.* The Journal of Clinical Investigation, 2017. **127**(7): p. 2829-2841.
171. Lang, S., et al., *Intestinal Fungal Dysbiosis and Systemic Immune Response to Fungi in Patients With Alcoholic Hepatitis.* Hepatology, 2020. **71**(2): p. 522-538.
172. Chu, H., et al., *The Candida albicans exotoxin candidalysin promotes alcohol-associated liver disease.* J Hepatol, 2020. **72**(3): p. 391-400.
173. Zeng, S., et al., *Candida albicans-specific Th17 cell-mediated response contributes to alcohol-associated liver disease.* Cell Host Microbe, 2023. **31**(3): p. 389-404.e7.
174. Lemoinne, S., et al., *Fungi participate in the dysbiosis of gut microbiota in patients with primary sclerosing cholangitis.* Gut, 2020. **69**(1): p. 92-102.
175. Little, R., et al., *Gut microbiome in primary sclerosing cholangitis: A review.* World J Gastroenterol, 2020. **26**(21): p. 2768-2780.
176. Demir, M., et al., *The fecal mycobiome in non-alcoholic fatty liver disease.* J Hepatol, 2022. **76**(4): p. 788-799.
177. World Health Organization. *Breast cancer*. 2024 13.03.2024 [cited 2024 10.06.2024]; Available from: https://www.who.int/news-room/fact-sheets/detail/breast-cancer.
178. Waks, A.G. and E.P. Winer, *Breast Cancer Treatment: A Review.* JAMA, 2019. **321**(3): p. 288-300.
179. Fragomeni, S.M., A. Sciallis, and J.S. Jeruss, *Molecular Subtypes and Local-Regional Control of Breast Cancer.* Surg Oncol Clin N Am, 2018. **27**(1): p. 95-120.
180. Inic, Z., et al., *Difference between Luminal A and Luminal B Subtypes According to Ki-67, Tumor Size, and Progesterone Receptor Negativity Providing Prognostic Information.* Clin Med Insights Oncol, 2014. **8**: p. 107-11.
181. Sarhangi, N., et al., *Breast cancer in the era of precision medicine.* Mol Biol Rep, 2022. **49**(10): p. 10023-10037.
182. Liu, C., et al., *Advances in Rodent Models for Breast Cancer Formation, Progression, and Therapeutic Testing.* Frontiers in Oncology, 2021. **11**.

183. Behbod, F., et al., *An intraductal human-in-mouse transplantation model mimics the subtypes of ductal carcinoma in situ.* Breast Cancer Research, 2009. **11**(5): p. R66.
184. Zeng, L., W. Li, and C.-S. Chen, *Breast cancer animal models and applications.* Zoological Research, 2020. **41**(5): p. 477-494.
185. Regua, A.T., et al., *Transgenic mouse models of breast cancer.* Cancer Letters, 2021. **516**: p. 73-83.
186. Ursini-Siegel, J., et al., *ShcA signalling is essential for tumour progression in mouse models of human breast cancer.* Embo j, 2008. **27**(6): p. 910-20.
187. Ruo, S.W., et al., *Role of Gut Microbiota Dysbiosis in Breast Cancer and Novel Approaches in Prevention, Diagnosis, and Treatment.* Cureus, 2021. **13**(8): p. e17472.
188. Bard, J.M., et al., *Relationship between intestinal microbiota and clinical characteristics of patients with early stage breast cancer.* The FASEB Journal, 2015. **29**: p. 914.2.
189. Zhu, J., et al., *Breast cancer in postmenopausal women is associated with an altered gut metagenome.* Microbiome, 2018. **6**(1): p. 136.
190. Goedert, J.J., et al., *Investigation of the association between the fecal microbiota and breast cancer in postmenopausal women: a population-based case-control pilot study.* J Natl Cancer Inst, 2015. **107**(8).
191. Nejman, D., et al., *The human tumor microbiome is composed of tumor type-specific intracellular bacteria.* Science, 2020. **368**(6494): p. 973-980.
192. Rosean, C.B., et al., *Preexisting Commensal Dysbiosis Is a Host-Intrinsic Regulator of Tissue Inflammation and Tumor Cell Dissemination in Hormone Receptor–Positive Breast Cancer.* Cancer Research, 2019. **79**(14): p. 3662-3675.
193. Kwa, M., et al., *The Intestinal Microbiome and Estrogen Receptor-Positive Female Breast Cancer.* J Natl Cancer Inst, 2016. **108**(8).
194. Parida, S., et al., *A pro-carcinogenic colon microbe promotes breast tumorigenesis and metastatic progression and concomitantly activates Notch and βcatenin axes.* Cancer Discovery, 2021.
195. Parhi, L., et al., *Breast cancer colonization by Fusobacterium nucleatum accelerates tumor growth and metastatic progression.* Nature Communications, 2020. **11**(1): p. 3259.
196. Fu, A., et al., *Tumor-resident intracellular microbiota promotes metastatic colonization in breast cancer.* Cell, 2022. **185**(8): p. 1356-1372.e26.
197. Banerjee, S., et al., *Prognostic correlations with the microbiome of breast cancer subtypes.* Cell Death Dis, 2021. **12**(9): p. 831.
198. Banerjee, S., et al., *Distinct Microbial Signatures Associated With Different Breast Cancer Types.* Frontiers in Microbiology, 2018. **9**.
199. Ahmadi, N., et al., *Systemic infection with Candida albicans in breast tumor bearing mice: Cytokines dysregulation and induction of regulatory T cells.* Journal de Mycologie Médicale, 2019. **29**(1): p. 49-55.
200. Sohrabi, N., et al., *Invasive aspergillosis promotes tumor growth and severity in a tumor-bearing mouse model.* Canadian Journal of Microbiology, 2010. **56**(9): p. 771-776.
201. Guiver, M., K. Levi, and B.A. Oppenheim, *Rapid identification of candida species by TaqMan PCR.* J Clin Pathol, 2001. **54**(5): p. 362-6.
202. Sugita, T., et al., *Quantitative analysis of cutaneous malassezia in atopic dermatitis patients using real-time PCR.* Microbiol Immunol, 2006. **50**(7): p. 549-52.
203. Jiang, T.T., et al., *Commensal Fungi Recapitulate the Protective Benefits of Intestinal Bacteria.* Cell Host Microbe, 2017. **22**(6): p. 809-816.e4.
204. Zmora, N., et al., *Personalized Gut Mucosal Colonization Resistance to Empiric Probiotics Is Associated with Unique Host and Microbiome Features.* Cell, 2018. **174**(6): p. 1388-1405.e21.
205. Chen, S., et al., *fastp: an ultra-fast all-in-one FASTQ preprocessor.* Bioinformatics, 2018. **34**(17): p. i884-i890.

206. Dobin, A., et al., *STAR: ultrafast universal RNA-seq aligner.* Bioinformatics, 2013. **29**(1): p. 15-21.
207. Love, M.I., W. Huber, and S. Anders, *Moderated estimation of fold change and dispersion for RNA-seq data with DESeq2.* Genome biology, 2014. **15**: p. 1-21.
208. Bolyen, E., et al., *Reproducible, interactive, scalable and extensible microbiome data science using QIIME 2.* Nature Biotechnology, 2019. **37**(8): p. 852-857.
209. Rivers, A., et al., *ITSxpress: Software to rapidly trim internally transcribed spacer sequences with quality scores for marker gene analysis [version 1; peer review: 2 approved].* F1000Research, 2018. **7**(1418).
210. Callahan, B.J., et al., *DADA2: High-resolution sample inference from Illumina amplicon data.* Nature Methods, 2016. **13**(7): p. 581-583.
211. Beghini, F., et al., *Integrating taxonomic, functional, and strain-level profiling of diverse microbial communities with bioBakery 3.* eLife, 2021. **10**: p. e65088.
212. Wood, D.E., J. Lu, and B. Langmead, *Improved metagenomic analysis with Kraken 2.* Genome biology, 2019. **20**: p. 1-13.
213. Lu, J., et al., *Bracken: estimating species abundance in metagenomics data.* PeerJ Computer Science, 2017. **3**: p. e104.
214. Malitsky, S., et al., *Viral infection of the marine alga Emiliania huxleyi triggers lipidome remodeling and induces the production of highly saturated triacylglycerol.* New Phytol, 2016. **210**(1): p. 88-96.
215. Zheng, L., et al., *Fumarate induces redox-dependent senescence by modifying glutathione metabolism.* Nature Communications, 2015. **6**(1): p. 6001.
216. Pang, Z., et al., *MetaboAnalyst 6.0: towards a unified platform for metabolomics data processing, analysis and interpretation.* Nucleic Acids Res, 2024.
217. Zheng, L., C.J. Kelly, and S.P. Colgan, *Physiologic hypoxia and oxygen homeostasis in the healthy intestine. A Review in the Theme: Cellular Responses to Hypoxia.* Am J Physiol Cell Physiol, 2015. **309**(6): p. C350-60.
218. Fearon, E.R. and B. Vogelstein, *A genetic model for colorectal tumorigenesis.* Cell, 1990. **61**(5): p. 759-767.
219. Sommariva, S., et al., *Computational quantification of global effects induced by mutations and drugs in signaling networks of colorectal cancer cells.* Scientific Reports, 2021. **11**(1): p. 19602.
220. Turgeon, M.-O., N.J.S. Perry, and G. Poulogiannis, *DNA Damage, Repair, and Cancer Metabolism.* Frontiers in Oncology, 2018. **8**.
221. Downs, J.A., N.F. Lowndes, and S.P. Jackson, *A role for Saccharomyces cerevisiae histone H2A in DNA repair.* Nature, 2000. **408**(6815): p. 1001-4.
222. Kuo, L.J. and L.X. Yang, *Gamma-H2AX - a novel biomarker for DNA double-strand breaks.* In Vivo, 2008. **22**(3): p. 305-9.
223. Cuddihy, G., et al., *The Development of Oral Amphotericin B to Treat Systemic Fungal and Parasitic Infections: Has the Myth Been Finally Realized?* Pharmaceutics, 2019. **11**(3): p. 99.
224. Shinde, R.B., J.S. Raut, and M.S. Karuppayil, *Biofilm formation by Candida albicans on various prosthetic materials and its fluconazole sensitivity: a kinetic study.* Mycoscience, 2012. **53**(3): p. 220-226.
225. Soll, D.R. and K.J. Daniels, *Plasticity of Candida albicans Biofilms.* Microbiol Mol Biol Rev, 2016. **80**(3): p. 565-95.
226. Karakousis, A., et al., *An assessment of the efficiency of fungal DNA extraction methods for maximizing the detection of medically important fungi using PCR.* Journal of Microbiological Methods, 2006. **65**(1): p. 38-48.
227. Kurtzman, C.P., et al., *Multigene phylogenetic analysis of pathogenic candida species in the Kazachstania (Arxiozyma) telluris complex and description of their ascosporic states*

as Kazachstania bovina sp. nov., K. heterogenica sp. nov., K. pintolopesii sp. nov., and K. slooffiae sp. nov. J Clin Microbiol, 2005. **43**(1): p. 101-11.
228. Koh, A.Y., *Murine Models of Candida Gastrointestinal Colonization and Dissemination.* Eukaryotic Cell, 2013. **12**(11): p. 1416-1422.
229. Palleja, A., et al., *Recovery of gut microbiota of healthy adults following antibiotic exposure.* Nat Microbiol, 2018. **3**(11): p. 1255-1265.
230. Dethlefsen, L. and D.A. Relman, *Incomplete recovery and individualized responses of the human distal gut microbiota to repeated antibiotic perturbation.* Proc Natl Acad Sci U S A, 2011. **108 Suppl 1**(Suppl 1): p. 4554-61.
231. Lefranc, M.P., *Immunoglobulin and T Cell Receptor Genes: IMGT(®) and the Birth and Rise of Immunoinformatics.* Front Immunol, 2014. **5**: p. 22.
232. Schroeder, H.W., Jr. and L. Cavacini, *Structure and function of immunoglobulins.* J Allergy Clin Immunol, 2010. **125**(2 Suppl 2): p. S41-52.
233. Cox, J.J., et al., *An SCN9A channelopathy causes congenital inability to experience pain.* Nature, 2006. **444**(7121): p. 894-8.
234. Mombaerts, P., et al., *RAG-1-deficient mice have no mature B and T lymphocytes.* Cell, 1992. **68**(5): p. 869-77.
235. Enguita, F.J. and A.L. Leitão, *Hydroquinone: Environmental Pollution, Toxicity, and Microbial Answers.* BioMed Research International, 2013. **2013**: p. 542168.
236. Whysner, J., et al., *Analysis of studies related to tumorigenicity induced by hydroquinone.* Regul Toxicol Pharmacol, 1995. **21**(1): p. 158-76.
237. Biswas, S.K. and W.L. Chaffin, *Anaerobic growth of Candida albicans does not support biofilm formation under similar conditions used for aerobic biofilm.* Curr Microbiol, 2005. **51**(2): p. 100-4.
238. Williams, S., I. Cleary, and D. Thomas, *Anaerobic conditions are a major influence on Candida albicans chlamydospore formation.* Folia Microbiol (Praha), 2023. **68**(2): p. 321-324.
239. Brown, A.J., et al., *Metabolism impacts upon Candida immunogenicity and pathogenicity at multiple levels.* Trends Microbiol, 2014. **22**(11): p. 614-22.
240. Dumitru, R., J.M. Hornby, and K.W. Nickerson, *Defined anaerobic growth medium for studying Candida albicans basic biology and resistance to eight antifungal drugs.* Antimicrob Agents Chemother, 2004. **48**(7): p. 2350-4.
241. Andreasen, A.A. and T.J. Stier, *Anaerobic nutrition of Saccharomyces cerevisiae. I. Ergosterol requirement for growth in a defined medium.* J Cell Comp Physiol, 1953. **41**(1): p. 23-36.
242. Ishtar Snoek, I.S. and H. Yde Steensma, *Factors involved in anaerobic growth of Saccharomyces cerevisiae.* Yeast, 2007. **24**(1): p. 1-10.
243. Burgain, A., et al., *Metabolic Reprogramming in the Opportunistic Yeast Candida albicans in Response to Hypoxia.* mSphere, 2020. **5**(1): p. e00913-19.
244. Mishra, P., et al., *Genome-scale metabolic modeling and in silico analysis of lipid accumulating yeast Candida tropicalis for dicarboxylic acid production.* Biotechnology and Bioengineering, 2016. **113**(9): p. 1993-2004.
245. Tomova, A.A., A.V. Kujumdzieva, and V.Y. Petrova, *Carbon source influences Saccharomyces cerevisiae yeast cell survival strategies: quiescence or sporulation.* Biotechnology & Biotechnological Equipment, 2019. **33**(1): p. 1464-1470.
246. Ene, I.V., et al., *Host carbon sources modulate cell wall architecture, drug resistance and virulence in a fungal pathogen.* Cell Microbiol, 2012. **14**(9): p. 1319-35.
247. Begum, N., et al., *Integrative functional analysis uncovers metabolic differences between Candida species.* Communications Biology, 2022. **5**(1): p. 1013.
248. Jouhten, P., et al., *Saccharomyces cerevisiae metabolism in ecological context.* FEMS Yeast Res, 2016. **16**(7).

249. Oliver, J.C., et al., *Metabolic profiling of Candida clinical isolates of different species and infection sources.* Sci Rep, 2020. **10**(1): p. 16716.
250. Yan, Q., et al., *A genomic compendium of cultivated human gut fungi characterizes the gut mycobiome and its relevance to common diseases.* Cell, 2024.
251. Torres, R., et al., *In Vitro Antifungal Activity of Three Synthetic Peptides against Candida auris and Other Candida Species of Medical Importance.* Antibiotics, 2023. **12**(8): p. 1234.
252. Pistoia, E.S., et al., *All-Trans Retinoic Acid Effect on Candida albicans Growth and Biofilm Formation.* Journal of Fungi, 2022. **8**(10): p. 1049.
253. Case, N.T., et al., *Respiration supports intraphagosomal filamentation and escape of Candida albicans from macrophages.* mBio, 2023. **14**(6): p. e02745-23.
254. Kämmer, P., et al., *Survival Strategies of Pathogenic Candida Species in Human Blood Show Independent and Specific Adaptations.* mBio, 2020. **11**(5).
255. Wilson, H.B. and M.C. Lorenz, *Candida albicans Hyphal Morphogenesis within Macrophages Does Not Require Carbon Dioxide or pH-Sensing Pathways.* Infect Immun, 2023. **91**(5): p. e0008723.
256. Fletcher, A.A., et al., *Revisiting the intrinsic mycobiome in pancreatic cancer.* Nature, 2023. **620**(7972): p. E1-E6.
257. Malik, A., et al., *SYK-CARD9 Signaling Axis Promotes Gut Fungi-Mediated Inflammasome Activation to Restrict Colitis and Colon Cancer.* Immunity, 2018. **49**(3): p. 515-530.e5.
258. Rafailidis, P.I., E.N. Ioannidou, and M.E. Falagas, *Ampicillin/sulbactam: current status in severe bacterial infections.* Drugs, 2007. **67**(13): p. 1829-49.
259. Geraci, J.E., *Vancomycin.* Mayo Clin Proc, 1977. **52**(10): p. 631-4.
260. Block, M. and D.L. Blanchard, *Aminoglycosides*, in *StatPearls*. 2024, StatPearls Publishing

261. Roy, U., et al., *Clinical and Neuroradiological Spectrum of Metronidazole Induced Encephalopathy: Our Experience and the Review of Literature.* J Clin Diagn Res, 2016. **10**(6): p. Oe01-9.
262. Förster, T.M., et al., *Enemies and brothers in arms: Candida albicans and gram-positive bacteria.* Cellular Microbiology, 2016. **18**(12): p. 1709-1715.
263. Liang, S.-H., et al., *The hyphal-specific toxin candidalysin promotes fungal gut commensalism.* Nature, 2024.
264. Martinez-Lomeli, J., et al., *Impact of various high fat diets on gene expression and the microbiome across the mouse intestines.* Sci Rep, 2023. **13**(1): p. 22758.
265. Huertas, B., et al., *Serum Antibody Profile during Colonization of the Mouse Gut by Candida albicans: Relevance for Protection during Systemic Infection.* J Proteome Res, 2017. **16**(1): p. 335-345.
266. Doron, I., et al., *Human gut mycobiota tune immunity via CARD9-dependent induction of anti-fungal IgG antibodies.* Cell, 2021. **184**(4): p. 1017-1031.e14.
267. Xue, Y., et al., *Pain behavior in SCN9A (Nav1.7) and SCN10A (Nav1.8) mutant rodent models.* Neuroscience Letters, 2021. **753**: p. 135844.
268. Böhm, L., et al., *The yeast form of the fungus Candida albicans promotes persistence in the gut of gnotobiotic mice.* PLOS Pathogens, 2017. **13**(10): p. e1006699.
269. Bratburd, J.R., et al., *Gut Microbial and Metabolic Responses to Salmonella enterica Serovar Typhimurium and Candida albicans.* mBio, 2018. **9**(6).
270. Liu, Z., et al., *Intestinal Candida albicans Promotes Hepatocarcinogenesis by Up-Regulating NLRP6.* Frontiers in Microbiology, 2022. **13**.

271. Markey, L., et al., *Colonization with the commensal fungus Candida albicans perturbs the gut-brain axis through dysregulation of endocannabinoid signaling.* Psychoneuroendocrinology, 2020. **121**: p. 104808.
272. Shuai, M., et al., *Mapping the human gut mycobiome in middle-aged and elderly adults: multiomics insights and implications for host metabolic health.* Gut, 2022. **71**(9): p. 1812-1820.
273. Burlikowska, K., et al., *Comparison of Metabolomic Profiles of Organs in Mice of Different Strains Based on SPME-LC-HRMS.* Metabolites, 2020. **10**(6).
274. Stöckli, J., et al., *Metabolomic analysis of insulin resistance across different mouse strains and diets.* Journal of Biological Chemistry, 2017. **292**(47): p. 19135-19145.
275. Qiao, Q., et al., *Metabolomic analysis of normal (C57BL/6J, 129S1/SvImJ) mice by gas chromatography–mass spectrometry: Detection of strain and gender differences.* Talanta, 2011. **85**(1): p. 718-724.
276. Sam, Q.H., M.W. Chang, and L.Y.A. Chai, *The Fungal Mycobiome and Its Interaction with Gut Bacteria in the Host.* International Journal of Molecular Sciences, 2017. **18**(2).
277. Krüger, W., et al., *Fungal-Bacterial Interactions in Health and Disease.* Pathogens, 2019. **8**(2).
278. Bajaj, J.S., et al., *Fungal dysbiosis in cirrhosis.* Gut, 2018. **67**(6): p. 1146-1154.
279. Dai, G., et al., *Acetaminophen Metabolism Does Not Contribute to Gender Difference in Its Hepatotoxicity in Mouse.* Toxicological Sciences, 2006. **92**(1): p. 33-41.
280. McConnachie, L.A., et al., *Glutamate Cysteine Ligase Modifier Subunit Deficiency and Gender as Determinants of Acetaminophen-Induced Hepatotoxicity in Mice.* Toxicological Sciences, 2007. **99**(2): p. 628-636.
281. Masubuchi, Y., J. Nakayama, and Y. Watanabe, *Sex difference in susceptibility to acetaminophen hepatotoxicity is reversed by buthionine sulfoximine.* Toxicology, 2011. **287**(1): p. 54-60.
282. Jensen, T., et al., *Fasting of mice: a review.* Laboratory Animals, 2013. **47**(4): p. 225-240.
283. Mossanen, J.C. and F. Tacke, *Acetaminophen-induced acute liver injury in mice.* Lab Anim, 2015. **49**(1 Suppl): p. 30-6.
284. Cover, C., et al., *Pathophysiological role of the acute inflammatory response during acetaminophen hepatotoxicity.* Toxicol Appl Pharmacol, 2006. **216**(1): p. 98-107.
285. Desai, P.R., et al., *Glutathione utilization by Candida albicans requires a functional glutathione degradation (DUG) pathway and OPT7, an unusual member of the oligopeptide transporter family.* J Biol Chem, 2011. **286**(48): p. 41183-41194.
286. Klünemann, M., et al., *Bioaccumulation of therapeutic drugs by human gut bacteria.* Nature, 2021. **597**(7877): p. 533-538.
287. Zimmermann, M., et al., *Mapping human microbiome drug metabolism by gut bacteria and their genes.* Nature, 2019. **570**(7762): p. 462-467.
288. Akay, C. and U. Tezel, *Biotransformation of Acetaminophen by intact cells and crude enzymes of bacteria: A comparative study and modelling.* Sci Total Environ, 2020. **703**: p. 134990.
289. Erb Downward, J.R., et al., *Modulation of Post-Antibiotic Bacterial Community Reassembly and Host Response by Candida albicans.* Scientific Reports, 2013. **3**(1): p. 2191.
290. Eichelberger, K.R., et al., *Candida–bacterial cross-kingdom interactions.* Trends in Microbiology, 2023. **31**(12): p. 1287-1299.
291. Jiang, Y., et al., *A Sucrose-Enriched Diet Promotes Tumorigenesis in Mammary Gland in Part through the 12-Lipoxygenase Pathway.* Cancer Res, 2016. **76**(1): p. 24-9.
292. Brown, K., et al., *Microbiota alters the metabolome in an age- and sex- dependent manner in mice.* Nature Communications, 2023. **14**(1): p. 1348.
293. Chang, S.W., et al., *Optimized synthesis of lipase-catalyzed l-ascorbyl laurate by Novozym® 435.* Journal of Molecular Catalysis B: Enzymatic, 2009. **56**(1): p. 7-12.

294. Kenseth, C.M., et al., *Synergistic O₃ + OH oxidation pathway to extremely low-volatility dimers revealed in β-pinene secondary organic aerosol.* Proceedings of the National Academy of Sciences, 2018. **115**(33): p. 8301-8306.
295. Vijayasarathy, M., et al., *In Vitro Detoxification Studies of p-Cresol by Intestinal Bacteria Isolated from Human Feces.* Curr Microbiol, 2020. **77**(10): p. 3000-3012.
296. Saito, Y., et al., *Identification of phenol- and p-cresol-producing intestinal bacteria by using media supplemented with tyrosine and its metabolites.* FEMS Microbiol Ecol, 2018. **94**(9).
297. McGinnis, C.S., et al., *The temporal progression of lung immune remodeling during breast cancer metastasis.* Cancer Cell.
298. Leonardi, I., et al., *Mucosal fungi promote gut barrier function and social behavior via Type 17 immunity.* Cell, 2022.

10 Acknowledgements

My PhD journey was definitely a rollercoaster: started during a pandemic, interrupted by a war, with many smaller bumps along the way. Almost at the end of the ride, there are many people that made it possible through their support and encouragement that I would like to thank and acknowledge:

Thanks Eran, for giving me the opportunity to delve into the fascinating world of the microbiome. Thank you for building not just one but two labs with smart, nice, and fun people and giving me the freedom to bounce between both, trusting me with my project and teaching me how to do science at a high level. I very much appreciate the encouragement and possibilities you gave me, as well as the times you told me to stop stressing ("no tears no fears"), even if I mostly ignored it.

Thank you, Jens, for your enthusiastic scientific input especially for bringing the organoids to the lab and freely sharing your knowledge and equipment. Thanks for making the lab a livelier and more social place – who knew we would end up in the same lab again (and letting me tell everyone that you followed me…)!

I would like to thank Ralf Bartenschlager for leading my TAC and thesis committee, Ferry Hagen, for being the fungi expert on my TAC, as well as Nina Papavasiliou and Ana Martin-Villalba for agreeing to be on my thesis committee.

Major thanks to Sara and Denise: you felt like the fairy godmothers of this PhD – I do not know what I would have done without you! Getting to work with you and learn from you science- and life-wise was the greatest joy of my PhD and I consider myself beyond lucky that you joined the fungi team, becoming not just my role models but also friends! Sara – thanks for volunteering to do the first "quick" GF fungi experiment, that then spiraled into a much bigger involvement… Thanks for your pep talks, listening to me, and spreading good mood! Denise – thank you for your relentless, never-ending, always reliable support in experiments and in life, even if it meant going to the Mamtak four times a day with me because I forgot something, and for taking over the project. I appreciate you both so much and will stop here before I get too sappy.

Thanks Dragos, for sharing the fungi-enthusiasm and always being up for discussing a project or plating yet another round of stool samples… or adrenal glands, just in case, you never know!

Rafa – thanks for your patient bioinformatics analysis and statistics support but even more for your care and friendship during some low times, and laughter, chats, and sharing your sweets during some happier times.

Nyssa – the fact that at some point I had asked you so many questions that you knew by the way I was breathing in that I was about to start talking and already turned your head towards me says it all already. Thanks for your advice and input on everything ranging from experimental planning to meme subtitles, helping me get more comfortable with mouse work, and non-diplomatic eyebrow-raises.

Thanks to Jasmin, for your excitement to explore fungi-organoid cocultures together, for learning things and becoming independent quickly so that you kept things going even when I wasn't there!

Thanks to Hagit, for your continuous support with the GF experiments and especially for keeping them going while I was stuck at DKFZ. Thanks Suhaib (Team Breast Cancer!), for your help with

the Erbb2 mice, running serum analyzer experiments, and teaching me how to catch mice again when they accidently get loose in the isolator.

Thanks to Sabine, for the highly competent and reliable support with all my sequencing endeavors and early lunch suggestions. And her WIS “counterpart” – thanks Mally, for help with the DNA extractions and nice lunch conversations, and thanks to Shahar for the RNA library preps.

Rogier - the #1 person to message when something in the DKFZ lab is off as the official lab MacGyver as well as high quality meme producer – I very much appreciate your sense of humor, scientific input, and continuous attempts to get me to read the manual even though you knew that I never would!

Many thanks to Dinara for being the “gute Seele” of the lab and always having an open ear, may it be for rants about my admin and travel issues (and gently finding solutions), or just kindly indulging me during my procrastination office visits. On the WIS side – thanks Anna, for dealing with all the behind-the-scenes arrangements for my frequent WIS visits and always welcoming me warmly anyways!

Thanks to Eli and Hanna for patiently answering my many beginner-coding questions and introducing me to the microbiome analysis world. Thanks Matina, for the initial mouse and FACS training. Thanks to Christoph, for help with writing my TVA and planning my first mice experiments.

Thanks to the core facilities that were supporting this thesis – on the DKFZ side the Electron Microscopy Facility and the FACS facility, and on the WIS side the Metabolomics facility, Histology unit, Alon Harmelin for scoring the slides, Bacteriology, and especially the GF facility!

Many thanks to my lovely friends, roommates, and colleagues at the WIS for all your help with experiments, scientific and less-scientific conversations, and for including me in social events from the start – you made me feel so welcome that I kept coming back and it got harder to leave every time! Special thanks to Igor, Yiming, Rosa, Lara, Paromita, Kim, and Melina, for jumping in to help with my sacrifices when I needed extra hands.

Thanks to all my friends and colleagues at the DKFZ, my home base, in particular:

Lena – I remember recruiting you with the humble goal of becoming PhD lab besties and now look at us! Every day I have to fight with you for the good office desk… but you make it worth it with your genuine interest in how people are doing, countless puns, legendary PhDinner dates, and many fun, deep, interesting conversations – thank you, I could not have imagined this PhD without you.

Thanks Sahana, for your calm and soft-spoken kindness, always ready to help with mice sacrifices, after we had started on the same day in the lab: you with your first internship and me with the PhD.

To the rest of the new PhD cohort: Kyanna, Kamil, Serena, and Nina (almost!): here is my curated list of best lab spots for crying, ranked by privacy: botanical garden, PCR room, FACS room, microbe room (now more busy), microinjection room, cell culture, robot room. You are welcome and I wish that you will not need it!

To the postdocs that shared some time in the lab with me: Camila, Ignacio, and Arun – thanks for sharing your perspectives and experiences!

Thanks to the many students and trainees that passed through the lab during this time – your enthusiasm and excitement were great to experience and you all brought so much life to the lab! Special shout-outs to Tomáš (secret project starter & Covid support extraordinaire), Luigi (music sessions in cell culture), Miguelito (pinche pendejo & great tour guide as well as roommate), Deepak (sharing your music), Dinah (long walks home along the Neckar), Toni (brightening many days), and Nina & Luisa (last minute thesis proofreading)!

Thanks to my fellow PhD office occupants for the shared support in our suffering that made my days there so much lighter – special thanks to Svenja, for answering many many PhD-related questions, and Tania, for the frequent writing motivation and reminders that the PhD is “only pages away” now.

Many thanks to my friends and family for their love and support and reminders that there is life outside the lab as well (or so I heard?). Special thanks to Katha and Kai, for letting me invite myself for meals, especially supporting me when I did not know anyone else in HD, and even hosting me when I was homeless without asking how long I was going to stay. Massive thanks to Ninouk, for being a fantastic travel buddy and always being there with an empathetic ear, listening to many rants, giving good advice, and being easily convinced to jump into a cold body of water.

Finally, I would like to thank my parents – your unwavering love and support made this possible! Thanks for trusting my decisions, picking me up when I was down, believing in me, encouraging me countless times, and filling up my fridge. This is for you.